MICROCOPY RESOLUTION TEST CHART
NATIONAL BUREAU OF STANDARDS 1963-A

② **LEVEL** III

A057654

R-981
FEASIBILITY STUDY OF GPS-INERTIAL
NAVIGATION FOR HELICOPTERS
AND
STUDY OF ADVANCED GPS
SIGNAL PROCESSING TECHNIQUES
FINAL REPORT FOR
SAMSO CONTRACT F04701-75-C-0212
VOLUME III
by
Duncan B. Cox, Jr, Bernard A. Kriegsman, William M. Stonestreet
John Kishel, Luigi V. Calicchia
March 1978

D D C
RECEIVED
AUG 15 1978
B

The Charles Stark Draper Laboratory, Inc.

Cambridge, Massachusetts 02139

78 08 07 059

REPORT DOCUMENTATION PAGE		READ INSTRUCTIONS BEFORE COMPLETING FORM
1. REPORT NUMBER SAMSO TR-77-120, Vol. III	2. GOVT ACCESSION NO.	3. RECIPIENT'S CATALOG NUMBER
4. TITLE *(and Subtitle)* Feasibility Study on GPS-Inertial Navigation for Helicopters and Study of Advanced GPS Signal Processing Techniques. Volume III.		5. TYPE OF REPORT & PERIOD COVERED Volume III of Final Report, November 1975 - March 1978
		6. PERFORMING ORG. REPORT NUMBER R-981, Vol. III
7. AUTHOR(s) Duncan B. Cox, Jr., Bernard A. Kriegsman, William M. Stonestreet, John Kishel, Luigi V. Calicchia		8. CONTRACT OR GRANT NUMBER(s) F04701-75-C-0212
9. PERFORMING ORGANIZATION NAME AND ADDRESS The Charles Stark Draper Laboratory, Inc. 555 Technology Square Cambridge, MA. 01239		10. PROGRAM ELEMENT, PROJECT, TASK AREA & WORK UNIT NUMBERS 63421F, 632075
11. CONTROLLING OFFICE NAME AND ADDRESS U.S. Air Force Space and Missile Systems Org. SAMSO/YEO, P.O. Box 92960, Worldway Postal Center, Los Angeles, CA. 90009		12. REPORT DATE March 1978
		13. NUMBER OF PAGES 192
14. MONITORING AGENCY NAME & ADDRESS *(if different from Controlling Office)* R-981-VOL-3		15. SECURITY CLASS. *(of this report)* Unclassified
		15a. DECLASSIFICATION/DOWNGRADING SCHEDULE

16. DISTRIBUTION STATEMENT *(of this Report)*

Approved for public release, distribution unlimited.

DDC RECEIVED AUG 15 1978 B

17. DISTRIBUTION STATEMENT *(of the abstract entered in Block 20, if different from Report)*

18. SUPPLEMENTARY NOTES

19. KEY WORDS *(Continue on reverse side if necessary and identify by block number)*

NAVSTAR, GPS, Satellite Navigation, Helicopter Navigation, GPS-Inertial Navigation, Signal Processing, Tracking Loops

20. ABSTRACT *(Continue on reverse side if necessary and identify by block number)*

This report is presented in two parts. Part 1 presents the results of a feasibility study of a low-cost integrated GPS-inertial (strapdown) navigation system for Army attack helicopters. The conclusion is reached that a GPS-Doppler navigation system can more easily attain the cost and performance goals. It was also concluded that an integrated GPS-Doppler-inertial system might be very attractive if it could be used for providing attitude and heading reference data as well as navigation data. There would be a cost

(O V E R)

DD FORM 1 JAN 73 1473 EDITION OF 1 NOV 65 IS OBSOLETE

408386 LB

20. Abstract (con't)

savings associated with avoiding the need for the usual attitude and heading reference system. Moreover, the integrated GPS-Doppler-inertial system would have excellent performance in the presence of aircraft dynamics and jamming.

Part 2 presents the results of a study of advanced GPS signal processing techniques. Covered in the study are data aiding, comparison of phase-locked loops with Costas loops, variable predetection bandwidths in code-tracking loops, code loop dithering, aided tracking, variable tracking bandwidths, and effective gains of detectors in the presence of noise. The results are from computer simulation and theoretical analysis.

R-981

FEASIBILITY STUDY OF GPS-INERTIAL NAVIGATION FOR HELICOPTERS AND STUDY OF ADVANCED GPS SIGNAL PROCESSING TECHNIQUES

FINAL REPORT FOR SAMSO CONTRACT F04701-75-C-0212

VOLUME III

by
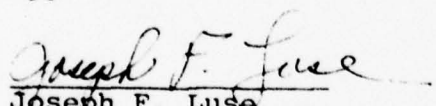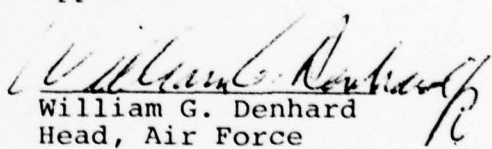
Duncan B. Cox, Jr.
Bernard Kriegsman
William Stonestreet
John Kishel
Luigi V. Calicchia

March 1978

Approved:

Joseph F. Luse
Project Officer
Space and Missile
Systems Organization

Approved:

William G. Denhard
Head, Air Force
Programs Department

The Charles Stark Draper Laboratory, Inc.
Cambridge, Massachusetts 02139

78 08 07 059

ACKNOWLEDGEMENT

This technical report has been reviewed and is approved for publication.

TABLE OF CONTENTS

TABLE OF CONTENTS (Cont.)

iv

TABLE OF CONTENTS (Cont.)

R-981

FEASIBILITY STUDY OF
GPS-INERTIAL NAVIGATION FOR HELICOPTERS

FINAL REPORT FOR SAMSO CONTRACT F04701-75-C-0212

VOLUME III, PART 1

By

John Kishel
Bernard A. Kriegsman
William M. Stonestreet
Duncan B. Cox, Jr.

March 1978

The Charles Stark Draper Laboratory, Inc.
Cambridge, Massachusetts   02139

SECTION 1

SUMMARY

A study was conducted in the Spring of 1977 to
determine the feasibility of developing in the near term
an integrated GPS-inertial navigator of low cost and ade-
quate performance for Army helicopters. A production cost goal of
$18K-$25K in FY76 dollars was adopted for the navigator.
To meet this goal a strapdown inertial measurement unit
(IMU) was considered with the inertial components, the
GPS receiver, and the navigation processor mounted in the
same assembly and utilizing common components wherever pos-
sible. The GPS receiver and navigation processor were as-
sumed to be approximately equivalent in cost and perfor-
mance to the hardware and software in the SAMSO/Magnavox
GPS User Equipment Z Set. The production cost goal for the
integrated GPS-inertial navigator was subdivided into the
following components: IMU, $10k-$12k; GPS receiver, with
computer and display, $12k; additional microprocessors for
strapdown coordinate transformation, instrument compensation,
and inertial navigation, $1k. The driving question was whe-
ther inertial components existed, or could confidently be
developed for engineering models by 1979, which could be
produced at a low enough cost and which would provide ade-
quate performance in helicopter application.

It was recognized that the GPS signals could be utilized in the integrated GPS-Inertial Navigator to calibrate certain IMU parameters in flight and, thereby, to provide enhanced inertial navigation performance during periods of heavy jamming when the GPS signals would be unavailable. But even with this synergistic benefit taken into account, inertial components with adequate performance and sufficiently low cost could not be projected confidently as being available by 1979. Hence, it was concluded that it was not feasible to develop in the near future an integrated GPS-Inertial navigator with the desired cost and performance parameters.

In the study it became clear that, for the helicopter application where flight speeds are often very low, only an IMU of relatively high cost can provide stand-alone performance that is comparable to what can be achieved by a Doppler radar navigator. It was recognized that a low cost strapdown IMU can provide better short-term navigation performance, and better antijam tracking performance through aiding the GPS receiver, than can a Doppler radar. But the very poor long-term performance of the low cost IMU when the GPS is jammed was considered to be quite unacceptable. Although the Doppler radar was not studied in detail, it was seen to be a more practical alternative than a strapdown INS for integration with a GPS receiver to provide a low cost navigator for Army helicopters.

4

A secondary conclusion was that, at a small increase in cost (on the order of $12K) over the Doppler-GPS Navigator, a GPS-Doppler-Inertial system could be developed with superior navigation and antijam performance. Superior performance would be obtained both in the normal operating mode and in backup modes when either the GPS or the Doppler sensors, or both, are inoperative. Moreover, this integrated system could be used to drive the attitude and heading reference system (AHRS) displays. The savings obtained through elimination of AHRS components and the enhancement in navigation and display performance would make the GPS-Doppler-Inertial system an attractive development for a new helicopter.

The pertinent results of a survey of strapdown technology are presented in Section 3. Then, in Section 4, an analysis of navigation performance with applicable components is presented. Evaluations of the results are presented in Sections 4 and 5. The conclusions of the report are summarized in Section 6.

SECTION 2

SURVEY OF STRAPDOWN INERTIAL TECHNOLOGY

This survey is directed at projecting the state-of-the-art in low cost strapdown inertial technology as it can be expected to exist in the time frame 1979 to 1984. The primary objective is to provide a data base for further analysis leading to a possible decision to develop a hybrid GPS/inertial system for use in tactical Army helicopter navigation.

To qualify for consideration in this study, an instrument must be at such a point in its design that at least an engineering development model could be available by early 1979, and the instrument production unit cost goal must be comparible with use in $8K to $12K strapdown IMU[*]. Based on evaluations at CSDL, the cost of a strapdown IMU in volume production is estimated to be a factor of 2 or 3 times the cost of all inertial instruments in the IMU taken together. Hence, to achieve the cost goal for the IMU, the gyros should cost no more than about $1K, and the accelerometers no more than about $0.6K, per axis.

The IMU should be suitable for substantially improving the anti-jam performance of a GPS receiver and for serving as a useful auxiliary navigation sensor during periods when GPS signals might be heavily jammed or other-

---

[*]Throughout this section $ refers to FY76 dollars.

wise masked. In combination with a flux-valve sensor, it should also be capable of providing all the data normally supplied by an AHRS (Attitude and Heading Reference System). It should be capable of providing data for an autopilot or for a stability augmentation system as an option. In advance of detailed performance analyses, a rough rule of thumb was used that the IMU should offer, after a period of in-flight calibration using the GPS, some promise of operation in a range of long-term error rates of 3 to 10 nmph, and substantially smaller short-term error rates. Additional qualification criteria could be imposed on the components, such as tolerance of certain environmental conditions, but such restrictions would be premature at this early stage of the investigation.

As a result of intense efforts on the part of the inertial component industry, there are a sizeable number of components, ranging from currently available off-the-shelf instruments to those in the early feasibility model stages of development, which qualify for consideration.

This report first covers the state-of-the-art of off-the-shelf components. Next, the newer developments are reviewed. Following this same conclusions and recommendations are provided.

Many quantitative estimates which are proprietary to industrial companies and/or which are unsubstantiated by hard evidence are purposely omitted from this report.

2.1   Gyroscopes

A number of single-degree-of-freedom gyro families are currently available off-the-shelf and appear to meet the cost criteria used here. Gyros identified by each manufacturer's family nomenclature are shown in Table 2.1. Within each family specific gyro versions can be selected. Generally, each family includes gyro versions that can be purchased in volume for approximately $1K each. Day-to-day turn-on-to-turn-on bias repeatabilities of several of these gyros in the $1K cost range are in the neighborhood of 1 to 2°/hr (1σ). However, these biases are thought to be capable of being calibrated to lower levels of uncertainty through preflight and in-flight calibration. In the past, these gyros were used in stand-alone applications where day-to-day repeatability was the principal acceptance criterion, and, therefore, their short-term and long-term performance characteristics were not precisely measured. Data on short-term stability of the biases is, therefore, not available on these components. The Draper Laboratory is currently carrying out test programs on the GG-1111 and the IG-10 to establish a data base in the context of short-term and long-term performance after calibration.

Table 2.1 Single-degree-of-freedom rate integrating gyros.

Manufacturer — Generic Nomenclature	Examples of Current Use
Lear Siegler — 1903	Anti-Shipping Missile Guidance
Northrop — GI-G6	Anti-Shipping Missile Guidance
Hamilton-Standard — Minirig-30	Missile guidance
US Time — IG-10	Torpedo Guidance
Honeywell — GG1111	Missile Guidance

Early tests at CSDL on a GG-1111-AJ indicate that the short-term bias uncertainty is about an order of magnitude less than the day-to-day turn-on-to-turn-on variation. Therefore, there is some promise that a drift rate of 0.15° per hour (1 meru) could be achieved with this low-cost gyro.

There is a small category of "Hooke's-Joint" support gyros which should also be considered. The oldest members of this category were developed for use in gimballed navigation systems. Recent work has produced modifications for higher rate inputs. Engineering models of the two instruments in this category shown in Table 2.2 are available for evaluation. Manufacturers' budgetary estimates for unit costs of gyros in Table 2.2 in large volume production are roughly $1.5K-$3K. The likelihood of meeting the cost and performance criteria is not really clear for these gyros since the G7 has not been committed to substantial use for strapdown attitude reference, and the Conex has not been used for strapdown attitude reference.

Table 2.2 Dry tuned gyros (two-degree-of-freedom).

Manufacturer — Generic Nomenclature	Status of Instrument
Litton — G7	Bench-test evaluation for strapdown attitude reference applications
Kearfott — Conex	In use in pointing system application which is not representative of strapdown attitude reference applications

Other dry tuned gyros such as the Teledyne SDG-5, Litton G-6, and Kearfott SKN 3920 are considered to be far outside the aforementioned cost criteria.

9

Laser gyros offer certain advantages for strapdown systems applications. Their performances are not limited by high rate inputs which are troublesome to the torqued gyros considered above. Moreover, they are not sensitive to orientation relative to earth's gravity and appear to have turn-on-to-turn-on repeatability comparable to that of higher-priced conventional gyro counterparts. However, the relatively high levels of white-noise drift rate exhibited by laser gyros should be considered with respect to their effect on the aiding of GPS tracking loops. Since these units are still going through producibility development, it is difficult to obtain reliable cost estimates of production units. Because of the advantages offered, and because they potentially could be low in cost, the list in Table 2.3 is offered for consideration. Manufacturers' budgetary estimates for unit production costs of these gyros in large volume are on the order of $2K-$6K.

Table 2.3 Laser gyros potentially applicable.

Manufacturer — Generic Nomenclature	Strapdown Guidance Status
Sperry SLG 15	Flight testing in strapdown IMU 8300 in F4
Honeywell GG 1328	Flight testing in strapdown ATIGS IMU in A7

Other laser gyros are under early development at Sperry and Honeywell, and at other companies such as Hamilton Standard, Autonetics, Raytheon, Litton, and Singer Kearfott. The Honeywell GG-1300 and the Hamilton Standard DILAG are not included in Table 2.3 because their budgetary cost estimates are much to high for consideration in this survey.

10

2.2 Unconventional Sensors

The devices shown in Table 2.4 represent high-risk but high-payoff technology for strapdown systems of the future. Confidence levels for meeting the aforementioned qualification criteria are to a large extent not known.

Table 2.4 Unconventional sensors potentially applicable.

Manufacturer — Generic Nomenclature	Intended Application	Status
Delco — Sonic Gyro	Strapdown missiles aircraft navigation	Laboratory feasibility tests
Teledyne — SCAG	Strapdown missiles aircraft navigation	Laboratory feasibility tests

The sonic gyro has essentially no practical angular rate limits for applications under consideration. A single SCAG offers the capability of measurement of two (2) orthogonal angular rates and two (2) orthogonal accelerations.

2.3 Accelerometers

Table 2.5 shows currently available inertial-grade pendulous accelerometers with adequately low costs.

Table 2.5 Low-cost pendulous accelerometers.

Manufacturer — Generic Nomenclature	Strapdown Status
Sundstrand — QA 1100	Volume production for aircraft and missiles (TOW)
Systron Donner — 4832	Volume production for aircraft and missiles (LANCE)

11

Delco is studying the design of a vibrating-beam accelerometer which is being considered for application to missile guidance initially. A very low target cost makes this device an important contender for application to low-cost strapdown inertial guidance. Honeywell has two models of a pendulous accelerometer in laboratory evaluation. The low target cost of this design makes it a possible contender also. Kearfott has an electrostatic accelerometer under development that also has the potential to meet the criteria discussed in the introduction. These accelerometers are shown in Table 2.6.

Table 2.6   Accelerometers in development.

Manufacturer — Generic Nomenclature	Strapdown Status
Delco–Vibrating beam	Early bench testing
Honeywell — G2550	Early bench testing
Kearfott — Electrostatic, ESA	Early bench testing

2.4   Summary of Inertial Sensor Survey

Suitable accelerometers probably can be obtained. But there is substantial doubt about the availability of suitable gyros. For a price of $1K or less per gyro axis a drift bias of 0.1°/hr can be projected with fair confidence. Drift biases of 0.05°/hr might be achieved within the cost bounds, but only with fortuitous technology advances. Better performance than 0.05°/hr will probably entail a factor of two or more increase in cost.

12

A summary of the approximate performance parameters expected from an IMU within the stated cost bounds is shown in Table 2.7.

Table 2.7   Projected parameter uncertainties for low-cost strapdown IMU after calibration.

Error Source	RMS Error
Gyro drift-rate bias	10 meru (0.15°/hr)
Gyro scale factor	300 ppm
Gyro scale factor asymmetry	30-100 ppm
Gyro g sensitivity	0.1°/hr/g
Accelerometer bias	50-100μg
Accelerometer scale factor	200 ppm

If technology beyond 1979 is considered, further substantial improvements in perfromance can be expected.   But quantitative projections cannot now be made with confidence.

In the next section, the expected performances of GPS-inertial navigators utilizing low-cost (i.e., meeting the stated cost criteria) and medium-cost (i.e., a factor of 2 or more outside of the stated cost bounds) IMUs are derived for a possible helicopter scenario.   It is seen that the performance of the navigator utilizing the low-cost IMU is less than what is desired in this application whenever GPS is jammed for long periods.

SECTION 3

PERFORMANCE ANALYSIS OF GPS-INERTIAL NAVIGATOR

3.1   Summary

The use of GPS and IMU data for navigation of an attack helicopter is studied here. Low and moderate cost strapdown IMUs are considered for use in the helicopter. A 1.5-g S-turn maneuver is performed after takeoff, during which time GPS data are used to in-flight align the IMU.

A sequential GPS receiver is assumed, which is switched between 4 different satellites at 2-second intervals. The tracking period for a given satellite is 1 second long, during which 2 range and 1 delta-range measurements are taken.

In the cases studied it was found that by using GPS data in the manner described above, the IMU alignment errors can be reduced from about 6 mr/axis (1-sigma) to about 1.5 mr in azimuth and 0.4 mr in level (1-sigma) in less than a 1-minute time period.

If no additional GPS data are provided after the first 1-2 minutes following takeoff, then the helicopter navigation-system errors will diverge with time, as is typical of unaided inertial navigation systems. With a low-cost IMU (10 merus), drift-rate bias errors will dominate, and position errors of the order of 10 n.miles (1-sigma) will result after a 1-hour flight. With a moderate-cost IMU (1 meru), on the other hand,

the errors at the end of a 1-hour flight will be about 1.5
n.miles (1-sigma), with gyro-scale-factor contributing sig-
nificant errors along with drift-rate bias.

3.2   General Information

The overall study involves the integration of a low-
cost strapdown IMU with a GPS receiver for accurate navi-
gation of an attack helicopter. To minimize navigation
system costs, only strapdown IMUs are considered here.
Likewise, the GPS receiver for this study is taken as a
single-channel receiver, which will be switched between
the different satellites being tracked.

The GPS will provide very accurate navigation infor-
mation during periods when the signals can be tracked.
Accurate in-flight alignment of the IMU is also possible
in relatively short time periods (1-2 minutes) using GPS
information. The IMU will provide the required navigation
information during periods when GPS is not available.

3.3   Basic Assumptions

A relatively simple mission scenario is considered
here. The helicopter is assumed to be traveling at a con-
stant speed of 100 kn at an altitude of about 100 feet.
Shortly after takeoff the vehicle executes a coordinated
S-turn maneuver, as indicated in Figure 3.1. The total
duration of this maneuver is about 24 seconds. The total
lateral force (directed downward in vehicle coordinates)
on the vehicle during this period is 1.5 g's. The vehicle
then flies at a constant heading in a northernly direction
for about 1800 sec., at which time a second S turn is per-
formed. The vehicle flies thereafter on a constant head-
ing in a northernly direction.

Fig 3.1   Trajectory Ground Track w.r.t. Earth

$$V = 100 \text{ kn}$$
$$\text{turn accel} = 1.5 \text{ g's}$$
$$\text{Lat}_0 = 0, \text{Lon}_0 = 0$$

t = 5400 s

t = 1833 s   t = 1810 s

N

E

t = 23 s   t = 0
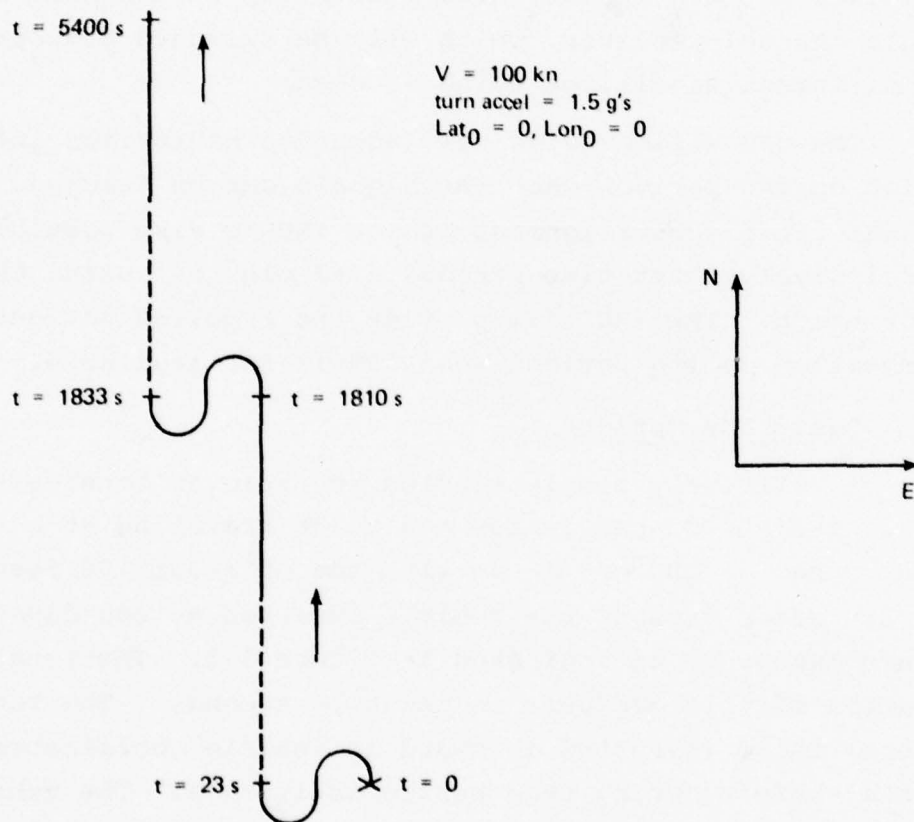
A single-channel GPS receiver is assumed here, which is sequentially switched between 4 appropriately selected satellites. The basic procedure is indicated in Fig 3.2. A 1-second period is assumed for acquisition of the new satellite. After acquisition a range measurement is taken, and the counting of Doppler cycles is begun. One second later (2 seconds after acquisition) a second range measurement is taken along with a delta-range measurement based on Doppler cycle counts for the 1-second interval. A set of three GPS range and delta-range measurements provides accurate information on helicopter position and velocity, if the receiver's clock is accurate. A fourth GPS measurement set permits accurate calibration of the receiver clock's time and frequency. Normally, the receiver's clock will not be accurate.

In the particilar case studied here, the primary interest was on the ability of the GPS to rapidly in-flight align an IMU and the implications on subsequent navigation-system performance thereafter. For this reason, a relatively large IMU alignment error was assumed initially, i.e., 6 mr/axis about all three axes. GPS tracking was assumed to take place, in the manner described earlier, for 60 seconds following takeoff. No GPS measurements are processed thereafter.

The study-model GPS errors are summarized in Table 3.1. Included here are receiver noise, satellite ephemeris uncertainties, and time offsets and drift in both the satellite and receiver frequency references. Propagation errors for transmission through the ionosphere and troposphere were included approximately within the other identified error parameters for this initial study.

17

Fig 3.2 Tracking Sequence
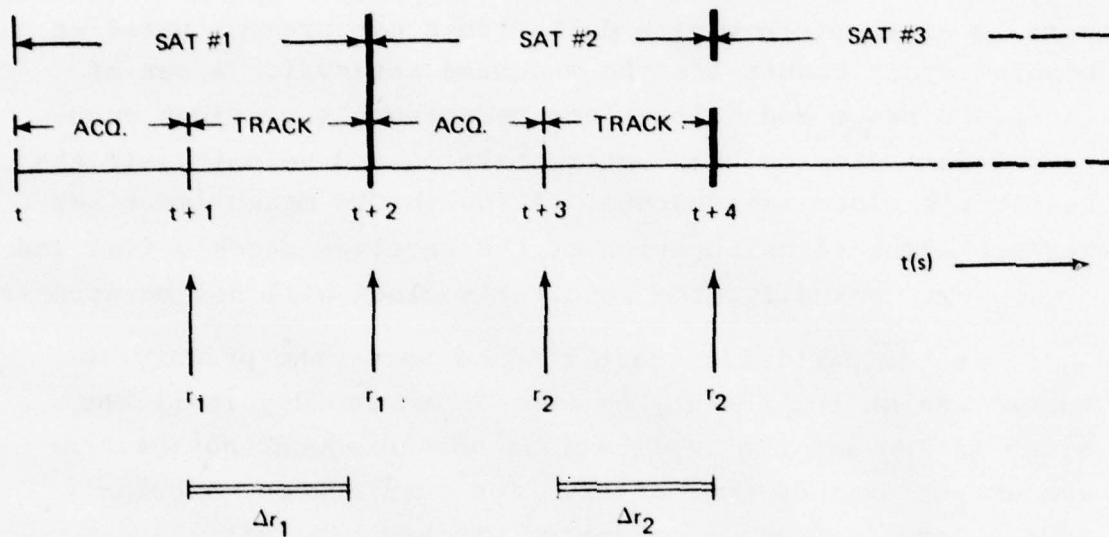
r   = RANGE MEASUREMENT

Δr = DELTA - RANGE MEASUREMENT

18

Table 3.1   GPS Error Model.

Error Type		RMS Value
Receiver Noise		10 ft (random)
		0.15 hz (random)
Satellite Ephemeris		10 ft/axis ($\tau = \infty$)
		0.001 fps/axis ($\tau = \infty$)
Receiver Clock	Init. Offset	2 µsec
	Drift	0.4 hz ($\tau = 2$ hrs)
	Noise	0.05 cycles (over 1s.)
Satellite Clock	Init. Offset	0.01 µs
	Drift	0.001 hz ($\tau = \infty$)
	Noise	0.05 cycles (over 1s.)

19

The IMU error models used in the study are summarized in Table 3.2. The errors here are all treated as bias errors ($\tau = \infty$), normally distributed about a zero mean value. Two different IMU models are considered: a low-cost IMU (meeting the cost objectives of the study) and a moderate-cost IMU. The primary difference in performance between the two is in the assumed gyro drift-rate bias errors.

3.4 Simulation Description

A detailed digital-computer simulation has been utilized to study the performance of the hybrid GPS-IMU navigator on an attack helicopter mission. The simulator uses a high-order state vector to model all IMU and GPS measurement errors given in Tables 3.1 and 3.2. A low-order state vector is used in a minimum-variance filter onboard the helicopter to process sequentially the GPS measurement data. The study-model onboard filter included position (3), velocity (3), IMU alignment (3), gyro drift-rate bias (3), user clock offset (1), and user clock drift (1) errors as state elements.

Two different types of data are generated from the simulation:

1) R.M.S. errors in the estimates of helicopter position, velocity, IMU alignment, and gyro drift-rate bias. These data are generated by integration and updating of the real-world estimation-error covariance matrix with consideration of the operation of the lower-order navigation filter, i.e., by linear covariance analysis.

2) Single-test-case or deterministic errors in the estimates of the navigation quantities. These data are generated from a single deterministic test

20

Table 3.2   IMU Error Model.

Error Source	RMS Error	
	Low-cost IMU	Medium-cost IMU
Initial Alignment	6 mr/axis	6 mr/axis
Gyro Drift-Rate Bias	10 meru	1 meru
Gyro Scale Factor	300 ppm	100 ppm
Gyro Scale-Factor Asymmetry	100 ppm	30 ppm
Accelerometer Bias	100 µg	50 µg
Accel. Scale Factor	200 ppm	100 ppm

run (not a statistical run) with the nonlinear model in which all initial-condition and bias errors are set at 1-sigma values. Simulated measurements are processed in the on-board filter in this type of run.

3.5   Simulation Results

The ability of the GPS to perform an in-flight alignment of the IMU is demonstrated in Fig 3.3 for the mission scenario and navigation-sensor models described earlier. The r.m.s. errors in the estimate of alignment errors (covariance analysis) are shown on the top half of Fig 3.3, and data for a typical deterministic case (all errors initially at 1-sigma values) are shown on the bottom. The alignment errors are presented as components along the vertical (V), east (E), and north (N) directions. GPS data are taken for 60 seconds, the first 24 of these are during the 1.5-g S-turn maneuver.

The data show that for the assumed conditions, the horizontal components of alignment error are estimated to an accuracy of better than 0.4 mr (1-sigma). The vertical component, on the other hand, is less accurately estimated, since the measurement geometry is poorer (e.g., after the S-turn the vehicle's lift force is essentially vertical). The r.m.s. error in this component is about 1.5 mr.

The reduction of helicopter navigation errors during the period of GPS tracking is shown in Fig 3.4. The r.m.s. errors in the estimates of vehicle position and velocity are given here along east and north directions. Single-test-case error time histories for the same case are given in Fig 3.5. The particular data shown in Figs 3.3-3.5 are for the moderate cost IMU, but essentially the same results were obtained with the low-cost IMU.

22

Fig 3.3   In-Flight Alignment of IMU with GPS Data

Notes: (1) Sequential receiver with $\tau=2s$, R+ΔR

(2) 60 seconds of GPS data

(3) S-turn at 1.5 g's for 24s, then level flight

(4) Moderate-cost or low-cost IMU

RMS ALIGNMENT EST. ERRORS
(covariance analysis)

U = ————————
E = +——+——+
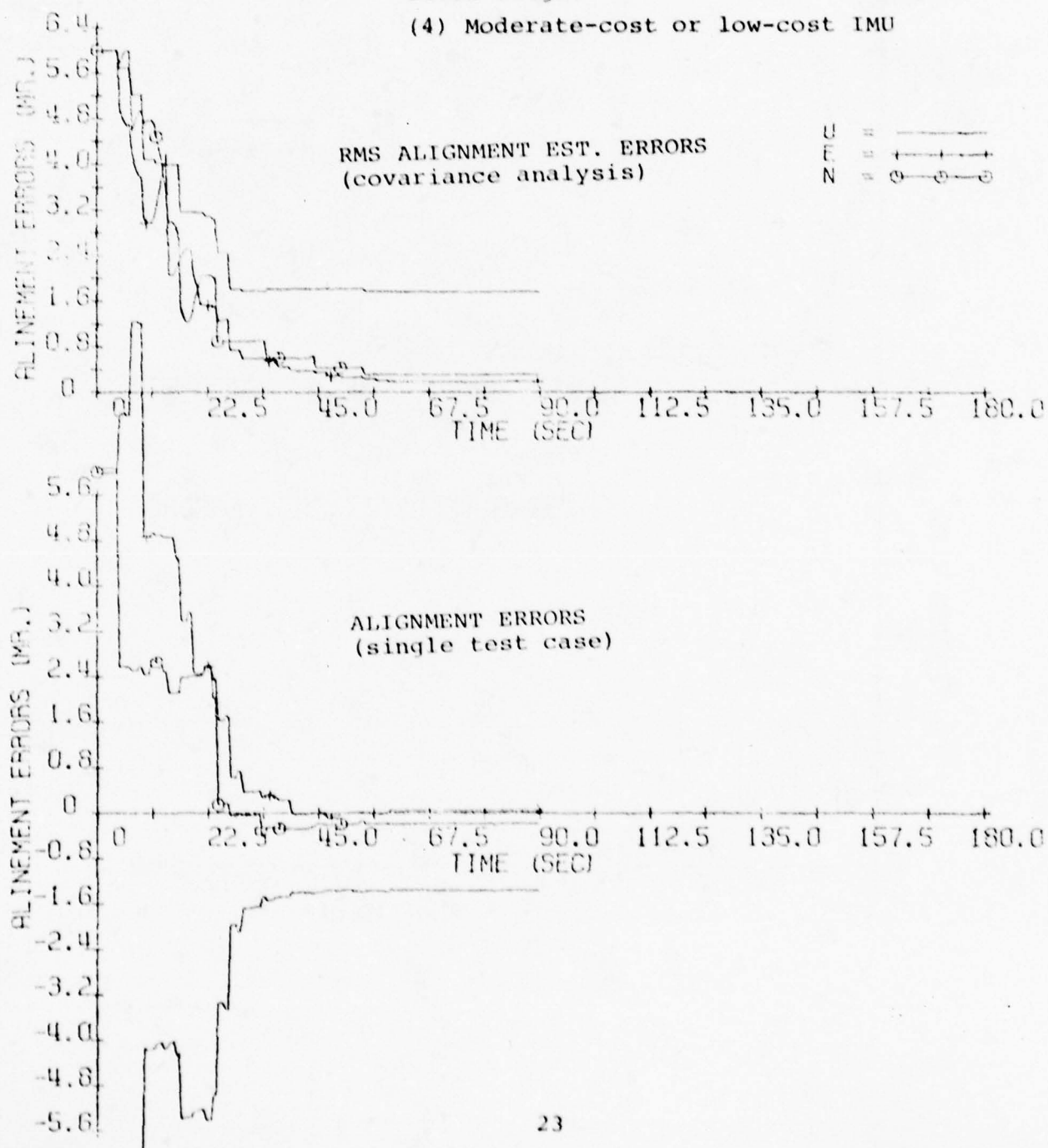N = ⊖——⊖——⊖

ALIGNMENT ERRORS
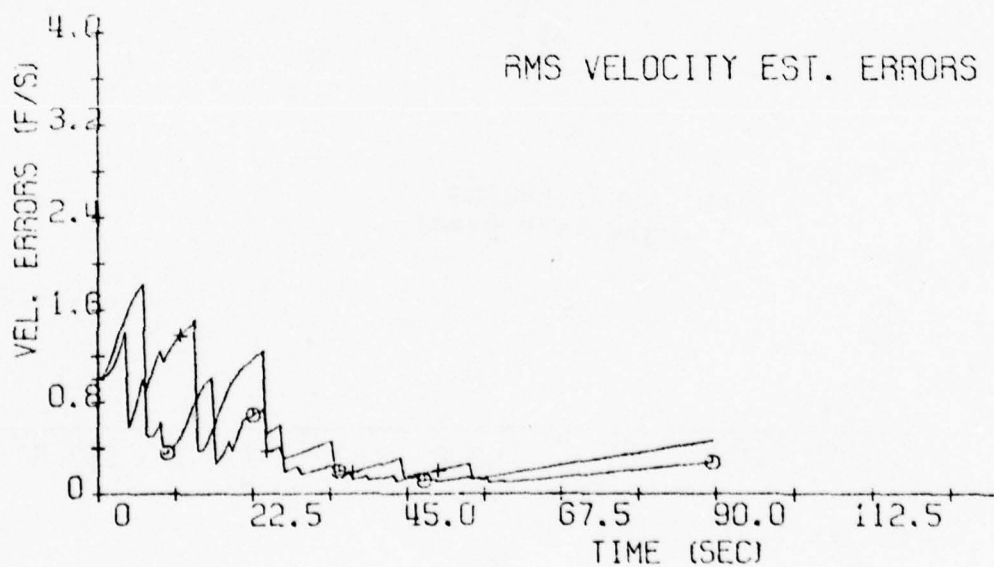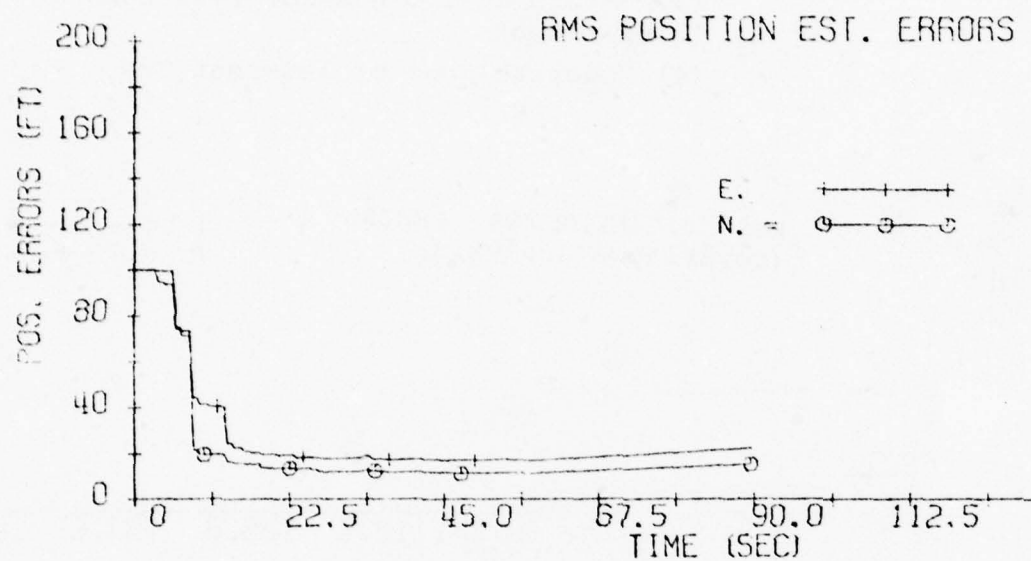(single test case)

23

Fig 3.4   Reduction of Navigation Errors
During GPS Tracking Period

Fig 3.5 Single-Test-Case Nav. Data

POSITION ERRORS

VELOCITY ERRORS

25
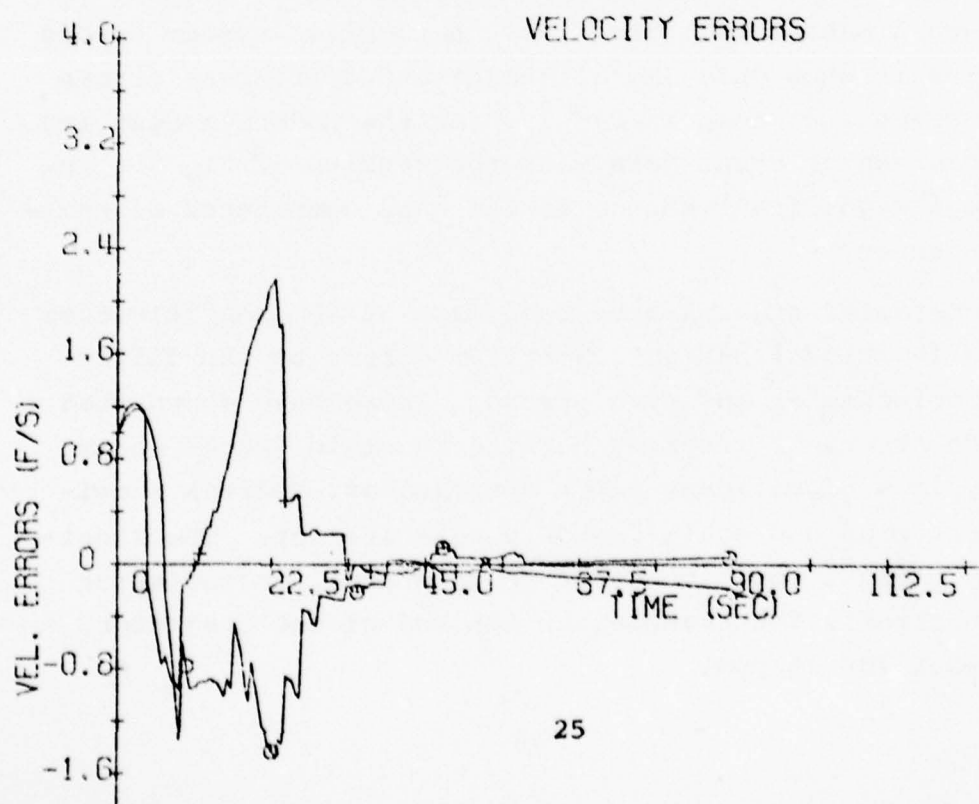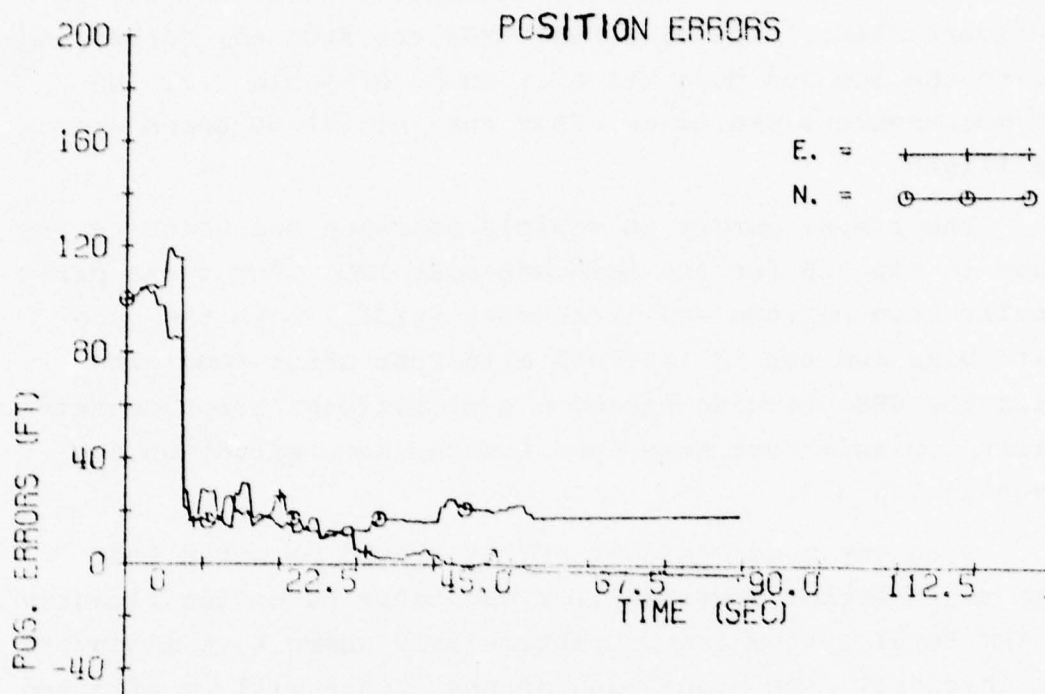
Inertial-navigation system performance for a 1.5-hour duration flight under the assumed conditions of Fig 3.1 is considered next. Two different IMUs are studied, corresponding to the low and moderate cost units of Table 3.2. No GPS measurements are taken after the initial 60 seconds of the flight.

The r.m.s. errors in vehicle position and velocity are shown in Fig 3.6 for the moderate-cost IMU. For these particular time periods and instrument errors, both the gyro drift bias and the IMU azimuth alignment error remaining after the GPS tracking period are significant error contributors. Single test case data for the same situation are given in Fig 3.7.

With the moderate-cost IMU it should be noted that gyro scale-factor uncertainties can contribute significantly to the total system error, particularly where turn maneuvers are involved. The magnitudes of the errors will be affected by the manner in which the maneuvers are implemented. Large changes in vehicle orientation occur during the course of the S-turn maneuvers. The r.m.s. navigation-system errors that result when only IMU alignment and drift-bias errors are present are shown in Fig 3.8 for the moderate-cost IMU. A comparison of these data with the results of Fig 3.6 indicate a significant change in the east components of navigation error.

Detailed studies have been made of the sensitivities of the individual navigation-system errors to the different accelerometer and gyro errors. These have shown that for the errors of interest here, gyro scale factor uncertainty is a significant error contributor, whereas accelerometer bias and scale-factor errors are not. The sensitivity of east position error to gyro scale factor error (pitch error), for example, at the end of the trajectory was about 150 ft/ppm.

26

Fig 3.6   Navigation Errors for 1.5-Hour Flight —
Moderate Cost IMU

RMS POSITION EST. ERRORS

RMS VELOCITY EST. ERRORS

RUN NO. - 123

7/13 8:55

27
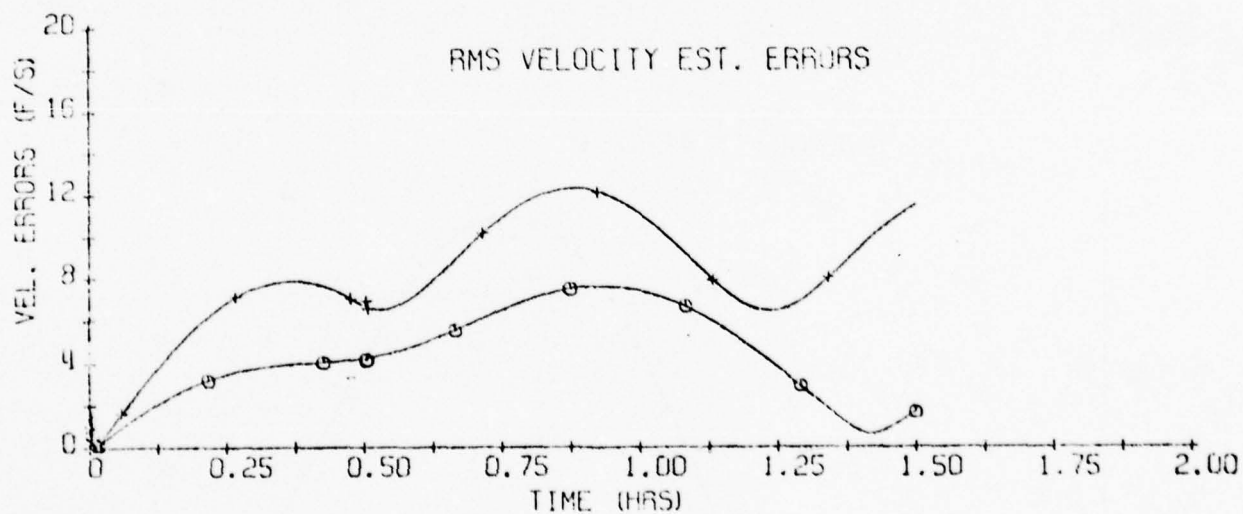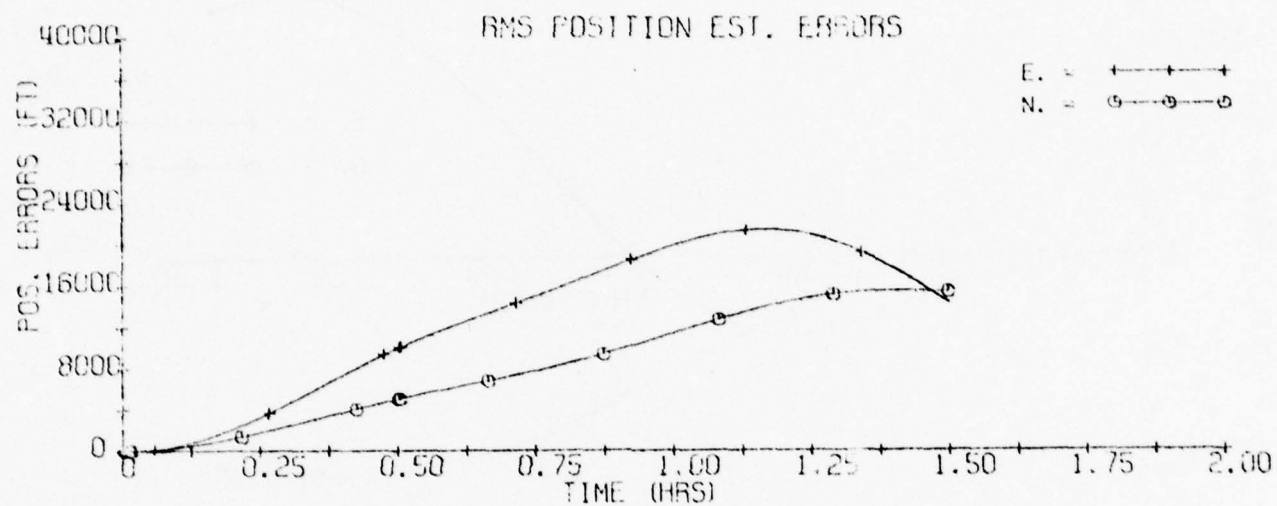
Fig 3.7   Navigation Errors for 1.5-Hour Flight — Moderate Cost IMU
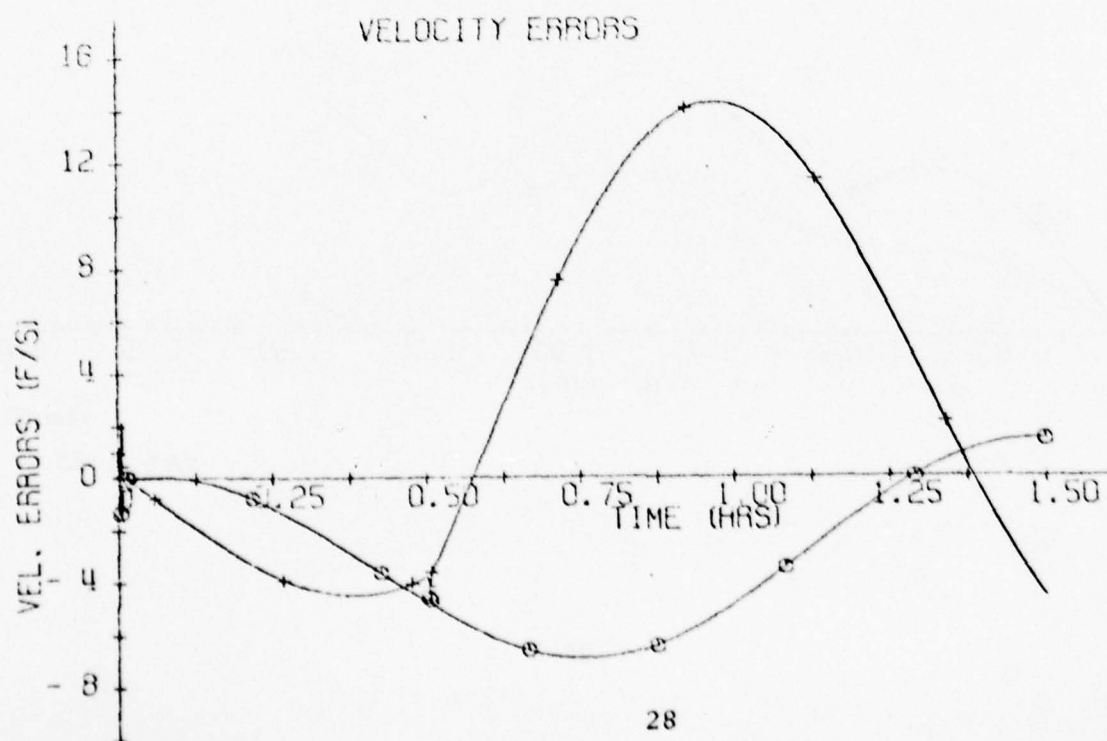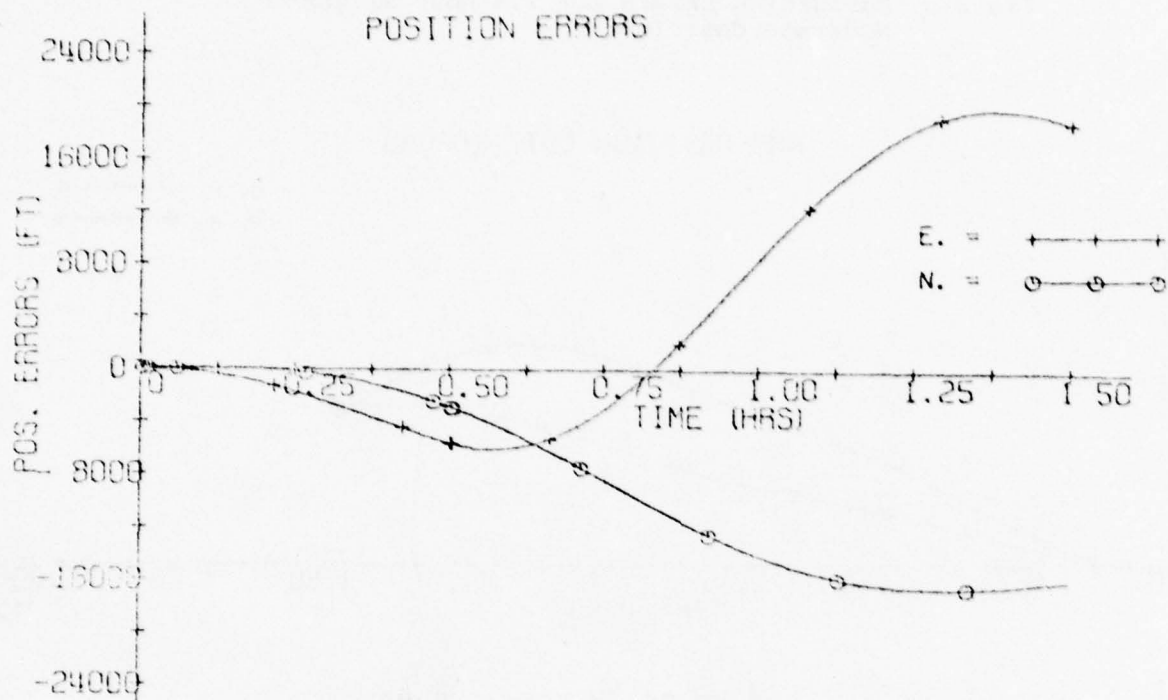
Fig. 3.8 Navigation Errors for 1.5-Hour Flight — Moderate-
Cost IMU with Drift and Alignment Errors Alone

RMS POSITION EST. ERRORS

E. = +——+——+

N. = θ——θ——θ

RMS VELOCITY EST. ERRORS

TIME (HRS)

POS. ERRORS (FT)

40000
32000
24000
16000
8000
0

0.25 0.50 0.75 1.00 1.25 1.50 1.75 2.00

TIME (HRS)

VEL. ERRORS (F/S)

20
16
12
8
4
0

0.25 0.50 0.75 1.00 1.25 1.50 1.75 2.00
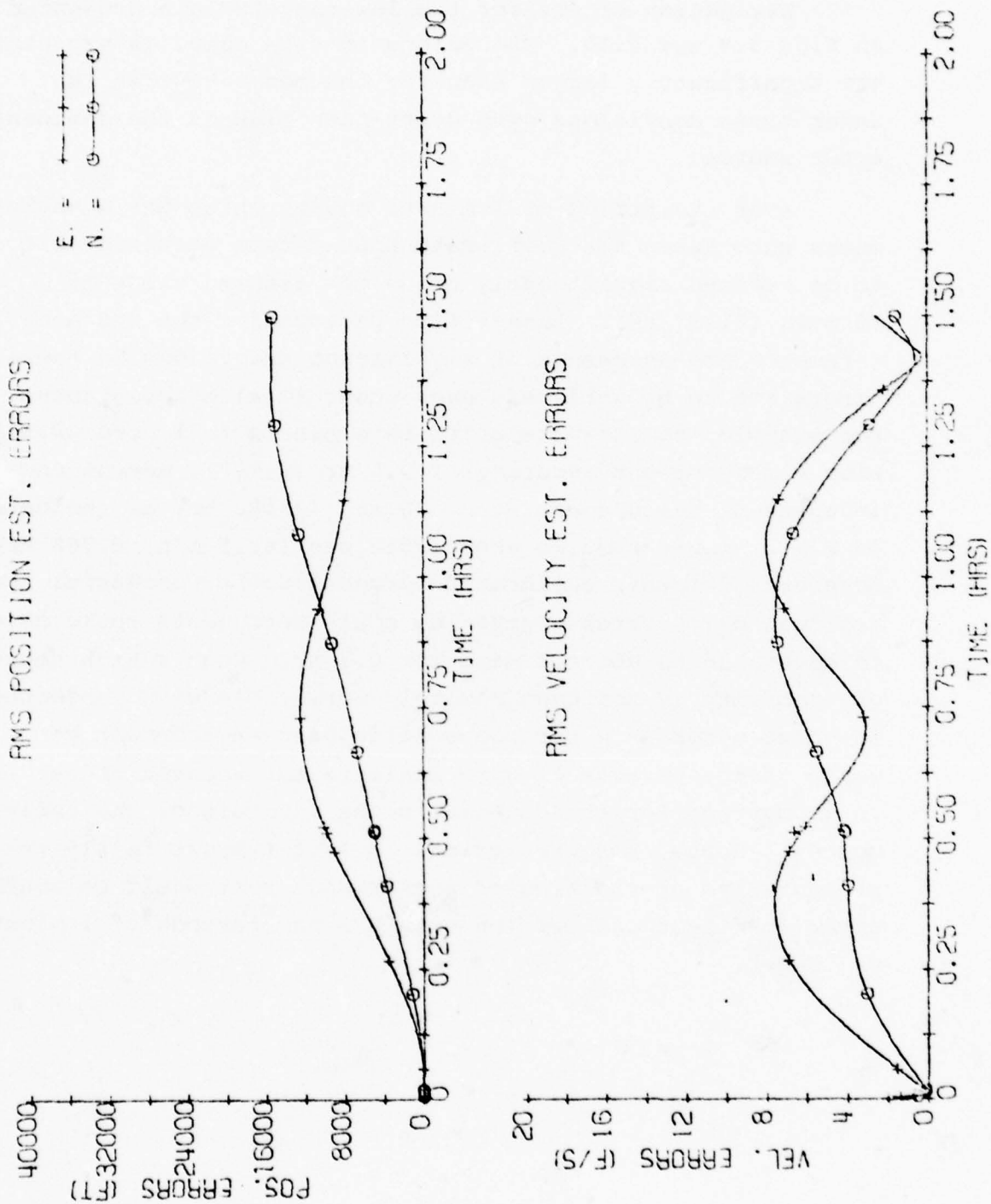
Navigation errors for the low-cost IMU are presented in Figs 3.9 and 3.10. The errors in this case, as expected, are significantly larger than for the moderate cost IMU. Under these conditions gyro drift-rate bias is the dominant error source.

Over the period of 1 minute during which GPS measurements were taken the drift-rate bias errors were not able to be reduced significantly below the assumed value of 10 meru (0.15°/hr). Longer time periods for the GPS measurements are necessary if significant reductions in these errors are to be achieved, even under ideal circumstances. For example, to estimate drift rate biases to 1 meru (0.015°/hr) with a measurement accuracy of 0.5 mr (0.03°), making one independent measurement every 20 sec (1/180 hr) as indicated in Fig 3, would require about 2550 sec (42.5 min, 0.708 hr). Moreover, for this calibration process to be successful the residual drift rates of the low cost instruments would have to be stable to about 1 meru for 0.7 hr. Such a high degree of stability is not even remotely achievable with projected low-cost gyros in a strapdown helicopter environment because of the effects of gyro scale factor uncertainties in accounting for the changes in the attitude of the helicopter. Hence, the predictions in Figs 6-9 are fairly representative of the kind of performance that would be achieved after in-flight calibration with GPS for periods of 1 minute or longer.

Fig 3.9 Navigation Errors for 1.5-Hour Flight — Low Cost IMU

31
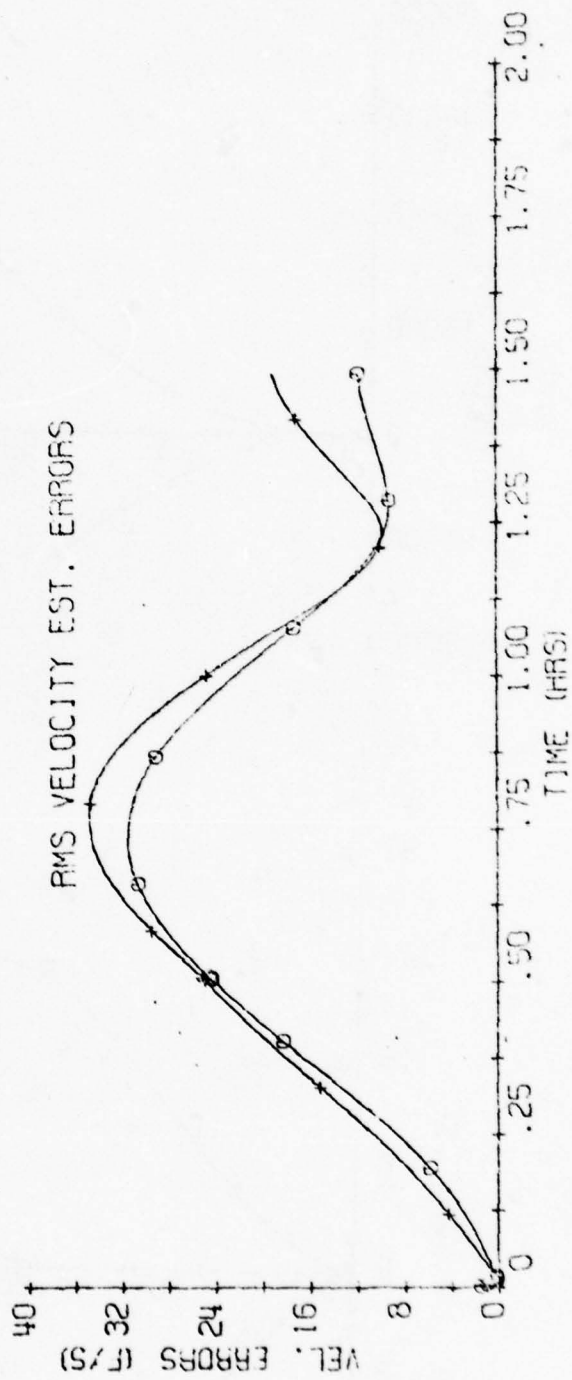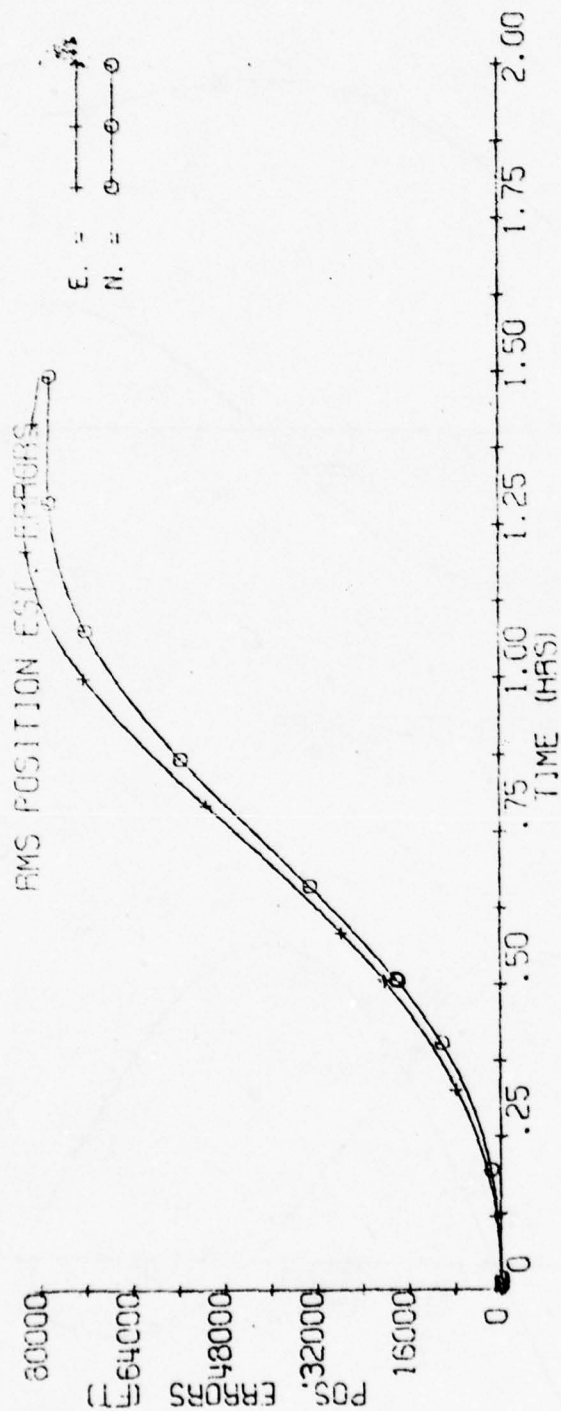
**Fig 3.10   Navigation Error for 1.5-Hour Flight —
Low Cost IMU**

POSITION ERRORS

VELOCITY ERRORS

32
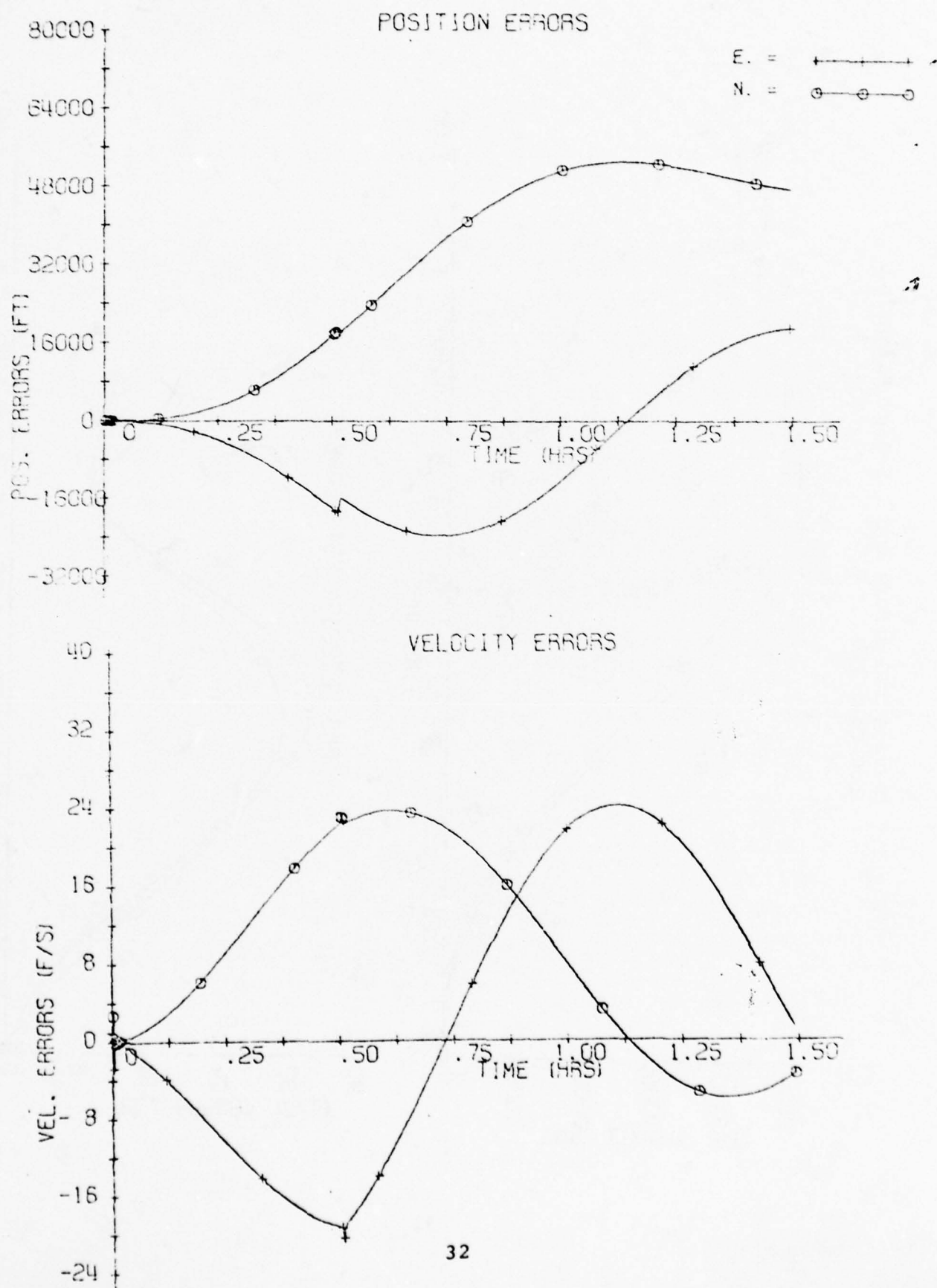
SECTION 4

EVALUATION OF RESULTS

The stand-alone navigation errors shown in Fig 3.9 for the low cost IMU are clearly unacceptable by a wide margin. Errors of about 18 nmi are indicated after a little over an hour of flight. Hence, we conclude that if GPS is jammed, or otherwise unavailable, the low-cost GPS-inertial navigator would not perform adequately for the helicopter application.

The stand-alone performance of the moderate-cost strapdown IMU, as shown in Fig 3.6 might be considered adequate under some circumstances. An error of about three miles accumulates in a little over an hour. However, becuase of the scale factor asymmetry error in Table 3.2 the error in position would be worse than indicated in Fig 3.6 if more S-turn maneuvers were employed during times when GPS was not available. Moreover, at a speed of 100 kt a Doppler radar navigator, utilizing the attitude and heading reference system (AHRS), would provide a CEP of roughly 2 miles in a little over an hour of flight ($\sim$ 1.7% of distance traveled at 100 kt). This is roughly comparable to what could be obtained with the postulated moderate-cost strapdown IMU. The cost of the Doppler radar (without computer, display, or AHRS) would be much less than the cost of the moderate cost strapdown IMU and roughly equal to the cost projection of $12K for the low-cost IMU. The relatively

33

good long-term performance of the Doppler radar in compari-
son with that of the low-cost strapdown IMU is due to the
low speed of flight and to the fact that the long-term
Doppler navigator errors are essentially proportional to
distance traveled (except at very low speeds), whereas
inertial navigation errors tend to grow as functions of
time.

We conclude that, if the choice is to be made between
a low-cost GPS-inertial navigator and a low-cost GPS-Doppler
navigator for tactical helicopters, the low-cost GPS-Doppler
navigator would be the better choice.

SECTION 5

EVALUATION OF OTHER SYSTEM CONFIGURATIONS

If the field of choice is to be broadened to include the possibility of saving the cost of the inertial AHRS components through utilization of the low-cost strapdown IMU for attitude and heading indication as well as for navigation, another option appears which is very attractive. This option is to utilize GPS, Doppler, and flux-valve sensors in confunction with a low-cost strapdown IMU, as shown in Figure 5.1 with this complement of sensors, performance is excellent and net cost is projected to be low.

The performance is expected to be excellent because of the synergism between the different kinds of sensors. The GPS receiver in conjunction with the IMU provides syneraccurate position (30 ft.) and velocity (0.1 ft/sec) data when GPS data is available and allows calibration of both the IMU and the Doppler radar. The IMU enhances the accuracy of velocity determination with GPS data by roughly an order of magnitude. The IMU (but not the Doppler radar) also improves the antijamming performance of the GPS tracking loops. The IMU also provides very accurate attitude data (with accuracies on the order of 0.1 degree) for use with the Doppler radar when GPS is unavailable, thus providing the capability stand-alone, Doppler-inertial navi-

Figure 5.1   An Integrated GPS-Doppler-Inertial System.
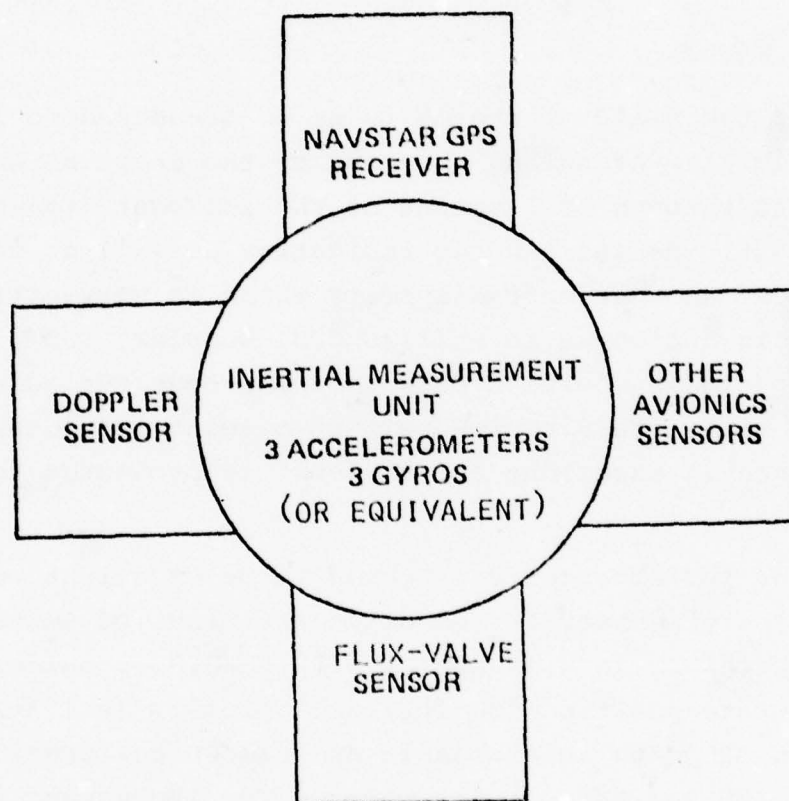
gation with errors on the order of 0.1 to 0.3 percent of distance traveled (much lower than Doppler-AHRS navigation errors). The IMU also provides accurate signals for AHRS displays. The flux-valve sensor provides backup heading information, in case GPS is never available for use in in-flight alignment, in order to provide the backup navigation with standard Doppler-AHRS errors on the order of 1.7% of distance traveled. This is a system with excellent performance and great tolerance to failures of subsytems.

This system could be made available at very low net cost by utilization of low-cost subsystems, by utilizing common elements in an integrated design, and by saving the cost of the AHRS components. A rough estimate of the production costs of such an integrated GPS-Doppler-Inertial integrated system is $39K, as indicated in Table 5.1. Furthermore, there would be a savings of about $16K in AHRS components leaving a net production cost of $23K for the integrated GPS-Doppler-Inertial system. This is an extremely low cost, within the cost goals of the study.

Because of its projected excellent performance and extremely low cost, the integrated GPS-Doppler-Inertial system should be considered for application to new helicopters and to a variety of other aircraft.

Table 3.5.1 Projected Production Cost of Integrated GPS-
Doppler-Inertial System.

Description	Large Volume Production Cost
Low Cost IMU (Comparable to LCIGS)	12K
GPS Receiver with Computer Control and Display (Comprable to Z Set)	12K
Doppler Radar (Comparable to ASN-128) without Computer or Display	12K
Flux Valve	1K
Attitude and Heading Display	1K
Additional Computation and Interface Electronics	4K
Commonality Savings	-3K
AHRS Savings (Comparable to ASN-43 without Display or Flux Valve	-16K
TOTAL	$23K

SECTION 6

STUDY CONCLUSIONS

A survey of inertial instruments shows that a strap-
down inertial measurement unit (IMU) can be developed with
a $10k-$12k production cost. A GPS receiver, computer, and
display could probably be integrated with this IMU to form
a navigation set with production cost of about $25k (FY76$).
But this IMU will have insufficient stand-alone navigation
performance for helicopter applications when GPS is jammed
or otherwise unavailable. Hence, an integrated GPS-inertial
navigator costing $18k-$25k (FY76$) would not be adequate
for Army tactical helicopter applications.

An integrated GPS-Doppler navigator probably could be
developed with production cost of $25k and would be pre-
ferable to the low cost GPS-Inertial navigator because of
its better performance whenever GPS is not available.

By replacing the standard attitude and heading refer-
ence system (AHRS) with a low cost strapdown IMU (such as
is being developed by CSDL under the Low Cost Inertial Guidance
Subsystem Program at AFATL) a cost savings can be realized.
Furthermore, by utilizing the low cost strapdown IMU as an
integral part of a GPS-Doppler-inertial navigation system
substantial improvements in performance in both normal and
degraded modes of operation would be achieved. Because of
its excellent performance and reliability and because of

its low net production cost, development of an integrated
GPS-Doppler-inertial system should be considered, especially
for new helicopters (or other low speed aircraft) for which
AHRS units have not already been procured.

R-981

STUDY OF ADVANCED GPS
SIGNAL PROCESSING TECHNIQUES

FINAL REPORT FOR SAMSO CONTRACT F04701-75-C-0212

VOLUME III, PART 2

By

Duncan B. Cox, Jr.
Bernard A. Kriegsman
Luigi V. Calicchia

March 1978

The Charles Stark Draper Laboratory, Inc.
Cambridge, Massachusetts 02139

SECTION 7

INTRODUCTION TO PART II

Study of Advanced GPS Signal Processing Techniques

This part of Volume III of Report R-981 describes
the results of a study that was carried out as an
extension of the work reported earlier in Volumes I and
II[1,2]. The earlier work developed a functional descrip-
tion of the SAMSO/Magnavox GPS X User Equipment Set and
developed quantitative data on the antijamming and dyna-
mic performance of its tracking loops when aided by data
from an inertial measurement unit. The results were ob-
tained via a detailed computer simulation of the X-Set
tracking loops and of the characteristics of the aiding
data. Emphasis was on the design of the interface re-
quirements for multiplexing and processing of data flow-
ing between the inertial measurement unit and the GPS
user equipment set in order to achieve various levels of
performance in high-dynamic and jamming environments.

The current study has been directed to obtaining
some special results relating to altering the design of
the GPS receiver so as to obtain improved performance in
tracking signals in high levels of noise. Emphasis has
been on the investigation of the effects of varying pre-
detection bandwidths*and the possible advantages of hav-

---

* The noise bandwidths of the filtering operations performed
  prior to data demodulation in Costas loops and prior to
  amplitude or power detection in delay-locked loops.

43

ing apriori knowledge of some or all of the GPS data bit stream. The GPS receiver simulation developed for the earlier study has been utilized for providing Monte Carlo results as predictions of performance gains that can be achieved with the suggested design changes. Analytical formulations are also provided to complement some of the simulation results.

The results of the study in Section 8 indicate that substantial advantages can be obtained by utilizing advance information concerning the GPS data bit stream and by appropriately minimizing predetection bandwidths. For example, the results show that an improvement of at least 6dB in the antijamming margins of the carrier tracking loops can be made by employing phase-locked loops instead of Costas loops. This improvement is due to increases in the detector ranges by a factor of 2. An additional improvement of about 7dB is expected at a signal-to-noise density ratio of 8dB-Hz because of the elimination of signal suppression effects.

Perhaps the most useful results, however, are the understandings of the nonlinear effects of the GPS signal detection algorithms under conditions of low signal-to-noise ratio. These results are presented in Section 9 and Appendices B and C. Results in other sections are of a more general nature, putting the results of Section 8 in focus, providing an organized approach to advanced designs, and pointing to some promising results reported elsewhere.

Because all of the quantitative results are focused on the GPS X-Set and are obtained from the X-Set simulation, a summary of the simulation and previous results is presented in References [1] and [2], which are Volumes I and II of this report. A reader not familiar with the earlier work should read Appendix A first.

44

SECTION 8

DATA AIDING AND VARIABLE PREDETECTION BANDWIDTHS

8.1 Data Aiding

The GPS waveform is modulated by data at a rate of 50 bits/sec. In typical application the data is not known apriori and must be detected by the GPS user equipment. Special provisions must be made to allow tracking of the codes and carriers in the presence of the unknown data. Carrier tracking is accomplished by means of Costas loops, wherein the data is estimated and demodulated internally to the loop. This operation is shown in Figure A-1 by the multiplication of Q_k by $SGN(I_k)$. Code tracking with unknown data is accomplished by means of an incoherent delay-locked loop. Code lock is maintained by balancing detected amplitudes in the 50 Hz data bandwidth between advanced and delayed code channels. This operation is shown in Figure A-2 as taking the difference between early amplitude and late amplitude to form the error indication e_{c0}. Refer to equations 3-34 and 3-35 of reference 2 for a precise definition of the incoherent detection operation carried out in the simulation of the X Receiver Set.

Although the Costas loops and incoherent delay-locked loops are able to track the carriers and codes in the presence of unknown data, some problems do arise. The Costas loop suffers from the fact that the range of

its error detector is effectively halved in comparison
to that of a phase-locked loop, and the range of errors
that it can withstand without losing lock is likewise
halved. Furthermore, if the signal-to-noise ratio of
the estimated data, I_k in Figure A-1, is less than 0 dB
the dominant noise in I_k suppresses the signal in Q_k.
The result is an effective suppression of the signal-to-
noise ratio seen by the tracking loop by an amount equal
to the noise-to-signal ratio of I_k. The suppression
occurs only when the signal-to-noise ratio of I_k is sub-
stantially less than 0 dB but such situations can oc-
cur when the receiver is tracking a GPS signal with low
effective dynamics and low signal-to-noise density
ratios.

With respect to the incoherent delay-locked loop,
a similar signal suppression effect occurs. The
signal is suppressed, and the signal-to-noise ratio seen
by the tracking loop is correspondingly reduced, when-
ever the signal-to-noise ratios for the I and Q channels
prior to the nonlinear amplitude detection operations
are less than unity. The presence of the GPS data re-
quires that the predetection bandwidth be about 50Hz,
which is wide enough to allow the suppression effects to
occur when the signal-to-noise-density ratios at the input
to the receiver are lower than about 17 dB-Hz. If the
data could be removed before the signal enters the code
tracking loop, the predetection bandwidth could be reduced,
with the lower limit being governed by the uncertainty
in the carrier frequency. Under some circumstances the
uncertainty in the carrier frequency (even without carrier
loop tracking) can be quite small, perhaps on the order
of 1 Hz.

If the GPS data were known in advance, they could be demodulated from the GPS waveform prior to the operations of carrier tracking and code tracking. Then phase-locked loops and delay-locked loops with lower predetection bandwidths could be employed and the anti-jam margins of the receiver could likewise be increased. A 6-dB improvement in the anti-jam margins of the phase-locked loops would occur because of the factor-of-2 extension of the detector ranges of the phase-locked loops in comparison with the Costas loops. Further improvements in the anti-jamming margins of the carrier and code tracking loops will occur because of the reduction of signal suppression effects whenever the signal-to-noise density ratio is less than 17dB-Hz (corresponding to a signal-to-noise ratio of 0dB in a 50-Hz predetection bandwidth of 50-Hz).

The problems of how to obtain and to store the GPS data in advance of reception of the GPS signals are special problems in themselves and will not be treated here. It should be noted here, though, that not all of the GPS data need be known in advance in order to obtain improvements in performance. If the data are known over major portions of the tracking time, but unknown over other portions, the operations of the loop may be shifted between the appropriate modes of tracking to obtain an overall improvement in performance without interruptions in the tracking operation. Hence, the interspersion of known data bits in the GPS bit stream would allow substantial improvement in tracking performance. In this report we concentrate on showing the performance advantages that can be obtained if all the data are known apriori.

8.2   Phase-Locked Loop Versus Costas Loop

When the GPS data are known apriori a phase-locked
loop instead of a Costas loop may be employed for carrier
tracking, as explained above. In this section we show,
via simulations of the carrier tracking loops of the Magnavox
X-set, the performance improvements that can be expected
in practice from the use of a phase-locked loop instead of the
Costas loop. We also show these results in the light of theo-
retical results obtained from the literature.

The first step is to look at the responses of
the loops to stationary signals (i.e., with no dynamics)
corrupted with noise, perhaps due to jamming. Figure A-3
of Appendix A shows how such results might be combined
with results on the responses of the loop to signal dy-
namics to predict tracking loop performance in practical
situations. As illustrated in Figure A-3, there is gen-
erally an optimum loop bandwidth which minimizes the
error in response to the combination of input noise
and signal dynamics. We concentrate first on input
noise.

Table 8.1 shows the RMS tracking errors of Costas*
and phase-locked loops tracking stationary signals with
signal-to-noise-density ratios of 12 dB-Hz and 8 dB-Hz utilizing
noise bandwidths of 5 Hz and 2 Hz. These are the results
of single sample runs with simulated non-linear carrier
tracking loops operating with code tracking loops as
described in Appendix A-1. It is clear from Table 8.1
that the phase-locked loop has superior performance to
that of the Costas loop.

To shed some light on the results of Table 8.1 it is
worth examining an expression for the RMS phase tracking

*These are modified Costas loops incorporating a sgn func-
 tion in the "I" channel as utilized in the X-Set.

Type	Noise Bandwidth (Hz)	S/N_o (dB-Hz)	RMS Tracking Error (ft)	Results
Costas	5	12	0.246	lost lock
	5	8	1.95	lost lock
	2	12	0.055	maintained lock
	2	8	0.163	lost lock
Phase-locked	5	12	0.050	maintained lock
	5	8	0.089	maintained lock
	2	12	0.028	maintained lock
	2	8	0.046	maintained lock

Table 8.1   Responses of Costas and Phase-locked loops to input noise.   Results of single runs of 4 seconds duration.   Predetection integration time = 20ms.   Code tracking loop also running to supply proper code to carrier loop.

error $\sigma_{\phi np}$ as provided in reference 3.

$$\sigma_{\phi np} = \sqrt{\frac{N_{oe} B_{\ell p}}{S_1}} \quad \text{radians RMS} \tag{8.1}$$

where N_{oe} is the single sided noise spectral density, $B_{\ell p}$ is the single-sided noise bandwidth of the tracking loop, and S is the signal power. This expression, which is based upon a linearized model of the tracking loop, is plotted as two solid lines, corresponding to signal-to-noise ratios of 12dB-Hz and 8dB-Hz, in Figure 8.1. For the Costas loop the expression for tracking error $\sigma_{\phi nc}$ is

$$\sigma_{\phi nc} = \sigma_{\phi np} \sqrt{1 + \frac{N_{oe} B_w}{2S}} \quad \text{radians RMS} \tag{8.2}$$

where B_w is the predetection bandwidth in Hertz (the inverse of the predetection integration time in seconds). The expression under the square-root sign in equation 8.2 accounts for the signal suppression effects described above. With B_w = 50 Hz, the tracking error is degraded by 4.1dB and 6.9dB at signal-to-noise-density ratios, S/N_{oe}, of 12dB-Hz and 8dB-Hz, respectively. Equation 8.2 is plotted as the two dashed lines in Figure 8.1. Clearly the performance of the phase-locked loop is better than the performance of the Costas loop at low signal-to-noise-density ratios.

The fact that the detector range of the phase-locked loop is twice as great as that of the Costas

50
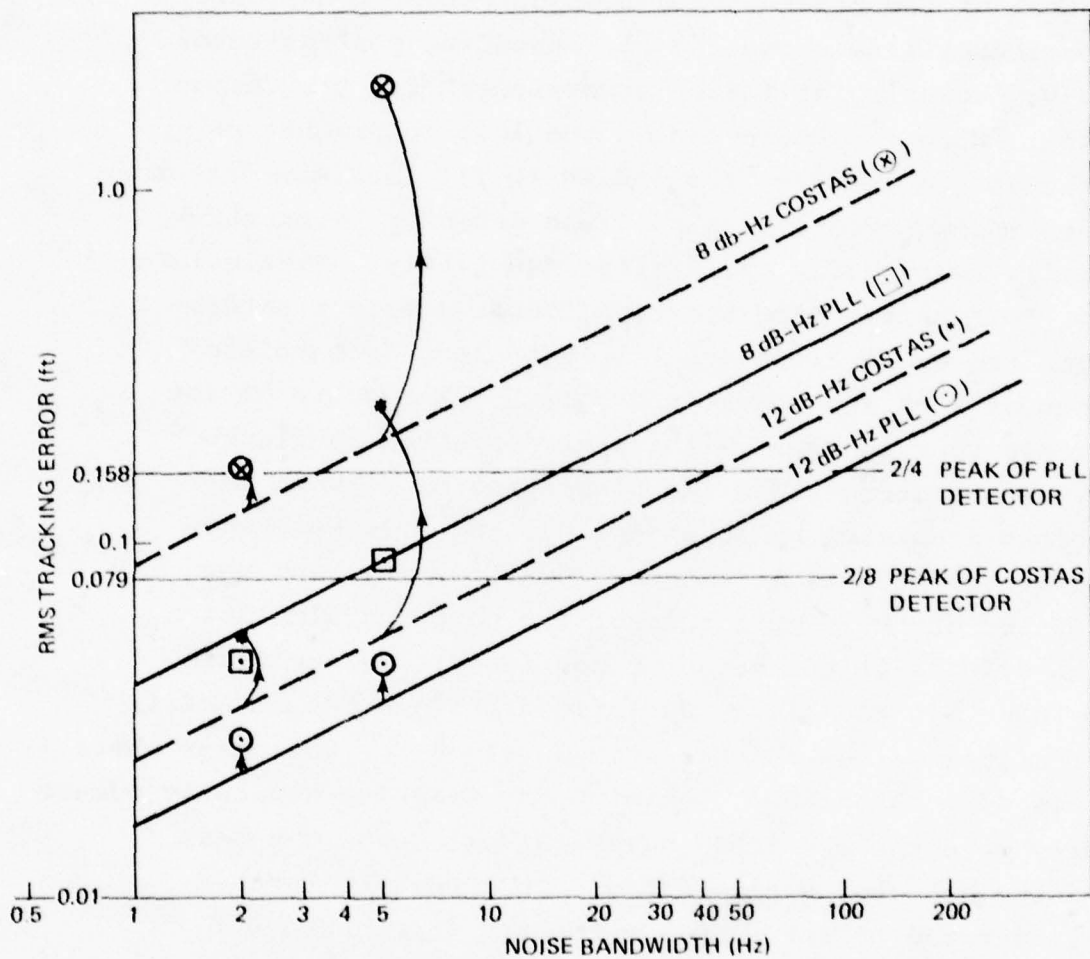
Figure 8.1 Tracking errors of Costas and phase-locked
loops due to input noise. Results of single
test cases of 4-sec duration.

loop is also indicated in Figure 8.1. The horizontal
line drawn at a level of 0.158 ft, or 1/4 of a wavelength,
indicates a tracking error corresponding to the maximum
output of the phase-locked-loop detector. The lower
horizontal line shows the corresponding peak detector
output occuring at 1/8 of a wavelength for the Costas
loop. When the RMS error of the loop approaches or
exceeds the level corresponding to its maximum detector
output, the effective gain of the detector is substan-
tially reduced and cycle slips are likely. Particular-
ly for third-order tracking loops, detector satura-
tion and cycle slips are likely to lead to complete
loss of lock and run-away errors. ¶ The results of the
sample runs in Table 8.1 are also plotted in Figure
8.1. The arrows show the discrepancies between the
errors predicted by equations 8.1 and 8.2, which ne-
glect the effects of detector nonlinearity, and the
results of the sample runs of the computer simulation.
The effects of the detector nonlinearities are quite
evident in the large deviations between the linearily
predicted values and the actual values for the cases where
loss of lock occurs. Satisfactory tracking generally occurs
only when the predicted value is well below the peak
of the detector nonlinearity. This fact is further
illustrated by the sample responses in Figures 8.2
through 8.5 corresponding to the cases identified
in Table 8.1. ¶ It is clear that the phase-locked loop
has a 6dB advantage and anti-jam margin over the Costas
loop because the former has a detector range that is
two times greater than that of the latter. The phase
locked loop has the further advantage of $(1 + N_{0e}B_w / 2 S_1)^{1/2}$,
which is equal to 4.1 dB at 12 dB-Hz and 6.9 dB
at 8dB-Hz, over the Costas loop. It is also clear that

52

CARRIER LOOP TRACKING ERROR
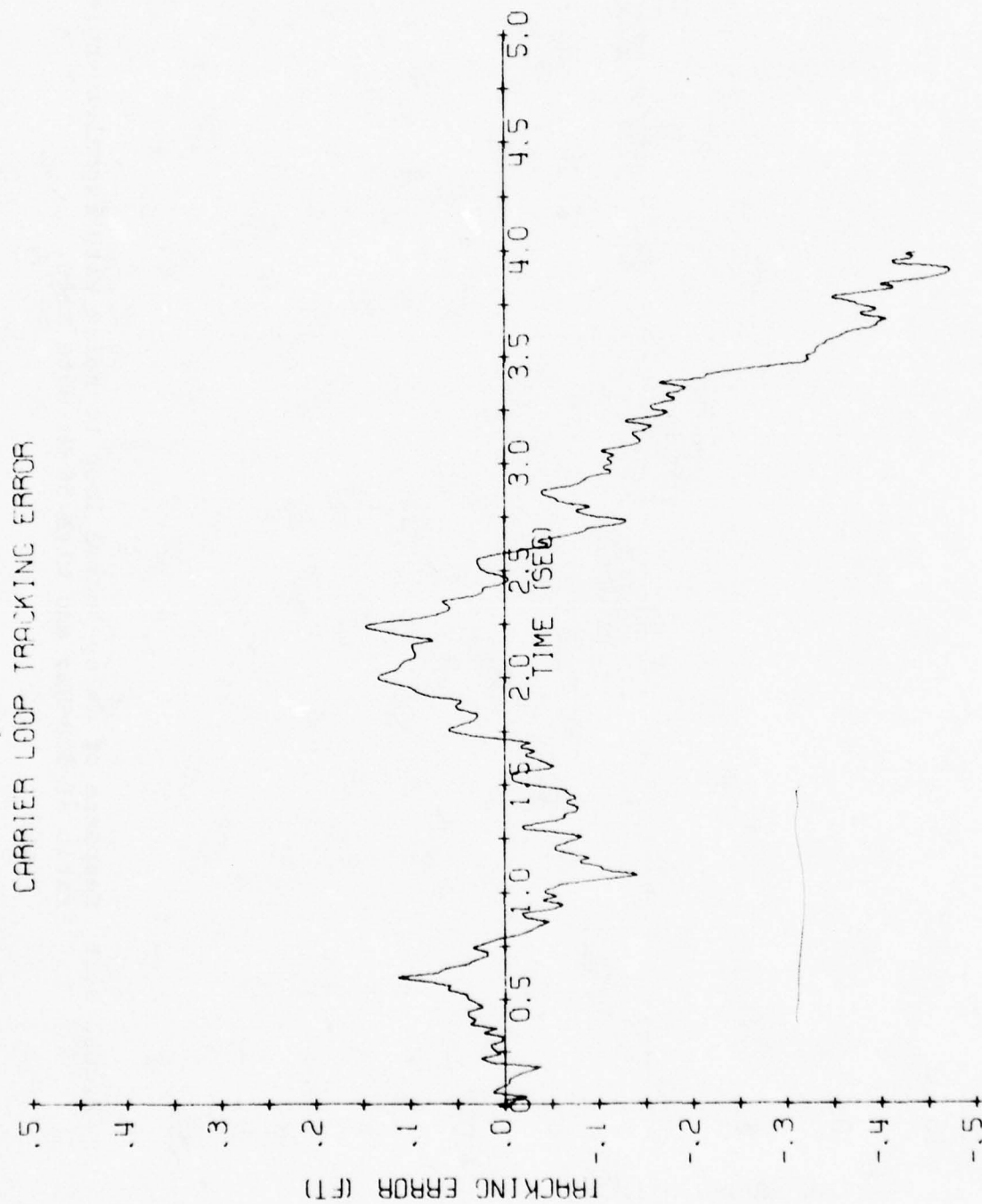
Figure 8.2a   Response of Costas carrier loop with 2-Hz noise bandwidth to noise with signal-to-noise ratio of 8dB-Hz, and with 50-Hz data rate.

53

Figure 8.2b Response of delay-locked loop to noise with signal-to-noise ratio of 8dB-Hz, and with 50-Hz data rate.

54
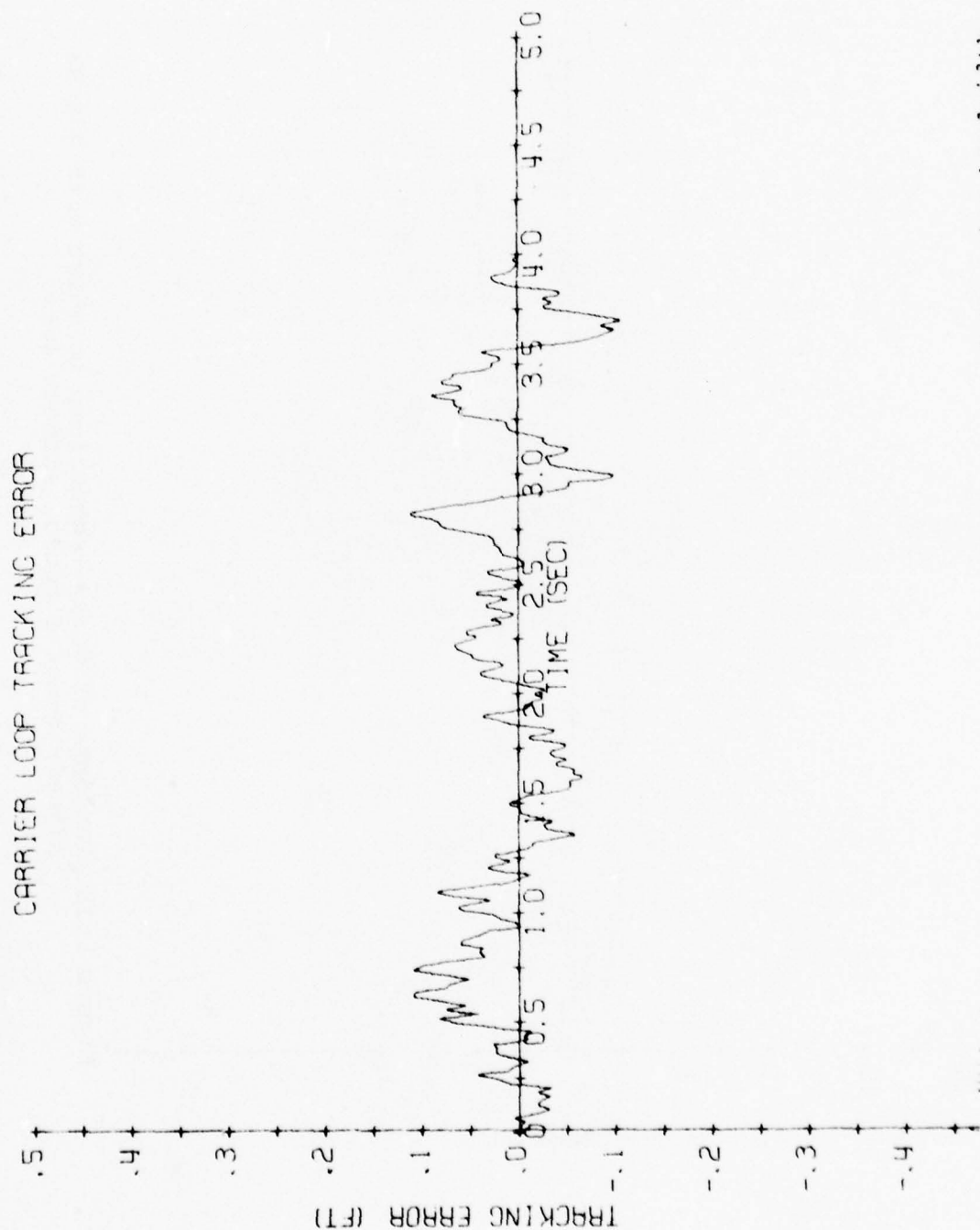
Figure 8.3a Response of phase-locked loop with 2-Hz noise bandwidth
to noise with a signal-to-noise ratio of 8dB-Hz, without data.

55

CODE LOOP TRACKING ERROR

Figure 8.3b Response of delay-locked loop to noise with 8dB-Hz signal-to-noise ratio, without data.
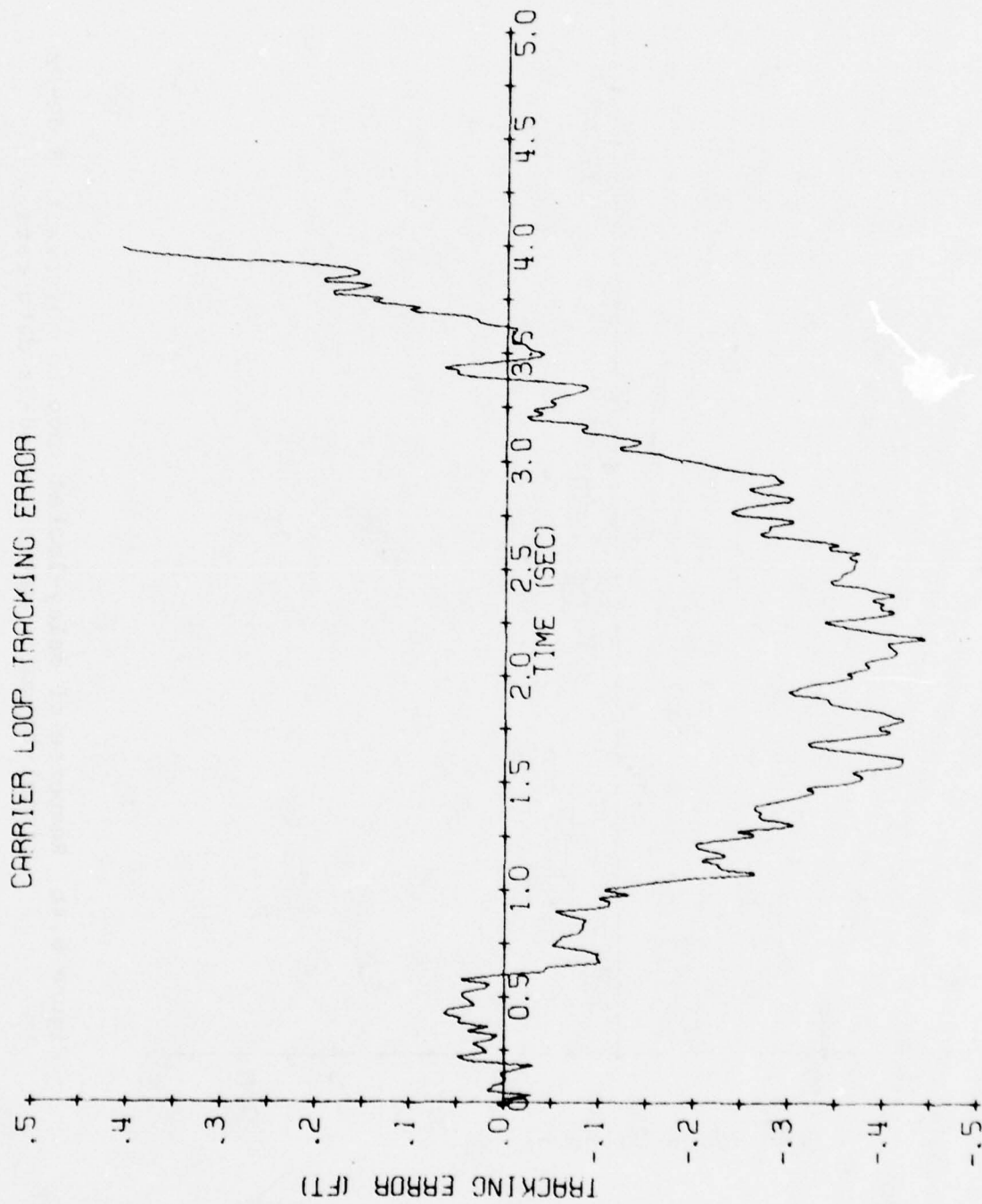
Figure 8.4a Response of Costas loop with 5-Hz noise bandwidth to noise with signal-to-noise ratio of 12 dB-Hz and 50-Hz data rate.

57

CODE LOOP TRACKING ERROR

Figure 8.4b Response of delay-locked loop to noise with 8 dB-Hz signal-to-noise ratio and 50-Hz data rate.
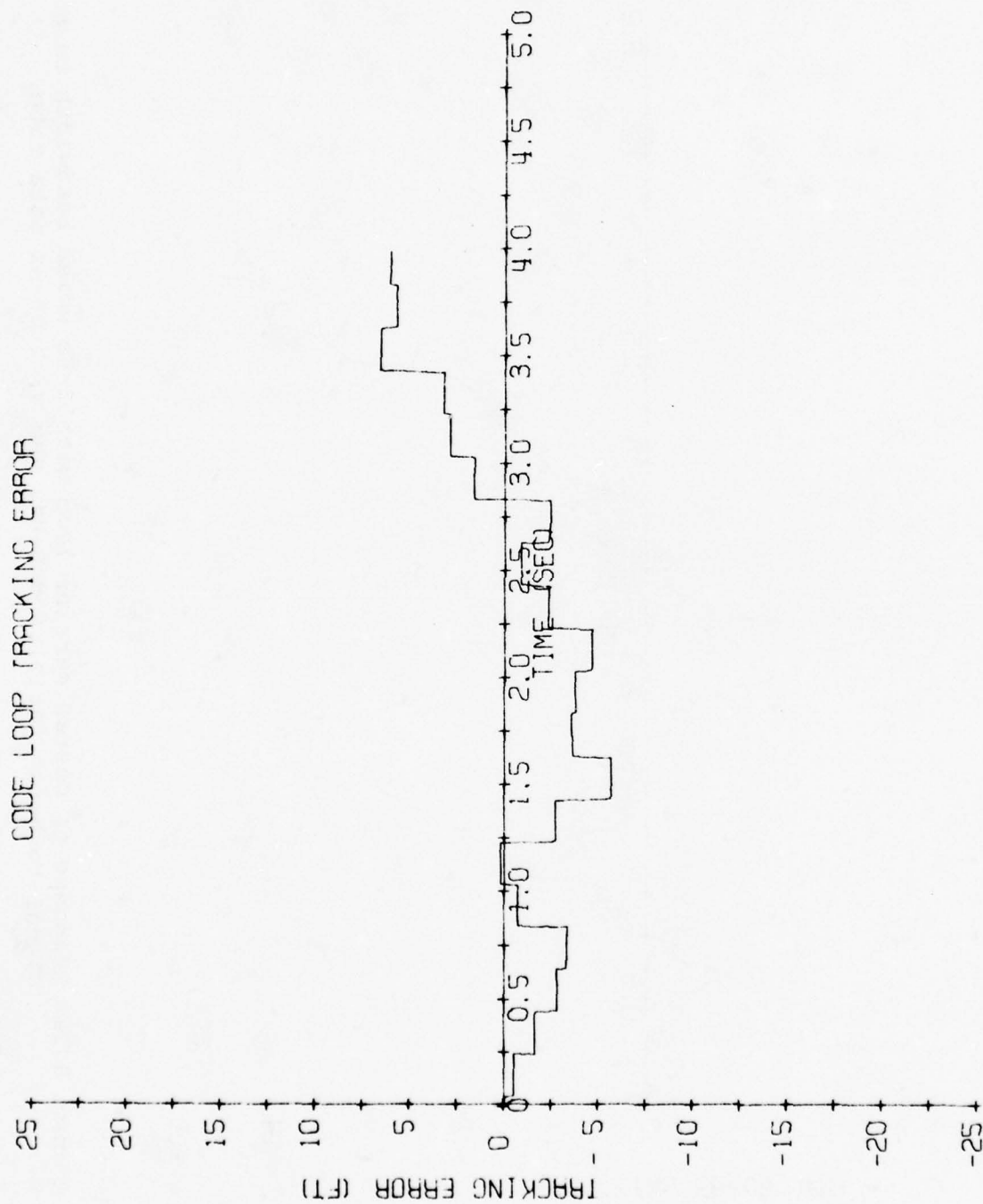
58
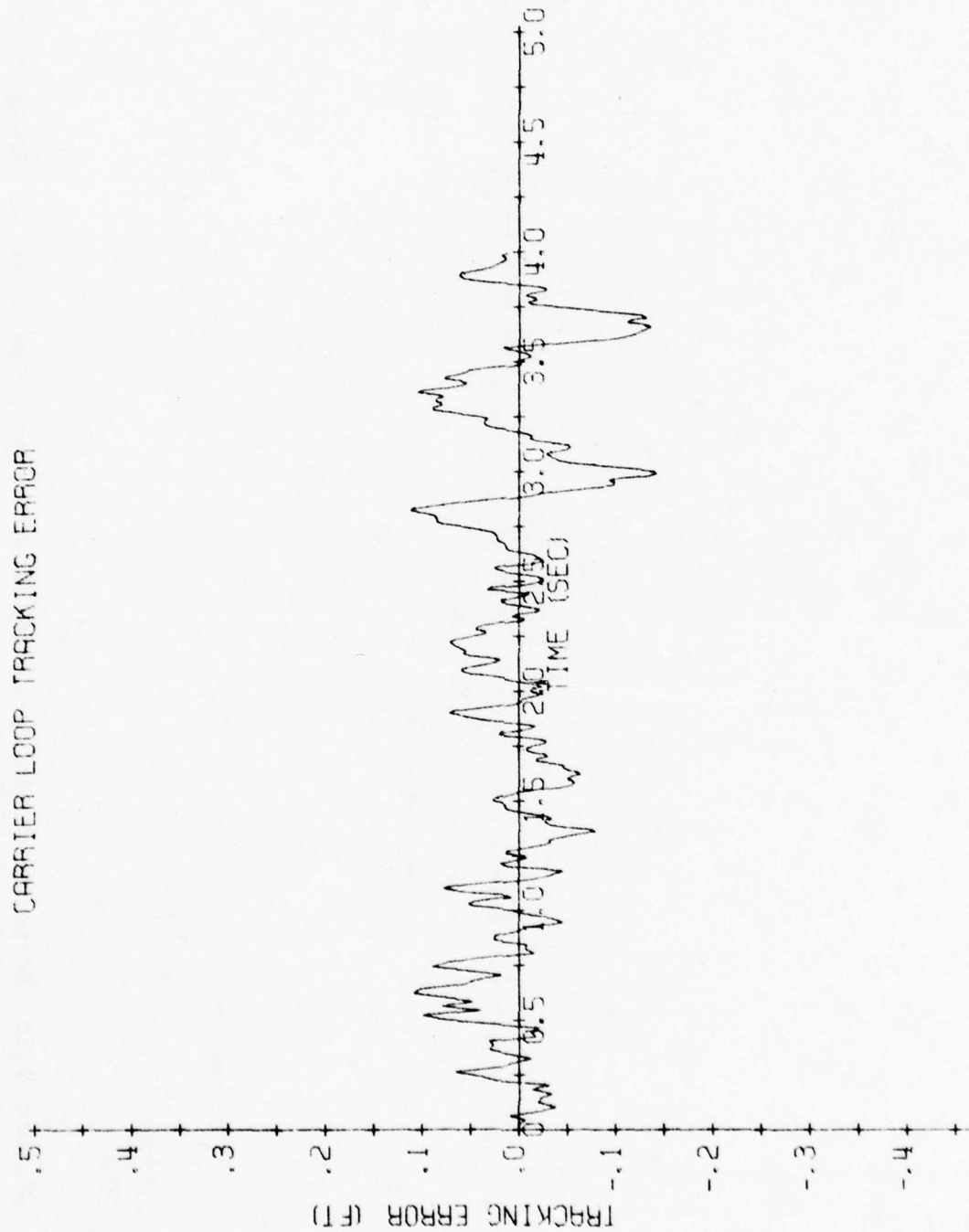
Figure 8.5a Response of phase-locked loop with 5-Hz noise bandwidth to noise with signal-to-noise ratio of 12 dB-Hz.

CODE LOOP TRACKING ERROR
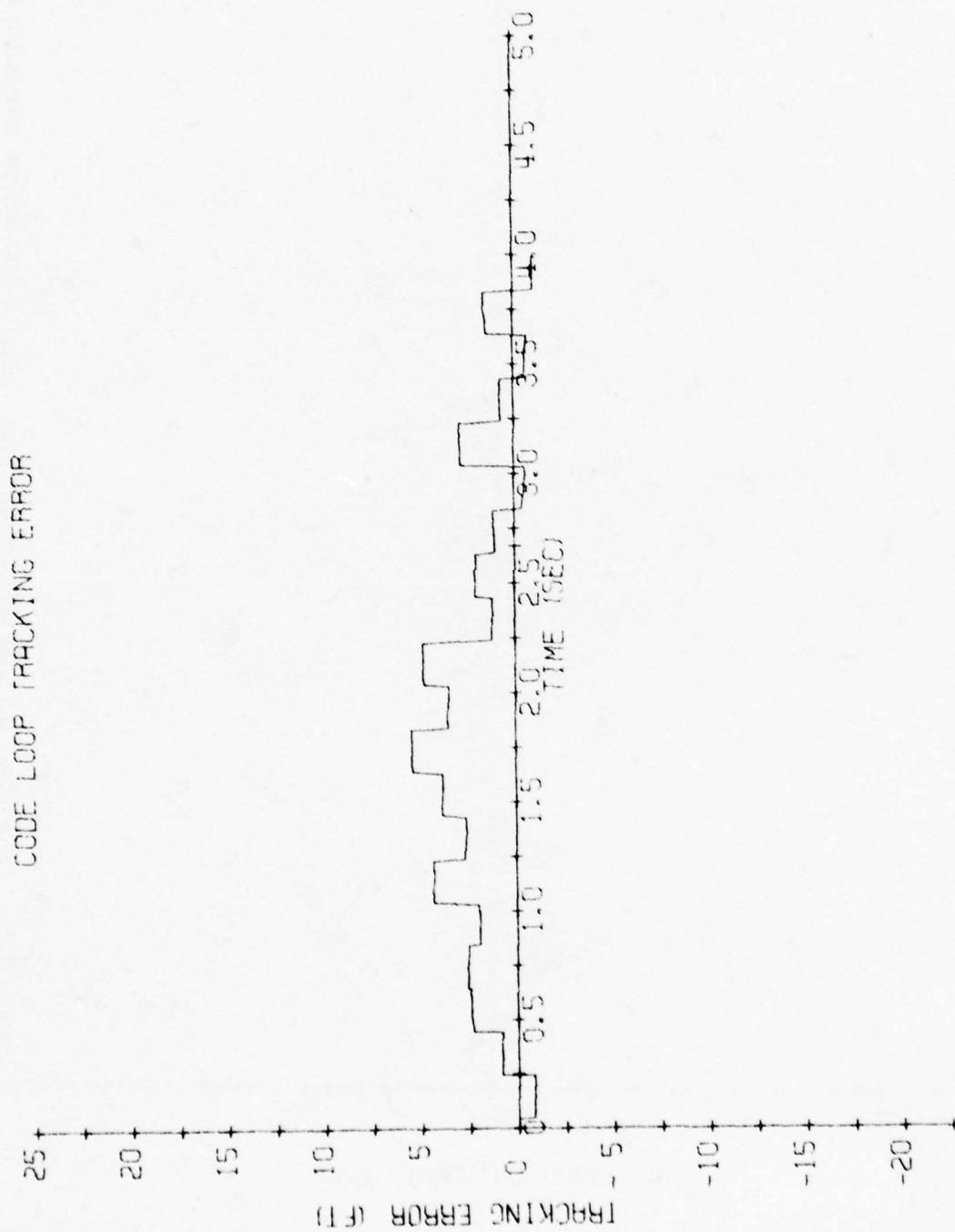
Figure 8.5b Response of delay-locked loop to noise with signal-to-noise ratio of 12 dB-Hz.

60

a complete loss of lock and a diverging error are likely
if the RMS error approaches 1/4 of a wavelength for
the phase-locked loop or 1/8 of a wavelength for the
Costas loop.

The previous data indicated the advantage of a
phase-locked loop in comparison with a Costas loop in
tracking a stationary signal in the presence of high
levels of jamming. Now we address the performance of
the two loops in tracking high-dynamic signals, again
in the presence of high levels of jamming. Whereas low
noise bandwidths are desired for tolerating noise (jam-
ming), high noise bandwidths are desired for minimizing
the tracking errors in response to input signal dynamics.
For a given noise level and a given dynamic signal to be
tracked, there is an optimum noise bandwidth for opti-
mizing tracking performance. Because the response to
noise is different for a phase-locked loop from that
of a Costas loop, the optimum bandwidth for the two
kinds of loops are different. By referring to the
preceding information in this section on responses to
noise and to the information in Figures A8, A9, and A17
in Appendix A on the responses to dynamics, some reason-
able guesses can be made as to the optimum bandwidth and
the tracking performance under practical conditions of
noise and dynamics. Once these parameters are estab-
lished, the performances can be verified via Monte-Carlo
analyses utilizing the GPS X-Set simulation. In what
follows we show the results of a limited number of
Monte-Carlo runs under various assumptions as to noise
levels, dynamics, and type of loop. Although the re-
sults are quantitative, they should be interpreted as
only approximate indications of levels of performance.

61

A large number of simulation runs is necessary if precise performance results are to be obtained. With the simulation tools at hand further analyses can be carried out in a straightforward fashion but the resulting computer cost is probably only warranted when a scenario and a measure of performance are precisely defined for a specific practical application.

In obtaining the results for tracking with dynamics and noise the receiver is assumed to be in a vehicle undergoing a linear jerk of 10 g/sec for 0.6 sec. The carrier loop is assumed to be aided by an IMU with a sampling interval of 10 ms, with aiding errors as indicated in Figure A-17. Various IMU errors and clock errors are also assumed. Each run corresponds to 4 seconds of realtime.

The first set of results is presented in Tables 8.2 and 8.3 and Figures 8.6 and 8.7. For these results the IMU is assumed to be error-free, but the GPS oscillator is assumed to have a drift rate that is perturbed by the vehicle acceleration with a scale factor of 10^{-10}/g. On the basis of the data in Figures A8 and A17, the clock errors are expected to be the dominant dynamic inputs to the carrier loops under these circumstances.

Table 8.2 shows the results utilizing a Costas loop. This table shows the results of 10 sets of 12 Monte-Carlo runs under the stated conditions of noise bandwidth and signal-to-noise ratio. A success is indicated when either the loop did not slip any cycles or appeared to successfully regain lock after slipping a few cycles. Failure is indicated when the (third order) loop appears to have a diverging error without any apparent indication of the ability to regain lock. Temporary slips are indicated whenever cycles are lost but lock is regained. With a noise bandwidth of 11 Hz, a signal-to-noise-density ratio of 18 dB-Hz or

62

Noise Bandwidth (Hz)	$\frac{S}{N}$ dB-Hz	Successes	Complete Failure	Temporary Slips
11	18	6/12	6/12	4/12
	14	0/12	12/12	0/12
	12	0/12	12/12	0/12
5	16	6/12	6/12	2/12
	14	0/12	12/12	0/12
	12	0/12	12/12	0/12
4	18	10/12	2/12	1/12
2	16	9/12	3/12	4/12
	14	5/12	7/12	5/12
	12	3/12	9/12	2/12

Table 8.2 Carrier tracking with Costas loop with high-noise and high-jerk inputs. (IMU aiding at 10 ms rate with latest algorithm, 10^{-10}/g oscillator drift, no IMU errors, 10 g/sec for 0.6 sec, 4-sec run length, X-Set receiver simulation.)
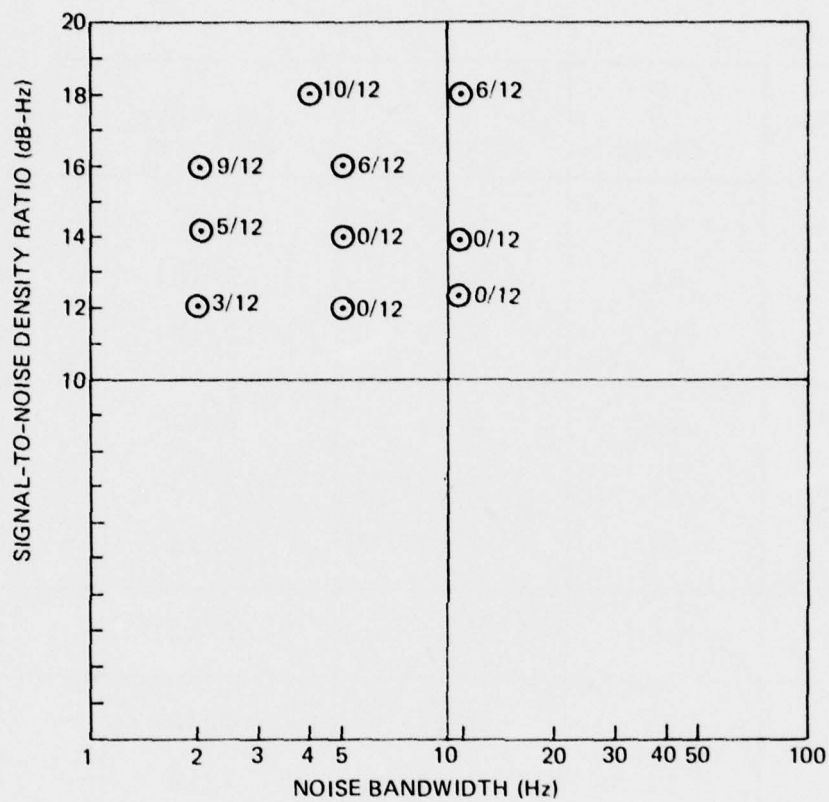
Figure 8.6 Success ratios for Costas carrier tracking as a function
of signal-to-noise ratio and noise bandwidth, from Table 8.2.

better is apparently required for successful tracking on 6 out of the 12 trials, each of which had a duration of 4 sec. Lowering the noise bandwidth to 2 Hz resulted in improvements in performance, with successful tracking being obtained in 9 trials out of 12 at 15 dB-Hz with 2-Hz bandwidth. The success ratios in Table 8.2 are plotted in Figure 8.6 as functions of signal-to-noise-density ratio and noise bandwidth. Ideally, a contour of constant success ratio in Figure 8.6 would have generally a U shape showing a minimum at an optimum noise bandwidth. Although the minimum is not fully illustrated in Figure 8.6 it is clear that reasonably good performance could be expected at 16 or 18 dB-Hz signal-to-noise ratio with a noise bandwidth of about 2 Hz.

Table 8.3 shows corresponding results for a phase-locked loop, with the GPS data having been demodulated apriori. The success ratios are again plotted in Figure 8.7. Even with a bandwidth as high as 5 Hz, completely successful tracking was obtained with signal-to-noise-density ratios of only 12 dB-Hz. Hence, a substantial improvement in performance of the phase-locked loop in comparison with the Costas loop is indicated even when tracking high dynamic inputs, as long as an oscillator with low g-sensitivity (10^{-10}/g) is employed and the sampling interval for aiding signals from the IMU is short (10 ms).

On the basis of the results in Appendix A, it can be concluded that a further reduction in oscillator sensitivity should improve the performance. Moreover, recent work at CSDL has shown that a sensitivity of 3×10^{-11}/g can be obtained[4]. Hence, a new set of Monte-Carlo runs was generated corresponding to this

65

Noise Bandwidth (Hz)	$\frac{S}{N}$ dB-Hz	Successes	Complete Failures	Temporary Slips
11	18	10/10	0/10	0/10
	14	10/10	0/10	1/10
	12	2/10	8/10	2/10
5	14	10/10	0/10	0/10
	12	10/10	0/10	0/10

Table 8.3 Carrier tracking with phase-locked loop with high-noise and high-jerk inputs. (IMU aiding at 10 ms rate with latest algorithm, 10^{-10}/g oscillator drift, no IMU errors, 10 g/sec for 0.6 sec, X-Set receiver simulation, 4-sec intervals.)

Figure 8.7 Success ratios for carrier tracking with phase-locked loops with
high-noise and high-jerk inputs. (IMU aiding at 10-ms rate with
latest algorithm, $10^{-10}/g$ oscillator drift, no IMU errors, 10
g/sec for 0.6 sec, X-set receiver simulation).

value of oscillator sensitivity. The sampling interval for the aiding signal was held at 10 ms. An accelerometer scale-factor error of 100 ppm was also assumed, in order to account both for important accelerometer errors and for a small error in IMU alignment. The IMU was assumed to have been aligned previously inflight via GPS signals. Velocity noise of 0.01 ft/sec RMS was also included in order to account for quantization noise in the aiding signals from the accelerometers. These parameters were considered to be representative of what could be achieved with a well integrated GPS inertial system incorporating a high quality inertial navigator. The results are shown in Tables 8.4 and 8.5, and in Figures 8.8 and 8.9.

Table 8.4 shows the results of employing a Costas loop. The success ratios in Table 8.4 are plotted in Figure 8.8. Successful tracking is obtained with a noise bandwidth of 2 Hz with signal-to-noise ratios somewhere in the range between 12 and 16 dB-Hz. The corresponding results for the phase-locked loop are shown in Table 8.5 and Figure 8.9. These results indicate completely successful tracking at 8 dB-Hz and partially successful tracking at even lower values of signal-to-noise ratio. Successful tracking was obtained with 8 of the 12 trials at a signal-to-noise-density ratio of only 2 dB-Hz. Clearly, excellent antijam performance of this aided phase-locked loop system is indicated by the Monte-Carlo data. The data also indicate that an improvement in antijam performance of 6 dB or more is obtainable using the phase-locked loop over what could be obtained with the Costas loop, even in a high-dynamic environment. An improvement by at least this amount was, of course, expected by virtue of the 2 times greater detector range of the phase-locked loop in comparison with the Costas loop.

Noise Bandwidth (Hz)	$\frac{S}{N}$ dB-Hz	Successes	Complete Failures	Temporary Slips
5	12	1/12	11/12	1/12
	10	0/12	12/12	0/12
4	18	11/12	1/12	0/12
	16	9/12	3/12	4/12
	14	0/12	12/12	0/12
2	16	12/12	0/12	0/12
	12	8/12	4/12	4/12
	10	7/12	5/12	7/12

Table 8.4   Carrier tracking with Costas loop with high-noise and high-jerk inputs.   (IMU aiding at 10-ms interval with latest algorithm, 3×10^{-11}/g oscillator drift, 100 ppm scale factor error, 0.01 ft/sec velocity noise).
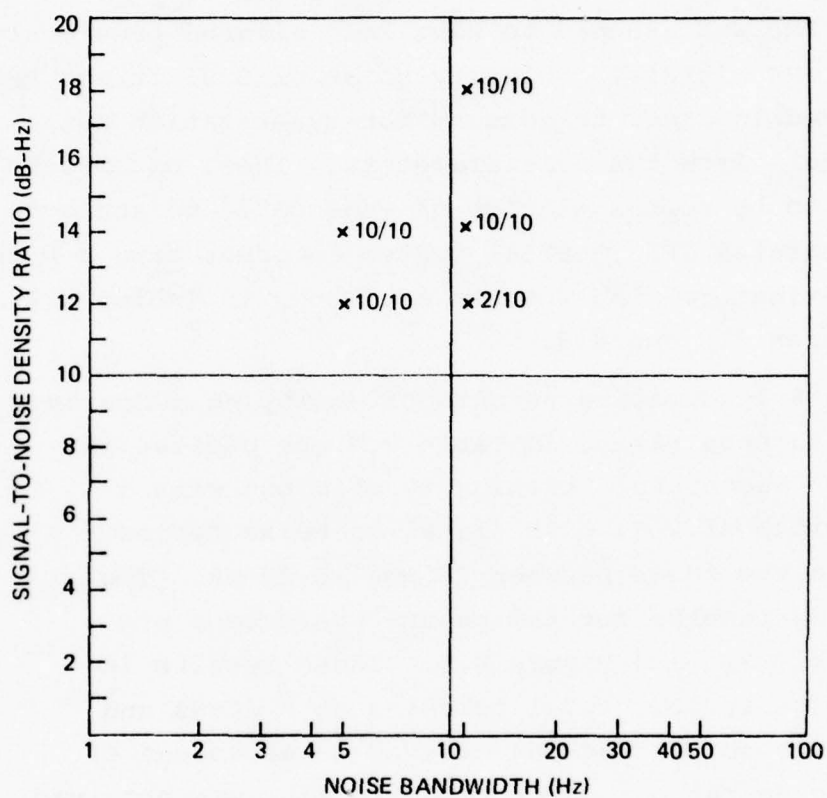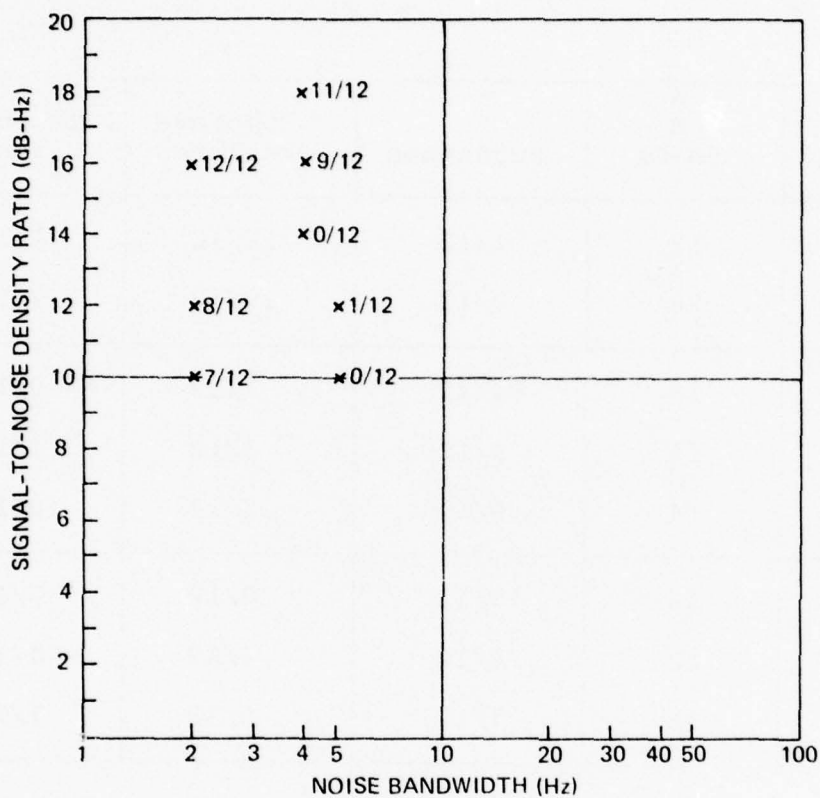
Figure 8.8   Success rates for carrier tracking with Costas loop with high-noise and high-jerk inputs.   (IMU aiding at 10-ms interval with latest algorithm, 3×10^{-11}/g oscillator drift, 100 ppm scale factor error, 0.01 ft/sec velocity noise).

Noise Bandwidth (Hz)	$\frac{S}{N}$ dB-Hz	Successes	Complete Failure	Temporary Slips
5	12	12/12	0/12	0/12
	10	9/12	3/12	3/12
	8	8/12	4/12	3/12
4	6	4/12	8/12	2/12
2	10	12/12	0/12	0/12
	8	12/12	0/12	0/12
	6	8/12	4/12	0/12
	4	9/12	3/12	2/12
	2	8/12	4/12	6/12

Table 8.5 Carrier tracking with phase-locked loop with high-noise and high-jerk inputs. (IMU aiding at 10-ms interval with latest algorithm, 3×10^{-11}/g oscillator drift, 100 ppm scale factor error, 0.01 ft/sec velocity error).

71
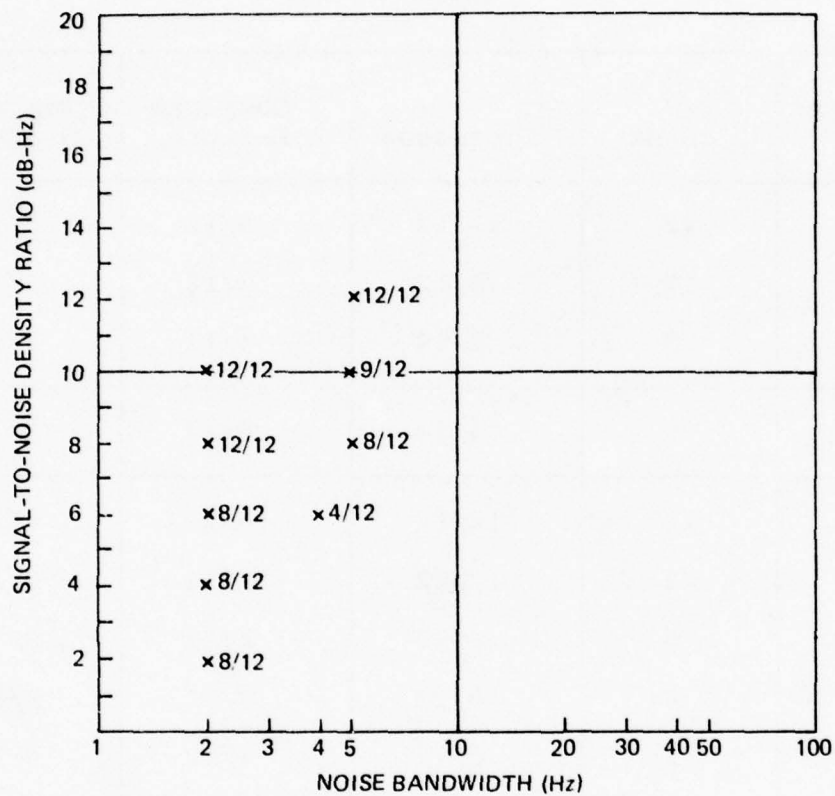
Figure 8.9 Success ratios for carrier tracking with phase-locked loop with high-noise and high-jerk inputs. (IMU aiding at 10 ms interval with latest algorithm $3 \times 10^{-11}/g$ oscillator drift, 100 ppm scale factor error, 0.01 ft/sec velocity error).

Sample loop error responses corresponding to
Tables 8.4 and 8.5 are shown in Figures 8.10 - 8.12.
Figures 8.10a and 8.10b show the response of the aided
Costas loop and its associated delay-locked loop
with a Costas noise bandwidth of 2 Hz and a signal-to-
noise-density ratio of 10 dB-Hz. This result was classified
as a "complete failure" in the statistics of Table
8.4, because the Costas loop has evidently lost lock.
Figures 8.11a and 8.11b show the responses of the
aided phase-locked loop and its associated delay-
locked loop with a phase-locked noise bandwidth of
2 Hz and a signal-to-noise ratio of only 4 dB-Hz.
In this example the error was quite large, but no
cycles were slipped over the four second-interval.
The result was classified as "successful" in arriving
at the statistics of Table 8.5.

In summary, it has been demonstrated that the
anti-jamming margin of the GPS X-Set for carrier track-
ing can be improved substantially by employing phase-
locked loops instead of Costas loops. The phase-
locked loop implementation requires that the GPS
communication data be removed from the waveform in
advance of the tracking loop operation. The improve-
ment in anti-jamming margin is at least 6 db, due to
an increase in the detector range of the phase-locked
loop by a factor of two in comparison with that of
the Costas loop. Additional improvement by
approximately 7 dB is expected with a signal-to-
noise ratio of 8 dB-Hz because of the elimination of
signal supression effects. Successful tracking at
8 dB-Hz with a phase-locked loop is shown to be very
probable if errors due to signal dynamics are negligible.

CARRIER LOOP TRACKING ERROR   10 ms, 2 Hz COSTAS 3×10^{-11} 10 dB-Hz

3/23/20:42
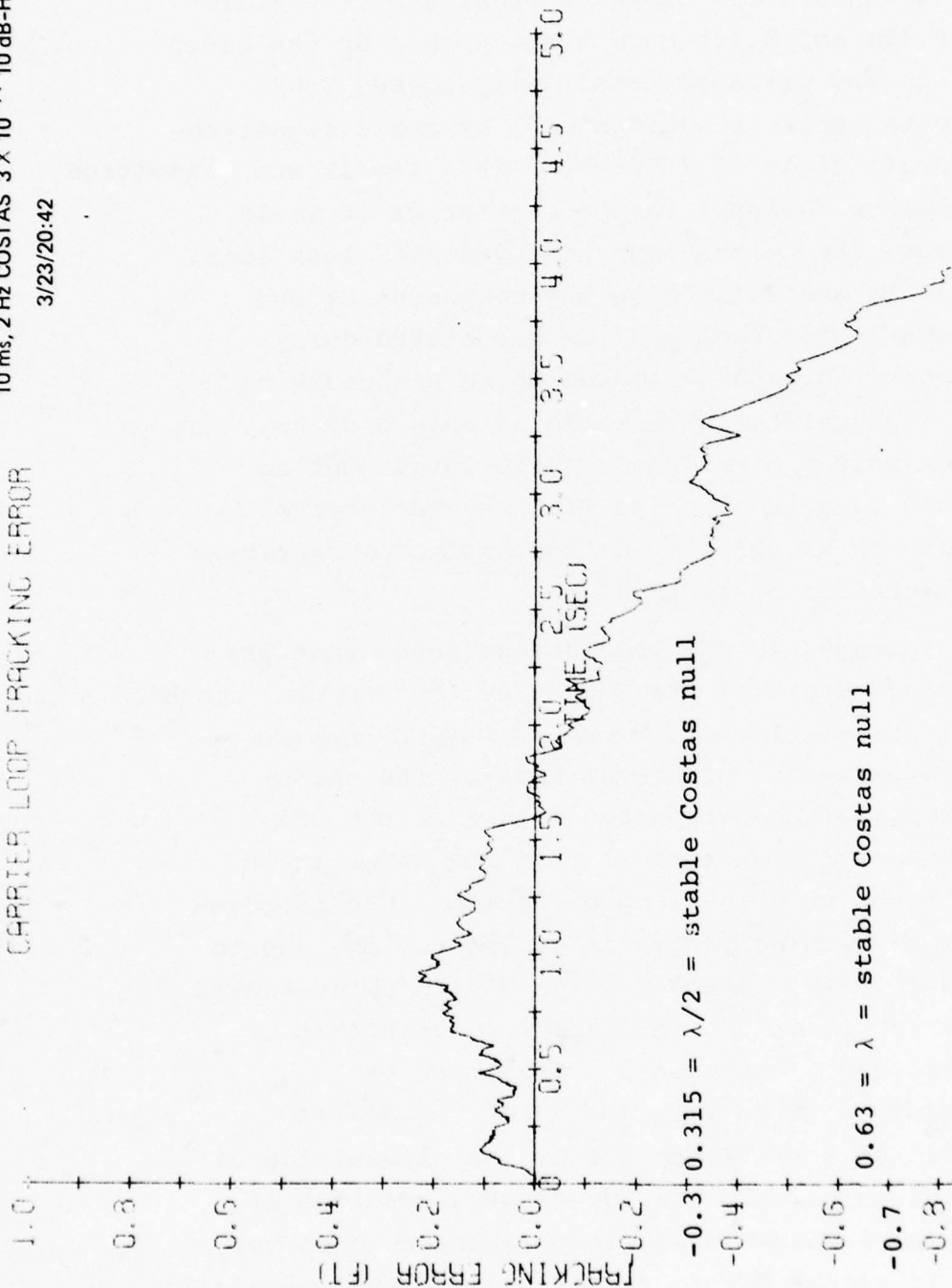
Figure 8.10a. Response of aided Costas loop to dynamics and noise.
(Conditions: 10 dB-Hz, 2 Hz Costas noise BW, 10-ms aiding, 3×10^{-11}/g oscillator, 100 ppm SF error, 0.01 ft/sec rms aiding error, 10 g/sec for 0.6 sec.)

74

CODE LOOP TRACKING ERROR
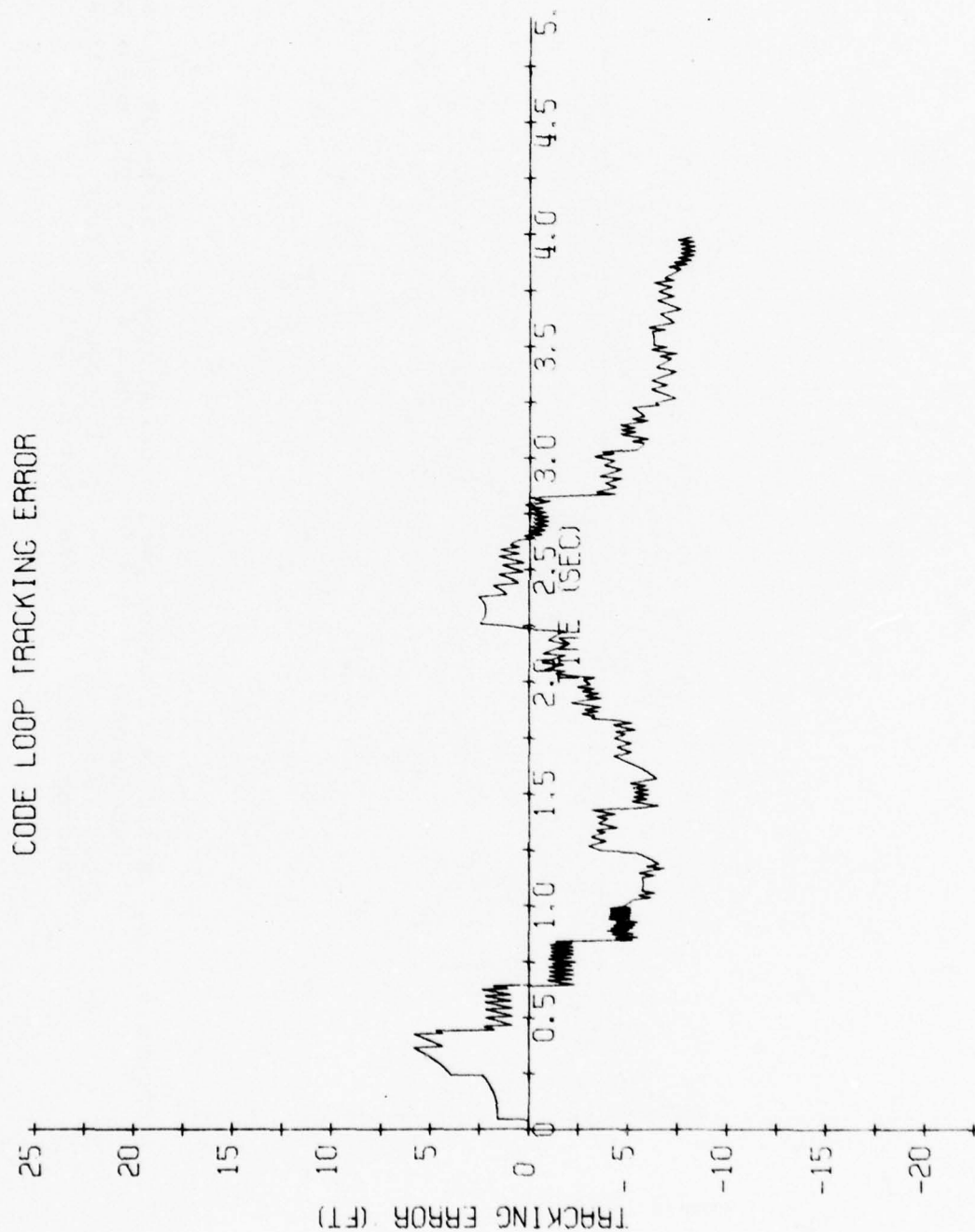
Figure 8.10b. Response of code loop, aided by Costas loop to dynamics and noise. (Conditions: 10 dB-Hz, 2-Hz Costas noise BW, Costas loop aided by IMU, 10-ms aiding, 3×10^{-11}/g oscillator, 100 ppm SF error, 0.01 ft/sec rms aiding error, 10 g/sec for 0.6 sec.)
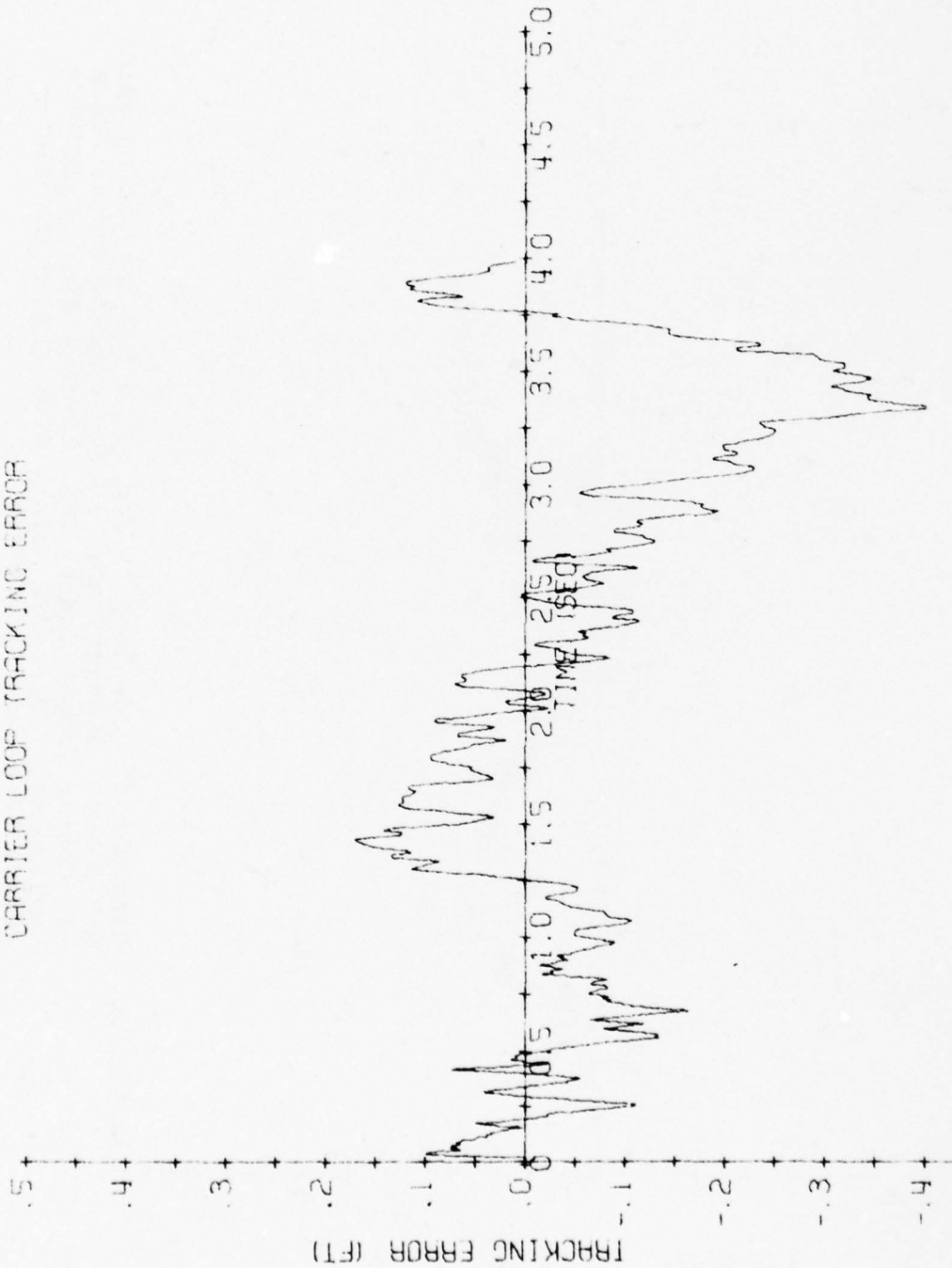
Figure 8.11a. Response of aided phase-locked loop to dynamics and noise. (Conditions: λ = 0.63 ft, S/N = 4 dB-Hz, PLL noise BW = 2 Hz, osc. sens. = 3 x 10⁻¹¹/g, 100 ppm SF error, 0.01 ft/sec rms aiding error, 10 g/sec for 0.6 sec).

CODE LOOP TRACKING ERROR
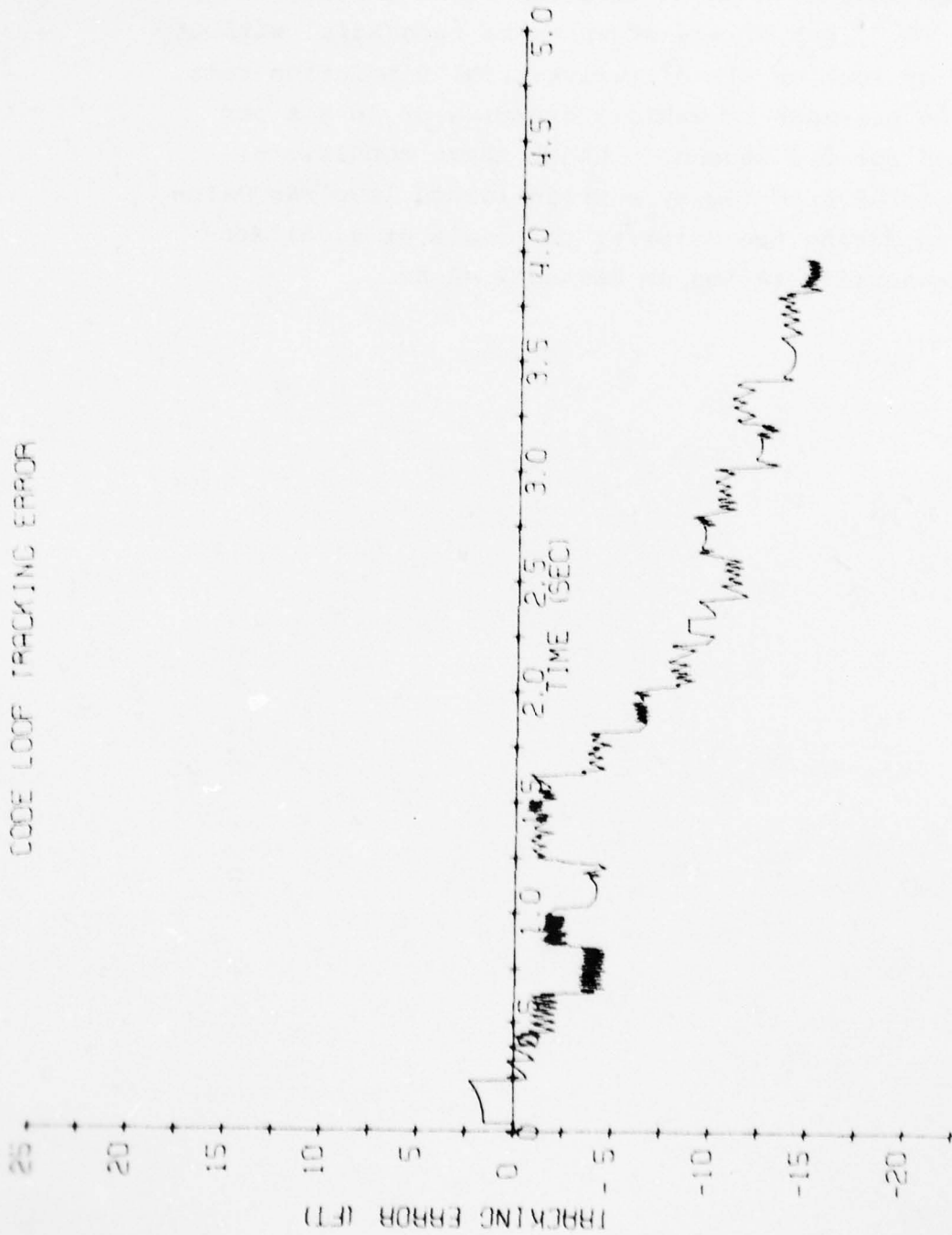
Figure 8.11b. Response of delay-locked loop (aided by IMU-aided PLL)
to dynamics and noise. (Conditions: chip length 100 ft,
S/N = 4 dB-Hz, PLL noise BW = 2 Hz, osc. sens. = 3x10-11/g,
100 ppm SF error, 0.01 ft/sec rms aiding error, 10 g/sec
for 0.6 sec input dynamics).

Tracking at 8 dB-Hz with an inertially aided phase-locked loop with an oscillator of low g-sensitivity (3×10^{-11} per g) was shown to be successful without loss of lock on all of twelve trial simulation runs, in the presence of vehicle dynamics of 10 g's per second for 0.6 seconds. Under these conditions, successful tracking by a phase-locked loop was maintained during the majority of trials at signal-to-noise-density ratios as low as 2 dB-Hz.

8.3 Variable Predetection Bandwidth in Code Tracking Loops

The delay-locked loop of the X-Set is shown in figure A-2, as modeled in the computer simulation. Integrate-and-dump operations over 4-ms intervals are performed on "I" and "Q" components of "early" and "late" and correlations. The outputs of the integrate-and-dump circuits are summed over five consecutive intervals to provide data samples that are equivalent to the outputs of integrate-and-dump operations over the full data-bit intervals of 20 ms. These results are denoted as $Q_{C0}^{(E)}$, $I_{C0}^{(E)}$, $Q_{C0}^{(L)}$, and $I_{C0}^{(L)}$ after Equation (A7) in Appendix A. The error in feet indicated by the code (delay-locked) loop error detector is, per Equations (A8 - A10),

$$\hat{e}_{CO} = \Delta \left| \frac{P_E - P_L}{P_E + P_L} \right| \tag{8.3}$$

where

$$P_E = \left| Q_{CO}^{(E)} \right| + \left| I_{CO}^{(E)} \right| \tag{8.4}$$

$$P_L = \left| Q_{CO}^{(L)} \right| + \left| I_{CO}^{(L)} \right| \tag{8.5}$$

79

In this implementation of a data-incoherent delay-locked loop, P_E and P_L are estimates of RMS signal after early and late correlations. The estimates are made over 20 ms intervals during which the data modulation (of unknown sign) is known to be constant. If the data could be demodulated in advance, the estimates of early and late rms signal could be made by integrating over intervals of longer than 20 ms. Increasing the integration intervals would increase the signal to noise ratios of $Q_{C0}^{(E)}$, $I_{C0}^{(E)}$, $Q_{C0}^{(L)}$ and $I_{C0}^{(L)}$ and would reduce the signal-supression effects due to the absolute value operations in Equations (8.4 - 8.5).

The signal-supression effects are similar to those described in Section 8.2 with regard to the Costas loop. These effects occur whenever the signal-to-noise ratios of the I's and Q's in Equations (8.4 - 8.5) are less than 0 db, and they act to decrease the effective signal-to-noise-density ratio seen by the delay-locked loop. An expression for the error of a delay-locked loop in tracking a signal with a cor-stant delay in the presence of noise is[3]

$$\frac{\sigma_\varepsilon}{L} = \frac{B_{LC}N}{2S} \left\{ \left[1 + \frac{2NB_W}{S} \right] \right\}^{1/2} \text{ chips} \qquad (8.6)$$

where, B_{LC} is the single-sided noise bandwidth in Hertz of the code loop for high signal to noise ratios, S/N

is the single-sided signal-to-noise-density ratio
in dB-Hz of the GPS signal to be tracked, B_W is the
predetection bandwidth (the inverse of the integration
time in seconds of the effective integrate-and-dump
operation) in Hertz, and L_C is the chip length. The
term $2NB_W/S$ in Equation 8.6 represents the effect of
signal supression. By lengthening the predetection
integration time B_W can be reduced, thereby reducing
the signal-supression effect.

     The X-Set code loop is time shared, with an er-
ror for each loop being estimated only once every
200 ms. For the simulation, the gain is adjusted so
that 0.1 of the estimated error is corrected every
200 ms. When the signal-to-noise ratio is high, this
leads to a time constant of about 1.8 seconds. Hence,
the prediction integration interval of 20 ms could be
increased to, say, 180 ms without directly adding
a significant amount to the filtering lag of the
delay-locked loop. However, there is another potential
problem with increasing the integration time. The I and
Q signals being integrated are sine and cosine functions
of the phase error between the estimated and actual re-
ceived carriers. A 1 ft/sec error in line-of-sight velo-
city would lead to sinusoidal and cosinusoidal I and Q
signals with the frequency 1.6 Hz. To process such sig-
nals without excessive attenuation, predetection inte-
gration should be performed over no more than about 1/4
of a cycle, or 160 ms for a 1 ft/sec error. In some
cases where increasing the predetection bandwidth will
be important, the carrier loop will have lost lock and
the code loop will be aided by the inertial navigation
system rather than by the carrier loop. Perhaps

81

l ft/sec is a reasonable value to assume for velocity
aiding error under these circumstances. Hence, lengthen-
ing the predetection integration time to approximately
160-200 ms would be a reasonable design option to con-
sider.

Because a single code-detector channel is time
shared in the X Set between early and late signals and
between the four GPS satellites, lengthening the pre-
detection integration time would involve taking mea-
surements over intervals where previously no measure-
ments were made. Thus, increasing the integration time
would also have the effect of decreasing the noise
bandwidth of the loop, improving its ability to reject
noise even without the signal suppression effect being
considered.

The elimination of time sharing entails the addi-
tion of extra detector hardware. To cover all four
signals simultaneously over the 200-ms cycle would re-
quire 8 I-Q detectors, instead of 1, for the code
channels. In many applications the improvement in
antijamming performance would not be worth the increase
in cost due to the extra detector hardware and the ex-
tra hardware and software required for acquisition,
storage, and predemodulation of the GPS data.

Evaluation of the increase in performance is most
easily made through reference to Equation 8.6. Increasing
the predetection integration time from 20 ms to 200 ms
would decrease both B_{LC} and B_W by a factor of 10. With
an integration interval of 20 ms, B_W is 50 Hz. If, for
example, S/N is 0 dB-Hz, then $2NB_W/S$ is 100 and is
the dominating term in the sum in Equation 8.6. Then

increasing the predetection integration time to 200 ms
(and performing the integration in parallel) would de-
crease σ_ε/L_C in Equation 8.6 by a factor of 10 RMS.
This corresponds to a 20 dB reduction in tracking er-
ror due to jamming without altering the tracking loop
response time of 1.8 sec.

To find the improvement in antijamming margin,
Equation 8.6 can be solved for S/N.   Because the
value of unity in the righthand side of Equation 8.6
is of negligible consequence at low signal-to-noise-
density ratios, the result is

$$\frac{S}{N} = \frac{\sigma_e}{L_C} \sqrt{B_{LC}B_W}$$

(8.7)

when

$$2NB_W/S \gg 1$$

(8.8)

From Equation 8.7 it is clear that a factor of 10 re-
duction in both B_{LC} and B_W provides a factor of 10
decrease in the value of S/N_{OE} needed to achieve a
desired RMS tracking error (σ_e/L_c). Hence, increas-
ing the predetection integration time from 20 ms to
200 ms provides a 10 dB improvement in antijamming
margin whenever the inequality (8.8) is valid.

These are very substantial gains in performance.
However, they can be achieved only if the aiding ac-
curacy is within about 1 ft/sec, as explained above.

Whether or not this accuracy can be maintained will depend upon the quality of the inertial navigation system and upon the details of the implementation of the aiding algorithms. Further work is necessary to postulate and evaluate via analysis and simulation a complete GPS inertial system with these advanced performance features.

The foregoing results in this section have been based substantially on Equation 8.6, which is based upon a square-law detection of signal power, rather than the absolute-value functions in Equations 8.4 and 8.5. However, the differences between the absolute-value and square-law implementation are expected to be small, within about 1 dB.

In applying Equation (8.6), however, signal-suppression effects must be taken into account in the calculation of the noise bandwidth B_{LC} of the loop. The term $2NB_W/S$ in Equation (8.6) accounts for the reduction in effective signal-to-noise ratio seen by the loop, but it does not account for changes in loop bandwidths. Signal suppression has the effect of reducing the gain of the delay-detection process, as defined by Equations (8.3-8.5). The reduction in detector gain results in a reduction in loop bandwidth. This reduction in bandwidth was identified in the computer simulations as being extremely important. It must be taken into account in predicting the performance of the loop.

With the detection algorithm of Equations (8.3-8.5) there are two gain-reduction effects, one associated with the numerator and one with the denominator. The term (P_E+P_L) in the denominator was meant to make the detector gain independent of signal level. This goal is well ac-

complished at high signal-to-noise ratios where $P_E + P_L$ is proportional to signal amplitude. But at low signal-to-noise ratios, $(P_E + P_L)$ is proportional to rms noise level and has the effect of reducing the gain of the detector by a factor that is directly proportional to rms noise-to-signal ratio. The numerator also provides a similar gain reduction, as will be described below. The combined effect of noise on the numerator and denominator of Equation (8.3) reduce the gain of the detector by a factor proportional to the noise-to-signal power ratio of the $I_{CO}^{(E)}$, etc., measurements when this ratio is substantially greater than unity. A precise theoretical expression for the gain reduction is not available. But emperical data is supplied by a Monte Carlo Analysis in Appendix B.

The reduction in gain at low signal-to-noise ratios is a good adaptive feature, dramatically improving the ability of the loop to track a stationary signal in high-noise conditions. The simulation demonstrated successful tracking by the X-Set at signal-to-noise ratios as low as 0 dB-Hz. However, the resulting low bandwidths may not be optimum when signal dynamics are taken into account. Care must be taken to take this gain reduction effect into account in any receiver designed to operate under conditions of severe jamming. The data in Appendix B should be of value in this regard.

After the date when the simulation design was finalized changes were made in the code-detection algorithm of the X-Set[1]. The denominator of Equation (8.3) was replaced by a constant factor and squaring operations were used as replacements for the absolute-value operations.

So it seems worthwhile to examine the gain-reduction effect
that remains when the denominator of Equation (8.3) is
replaced by a constant. An analytical expression for
this effect has been obtained, and two trial examples
were run on the simulation with the modified detector.

Equation (8.3) with the denominator replaced by
2Δ becomes

$$\hat{e}_{CO} = \frac{1}{2} \left[-P_E + P_L \right] \qquad (8.9)$$

If we adjust the carrier so that all the signals appear
in the I channels, Equations (8.9, 8.4, 8.5) can be used
to derive an expression for $\hat{e}_{CO}$ as a function of the
tracking error ε. The result is

$$\hat{e}_{CO} = \frac{1}{2} \left[-|(\Delta-\varepsilon)+N_{IE}| - |N_{QE}| + |(\Delta+\varepsilon)+N_{IL}| + |N_{QL}| \right] \qquad (8.10)$$

subject to

$$|\varepsilon| < \Delta \qquad (8.11)$$

where N_{IE}, etc., are samples of Gaussian noise with
variance σ^2. By setting the noise values equal to zero
in Equation (8.10) the gain $(\partial \hat{e}_{CO}/\partial \varepsilon)$ is seen to be equal
to +1. We want to know how the effective gain varies with
the rms noise level σ. The result, as shown in Appendix C,
has been found to be

$$\left. \frac{\partial \overline{\hat{e}_{CO}}}{\partial \varepsilon} \right|_{\varepsilon=0} = \mathrm{erf}(\Delta/\sqrt{2}\sigma) \qquad (8.12)$$

86

where erf is the standard error function

$$\text{erf}(\alpha) = \frac{2}{\sqrt{\pi}} \int_0^\alpha e^{-x^2} dx \tag{8.13}$$
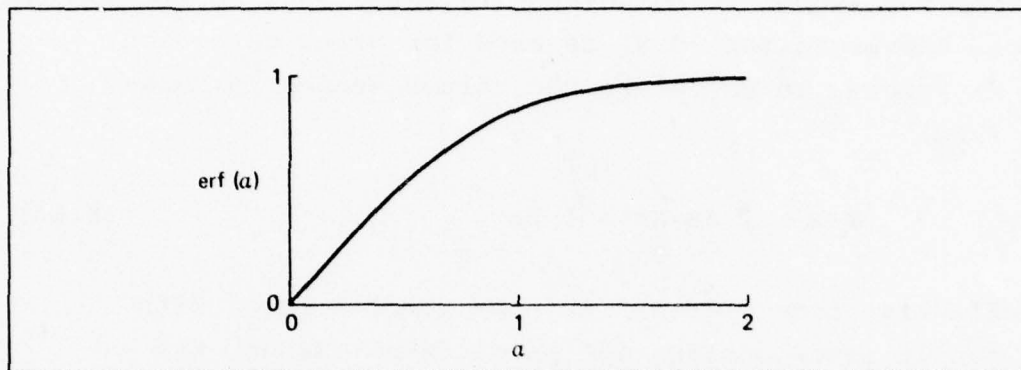
Figure 8.12   Error Function

This function is plotted in Figure 8.12.   When $\Delta/\sqrt{2}\sigma$ is small in Equation (8.12) the gain becomes unity, as expected. For small values of $(\Delta/\sqrt{2}\sigma)$ the error function becomes linear and the gain can be approximated by

$$\frac{\partial \overline{e_{CO}}}{\partial \varepsilon}\bigg|_{\varepsilon=0} = \left(\frac{2}{\sqrt{\pi}}\right)\left(\frac{\Delta}{\sqrt{2}\sigma}\right) = 0.798 \frac{\Delta}{\sigma} \tag{8.14}$$

subject to

$$\frac{\Delta}{\sqrt{2}\sigma} << 1 \tag{8.15}$$

It is clear from Equation (8.14) that the gain of the detector is inversely proportional to the rms noise level in the I and Q samples when the rms noise level is large in comparison to $\Delta/\sqrt{2}$.

To see how these results are utilized consider the
following example. Suppose that the integrate-and-dump
operations are carried out in parallel over 180 ms (aver-
aging over 45 4-ms samples in the X-Set implementation)
and that the signal-to-noise-density ratio is 1 dB-Hz. Further,
suppose that Equation (8.9) is used for error detection.
Then we procede to calculate the values needed in Equa-
tion (8.6)

$$S/N = 1 \text{ dB-Hz} = 1.26 \tag{8.16}$$

The effective time constant is nine samples long, with
each sample incorporating 180 ms of data. Hence, the
noise bandwidth of the loop without gain reduction is

$$B_{LC(normal)} = \left(\frac{1000}{9 \times 180}\right)\left(\frac{1}{4}\right) = 0.154 \text{ Hz} \tag{8.17}$$

and the predetection bandwidth is the inverse of the pre-
detection integration time

$$B_W = \frac{1000}{180} = 5.55 \text{ Hz} \tag{8.18}$$

At 1 dB-Hz the rms value of the noise σ in the 4-ms I and
Q samples is 9.96 chips (Ref. 2, Eq. 3-31) and the rms
value of the noise in the average of 45 samples is

$$\sigma = \sqrt{N/2ST}\bigg|_{T=0.130} = 9.96/\sqrt{45} = 1.48 \text{ chips} = 148 \text{ ft rms} \tag{8.19}$$

88

From Equations (8.14, 8.17, 8.19) with Δ = 50 ft, the effective loop bandwidth can be calculated

$$B_{LC} = (0.154) \left| (0.798) \, \frac{(50)}{(148)} \right| = 0.0415 \text{ Hz} \qquad (8.20)$$

and the effective bandwidth is seen to have been reduced by a factor of about 4 from its normal value. The rms tracking error is then computed from Equation (8.6)

$$\frac{\sigma_\varepsilon}{L} = \left\{ \frac{(0.0415)}{(2) \, (1.26)} \left[1 + \frac{(2) \, (5.55)}{(1.26)} \right] \right\}^{1/2}$$

$$= [(0.016) \, (1 + 8.81)]^{1/2} = (0.161)^{1/2} = 0.4 \text{ chips} \qquad (8.21)$$

which corresponds to a 40-ft rms tracking error. Notice the factor of 9.91 increase in noise power due to signal suppression.

With an rms tracking error as large as 40 ft and a chip width of 50 ft the nonlinearily of the code detection function[2] comes into play, further reducing the loop gain. So we expect an error of somewhat less than 40 ft in tracking a stationary signal. A single run of 30 seconds duration of the modified simulation produced an rms error of 23 ft, which is considered to be within the expected margin of errors (statistical and analytical) for this example.

Once the changes in loop bandwidth due to nonlinear effects of noise on the delay-detection algorithm are understood, changes may be made in the loop filter to provide whatever loop gain is desired. Then the conclusions at the beginning of this section as to the benefits of extending the predetection integration interval remain accurate.

Similar considerations concerning variations in loop bandwidth as a function of signal-to-noise ratio presumably apply to the Costas loop, considered in Section 8.2. Further work is needed to extend these results for the delay-locked loop to the Costas loop.

In summary, increasing the predetection integration time is shown to be an effective means of increasing the antijamming margin of the Code-tracking loops of the X-Set. Increasing the integration time from 20 ms to 200 ms results in a 10 dB increase in antijamming margin, and a 20 dB reduction in error due to jamming, at a fixed loop bandwidth. But the increase in integration time requires 8 sets of I-Q detectors for 4 receiver channels. In the current design, 1 set of I-Q detectors is time-shared between early and late detections and between four satellite channels. The increase in the predetection integration interval to 200 ms should be implemented only when inertial aiding is accurate to about 1 ft/sec. Verification of this accuracy over long missions and with a specified GPS inertial system design should be carried out, but is beyond the scope of this study. The effective loop bandwidth at low signal-to-noise ratios is shown to be critically dependent upon the choice of the detection algorithm. Analytical and imperical results relating the effective gains of two common algorithms to signal-to-noise ratio are provided.

1.0

1.1

1.25   1.4   1.6

1.8

2.0

2.2

2.5

2.8

MICROCOPY RESOLUTION TEST CHART

NATIONAL BUREAU OF STANDARDS-1963-A
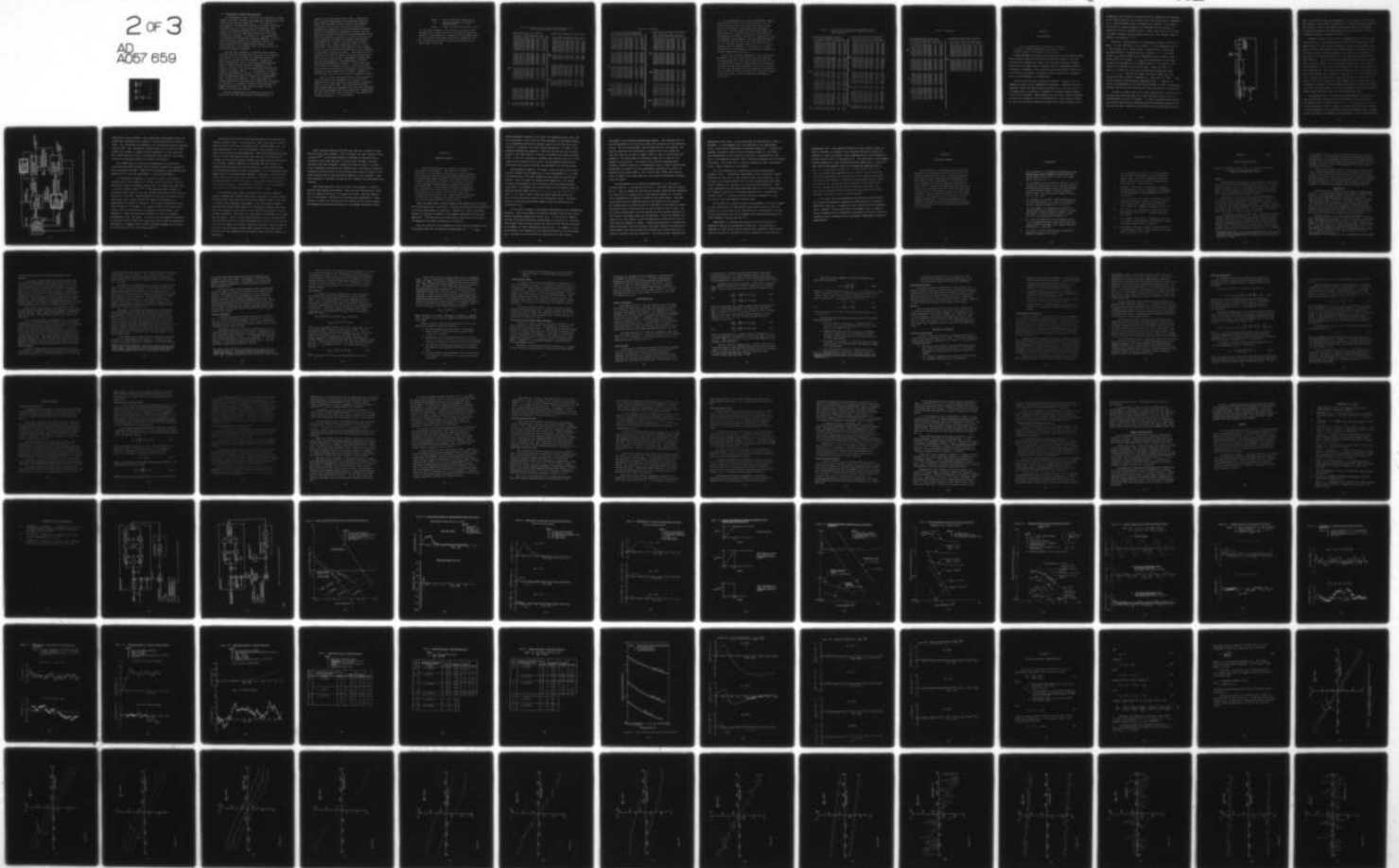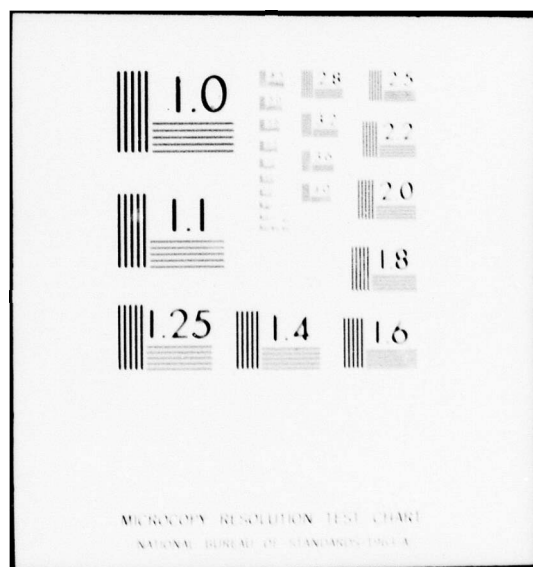
8.4 Elimination of Code-Loop Dithering

In the Magnavox X-Set, one set of I-Q detectors is time-shared ("dithered") between early and late code detection and between four satellite channels.[1,2] For each one of the channels, the detectors operate for 20 ms on the early waveforms, then for 20 ms on the late waveforms, then return to the early waveforms after a total time (including the first two sampling intervals of 20 ms each) of 200 ms has elapsed. In Section 8.3, the possibility of extending the integration times was examined. In this section possible benefits are examined of making the early-late detections simultaneously during a single 20 ms interval. To accomplish this, an extra set of I-Q detection hardware is needed.

Once the extra hardware is available and is being used for simultaneous detection during one 20 ms interval per channel, it is available for operation during one extra 20 ms interval for each channel. Forming two error estimates per 200 ms cycle would be desirable because it would decrease the noise bandwidth of the loop by a factor of two without appreciably altering the response to dynamic inputs. If, furthermore, the data could be demodulated in advance, a single error estimate could be made based upon an average of I-Q measurements over a single 40 ms interval. This would have the further advantage of decreasing the predetection bandwidth by a factor of 2, leading to greater gain stability and reduced sensitivity to high levels of noise, as discussed in the previous section.

Here we concentrate on the effects of making the 20 ms early and late measurements simultaneously in a

91

single 20 ms interval per 200 ms cycle. Making the
early and late measurements over different intervals
rather than the same interval causes no degradation
in signal-to-noise ratio and does not affect the
predetection bandwidth or the post-detection bandwidth.
There is the theoretical possiblity, though, that the
time delay between the early and late measurements could
lead to an erroneous indication of error during carrier-
loop transients in response to pseudo range dynamics.
The problem that arises is that the early and late
measurements are slightly dependent upon the carrier
phase error. This phase error appears as the argument
of the sine and cosine functions of the I and Q channels,
as specified in Equations (A6-A7). The absolute value
operations (A9-A10) are meant to provide indications of
early and late signal power independent of phase-angle.
But the indications are only approximate, and some
phase-angle dependence is present. If the square root
of the sum of the squares of the I's and Q's had been
used instead of the sum of the absolute values, this de-
pendence on phase angle would be absent. However, as
will be seen, the effect is of minor consequence anyway.

Table 8.6 shows selected regions of the printout of
code and carrier loop responses to a step of 10 ft.
applied to just the code loop, with the code loop being
aided by the carrier loop. The left-hand and right-
hand columns show the responses with early-late dithering
and with simultaneous early-late detection, respectively.
No input noise, VCO noise, VCO drift, or A/D conversion
errors were present. In the printout

92

$$\text{EPSCO} \equiv \text{actual code-loop tracking error}$$

$$\text{ECO} \equiv \text{code-loop detector's estimate of tracking error.}$$

$$\text{EPSCA} \equiv \text{actual carrier-loop tracking error}$$

As indicated in Table 1, when there is no carrier-loop tracking error, EPSCO and ECO are essentially identical whether or not dithering is employed. The presented data are for selected time points during the simulation run, but essentially the same results were obtained at all other times in the run.

Table 8.6: Comparison of Dithered and Simultaneous Early-
Late Correlation with no Carrier Error

Dithered Early-Late Correlation

TIME (SEC)	CAR I N B V	K Q	EPSCA (FT)	ECA(E) (FT)	EPSCO (FT)	ECO(E) (FT)
0.000	0 0 1 1	1 1	- 0.000	0.000	10.00	0.00
0.002	0 0 0 0	1 1	- 0.000	0.000	10.00	0.00
0.004	1 0 0 1	1 1	0.000	0.000	10.00	0.00
0.006	0 0 0 0	1 1	- 0.000	0.000	10.00	0.00
0.008	1 0 0 1	1 1	- 0.000	0.000	10.00	0.00
0.010	0 0 0 0	1 1	0.000	0.000	10.00	0.00
0.012	1 0 0 1	1 1	- 0.000	0.000	10.00	0.00
0.014	0 0 0 0	1 1	0.000	0.000	10.00	0.00
0.016	1 0 0 1	1 1	0.000	0.000	10.00	0.00
0.018	0 0 0 0	1 1	0.000	0.000	10.00	0.00
0.020	1 1 1 1	1 1	0.000-	0.000	10.00	0.00
0.022	0 0 0 0	1 1	0.000-	0.000	10.00	0.00
0.024	1 0 0 1	1 1	0.000-	0.000	10.00	0.00
0.026	0 0 0 0	1 1	0.000-	0.000	10.00	0.00
0.028	1 0 0 1	1 1	- 0.000-	0.000	10.00	0.00
0.030	0 0 0 0	1 1	- 0.000-	0.000	10.00	0.00
0.032	1 0 0 1	1 1	- 0.000-	0.000	10.00	0.00
0.034	0 0 0 0	1 1	- 0.000-	0.000	10.00	0.00
0.036	1 0 0 1	1 1	- 0.000-	0.000	10.00	0.00
0.038	0 0 0 0	1 1	- 0.000-	0.000	10.00	0.00
0.040	1 1 1 1	1 1	- 0.000-	0.000	10.00	10.00
0.042	0 0 0 0	1 1	- 0.000-	0.000	10.00	0.00
0.044	1 0 0 1	1 1	- 0.000-	0.000	10.00	0.00
0.046	0 0 0 0	1 1	- 0.000-	0.000	9.50	0.00
0.048	1 0 0 1	1 1	- 0.000-	0.000	9.00	0.00
0.050	0 0 0 0	1 1	- 0.000-	0.000	9.00	0.00
0.052	1 0 0 1	1 1	- 0.000-	0.000	9.00	0.00
0.054	0 0 0 0	1 1	- 0.000-	0.000	9.00	0.00
0.056	1 0 0 1	1 1	- 0.000-	0.000	9.00	0.00
0.058	0 0 0 0	1 1	- 0.000-	0.000	9.00	0.00
0.420	1 1 1 1	1 1	0.000	0.000	8.10	0.00
0.422	0 0 0 0	1 1	0.000	0.000	8.10	0.00
0.424	1 0 0 1	1 1	0.000	0.000	8.10	0.00
0.426	0 0 0 0	1 1	0.000	0.000	8.10	0.00
0.428	1 0 0 1	1 1	0.000	0.000	8.10	0.00
0.430	0 0 0 0	1 1	0.000	0.000	8.10	0.00
0.432	1 0 0 1	1 1	0.000	0.000	8.10	0.00
0.434	0 0 0 0	1 1	0.000	0.000	8.10	0.00
0.436	1 0 0 1	1 1	- 0.000	0.000	8.10	0.00
0.438	0 0 0 0	1 1	0.000	0.000	8.10	0.00
0.440	1 1 1 1	1 1	- 0.000	0.000	8.10	8.10
0.442	0 0 0 0	1 1	- 0.000	0.000	8.10	0.00
0.444	1 0 0 1	1 1	- 0.000	0.000	8.10	0.00

Simultaneous Early-Late Correlation

TIME (SEC)	CAR I N B V	K Q	EPSCA (FT)	ECA(E) (FT)	EPSCO (FT)	ECO(E) (FT)
0.000	0 0 1 1	1 1	- 0.000	0.000	10.00	0.00
0.002	0 0 0 0	1 1	- 0.000	0.000	10.00	0.00
0.004	1 0 0 1	1 1	0.000	0.000	10.00	0.00
0.006	0 0 0 0	1 1	0.000	0.000	10.00	0.00
0.008	1 0 0 1	1 1	0.000	0.000	10.00	0.00
0.010	0 0 0 0	1 1	0.000	0.000	10.00	0.00
0.012	1 0 0 1	1 1	- 0.000	0.000	10.00	0.00
0.014	0 0 0 0	1 1	0.000	0.000	10.00	0.00
0.016	1 0 0 1	1 1	0.000	0.000	10.00	0.00
0.018	0 0 0 0	1 1	0.000	0.000	10.00	0.00
0.020	1 1 1 1	1 1	0.000	0.000	10.00	10.00
0.022	0 0 0 0	1 1	0.000	0.000	10.00	0.00
0.024	1 0 0 1	1 1	- 0.000	0.000	10.00	0.00
0.026	0 0 0 0	1 1	- 0.000	0.000	9.50	0.00
0.200	1 1 1 1	1 1	0.000	0.000	9.00	0.00
0.202	0 0 0 0	1 1	0.000	0.000	9.00	0.00
0.204	1 0 0 1	1 1	0.000	0.000	9.00	0.00
0.206	0 0 0 0	1 1	0.000	0.000	9.00	0.00
0.208	1 0 0 1	1 1	- 0.000	0.000	9.00	0.00
0.210	0 0 0 0	1 1	- 0.000	0.000	9.00	0.00
0.212	1 0 0 1	1 1	- 0.000	0.000	9.00	0.00
0.214	0 0 0 0	1 1	- 0.000	0.000	9.00	0.00
0.216	1 0 0 1	1 1	- 0.000	0.000	9.00	0.00
0.218	0 0 0 0	1 1	- 0.000	0.000	9.00	0.00
0.220	1 1 1 1	1 1	- 0.000-	0.000	9.00	9.00
0.222	0 0 0 0	1 1	- 0.000-	0.000	9.00	0.00
0.224	1 0 0 1	1 1	- 0.000-	0.000	9.00	0.00
0.226	0 0 0 0	1 1	- 0.000-	0.000	8.55	0.00
0.228	1 0 0 1	1 1	0.000-	0.000	8.10	0.00
0.230	0 0 0 0	1 1	- 0.000-	0.000	8.10	0.00

Table 8.6 (Continued)

Dithered Early-Late Correlations

TIME (SEC)	CAR I N B V	K Q	EPSCA (FT)	ECA(E) (FT)	EPSCO (FT)	ECO(E) (FT)
0.800	1 1 1 1	1 1	- 0.000-	0.000	6.55	0.00
0.802	0 0 0 1	1 1	- 0.000-	0.000	6.55	0.00
0.804	1 0 0 1	1 1	- 0.000-	0.000	6.56	0.00
0.806	0 0 0 1	1 1	- 0.000-	0.000	6.56	0.00
0.808	1 0 0 1	1 1	- 0.000-	0.000	6.56	0.00
0.810	0 0 0 1	1 1	- 0.000-	0.000	6.56	0.00
0.812	1 0 0 1	1 1	- 0.000-	0.000	6.56	0.00
0.814	0 0 0 1	1 1	- 0.000-	0.000	6.56	0.00
0.816	1 0 0 1	1 1	- 0.000-	0.000	6.55	0.00
0.818	0 0 0 1	1 1	- 0.000-	0.000	6.56	0.00
0.820	1 1 1 1	1 1	- 0.000-	0.000	6.56	0.00
0.822	0 0 0 1	1 1	- 0.000-	0.000	6.56	0.00
0.824	1 0 0 1	1 1	- 0.000-	0.000	6.56	0.00
0.826	0 0 0 1	1 1	- 0.000-	0.000	6.56	0.00
0.828	1 0 0 1	1 1	- 0.000-	0.000	6.56	0.00
0.830	0 0 0 1	1 1	- 0.000-	0.000	6.56	0.00
0.832	1 0 0 1	1 1	- 0.000-	0.000	6.56	0.00
0.834	0 0 0 1	1 1	- 0.000-	0.000	6.56	0.00
0.835	1 0 0 1	1 1	- 0.000-	0.000	6.56	0.00
0.833	0 0 0 1	1 1	- 0.000-	0.000	6.56	0.00
0.840	1 1 1 1	1 1	- 0.000-	0.000	6.56	6.56
0.842	0 0 0 1	1 1	- 0.000-	0.000	6.55	0.00
0.844	1 0 0 1	1 1	- 0.000-	0.000	6.56	0.00
0.846	0 0 0 1	1 1	- 0.000-	0.000	6.23	0.00
0.848	1 0 0 1	1 1	- 0.000-	0.000	5.90	0.00
0.850	0 0 0 1	1 1	- 0.000-	0.000	5.90	0.00
0.852	1 0 0 1	1 1	- 0.000-	0.000	5.90	0.00
0.854	0 0 0 1	1 1	- 0.000-	0.000	5.90	0.00
0.856	1 0 0 1	1 1	- 0.000-	0.000	5.90	0.00
0.853	0 0 0 1	1 1	- 0.000-	0.000	5.90	0.00
2.000	1 1 1 1	1 1	- 0.000	0.000	3.48	0.00
2.010	0 0 0 1	1 1	- 0.000	0.000	3.48	0.00
2.020	1 1 1 1	1 1	- 0.000-	0.000	3.48	0.00
2.030	0 0 0 1	1 1	- 0.000-	0.000	3.48	0.00
2.040	1 1 1 1	1 1	- 0.000-	0.000	3.48	3.48
2.050	0 0 0 1	1 1	- 0.000-	0.000	3.13	0.00
2.060	1 1 1 1	1 1	0.000	0.000	3.13	0.00
2.070	0 0 0 1	1 1	0.000	0.000	3.13	0.00
2.080	1 1 1 1	1 1	0.000	0.000	3.13	0.00
2.090	0 0 0 1	1 1	0.000	0.000	3.13	0.00

Simultaneous Early-Late Correlations

TIME (SEC)	CAR I N B V	K Q	EPSCA (FT)	ECA(E) (FT)	EPSCO (FT)	ECO(E) (FT)
0.800	1 1 1 1	1 1	- 0.000-	0.000	6.56	0.00
0.802	0 0 0 1	1 1	- 0.000-	0.000	6.56	0.00
0.804	1 0 0 1	1 1	- 0.000-	0.000	6.56	0.00
0.806	0 0 0 1	1 1	- 0.000-	0.000	6.56	0.00
0.808	1 0 0 1	1 1	- 0.000-	0.000	6.56	0.00
0.810	0 0 0 1	1 1	- 0.000-	0.000	6.55	0.00
0.812	1 0 0 1	1 1	- 0.000-	0.000	6.56	0.00
0.814	0 0 0 1	1 1	- 0.000-	0.000	6.56	0.00
0.816	1 0 0 1	1 1	- 0.000-	0.000	6.56	0.00
0.818	0 0 0 1	1 1	- 0.000-	0.000	6.56	0.00
0.820	1 1 1 1	1 1	0.000-	0.000	6.56	6.56
0.822	0 0 0 1	1 1	0.000-	0.000	6.56	0.00
0.824	1 0 0 1	1 1	0.000-	0.000	6.56	0.00
0.826	0 0 0 1	1 1	0.000-	0.000	6.23	0.00
0.828	1 0 0 1	1 1	0.000-	0.000	5.90	0.00
0.830	0 0 0 1	1 1	0.000-	0.000	5.90	0.00
0.832	1 0 0 1	1 1	0.000-	0.000	5.90	0.00
0.834	0 0 0 1	1 1	0.000-	0.000	5.90	0.00
0.836	1 0 0 1	1 1	0.000-	0.000	5.90	0.00
0.838	0 0 0 1	1 1	0.000-	0.000	5.90	0.00
1.600	1 1 1 1	1 1	0.000	0.000	4.30	0.00
1.610	0 0 0 1	1 1	0.000	0.000	4.30	0.00
1.620	1 1 1 1	1 1	0.000	0.000	4.30	4.30
1.630	0 0 0 1	1 1	0.000	0.000	3.87	0.00
1.640	1 1 1 1	1 1	0.000	0.000	3.87	0.00
1.650	0 0 0 1	1 1	0.000	0.000	3.87	0.00
1.660	1 1 1 1	1 1	- 0.000	0.000	3.87	0.00
1.670	0 0 0 1	1 1	- 0.000	0.000	3.87	0.00
1.680	1 1 1 1	1 1	- 0.000-	0.000	3.87	0.00
1.690	0 0 0 1	1 1	- 0.000-	0.000	3.87	0.00
1.700	1 1 1 1	1 1	- 0.000-	0.000	3.87	0.00
1.710	0 0 0 1	1 1	- 0.000-	0.000	3.87	0.00
1.720	1 1 1 1	1 1	- 0.000-	0.000	3.87	0.00
1.730	0 0 0 1	1 1	- 0.000-	0.000	3.87	0.00
1.740	1 1 1 1	1 1	- 0.000-	0.000	3.87	0.00
1.750	0 0 0 1	1 1	- 0.000-	0.000	3.87	0.00
1.760	1 1 1 1	1 1	- 0.000-	0.000	3.87	0.00
1.770	0 0 0 1	1 1	- 0.000-	0.000	3.87	0.00
1.780	1 1 1 1	1 1	0.000	0.000	3.87	0.00
1.790	0 0 0 1	1 1	0.000	0.000	3.87	0.00
1.800	1 1 1 1	1 1	0.000	0.000	3.87	0.00
1.810	0 0 0 1	1 1	0.000	0.000	3.87	0.00
1.820	1 1 1 1	1 1	0.000	0.000	3.87	3.87
1.830	0 0 0 1	1 1	- 0.000	0.000	3.48	0.00
1.840	1 1 1 1	1 1	- 0.000	0.000	3.48	0.00
1.850	0 0 0 1	1 1	- 0.000	0.000	3.48	0.00
1.860	1 1 1 1	1 1	- 0.000-	0.000	3.48	0.00

In the subsequent test cases, high dynamic inputs were provided to the full receiver so that variable carrier loop tracking errors and code loop tracking errors were present. The results are presented in Table 8.7. The left-hand and right-hand columns show the results for dithered early-late correlation and simultaneous early-late correlation, respectively. Note, for example, the discrepancy with the dithered system at 0.440 sec between the actual code-loop error of 0.13 ft. and the indicated code-loop error of 1.94 ft. Although this discrepancy is very small, it is much larger than any discrepancies found with the system employing simultaneous detection.

Early-late dithering apparently causes only minor problems. The only significant reason for shifting to simultaneous detection would be to extend the interval during which data for each channel is processed so that the post-detection bandwidth (and possibly, with a priori data demodulation, the predetection bandwidth) can be decreased with lengthening the transient response time of the loop. These benefits were discussed in Section 8.3.

Table 8.7: Comparison of Dithered and Simultaneous Early-
Late Code Loop Correlation During Carrier Loop
Error Transients

Dithered Early-Late Correlation

TIME (SEC)	CAR I N B V	K Q	EPSCA (FT)	ECA(E) (FT)	EPSCO (FT)	ECO(E) (FT)
0.0000	0 0 1 1	1 1	- 0.000	0.000	- 0.00	0.00
0.0020	0 0 0 1	1 1	0.000	0.000	0.00	0.00
0.0044	1 0 0 1	1 1	0.000	0.000	0.00	0.00
0.0060	0 0 0 1	1 1	0.000	0.000	0.00	0.00
0.0083	1 0 0 1	1 1	0.000	0.000	0.00	0.00
0.0100	0 0 0 1	1 1	0.000	0.000	0.00	0.00
0.0121	1 0 0 1	1 1	0.000	0.000	0.00	0.00
0.0140	0 0 0 1	1 1	0.000	0.000	0.00	0.00
0.0161	1 0 0 1	1 1	0.000	0.000	0.00	0.00
0.0180	0 0 0 1	1 1	0.000	0.000	0.00	0.00
0.0201	1 1 1 1	1 1	0.000	0.000	0.00	0.00
0.0220	0 0 0 1	1 1	0.000	0.000	0.00	0.00
0.0241	1 0 0 1	1 1	0.001	0.000	0.00	0.00
0.0260	0 0 0 1	1 1	0.001	0.000	0.00	0.00
0.0281	1 0 0 1	1 1	0.001	0.000	0.00	0.00
0.0300	0 0 0 1	1 1	0.001	0.000	0.00	0.00
0.0321	1 0 0 1	1 1	0.002	0.000	0.00	0.00
0.0340	0 0 0 1	1 1	0.002	0.000	0.00	0.00
0.0361	1 0 0 1	1 1	0.002	0.000	0.00	0.00
0.0380	0 0 0 1	1 1	0.003	0.000	0.00	0.00
0.0400	1 1 1 1	1 1	0.003	0.001	0.00	0.43
0.0420	0 0 0 1	1 1	0.004	0.001	0.00	0.00
0.0441	1 0 0 1	1 1	0.005	0.001	0.00	0.00
0.0460	0 0 0 1	1 1	0.005	0.001	0.02	0.00
0.0483	1 0 0 1	1 1	0.005	0.001	0.05	0.00
0.4001	1 1 1 1	5 5	0.025	0.018	0.14	0.00
0.4021	0 0 0 1	5 5	0.024	0.018	0.14	0.00
0.4041	0 0 0 1	5 5	0.026	0.018	0.15	0.00
0.4061	0 0 0 1	5 5	0.024	0.018	0.14	0.00
0.4083	1 0 0 1	5 5	0.023	0.018	0.14	0.00
0.4100	0 0 0 1	5 5	0.022	0.018	0.14	0.00
0.4121	0 0 0 1	5 5	0.021	0.018	0.14	0.00
0.4140	0 0 0 1	5 5	0.020	0.018	0.14	0.00
0.4161	0 0 0 1	5 5	0.019	0.018	0.14	0.00
0.4180	0 0 0 1	5 5	0.018	0.018	0.14	0.00
0.4201	1 1 1 1	5 5	0.017	0.022	0.14	0.00
0.4221	0 0 0 1	5 5	0.016	0.022	0.14	0.00
0.4241	1 0 0 1	5 5	0.015	0.022	0.13	0.00
0.4261	0 0 0 1	5 5	0.014	0.022	0.13	0.00
0.4281	1 0 0 1	5 5	0.013	0.022	0.13	0.00
0.4300	0 0 0 1	5 5	0.011	0.022	0.13	0.00
0.4321	1 0 0 1	5 5	0.011	0.022	0.13	0.00
0.4340	0 0 0 1	5 5	0.009	0.022	0.13	0.00
0.4351	1 0 0 1	5 5	0.009	0.022	0.13	0.00
0.4380	0 0 0 1	5 5	0.007	0.022	0.13	0.00
0.4401	1 1 1 1	5 5	0.007	0.012	0.13	1.94
0.4421	0 0 0 1	5 5	0.006	0.012	0.12	0.00

Simultaneous Early-Late Correlation

TIME (SEC)	CAR I N B V	K Q	EPSCA (FT)	ECA(E) (FT)	EPSCO (FT)	ECO(E) (FT)
0.0000	0 0 1 1	1 1	- 0.000	0.000	- 0.00	0.00
0.0020	0 0 0 1	1 1	0.000	0.000	0.00	0.00
0.0041	1 0 0 1	1 1	0.000	0.000	0.00	0.00
0.0060	0 0 0 1	1 1	0.000	0.000	0.00	0.00
0.0081	1 0 0 1	1 1	0.000	0.000	0.00	0.00
0.0100	0 0 0 1	1 1	0.000	0.000	0.00	0.00
0.0121	1 0 0 1	1 1	0.000	0.000	0.00	0.00
0.0140	0 0 0 1	1 1	0.000	0.000	0.00	0.00
0.0161	1 0 0 1	1 1	0.000	0.000	0.00	0.00
0.0180	0 0 0 1	1 1	0.000	0.000	0.00	0.00
0.0201	1 1 1 1	1 1	0.000	0.000	0.00	0.00
0.0220	0 0 0 1	1 1	0.000	0.000	0.00	0.00
0.0241	1 0 0 1	1 1	0.001	0.000	0.00	0.00
0.0260	0 0 0 1	1 1	0.001	0.000	0.00	0.00
0.0281	1 0 0 1	1 1	0.001	0.000	0.00	0.00
0.0300	0 0 0 1	1 1	0.001	0.000	0.00	0.00
0.0321	1 0 0 1	1 1	0.002	0.000	0.00	0.00
0.0340	0 0 0 1	1 1	0.002	0.000	0.00	0.00
0.0361	1 0 0 1	1 1	0.002	0.000	0.00	0.00
0.0330	0 0 0 1	1 1	0.003	0.000	0.00	0.00
0.2001	1 1 1 1	5 5	0.013	0.012	0.01	0.00
0.2020	0 0 0 1	5 5	0.013	0.012	0.01	0.00
0.2041	1 0 0 1	5 5	0.019	0.012	0.01	0.00
0.2061	0 0 0 1	5 5	0.013	0.012	0.01	0.00
0.2081	1 0 0 1	5 5	0.013	0.012	0.01	0.00
0.2100	0 0 0 1	5 5	0.012	0.012	0.01	0.00
0.2121	0 0 0 1	5 5	0.012	0.012	0.01	0.00
0.2140	0 0 0 1	5 5	0.011	0.012	0.01	0.00
0.2161	1 0 0 1	5 5	0.013	0.012	0.01	0.00
0.2180	0 0 0 1	5 5	0.010	0.012	0.01	0.00
0.2201	1 1 1 1	5 5	0.009	0.012	0.00	0.01
0.2221	0 0 0 1	5 5	0.009	0.012	0.00	0.00
0.4001	1 1 1 1	5 5	0.025	0.017	0.02	0.00
0.4021	0 0 0 1	5 5	0.024	0.017	0.02	0.00
0.4041	1 0 0 1	5 5	0.026	0.017	0.02	0.00
0.4061	0 0 0 1	5 5	0.024	0.017	0.02	0.00
0.4081	1 0 0 1	5 5	0.023	0.017	0.02	0.00
0.4100	0 0 0 1	5 5	0.022	0.017	0.02	0.00
0.4121	0 0 0 1	5 5	0.021	0.017	0.02	0.00
0.4140	0 0 0 1	5 5	0.020	0.017	0.01	0.00
0.4161	1 0 0 1	5 5	0.019	0.017	0.01	0.00
0.4180	0 0 0 1	5 5	0.018	0.017	0.01	0.00
0.4201	1 1 1 1	5 5	0.017	0.022	0.01	0.02
0.4221	0 0 0 1	5 5	0.016	0.022	0.01	0.00
0.4241	1 0 0 1	5 5	0.015	0.022	0.01	0.00

97

Table 8.7 (Continued)

Dithered Early-Late Correlation

TIME (SEC)	I N B V	K Q	EPSCA (FT)	ECA(E) (FT)	EPSCO (FT)	ECO(E) (FT)
3.200	1 1 1	3 3	- 0.007	- 0.002	0.16	0.00
3.210	0 0 0	3 3	- 0.008	- 0.002	0.16	0.00
3.220	1 1 1	3 3	- 0.004	- 0.008	0.17	0.00
3.230	0 0 0	3 3	- 0.000	- 0.008	0.17	0.00
3.240	1 1 1	3 3	0.003	- 0.000	0.17	1.90
3.250	0 0 0	3 3	0.005	- 0.000	0.01	0.00
3.260	1 1 1	3 3	0.006	0.005	- 0.00	0.00
3.270	0 0 0	3 3	0.006	0.005	- 0.00	0.00
3.280	1 1 1	3 3	0.004	0.006	- 0.01	0.00
3.290	0 0 0	3 3	0.000	0.006	- 0.01	0.00
3.300	1 1 1	4 4	- 0.003	0.000	- 0.01	0.00
3.310	0 0 0	4 4	- 0.004	0.000	- 0.02	0.00
3.320	1 1 1	4 4	- 0.000	- 0.004	- 0.01	0.00
3.330	0 0 0	4 4	0.002	- 0.004	- 0.01	0.00
3.340	1 1 1	4 4	0.005	0.002	- 0.00	0.00
3.350	0 0 0	4 4	0.007	0.002	- 0.00	0.00
3.360	1 1 1	4 4	0.003	0.007	- 0.00	0.00
3.370	0 0 0	4 4	0.006	0.007	- 0.00	0.00
3.380	1 1 1	4 4	0.004	0.006	- 0.01	0.00
3.390	0 0 0	4 4	0.000	0.006	- 0.01	0.00
3.400	1 1 1	5 5	- 0.004	0.000	- 0.02	0.00
3.410	0 0 0	5 5	- 0.005	0.000	- 0.02	0.00
3.420	1 1 1	5 5	- 0.002	- 0.005	- 0.01	0.00
3.430	0 0 0	5 5	0.000	- 0.005	- 0.01	0.00
3.440	1 1 1	5 5	0.004	0.000	- 0.01	- 1.09
3.450	0 0 0	5 5	0.005	0.003	0.09	0.00
3.460	1 1 1	5 5	0.006	0.005	0.10	0.00
3.470	0 0 0	5 5	0.005	0.005	0.09	0.00
3.480	1 1 1	5 5	0.002	0.005	0.09	0.00
3.490	0 0 0	5 5	- 0.001	0.005	0.09	0.00
3.500	1 1 1	0 0	- 0.006	- 0.001	0.08	0.00
3.510	0 0 0	0 0	- 0.007	- 0.001	0.08	0.00
3.520	1 1 1	0 0	- 0.003	- 0.007	0.09	0.03
3.530	0 0 0	0 0	- 0.000	- 0.007	0.09	0.00
3.540	1 1 1	0 0	0.002	- 0.000	0.09	0.00
3.550	0 0 0	0 0	0.004	- 0.000	0.09	0.00
3.560	1 1 2	0 0	0.005	0.004	0.09	0.00
3.570	0 0 0	0 0	0.004	0.004	0.09	0.00
3.580	1 1 1	0 0	0.002	0.004	0.09	0.00
3.590	0 0 0	0 0	- 0.001	0.004	0.09	0.00

Simultaneous Early-Late Correlation

TIME (SEC)	I N B V	K Q	EPSCA (FT)	ECA(E) (FT)	EPSCO (FT)	ECO(E) (FT)
0.800	1 1 1	3 3	- 0.096	- 0.086	- 0.09	0.00
0.802	0 0 0	3 3	- 0.099	- 0.086	- 0.10	0.00
0.804	0 0 1	3 3	- 0.101	- 0.086	- 0.10	0.03
0.805	0 0 0	3 3	- 0.100	- 0.086	- 0.10	0.00
0.806	0 0 1	3 3	- 0.093	- 0.086	- 0.10	0.00
0.810	0 0 0	3 3	- 0.097	- 0.086	- 0.09	0.00
0.812	0 0 1	3 3	- 0.095	- 0.086	- 0.09	0.03
0.814	0 0 0	3 3	- 0.093	- 0.086	- 0.09	0.00
0.816	0 0 1	3 3	- 0.091	- 0.086	- 0.09	0.00
0.818	0 0 0	3 3	- 0.090	- 0.086	- 0.09	0.00
0.820	1 1 1	3 3	- 0.083	- 0.096	- 0.09	- 0.09
0.822	0 0 0	3 3	- 0.087	- 0.096	- 0.09	0.00
0.824	0 0 1	3 3	- 0.085	- 0.096	- 0.08	0.00
0.826	0 0 0	3 3	- 0.083	- 0.096	- 0.08	0.00
0.828	0 0 1	3 3	- 0.081	- 0.096	- 0.07	0.00
0.830	0 0 0	3 3	- 0.080	- 0.096	- 0.07	0.00
0.832	0 0 1	3 3	- 0.077	- 0.096	- 0.07	0.00
0.834	0 0 0	3 3	- 0.076	- 0.096	- 0.06	0.00
0.836	0 0 1	3 3	- 0.074	- 0.096	- 0.06	0.00
0.838	0 0 0	3 3	- 0.072	- 0.096	- 0.06	0.00

SECTION 9

AIDED TRACKING

As an introduction to the subject of adaptive
tracking, a general discussion of inertial aiding of
tracking loops is presented in this section.

Useful GPS data is obtained only while the carrier-tracking and/or
code-tracking loops are locked onto the desired signals. When any
tracking error becomes too large, the correlation detector becomes
excessively nonlinear and its effective gain is accordingly lowered.
Progressive increases in the tracking error and attendant reductions in
the detector gain lead to a complete loss of lock and to a complete
loss of that component of the GPS data.

Loss of lock can occur because of excessive tracking error in
response to radio noise, perhaps due to jamming. Lowering the loop
bandwidth lowers the noise-induced tracking error, but also acts to
increase errors in response to dynamics in the pseudorange variable
that is to be tracked. These dynamics can be due to vehicle dynamics,
to oscillator dynamics, and to perturbations in the propagation path.
By utilizing the IMU to measure the short-term signal dynamics due to

translation and rotation of the vehicle and by supplying the IMU data as an aiding signal to the tracking loop, the tracking-error components due to vehicle dynamics can be substantially reduced. With reduced errors due to vehicle dynamics, the bandwidth of the loop may be reduced to further attenuate jamming. Hence, IMU aiding of the tracking loops increases the antijamming margins of the tracking loops in dynamic environments.[2,3,5-7]

Generally, aiding signals are introduced as shown in Figure 9.1, where τ is the time delay to be tracked, $\hat{\tau}$ is the estimated value of τ, and $\dot{\tau}_{aid}/K_{FC}$ is an aiding signal. Alternatively, with exactly the same effect on the detected error signal $D(\tau - \hat{\tau})$, the aiding signal τ_{aid} could be added to the feedback signal as shown by the dotted line in the figure. If τ_{aid} were subtracted from the input τ instead of being added to the feedback signal $\hat{\tau}$, its effect on the output of the detector would be the same. Hence the effect of aiding is to make the loop track an effective pseudorange signal $\tau_e \equiv (\tau - \tau_{aid})$. The IMU can supply an aiding signal τ_{aid} that matches the high-frequency components of τ quite well so that $\tau - \tau_{aid}$ contains smaller high-frequency components than τ. Then, with aiding, the bandwidth of the loop can be lowered in order to attenuate jamming noise while still maintaining linear operation of the detector.

In order to avoid loss of lock, the tracking error of each carrier-tracking loop should be kept well within the small value of 0.1 ft (phase-locked) or 0.05 ft (Costas). In order to provide this accuracy with narrow tracking-loop bandwidths during high-dynamic maneuvers of tactical aircraft, aiding velocity signals must be delivered from the

100
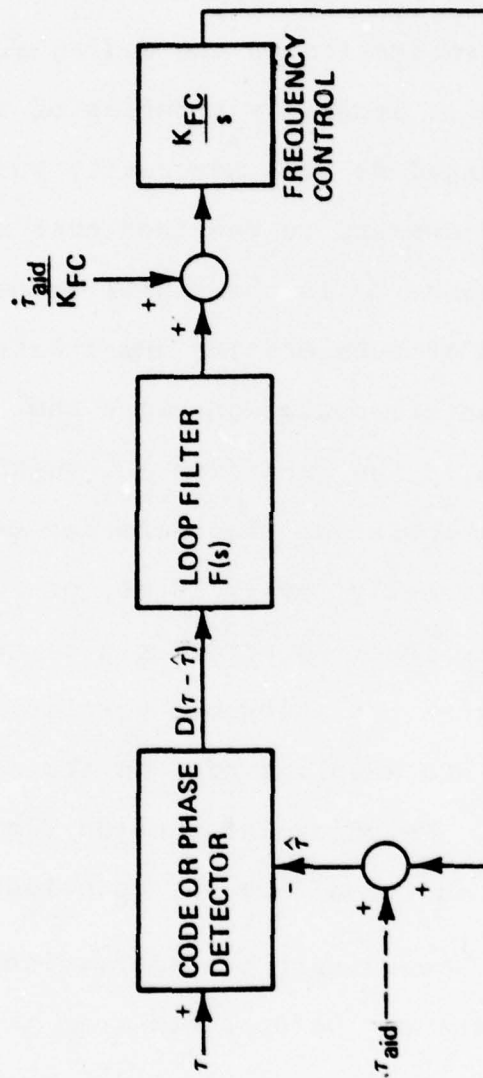
Figure 9.1. The use of an aiding signal in a tracking loop

101

IMU to the carrier loops very frequently, on the order of every 10 ms, and transport delays must be accounted for. Because data are generally not available from the INS mechanization algorithms this frequently, the aiding data should be obtained directly from the IMU, or from its strapdown processor, as shown in Figure 9.2.

Transport delays can occur in the implementation of the tracking loop as well as in the implementation of the aiding algorithms. The aiding signal for each loop is generally a series of increments Δr_{aid} each of which, when implemented at some accurately specified time in the future as the frequency command to the loop over an interval Δt, represents the predicted change Δr in the signal to be tracked over that interval. Past values of acceleration and attitude data from the IMU are used as inputs to an extrapolation algorithm. The output of the extrapolation algorithm is the predicted $\hat{\Delta r}$, which is delivered to the tracking loop. The extrapolation algorithm can be very simple, but should be repeated very frequently, every 10 ms, or so for each carrier loop. Because the code-loop tracking errors can be on the order of tens of feet, much larger than the allowable carrier-loop errors, the problems of transport lags and sampling periods are relatively insignificant for code-loop aiding. Velocity information from the INS mechanization algorithms may be used for aiding the code loops.

The parameters for the coordinate transformation and scaling of the translational aiding data can be obtained from the integrated navigation filter, as shown in Figure 9.2. These parameters, relating to the bearings of lines of sight to the GPS satellites, and relating to the orientation of the gyro-stabilized accelerometer frame, change slowly and need to be updated only infrequently. With these parameters

102
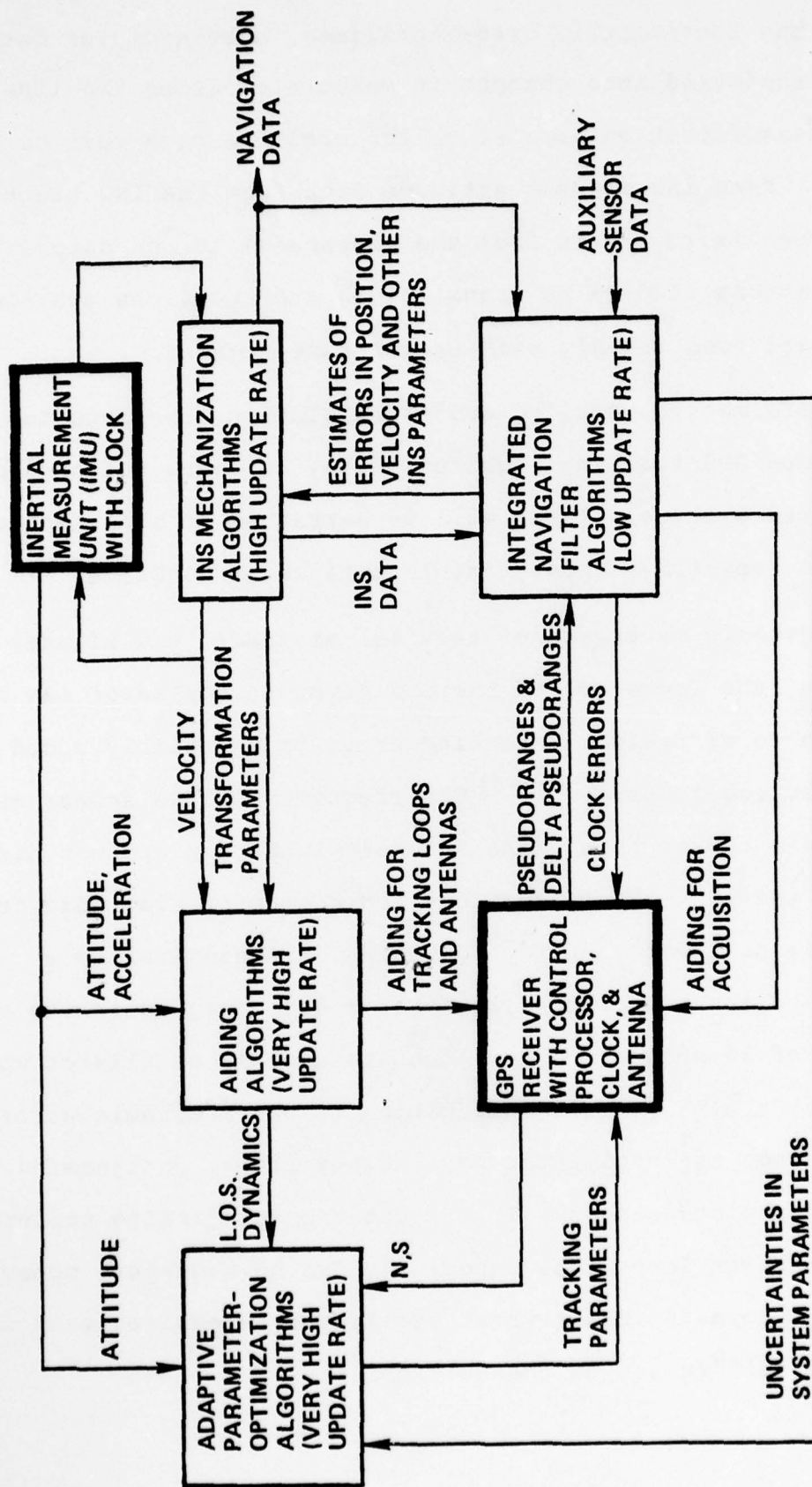
Figure 9.2. Structure for integrated GPS inertial navigation system.

being known, the incremental, gyro-stabilized, accelerometer data are scaled and transformed into changes in velocities along the lines of sight. The transformation parameters for attitude data must be obtained from the IMU. Then incremental attitude data from the IMU are transformed into changes in ranges from the antenna(s) to the satellites. The transformations of data on translations and rotations are simple, but must be performed rapidly with proper time-tagging.

The transformation, scaling and extrapolation functions for inertially-aided GPS tracking require special software not needed for the unintegrated systems. These will be warranted in some applications because of the resulting improvement in antijam performance.

In high-dynamic maneuvers of tactical aircraft, the effects of acceleration on the frequency of the GPS crystal oscillator can be a significant cause of residual tracking error in inertially aided code or carrier tracking loops.[2-4,6-9] The frequency shifts appear as pseudorange-rate inputs to all the tracking loops and are not directly detectable by the IMU. Specifications for currently available crystal oscillators are no lower than 10^{-9}/g, which is equivalent to a pseudorange rate input of $1(ft/s)/g$. For a code loop operating with a time constant of 30 seconds, a 2-g input to such an oscillator would lead to a 60-ft tracking error in addition to other dynamic error components. Hence the oscillator sensitivity limits antijamming performance of the code loops. It affects the antijamming performance of IMU-aided carrier loops too, especially during high-jerk maneuvers. Fortunately, it appears that crystal oscillator assemblies with sensitivities below 10^{-10}/g are on the horizon.[4]

IMU errors also limit the antijam performance of aided code and carrier tracking loops. For the carrier loops, care must be taken to keep tracking errors due to attitude errors, bending modes, etc., to less than about 0.1 ft, with loop response times of about 0.5 s, or less, during severe attitude maneuvers. With one milliradian attitude errors, a lever arm length of much less than 100 ft would not be a problem, but structural flexure between the antenna and the IMU could be a problem. Either gimballed or strapdown IMUs are capable of supplying sufficiently accurate attitude data in most applications. For the gimballed IMUs the pacing requirement is on the accuracies and update rates of the gimbal angle encoders. Reference 2 and Appendix A provide quantitative data on the effects of a variety of error sources on the performance of IMU-aided carrier loops under jamming and with high dynamic maneuvers. Improvements of 10 dB or so in AJ performance can be achieved through inertial aiding of carrier loops.

For aiding the code loops, the ability of the INS to measure dynamic translational motions sufficiently accurately so that tracking errors are much less than 100 ft with loop response times on the order of 1-100 s is the dominant requirement. Only high-quality stable-platform IMUs are currently capable of successfully aiding code loops with time constants on the order of 100 s during high-dynamic tactical aircraft maneuvers. The code-loop time constant determines the ultimate antijam margin. Hence, the antijam performance of the integrated GPS inertial system will be strongly dependent upon the accuracy of the IMU over the full range of accuracy of available designs. This conclusion is true to an even greater extent when navigation performance after loss of lock, and reacquisition performance under moderate jamming, are considered.

Aided tracking loops provide GPS data that are corrupted to some extent by the aiding signals. This corruption has been reported in the literature[54] as sometimes leading to problems of instabilities in navigation algorithms designed to receive pure GPS data, and some solutions have been proposed. Because the aiding signal τ is effectively high-pass filtered by the tracking loop, subtracting a similarly high-pass filtered version of the aiding signal from the output of the aided tracking loop is an alternative approach to this problem. Some extra hardware or software is required for creating the high-pass-filter function.

Aided code loops will have very long time constants in order to maximize anti-jamming performance. When the time constants are longer than the sampling period of the navigation filter, the data samples will be correlated. Whitening filters have been implemented in some designs to reduce the correlations and thereby to more nearly satisfy the assumptions governing the design of the Kalman navigation filter.

SECTION 10

ADAPTIVE TRACKING

Adaptive tracking was not treated in detail during
the course of this study.   But some of the general
principles are described in this section, and references
are provided to some of the latest results which have been
developed under other contracts.   The latest results in-
clude the possibility of adaptively varying the range of
P-code detection through the use of multi-chip correla-
tion techniques.   A key element of adaptive tracking is
the incorporation of the effects of noise in suppressing
the signals and in lowering the detector gains when
signal-to-noise ratios are low.   These effects, described
in Section 8, are assumed to be taken into account in
the optimizations described in this section.

When the conditions of signal dynamics and jamming noise are such
that maintaining lock is difficult, choosing the tracking-loop parameters
to optimize performance is important.   Because the conditions usually
cannot be predicted in advance, the parameter adjustment is best done
adaptively.   The availability of data from an IMU greatly facilitates
the adaptation process, as indicated in Figure 9.2.

The best values for the parameters of each loop are dependent upon
the dynamic model for the effective pseudorange $\tau_e \equiv (\tau - \tau_{aid})$

being estimated (tracked) by the loop, the signal-to-noise ratio, and the covariances of the tracking loop's estimates of the model states. In an integrated GPS-inertial system, data from the INS can be used directly to determine the time-variable parameters in a model of the effective pseuodrange dynamics. Data from the INS can also be used, together with data from the receiver to determine the signal-to-noise ratio. From this information, together with initial values for covariances of the tracking error states, the succeeding tracking-error covariances and optimum tracking loop parameters can be calculated.

Each optimally adaptive, n^{th} order, tracking loop can be considered as a Kalman filter operating on noisy measurements of τ_e, which is generated by an nth order dynamic process model with white noise sources. Once the model is characterized adaptively, the optimal tracking-loop parameters can be obtained from the standard Kalman algorithms. For example, for a third-order carrier tracking loop, an adequate process model might be $\dot{\tau}_e = v_e$, $\dot{v}_e = a_e$, $\dot{a}_e = -a_e/T + n_j$, where n_j is a white noise source with power spectral density N_j, and T is the correlation time of the acceleration state. The variations in effective pseudorange dynamics could be represented by variations in N_j.

If the loop is unaided, this process represents the full pseudorange dynamics. Then accelerometer and attitude outputs from the IMU can be used to designate appropriate values of N_j. If the loop is aided by the INS the process represents the dynamics of aiding error. Then the accelerometer and attitude outputs are used with the INS and oscillator error models to obtain appropriate values of N_j. For example, if the uncertainties in alignments of the stabilized axes are 10 milliradians rms, 1 percent of the acceleration indicated by the IMU could be

allocated to the effective pseudorange dynamics. The uncertainties of the INS parameters will vary only slowly (as solutions of the navigation filter), but the accelerometer and attitude data can vary rapidly, and must be converted into selections of values for N_j very rapidly so that the loop will be able to adapt itself in time to follow high-jerk dynamics. The algorithms for selecting values for N_j must be very simple to be practical. The values of N_j should be appropriately bounded to prevent selection of excessively large or small tracking-loop bandwidths, but need to be only approximate indications of levels of dynamics within these bounds. For a first-order aided code-tracking loop, a simple first-order model for the effective pseudorange dynamics would be chosen.

The measurement of the effective pseudorange τ_e by the code or carrier detector is corrupted by noise n_τ. The power spectral density N_τ of n also is needed for deriving the optimum tracking-loop parameters. The value of N_τ is proportional to the spectral density of the radio noise (perhaps due to jamming) divided by the signal power. The radio noise density can be measured directly and rapidly by the receiver. The signal power is a weak function of the angle of the satellite above the horizon and a strong function of the attitude of the aircraft. By utilizing attitude data from the IMU and the known antenna patterns of the vehicle, the signal power can be predicted. Since the signals will usually be at full power, it may be sufficient to characterize each of them merely as present or absent. Because malfunctions or interveining fixed structures, such as mountains, can cause unpredicted blackouts of some signals, the receiver must also estimate the signal power that is actually received from each satellite. But this estimate requires code

109

demodulation and, hence, is not valid when the code detector range is exceeded. It also depends upon the parameters of the measurement filter, which should themselves be optimized adaptively. Although the response time may be slow, provision should be made for the signal power measurement by the receiver to provide a "signal-absent" override to the adaptive algorithm, and to satellite-selection and navigation algorithms. The values for N should be bounded so that unreasonably large or small values are not utilized.

With the parameters N_j (representing effective pseudorange dynamics) and N (representing measurement noise) determined, Kalman solutions for the gains in the tracking loops can be obtained. The solutions are straightforward, but are time consuming when performed rapidly enough to be accurate for a loop with wide bandwidth. Time-scales approximation techniques have been applied to the simplification of a numerical solution of the Kalman equations for a second-order tracking loop[11], thereby providing a practical approach to that part of the real-time adaptive tracking task.

The solution for optimum tracking loop parameters has been extended to cover the effects of code-detector nonlinearity and to cover the possibility of also varying the code-detection range optimally so that tracking and acquisition can be handled with improved performance by a single adaptive tracking process.[12].

Improvements in antijam performance can also be obtained by adaptively varying the predetection bandwidth. The predetection bandwidth of each Costas carrier-tracking and incoherent code-tracking loop can be varied in proportion to the uncertainty in the effective

110

pseudorange rate. Each bandwidth should be large enough to pass the carrier and data (if present), but otherwise should be as small as possible in order to minimize signal suppression when the predetection signal-to-noise ratio is less than unity. The improvement in performance through adaptation is most pronounced during acquisition, or when the code loop is data-aided so that its predetection bandwidth can be small[3], as described in Section 8. If the carrier loop is in lock, the predetection bandwidths of the carrier loop and its associated code loop should be proportional to the frequency uncertainty of carrier-loop tracking, as indicated by the Kalman adaptive tracking equations for the carrier loop. When the carrier loop is not in lock, and both the carrier and code loops are IMU-aided, the much slower navigation filter solutions for uncertainties in clock frequency and vehicle velocity can be utilized.

It is clear that the availability of data from an IMU greatly facilitates the process of adapting the GPS receiver to different operating conditions. An approach to the process has been suggested above. However, further exploratory development work is needed to develop complete sets of adaptation algorithms of different levels of complexity and to determine their performance advantages in specific applications.

SECTION 11

CONCLUDING SUMMARY

The simulation of the SAMSO/Magnavox GPS User
Equipment Set X has been utilized to illustrate per-
formance advantages that can be obtained through ap-
propriately minimizing predetection bandwidths of
the tracking loops. The benefits of utilization of
prior knowledge of GPS data have been described in
this context. Theoretical expressions and Monte Carlo
results for nonlinear effects of detection algorithms
in conditions of low signal-to-noise ratio have been
developed. These results are important to the under-
standing of the behavior of GPS receivers in high
jamming environments. New design techniques for
adaptive receivers have been described and references
have been provided to recent results developed under
other contracts.

REFERENCES

1.   W.M. Stonestreet, <u>A Functional Description of the</u>
      <u>NAVSTAR GPS Receiver Model-X,</u> Draper Laboratory
      Report R-981, Vol. I, Rev. I, Feb. 1977; SAMSO
      Report TR77-120, Vol. I.

2.   B.A. Kriegsman, W.M. Stonestreet, and D.B. Cox, Jr.,
      "Functional Requirements of the Interface Between
      the NAVSTAR GPS Receiver Model X and the Advanced
      Inertial Reference Sphere," Draper Laboratory
      Report R-981, (Air Force Report SAMSO TR77-120),
      Vol. II, Dec. 1977.

3.   L.L. Horowitz, J.R. Sklar, "ECM Vulnerability of
      the GPS User Receiver in a Tactical Environment",
      Lincoln Laboratory Report XR-1, 7 May 1976.

4.   J.M. Przyjemski, "A Compensation Technique for
      Acceleration-Induced Frequency Changes in Crystal
      Oscillators," Draper Laboratory Report P-606,
      May 1978, to be presented at NAECON '78.

5.   P.P. Yeh, "A Treatise on the Antijamming Margin
      of an IMU/Computer-Aided Global Positioning Navi-
      gation System," Aerospace Corp. Report TOR-0076-
      (6473-01)-1, 15 Oct 1975.

6.   E.H. Martin, "Aiding GPS Navigation Functions,"
      <u>NAECON '76 Record</u>, pp 849-856.

REFERENCES (CON'T)

7. B.A. Kriegsman, D.B. Cox, Jr., W.M. Stonestreet, "An IMU Aided GPS Receiver," Draper Laboratory Report P-490, June 1977, Presented at the 33rd Annual Meeting of the Institute of Navigation, Costa Mesa, CA., 22-24 June 1977.

8. R. Maher, "Oscillator and Frequency Management Requirements for GPS User Equipment," Proceedings of 1976 Frequency Control Symposium, June 1976, pp 384-389.

9. J.M. Przyjemski, P.L. Konop, "Limitations on GPS Receiver Performance Imposed by Crystal Oscillator G-Sensitivity," Draper Laboratory Report P-432, March 1977, NAECON '77 Record, pp 319-322.

10. R.W. Carrol, W.A. Mickelson, "Velocity Aiding of Non-Coherent GPS Receiver," NAECON '77 Record, pp 311-318.

11. R.V. Ramnath, W.M. Bowles, "Asymptotic Analysis of a Class of Time-Varying Linear Filters," Draper Laboratory Report R-994, 25 Aug 1976.

12. W.M. Bowles, "Optimal Acquisition and Tracking of a Pseudo-Random Code," Draper Laboratory Internal Memo 15L-76-005, 8 Jan 1976.

114

APPENDIX A   P-490

AN IMU-AIDED GPS RECEIVER

by

Bernard A. Kriegsman, Duncan B. Cox, Jr., William M. Stonestreet

The Charles Stark Draper Laboratory, Inc.
Cambridge, Massachusetts 02139

ABSTRACT

The performance requirements for the GPS X-set[*] impose diffi-
cult and conflicting design problems on the receiver. To accurately
track the incoming signals in a high-dynamics environment, a wide-
bandwidth tracking loop is reuqired with a high-order tracking net-
work. For best performance in the presence of noise, on the other
hand, a narrow bandwidth tracking loop is desired.

Techniques for utilizing an IMU (inertial measurement unit)
to aid the receiver tracking loops are studied here. The IMU
can provide accurate information on translational accelerations and
orientation changes experienced by the receiver. By properly using
the IMU data, the receiver bandwidth can be reduced without increasing
the dynamics-induced tracking error. The end result is an improve-
ment in performance in noisy or jamming situations.

To evaluate the benefits of IMU aiding, a comprehensive digital-
computer simulation was developed for the IMU-aided X-set receiver.
Included in the simulation of the receiver were detailed models for
the error detectors, integrate-and-dump circuits, digital tracking
networks, and RM/IPMs (digital VCOs) for both the code and carrier
tracking loops. The effects of RM/IPM quantization, cross-coupling
between code and carrier tracking loop, dynamic clock errors, and the

_____

[*]The NAVSTAR GPS X-set is one of several baseline Phase I GPS receivers
being developed by Magnavox Advanced Products Division under sub-
contract to General Dynamics under a contract with the GPS Joint Pro-
gram Office at SAMSO.

115

finite sampling rates in each tracking loop were among the effects accounted for. In the IMU model, provisions were made for measuring the orientation and translational acceleration of the support vehicle. Included as IMU error sources were attitude readout errors, IMU mis-alignment, gyro drift bias, accelerometer bias, and accelerometer scale-factor uncertainty.

The simulation results present code and carrier tracking-loop errors, based on Monte-Carlo runs, for a wide range of conditions. Of particular interest are the thresholds of input noise and vehicle dynamics at which the tracking loops lose lock. Performance-comparison data are presented for the aided and unaided receiver as a function of system variables such as tracking loop bandwidth, RM/IPM noise, IMU errors, clock errors, and sampling rates for receiver and IMU.

INTRODUCTION

The incoming GPS (Global Positioning System) considered here consists of a high-frequency L-band carrier signal (1.575 GHz) modu-lated by a PRN (Pseudo-Random-Noise) code signal (10.23 MHz).[+] Binary data with satellite ephemeris and other information are modu-lated on these signals at 50 b.p.s. The function of the receiver is to demodulate the transmitted data, and simultaneously track both the carrier and code signal components. From the code signal information can be derived on the pseudo-range from the receiver to satellite (corrupted by various errors), and from the carrier signal the time rate-of-change of this pseudo-range can be found.

Receiver operation in a high-dynamics environment, such as might be encountered in a missile or tactical aircraft, is considered here. The design-reference input signal to the X-set receiver is assumed to consist of a 10 g/s jerk (rate of change of acceleration) for 0.6 seconds, followed by a constant acceleration of 6 g's. If the receiver can cope with an input of this magnitude without losing lock (or rapidly slipping cycles), then it is felt that it will

---

[+]See Reference 1 for a description of the complete GPS signal structure.

116

not have difficulty with the normally-encountered input dynamics.

The extremely severe dynamic inputs mentioned above pose very stringent requirements on the X-set carrier-tracking loop. In order to avoid loss of lock (or cycle slipping), the carrier-loop tracking error (as will be shown later) must be limited to about 0.15 ft. (about 0.25 cycles at 1.575 GHz). To hold the peak transient error to values of this magnitude a wide-bandwidth tracking loop is required. A third-order tracking loop is also necessary to track a constant-acceleration input with zero steady-state error. The requirements of wide bandwidth and high-order tracking network in the presence of sampling and transport lags tend to make stabilization of the carrier tracking loop difficult.

Input noise to the receiver, on the other hand, leads to receiver-design requirements diametrically opposed to those imposed by input dynamics. Small tracking-loop bandwidths are desired in this case in order to minimize the tracking errors caused by the input noise.

If the carrier-tracking loop maintains lock, it can be used to aid the code loop and essentially isolate it from the incoming high-dynamics input signal. Under these conditions it is relatively easy to limit the code-loop tracking error to 25 ft. (1/4 chip), which is necessary for proper code-loop tracking. If, however, the carrier-tracking loop loses lock and starts slipping cycles at a rapid rate, then it will no longer be able to meaningfully aid the code-tracking loop. Under these conditions the unaided code loop will lose lock in a very short time if any significant input dynamics are present, since the current X-set code-tracking loop has only a first-order tracking-loop capability and a relatively narrow bandwidth.

An inertial measurement unit (IMU) mounted in the missile (or aircraft) is capable of providing information on the motion of the receiver antenna w.r.t. an inertially-fixed frame. If the IMU

117

is collocated with the receiver antenna, then only gravity-corrected accelerometer data are required. If, on the other hand, the IMU is a significant distance from the receiver antenna, then attitude data are required to compute the rotational velocity of the antenna w.r.t. the IMU.

By properly using IMU-derived data to aid the X-set tracking loops, the effective input dynamics to which these loops are subjected can be significantly reduced. For the carrier loop[*] this means a lower-bandwidth loop for a given input-dynamics level. The end result is a less difficult tracking-loop stabilization problem, and a reduction of the input-noise induced tracking error. For the code loop, IMU-derived data is very useful in the loss-of-carrier-lock situation. Under these conditions external input-dynamics information is necessary to help the low-bandwidth first-order code-tracking loop maintain lock.

This paper is concerned with techniques for utilizing IMU-derived information to aid the X-set code and carrier tracking-loop channels. Extremely important factors here are the rate at which new IMU-derived aiding information can be obtained, and the aiding prediction algorithms that are employed. The finite read times for the IMU (the basic measurement is average acceleration) and the required information processing times are both relevant. In addition, several different IMU-related error sources must be considered. The most important of these are attitude readout errors, IMU alignment errors, accelerometer bias, and accelerometer scale-factor uncertainties.

In the immediately-following sections a detailed description is given of the study-model X-set receiver. For simplicity and clarity, only baseband models are considered. The primary emphasis

_____

[*]The current design of the X-set does not provide for aiding of the carrier loop. Implementation of the aiding techniques presented herein would require modifications to the receiver design and to the interfaces between the receiver, data processor, and IMU.

is on those items that significantly affect the stability and accuracy of the tracking loops. A discussion of the IMU-aiding schemes examined follows next. Included here are the algorithms used to extrapolate IMU-derived information between successive data processing times.

The final two major sections present detailed tracking-loop simulation results for study and evaluation of IMU-aided tracking systems. Peak-transient and rms tracking errors are shown as a function of tracking-loop noise bandwidth for several different assumed conditions. Both aided and unaided system data are presented so that meaningful performance tradeoffs can be made. Monte-Carlo simulation results are also included for selected cases to provide data on the minimum C/N_0 (signal/noise power spectral density) at which tracking-loop lock can be maintained with the high-dynamics input present.

General Information

A functional description of the X-set receiver is given in Ref. 2,[*] including detailed information-flow charts for both the code and carrier tracking-loop channels. The receiver descriptions presented here and in the following section are based heavily on the information given in this reference.

The primary function of the carrier-tracking loop is to track the phase of the incoming carrier signal. A baseband information-flow diagram showing how this is currently accomplished in the X-set receiver is given in Figure 1. For convenience the tracking loop can be broken down into three major subsystems: 1) the error detector, 2) the digital tracking-loop network, and 3) the rate multiplier incremental-phase modulator (RM/IPM).

---

[*] During the course of this study the design of the X-set was in a process of evolution. The study is based upon information on the design made available to the authors as of approximately January 1977. Ref. 2 contains information on some of the more recent changes.

The error detector provides the basic measurement of tracking error between the phase of the incoming carrier signal and that provided by the tracking loop. The tracking-loop network performs the operations on the error signal that are necessary to maintain accurate tracking. The RM/IPM functions essentially as a digital voltage controlled oscillator (VCO), i.e. it advances or retards receiver-carrier phase estimates at rates based on the tracking-network commands.

Error Detector

To accurately estimate tracking error, the error-detector must remove both code and data modulations from the incoming signal. The code-signal demodulation is accomplished first, as shown in Fig. 1, by correlating the actual incoming signal with the receiver's estimate of this signal (obtained by modulating the carrier-loop RM/IPM output with the receiver's on-time estimate of the PRN code). Inphase and quadrature baseband error signals ($e_{Q_{CA}}$ and $e_{I_{CA}}$) are obtained continuously from the correlator as described in Ref. 2.

The quadrature error signal $e_{Q_{CA}}$ is given by:

$$e_{Q_{CA}} = k_{COD} \, d(t) \sin (e_{CA}) \qquad A(1)$$

where e_{CA} is the phase-tracking error of the carrier loop, and $d(t)$ is the binary data-modulation on the incoming signal (+1 or -1). The coefficient k_{COD}, which directly affects $e_{Q_{CA}}$, is a function of code-loop tracking error (e_{CO}), as indicated in Figure 1. The value of k_{COD} varies linearly from unity when the code loop is tracking perfectly, to zero when the code-loop error increases to about 100 feet (the code-loop chip width). For code loop errors greater than 100 ft., k_{COD} remains at zero. The inphase signal $e_{I_{CA}}$ is given by:

$$e_{I_{CA}} = k_{COD} \, d(t) \cos (e_{CA}) \qquad A(2)$$

where e_{CA}, k_{COD}, and $d(t)$ have the same meanings as in Eq. (1).

120

If the code and carrier tracking-loop errors are reasonably small, then $e_{Q_{CA}}$ can be used to estimate the carrier loop tracking error e_{CA}, and $e_{I_{CA}}$ can be used to estimate the data-bit polarity $d(t)$. The X-set receiver employs these two ideas, as described in Ref. 2 and shown in Fig. 2, in a Costas-loop configuration to measure carrier-loop tracking error. In the actual receiver mechanization, the 20-ms data-bit interval is subdivided into five 4-ms intervals, and average values of $e_{Q_{CA}}$ and $e_{I_{CA}}$ are computed for these subintervals using integrate-and-dump circuits. These subinterval values are in turn averaged over the data-bit interval to provide the averaged quadrature and inphase signals Q_k and I_k at the data-bit transition time t_k. An estimate of the carrier error $\hat{e}_{CA_k}$ is then computed from the relation

$$\hat{e}_{CA_k} = Q_k \, \text{SIGN} \, (I_k) \hspace{2cm} A(3)$$

where the caret (^) is used to indicate an estimated or computed value, and SIGN(·) means that the algebraic sign associated with (·) is used.

There are several important characteristics of this error detector that should be carefully noted here:

1) The error detector output $\hat{e}_{CA}$ will be a reasonably linear function of the input only for small values of e_{CA}, e.g. < 1 radian.

2) The data-bit polarity estimate reverses sign, and the Costas loop starts to slip a cycle, when the average carrier-loop tracking error for the data-bit interval exceeds 90°.

3) The code-loop tracking error e_{COD} affects the carrier-loop detector gain through the correlation coefficient k_{COD}.

4) The error detector provides updated error estimates only at the data-bit transition times (t_k) which are spaced 20 ms apart.

121

5) The tracking-error estimates $\hat{e}_{CA_k}$ in effect represent averaged values for the 20-ms period preceding the time t_k.

Tracking-Loop Network

In order to track the design-reference high-dynamics input with an acceptable accuracy, it is necessary to pass the carrier-loop error signal $\hat{e}_{CA_k}$ through a tracking network before feeding it to the RM/IPM. A digital tracking network is used in the X-set receiver, as shown in Fig. 1, with three parallel paths: a proportional path, an integral path, and a double-integral path. The digital-network input signal is sampled at 20-ms intervals (synchronized with respect to the data-bit transition times), and the contents of the integrators (accumulators) are updated at these times (t_k).

The proportional path signal is sent through the tracking network without additional delay. Because of computer-throughput limitations, however, there is an additional delay of up to 20 ms in the transmission of the signal and double integral path data to the RM/IPM, as indicated in Fig. 1.

Rate Multiplier/Incremental-Phase Modulator

The RM/IPM is used to control the phase or frequency of the carrier-channel's output signal. The operation of the RM/IPM or digital VCO is described in Ref. 2. Functionally the RM/IPM provides changes in output frequency directly proportional to the magnitude of the input command to the RM/IPM. If the output of the RM/IPM is viewed as phase rather than frequency, then the RM/IPM acts essentially as an integrator, i.e. the rate at which its output-signal phase is changed w.r.t. a reference frequency is proportional to the input-commanded signal.

The input to the carrier-loop RM/IPM in the X-set is sampled at 4-ms intervals, and the phase of the carrier-loop output signal

122

is advanced (or retarded) at a rate dependent on the magnitude of the command, as indicated in Fig. 1. The input command may be delayed by as much as 4 ms during the process of asynchronous transmission from the tracking network to the RM/IPM. Finally, there is a 1/64th of a cycle quantization level in the RM/IPM, i.e. the resolution of the incremental phase changes than can be made by the RM/IPM at a given time is about 0.01 feet. Any unused remainder from the current input command is saved for use on the next computation cycle.

CODE-TRACKING LOOP

General Information

The primary function of the code tracking loop is to follow the incoming PRM code, using a replica of the PRN pattern provided in the receiver. The X-set design, which is described in Ref. 2, utilizes a non-coherent error detector, i.e. knowledge of carrier frequency but not carrier phase is utilized to separate the incoming-signal code from its carrier. In addition, the code-loop error detector of interest here is time-shared between five different channels as described in Ref. 2. The end result is that the signal from a particular satellite is tracked for 40-ms time periods, spaced 200 ms apart. Aiding data from the carrier-tracking loop is used between the code-loop tracking periods to maintain code lock.

The code-tracking loop is again for convenience subdivided here into three major parts: 1) the error detector, 2) the tracking network, and 3) the RM/IPM. An information-flow diagram for the code tracking loop is given in Fig. 2.

Error Detector

Code-loop error estimates are based on correlations between the incoming signal and the signal estimates provided by the receiver. The operation is identical to that previously described for the carrier loop, except that the correlator uses early and late receiver-code estimates rather than on-time code estimates as in the carrier tracking loop. The procedure here is

123

to correlate w.r.t. early estimated code for half of each 40-ms
tracking period, and w.r.t. late estimated code for the other
half of the interval. The early and late code estimates used here
are displaced by $\pm 1/2$ chip ($\approx$ 50 ft.) w.r.t. the on-time code estimate.

Quadrature and inphase correlator output signals ($e_{Q_{CO}}$ and
$e_{I_{CO}}$) similar to those for the carrier tracking loop are obtained
first. For the early-code correlation period, the output signals
are:

$$e_{Q_{CO}}^{(E)} = k_{COD}^{(E)} \, d(t) \sin (e_{CA}) \qquad\qquad A(4)$$

and

$$e_{I_{CO}}^{(E)} = k_{COD}^{(E)} \, d(t) \cos (e_{CA}) \qquad\qquad A(5)$$

where the superscript (E) is used to denote that the correlations
are w.r.t. early-code estimates. The correlation coefficient
$k_{COD}^{(E)}$ is identical in form to the k_{COD} of Eqs. (1) and (2), except
that it is unity when the receiver's code estimate is 1/2 chip
(about 50 ft.) late. For the late-code correlation period
the output signals are:

$$e_{Q_{CO}}^{(L)} = k_{COD}^{(L)} \, d(t) \sin (e_{CA}) \qquad\qquad A(6)$$

and

$$e_{I_{CO}}^{(L)} = k_{COD}^{(L)} \, d(t) \cos (e_{CA}) \qquad\qquad A(7)$$

where the superscript (L) is used to indicate correlations w.r.t.
late-code estimates. The correlation coefficient $k_{COD}^{(L)}$ is similar
in form to $k_{COD}^{(E)}$, except that it is unity when the receiver's code
estimate is 1/2 chip early.

The error detector computes 4-ms average values for the
correlator outputs, using integrate-and-dump circuits in a similar
manner as in the carrier loop. These quantities are then averaged
over the appropriate data-bit interval to obtain the 20-ms
averaged signals $Q_{CO}^{(E)}$, $I_{CO}^{(E)}$, $Q_{CO}^{(L)}$, and $I_{CO}^{(L)}$.

The X-set receiver computes the code-loop tracking error $(\hat{e}_{CO})$ from the relation*

$$\hat{e}_{CO} = \frac{\Lambda}{2} \left[\frac{P_E - P_L}{P_E + P_L} \right] \qquad\qquad A(8)$$

where Λ is the PRN chip width (about 100 ft.). For mechanization convenience, the terms P_E and P_L are computed from the magnitudes of the I and Q signals rather than (in the more conventional way) from their squared values. The mathematical relations are:

$$P_E = |Q_{CO}^{(E)}| + |I_{CO}^{(E)}| \qquad\qquad A(9)$$

and

$$P_L = |Q_{CO}^{(L)}| + |I_{CO}^{(L)}| \qquad\qquad A(10)$$

where the notation $|(\cdot)|$ implies that the magnitude alone of $(\cdot)$ is to be used.

Certain basic characteristics of the code-loop error detector should be noted here:

1) The error detector output $\hat{e}_{CO}$ is a linear function of the true error e_{CO} only if the magnitude of e_{CO} is less than 1/2 chip (about 50 feet).

2) Updated estimates of $\hat{e}_{CO}$ for a particular code channel (satellite transmission) are provided only at 200-ms intervals, using correlation data for the preceding pair of 20-ms time intervals.

3) The detector is dithered, i.e. the early and late correlations are made for successive 20-ms time intervals rather than simultaneously.

4) The carrier-loop tracking error couples directly into into the code-loop detector, as indicated in Eqs(4)-(7).

---

*Since the completion of this study, the algorithm utilized in the computation of code-tracking error in the X-set has been modified. See Reference 2.

125

If the carrier loop starts to slip cycles at a rapid rate then the averaged correlator outputs Q_{CO} and I_{CO} will not provide useful error-detection information.

Tracking-Loop Network

The code-loop tracking network used in the current X-set receiver consists simply of a proportional path with no integrations. Tracking-error data from the detector is sampled at 200-ms intervals and sent forward to the code-loop RM/IPM. The code-tracking loop under these conditions is only a first-order system. Accordingly, velocity aiding data from the carrier loop or from the IMU is required to permit code-loop tracking of high-dynamics input signals.

RM/IPM

The code-loop RM/IPM functions basically as a digital VCO to advance or retard the phase of the receiver-indicated code at a rate proportional to its input command, i.e. dynamically it acts like an integrator. The RM/IPM is quantized to 1/64th of a chip, i.e. the resolution of the incremental phase change that can be made at a given time is about 1.6 feet. Any unused remainder from the current input command is saved for use on the next computation cycle.

IMU AIDING OF RECEIVER

Scope of Investigation

In order to keep the study within reasonable bounds, certain ground rules were established at the outset. Since these assumptions significantly affect the subsequent study results, it is appropriate to mention them here.

1) The X-set receiver model to be used would follow closely that given in the preceding sections, e.g. the sampling procedures and tracking-network structure would not be changed.

2) Only floated or gimballed IMUs would be considered here, i.e. strapdown IMUs would not be investigated.

126

3) An IMU of high accuracy is assumed, i.e. one with performance characteristics on the order of 1 nmi/hr or better.

4) To simplify the interface with the receiver, it is assumed that the IMU-aiding data are fed into the tracking loops following the tracking networks.

5) A dedicated computer (microprocessor) is assumed to be available for rapid computation of the necessary aiding information from the IMU-measured data.

6) Aiding of the inertial-navigation system with GPS updates to bound its errors is not investigated here.

7) A rigid structure is assumed between the IMU and receiver antenna, i.e. no bending or flexure is assumed to be present.

Basic Design Considerations

An IMU is capable of aiding the code and carrier channels of the X-set receiver by providing information on the motion of the vehicle in which the antenna is mounted. If the IMU is located extremely close to the antenna, then only accelerometer-derived data are required for keeping track of antenna motion. If, on the other hand, there is a significant displacement between the IMU and receiver-antenna of interest, then IMU-derived attitude data will be required to compute any angular rotation of the IMU w.r.t. the receiver antenna.

An inertially-fixed instrument package is assumed, containing three single-degree-of-freedom gyros and integrating accelerometers. To properly aid the receiver with IMU data, it is necessary to determine the component of antenna motion along the line-of-sight from the satellite to the antenna. This information can then be used as an input to the carrier and code RM/IPMs to improve tracking-loop performance when significant vehicle (antenna) motions are present.

There are several problems associated with the use of IMU data for receiver aiding. First of all, the basic integrating-

127

accelerometer output is the vehicle velocity change (due to non-gravitational forces) over a finite read interval. In effect the measurement is average rather than instantaneous acceleration. Errors will be introduced in the estimates of position if the vehicle undergoes rapid motion changes over the measurement interval. In addition, certain operations required in the processing of the IMU data, e.g. coordinate transformations and gravitational-force computations, can introduce delays in the computation of antenna position and velocity. As a point of reference, the delays for carrier-loop aiding in the design-reference environment, should be no more than a few milliseconds.

To most effectively utilize IMU-derived accelerometer data under the above mentioned conditions, it is necessary to extrapolate the position and velocity estimates until the next data are received. A similar problem exists when rotational velocity is to be computed and extrapolated based on a series of discrete IMU-derived angular-orientation measurements. Relations used to accomplish these operations are given in the following section.

The ability of the IMU to measure motion of the receiver antenna is limited by various error sources such as IMU alignment, accelerometer bias and noise, and accelerometer scale-factor uncertainties. Insofar as the receiver is concerned, these errors are like disturbance inputs to the tracking loops. The tracking loops must have sufficient bandwidth to limit the tracking errors introduced by these sources to acceptable values. This can be a problem in the first-order code loop, if carrier-loop aiding is not available.

In concluding this section, it should be noted that IMU aiding will permit the tracking loops to handle high-dynamics inputs with reduced bandwidths. The minimum tracking-loop bandwidths must, however, be sufficiently large to handle input commands and system disturbances not measured by the IMU, e.g. frequency-reference noise, satellite ephemeris variations, ionosphere-induced propagation-velocity changes, and IMU measurement errors.

IMU-Data Extrapolation

To circumvent the problem of discrete-time IMU data, a predictor is used to estimate antenna position changes at times following the last available IMU data. The basic relations are developed.

The antenna position (r) at time t is given by:

$$r = r_k + v_k(t - t_k) + \frac{a_k}{2}(t - t_k)^2 + \frac{j_k}{6}(t - t_k)^3 \quad A(11)$$

where r_k and v_k are IMU-derived estimates of vehicle position and velocity at the last IMU-processing time t_k. The estimated acceleration and jerk components at this time are a_k and j_k. For convenience, only the scalar, single-component relations are given here.

The IMU-derived estimate of future vehicle position change between times t and t + T (both between t_k and t_{k+1}) is obtained by using t and t + T in Eq.(11), and taking the difference between the resultant position estimates. The resultant expression for the position change δr for the computation interval T is:

$$\frac{\delta r}{T} = v_k + a_k(t - t_k + \frac{T}{2}) + j_k\left[\frac{(t - t_k)(t - t_k + T)}{2} + \frac{T^2}{6}\right] \quad A(12)$$

where v_k, a_k, and j_k represent IMU-derived estimates of vehicle velocity, acceleration, and jerk at the most recent IMU-data processing time t_k. The constant-rate signal applied to the RM/IPM over the interval T to implement the δr is simply $\delta r/T$.

To compute a_k from the integrating-accelerometer data, the last two measurements are used in the relation:

$$a_k = \frac{(1.5 \Delta v_k - 0.5 \Delta v_{k-1})}{t_k - t_{k-1}} - g_k \quad A(13)$$

where Δv_k represents the accelerometer-measured velocity change over the time interval from t_{k-1} to t_k, and j_k is the average gravitational specific force acting on the vehicle during this period. The jerk

129

j_k is obtained simply from the back difference $a_k - a_{k-1}$ divided by $t_k - t_{k-1}$.

When the antenna and IMU are not collocated, it is necessary to compute the rotational velocity of the antenna w.r.t. the point at which the IMU is located. To accomplish this, it was assumed that over short time intervals the orientation angles (θ) of the antenna with respect to the inertial-reference frame could be represented as polynomial functions of time (τ), e.g.

$$\theta(\tau) = C_0 + C_1\tau + C_2\tau^2 + C_3\tau^3 \qquad A(14)$$

where the coefficients C_0, C_1, C_2, and C_3 are functions of the IMU-angle measurements. For computational simplicity, a least-squares fit to the five most-recent angle measurements (assumed equally spaced in time) was used to determine C_0, C_1, C_2, and C_3, as described in Ref. 3. Better estimation accuracy might be possible using larger or smaller data sets, or even other estimation schemes, but the one described above was felt to be adequate for the problem of interest here.

The coefficients C_i in Eq.(14) are weighted sums of the angle measurements sets $\underline{\theta}$, i.e.,

$$C_i = \underline{W}_i \cdot \underline{\theta} \qquad A(15)$$

where $\underline{W}_i$ represents the set of weighting factors to be used with the angle-measurement set $\underline{\theta}$ to compute C_i. If a specific number of angle measurements with fixed spacing is always used, then $\underline{W}_i$ needs to be computed only a single time. The detailed relations for $\underline{W}_i$ are given in Refs. 3 and 4.

Using the coefficients C_i in Eq.(14), the orientation of the antenna at a given time t, follwoing the last angle measurement θ_k at time t_k, can readily be computed. The desired antenna position change (δr) over the computation interval T is then obtained using the predicted angle change ($\delta\theta$) in combination with the lever arm (ℓ) from the IMU to the antenna.

130

SIMULATION RESULTS

Description of Simulation

A comprehensive single-channel simulation has been developed to study the problem of IMU aiding of the GPS X-set receiver. The simulation is basically at baseband, and is described in detail in Ref. 4. Some of the key features will be mentioned briefly here.

The receiver simulation is extremely detailed. Included in the error-detector models are the correlator nonlinearities, the cross-coupling between code and carrier channels, the integrate-and-dump circuits, the A/D converters, and the different sampling rates present in the system. The tracking networks are modeled as digital systems, updated at discrete time periods and with transport lags present. The RM/IPMs are modeled as digital integrators, appropriately quantized.

The IMU model provides for both velocity-change (from accelerometers) and angular-orientation measurements. The measurements are provided at discrete time periods with transport lags present. The typical IMU errors such as IMU alignment, gyro drift-rate bias, acceleration-sensitive drift, accelerometer bias, accelerometer scale-factor, accelerometer measurement noise, attitude measurement bias, and attitude-measurement noise are all included.

Provisions are made for aiding either or both the code and carrier loops with IMU-derived antenna position-change predictions. Alternately, carrier-loop data can be used alone to aide the code loop.

The current simulation provides models for both receiver input noise and various user frequency-reference disturbances. The input noise is represented by a random sequence providing a flat

131

power spectral density over the system frequencies of interest. The frequency-reference model includes both white and flicker frequency noise, in combination with acceleration-sensitive frequency drift.

Computation of Noise Bandwidth

In the following sections, tracking-performance data will be presented for both aided and unaided tracking configurations. Much of the data will be in the form of peak and rms tracking errors, since these are useful indicators of the probability of loss-of-lock or cycle-slipping. The tracking-error data will for convenience be presented as a function of noise bandwidth, since this provides a convenient measure of noise transmission through the tracking loops. A clarification of the term "noise bandwidth" as used in this paper will be given next.

For a linear continuous system with a low-pass closed-loop frequency-response function $H(\omega)$, it can be shown that the output power (σ_0^2) for a white noise input with flat power-spectral density N_i is given by the relation

$$\sigma_0^2 = \frac{1}{2\pi} \int_0^\infty N_i |H(\omega)|^2 \, d\omega \qquad\qquad A(16)$$

where ω is angular frequency in rad/s. The input power spectral density (N_i) is single-sided and in units of power/Hz. The units of the output (σ_0^2) are also power, e.g. ft^2 or rad^2. It is convenient to rewrite Eq.(16) in the form

$$\sigma_0^2 = N_i B_n \qquad\qquad A(17)$$

where B_n is called the single-sided low-pass noise bandwidth. The defining relation for B_n is thus

$$B_n = \frac{1}{2\pi} \int_0^\infty |H(\omega)|^2 \, d\omega \qquad\qquad A(18)$$

where the units of B_n as defined here are Hz or cycles/second.

132

An accurate computation of B_n for this problem requires that the effects of sampling and transport lags be accounted for. To determine B_n as a function of tracking-loop network parameter values under these conditions the output power from the tracking loops (i.e. the rms errors) was measured for white-noise (random-sequence) input signals, using the detailed X-set simulation. To obtain meaningful results, it was necessary to make the following modifications for these particular test runs: linear error detector, uncoupled code and carrier loops, no quantization of A/D conversion errors, and no receiver frequency-reference noise. The important sampling and transport lags present in the receiver do, however, enter into the computation of B_n.

Carrier-Loop Aiding Under Ideal Conditions

As a starting point, the tracking loop performance was investigated under ideal conditions: linear error detector, no frequency-reference noise, no quantization errors, and no input noise. All sampling and transport delays were included.

In these initial test runs, no IMU velocity-change measurement errors were present. It was assumed, however, that IMU measurements data would be processed at discrete time periods, e.g. every 10 or 100 ms.

The tracking-network parameters used in these test runs (proportional and integral-path gains) were based on Mallinckrodt network designs for continuous, linear systems with no transport lags (Refs. 5 and 6). Mallinckrodt design parameters were used here rather than those for Wiener designs (Refs. 7 and 8) because in the presence of the assumed sampling and transport lags, they provided better tracking-loop stability at the larger noise bandwidths.*

The peak-transient tracking errors for the carrier loop are presented in Fig. 3 as a function of measured tracking-loop noise

---

*Even better performance might be achieved via an iterative optimization of loop-filter parameters.

133

bandwidth (B_n). For convenience, both of these quantities are plotted
using logarithmic scales, to cover the wide range of numerical values.
The tracking errors are presented in feet. To convert these
errors to radians at the carrier frequency of 1.575 GHz, a multi-
plication by a factor of approximately 10 is required.

A horizontal line is shown in the various data plots at an
error of about 0.15 feet (about 90 degrees). If the average carrier-
loop tracking error over the 20-ms data-bit interval exceeds this
value, then the tracking loop will generally start to slip cycles.

To more clearly indicate the significance of noise bandwidth,
curves of rms tracking error corresponding to different values
of input signal to noise spectral density (C/N_0) are superposed
on Fig. 3 as dashed lines. The basic system-design tradeoff
is clearly shown: increasing the noise bandwidth reduces the errors
caused by input dynamics, but the noise-input tracking errors are
increased.

There are several points of interest in the data of Figure 3.
First of all, even for the assumed idealized conditions, the unaided
carrier tracking loop is unable to hold the peak-transient tracking
error for the high-jerk trajectory below the desired 0.15-ft. value,
unless a very wide noise bandwidth is used. Under these conditions,
the overall tracking loop has a large peak overshoot in response
to a small phase-step input, as indicated in Figure 4, even though
its response to a high-jerk input is seen to be well behaved.

When IMU aiding is employed, a significant reduction in peak-
transient carrier-track loop error is obtained, as indicated in Figure 3.
The minimum noise bandwidth to limit the peak error to 0.15 feet, as
can be seen, is reduced from an unaided value of about 30 Hz to a
much lower value of about 1-2 Hz with IMU aiding. At the larger
values of noise bandwidth shown in Figure 3, a significant reduction
in peak error is obtained by decreasing the interval at which IMU
data are processed from 100 to 10 ms.   At the lower noise band-
widths, on the other hand, the differences in peak error are much
less.

134

In order to properly interpret the data of Fig. 3, two important points should be noted. First of all, for most effective aiding, the IMU-derived information must get to the tracking-loop input point (where it can reduce the effective input dynamics) with a minimum delay. In this regard, computation delays in the IMU-data processing and transmission to the RM/IPM can limit the ability of the IMU to aid the receiver. Secondly, the algorithm used to extrapolate (i.e. predict) aiding signals in between IMU-data processing times is extremely important, particularly at low IMU-data rates such as 10 Hz (100-ms intervals). In the problem of interest here, for example, a 3rd-order extrapolation algorithm including all terms up to jerk, provides better performance than a 2nd-order algorithm including only terms up to acceleration.

As a result of the above-mentioned computation lags and extrapolation-algorithm imperfections, errors were introduced into the IMU-aiding process (in addition to those caused by the basic instrument errors and finite sampling rate). These errors must ultimately be tracked out by the receiver and, hence, place lower limits on the permissible tracking-loop noise bandwidths. With large noise bandwidths, as can be seen in Fig. 3, the peak-transient tracking errors for the aided systems are small, because of the greater tracking capability of the receiver.

A detailed analysis of the results shown in Fig. 3 indicates that the 100-ms aiding-algorithm extrapolation errors tended to cancel in part the errors caused by the 4-ms delay in transferring the IMU-aiding data to the RM/IPM. Because of this phenomenon, the data indicate slightly smaller peak-trnasient errors with a 10-Hz update-rate than with a 100-Hz rate at very low noise bandwidths (e.g. 0.3 Hz). With a more sophisticated extrapolation algorithm that properly accounts for all delays in the transmission of information from the IMU to the RM/IPM, the 100-Hz update-rate will provide better performance than the 10-Hz update-rate at all noise bandwidths. The data in Fig. 3 indicate performance improvements achievable with IMU aiding, although they are not necessarily the absolute optima.

135

Time histories of carrier-loop tracking error for the same
conditions as in Fig. 3 are shown in Figs. 5 and 6 for noise band-
widths of 1, 3, and 7 Hz, with IMU-data processing intervals of 10 and
100 ms. Two distinct transients occur: one at the time that the
10-g/s pulse is applied, the other when it is removed. For the
case where IMU data are processed at 100-ms intervals the character-
istics of the algorithm used to extrapolate the IMU-derived velocity
estimate are important, as can be seen in Fig. 6.

Frequency-Reference Errors

The receiver error detector correlates its own estimates
of the incoming signal (code and carrier) with the actual incoming
signal to derive code and carrier loop tracking errors. Accordingly,
any drift or noise present in the receiver's frequency reference
will introduce errors into the tracking loop. These disturbances, if
of significant magnitude, must be tracked out (followed) by the
code and carrier loops to avoid the buildup of significant tracking
error. The tracking loops themselves must have significant band-
width to accomplish this, since IMU-derived velocity-change data
will not help here except that acceleration data could be used to
compensate for errors in the freuqency reference on the basis of a
precalibrated dynamic model.

Three sources of frequency-reference error are considered
here: acceleration-sensitive frequency drift, white frequency noise,
and flicker frequency noise. On the basis of currently-available
frequency-reference information (Refs. 9-12) it is felt that
acceleration-sensitive drift will introduce the largest error of the
above three sources. For a drift of 1×10^{-9}/g, which is repre-
sentative of current frequency standards, the equivalent disturbance
input to the tracking loop caused by the high-jerk trajectory is an
acceleration pulse of about 10 f/s^2 for 0.6 seconds, followed by a
constant-velocity disturbance thereafter as shown in Fig. 7.

The carrier-loop tracking errors introduced by the above
mentioned frequency-reference-source errors are shown in Fig. 8.

For the typical acceleration-sensitive drift of 1×10^{-9}/g it can be seen that the minimum required noise bandwidth for successful tracking during the high-jerk trajectory is about 6 Hz. If the drift could be reduced (or compensated) down to 1×10^{-10}/g, then a lower noise bandwidth of about 1 Hz would be acceptable.

For the assumed values of white and flicker frequency noise, which are representative of current references, it can be seen that the resultant rms tracking errors are very small over the range of noise bandwidths of interest here, i.e. 1 - 10 Hz. If the desired noise bandwidths were extremely small, e.g. 0.01 Hz, then these noise sources would be significant error contributors.

IMU Measurement Errors

Errors in the IMU-derived velocity estimates used to aid the carrier tracking loop in effect represent disturbance inputs, which must be handled by the tracking loops in a similar manner as with the frequency-reference disturbances. The particular error sources considered here are random velocity-readout error, accelerometer-bias error, and accelerometer scale-factor error. IMU alignment errors, which were not explicitly considered here, exhibit short-term characteristic similar to those for accelerometer scale-factor errors.

Carrier-loop tracking errors from the three above-mentioned error sources are shown in Fig. 9 for the high-jerk input trajectory as a function of noise bandwidths. For illustrative purposes the numerical values used here for the instrument errors are roughly representative of an IMU that might be used in the shuttle orbiter vehicle. The instrument errors for a strategic missile IMU would probably be smaller. Under these assumed conditions it is evident that the IMU-measurement errors are not a significant factor in determining carrier-loop tracking errors.

With lower quality inertial instruments or smaller noise bandwidths, on the other hand, IMU measurement errors could significantly affect the tracking errors. If, for example, the desired

137

noise bandwidth were 0.3 Hz, then a 100-ppm scale-factor error
would contribute more than 0.1 feet of peak carrier-loop tracking
error.

Rotational-Input Errors

   IMU-derived velocity estimates can provide useful informa-
tion for the carrier-tracking loop as noted in this paper. If
there is significant rotational motion of the vehicle and the IMU
is not colocated with the receiver antenna, then the rotational
velocity of the antenna w.r.t. the IMU must also be computed.
Angular-orientation measurements from the IMU can be used to
estimate this rotational velocity, as described earlier in this
paper.

   As a basis for study of this problem, a sinusoidally-varying
angular rotation of the vehicle is assumed with a peak-to-peak
amplitude of 1.4 degrees at a frequency of 1.1 Hz. This rotational
motion provides a maximum angular velocity of 5 deg/s and a maxi-
mum angular acceleration of about 0.5 rad/s^2. The IMU is assumed
to be displaced from the antenna, as indicated in Figure 10, i.e. the
rotational-velocity lever arm is 2 feet.

   The rms carrier-loop tracking errors from the rotational
velocity are shown in Fig. 10 as a function of tracking-loop noise
bandwidth. Several cases are considered with different IMU-data
update rates and extrapolation algorithms.

   It should be noted that a significant reduction in tracking
error is obtained from IMU aiding even with no rotational correc-
tions, if the IMU is located reasonably close to the antenna.
The rotation-velocity lever arm, as can be seen in Figure 10, is
reduced in this case from the distance between antenna and axis of
rotation (m) to the distance between antenna and IMU (ℓ).

   When angular-orientation measurements are utilized to
estimate the rotational velocity component, a larger reduction in
tracking error can be obtained, as can be seen in Figure 10.

138

The angular rotational velocity estimates, as noted earlier, are
based on a least-squares fit to polynomial functions of time, using
the 5 latest angular-orientation measurements. When angle measure-
ments were provided at 100-ms intervals, a 3rd-order polynomial
was required to obtain reasonable velocity prediction accuracies.
When angle measurements were provided at 10-ms intervals, on
the other hand, a 2nd-order polynomial was satisfactory. A
significant reduction in error, as indicated in Fig. 10, was obtained
by increasing the frequency of measurements from 10 to 100 Hz.

To assess the effect of measurement noise, a 1-mr rms
uncorrelated error was assumed to be present in each angle measure-
ment. This magnitude of error is again representative of IMUs
currently under consideration for the shuttle orbiter vehicle.
For the data shown in Fig. 10, it is evident that the measurement
errors cause a significant degredation in tracking error. It
also appears that the higher-order prediction algorithm (3rd-order)
is more sensitive to measurement errors than the lower order algorithm.

Time histories of the carrier-loop tracking errors for the same
input conditions as in Figure 10 are shown in Figure 11. A noise
bandwidth of 1 Hz is assumed in all three cases shown. A signi-
ficant reduction in rms tracking error is obtained with IMU
angle-measurement data, as can be seen, when a 100-Hz data rate
is used (angle measurements at 10-ms intervals).

Monte-Carlo Study Results

A series of Monte-Carlo test runs were made for the X-set
receiver to determine the lowest value of C/N_0 at which the tracking
loops would reliably track the high-jerk design-reference trajectory.
An extremely high accuracy IMU was assumed in these test runs such
that its measurement errors did not sufficiently affect the tracking-
loop performance. Detector nonlinearities, receiver sampling and
transport lags, receiver frequency-reference disturbances,
and RM/IPM quantization errors were all included here. IMU aiding
was provided to the carrier loop, which in turn was used to aid the
code loop.

139

In the presentation of data, certain special terminology is used. A successful run in one in which the carrier loop either continuously maintained lock or temporarily slipped cycles during the run-time period of interest. A failed run is one in which the carrier loop lost lock and did not recover it during the run-time period.

As a starting point, data are presented in Table 1 for the unaided X-set receiver. To obtain satisfactory performance under these conditions, extremely wide noise bandwidths are required. The end results is that the minimum C/N_0 for successful carrier-loop tracking during the high-jerk trajectory was relatively large, i.e. about 28 dB-Hz. Time histories of code and carrier loop tracking errors for a typical test run under these conditions are shown in Fig. 12.

When IMU-aiding data are provided to the carrier loop at 100-ms intervals, a reduction in the minimum C/N_0, i.e. the threshold, for successful tracking during the high-jerk trajectory is obtained, as indicated in Table 2. With a frequency-reference drift of 1×10^{-9}/g present, a threshold of about 24 dB-Hz is obtained. This can be reduced further to about 20 dB-Hz if the frequency-reference drift is lowered to 1×10^{-10}/g.

Aiding the carrier loop more frequently at 10-msec intervals provides at best a small additional reduction in threshold, as indicated in Table 3. With a frequency-reference drift of 1×10^{-9}/g, the threshold is essentially unchanged at about 24 dB-Hz. With a reduction in frequency-reference drift to 1×10^{-10}/g, the threshold is lowered slightly to about 18-20 dB-Hz.

Representative time histories of code and carrier loop tracking errors are shown in Figures 13 and 14 for values of C/N_0 close to threshold. IMU-aiding information is provided in Figure 13 at 100-ms intervals, and in Fig. 14 at 10-ms intervals. The peak carrier-loop tracking errors in these runs are held below about 0.15 feet, which is typical of test cases in which lock is continuously maintained. The code-loop tracking errors, as can

140

be seen, are well behaved and generally smaller than 10 feet, provided that reasonably accurate velocity-aiding information is furnished from the carrier loop (which itself is IMU aided).

Under certain conditions it is possible for the aided receiver to slip cycles, but ultimately regain lock. This is shown in Fig. 15 where the carrier loop has slipped 1.5 cycles during the high-jerk portion of the trajectory. The code-tracking loop in this case is not significantly affected by the slipped cycles.

IMU Aiding When Carrier-Loop Has Lost Lock

Under certain conditions, e.g. at very small values of C/N_0, it is possible for the carrier loop to lose lock or start to slip cycles at a rapid rate. IMU aiding in this type of situation can often permit the code loop to remain in lock until carrier-loop reacquisition is obtained.

For meaningful code-loop tracking to take place, it is necessary to limit the error in the frequency reference to values below the data-bit rate. If a greater frequency-reference error occurs, the end result is that the code and carrier loop correlator outputs averaged over the data-bit interval become very small, and error-detection capability is lost. By using IMU information to control the receiver's carrier-frequency estimate, the detection of the incoming carrier and code can be improved.

If the rate of cycle-slipping in the carrier loop is reasonably well controlled, then direct IMU-aiding of the code loop can help the code loop stay in lock as is accomplished by the X-set in the "HOBYT" mode. The decision as to whether IMU-derived data or carrier tracking-loop information should be used to aid the code loop, depends on how well the carrier loop is tracking.

Tracking-error data are presented in Fig. 16 for a simulated situation where IMU aiding of the code loop permits it to stay in lock during a period where the carrier loop had lost lock. The IMU is used for estimating the Doppler shift for error detection. The dynamic input signal used here is the design-reference high-jerk

141

trajectory described earlier. The assumed C/N_0 in the test run was 14 dB-Hz.

A key point shown in Fig. 16 is that by IMU-aiding the X-set receiver, it is possible to maintain code-loop lock during periods when the carrier loop is slipping cycles at a very high rate. Because of the 1st-order characteristics of the code loop, however, it is subject to tracking errors from sources such as frequency-reference acceleration sensitive drift of IMU bias and scale-factor errors. Unless these errors are reasonably small, or a higher-order code-tracking loop is used, or the carrier loop regains lock, these errors could ultimately cause the code loop to eventually break lock.

SUMMARY AND CONCLUSIONS

An investigation has been made of the use of IMU-derived information to aid the X-set carrier and code tracking loops in a high-jerk environment. *Detailed simulations of the X-set receiver* and an IMU have been developed and used to accomplish this study.

Without IMU aiding, a carrier tracking loop threshold of about 28 dB-Hz is obtained. When IMU aiding is employed, the carrier-tracking loop bandwidth can be reduced. Acceleration-sensitive frequency-reference drift, which must be tracked out by the receiver, is an important factor in limiting the minimum noise bandwidths that can be used. With an acceleration-sensitive drift of $1 \times 10^{-9}/g$, a threshold of about 24 dB-Hz was obtained. If the drift were limited to a value of $1 \times 10^{-10}/g$, then a lowering of the carrier threshold to about 20 dB-Hz would be possible.

Improvements in tracking-loop performance were obtained when the rate at which IMU-derived data were processed was increased from 10 Hz (100-ms intervals) to 100 Hz (10-ms intervals). Carrier-loop thresholds were not, however, significantly affected by this data-rate change, because of the dominant *effect of acceleration-sensitive frequency-reference drift.* Rotational-velocity estimates, on the other hand, were much improved by an increase in IMU-angle data rates.

142

Finally, it should be noted that to most effectively IMU-aid the X-set receiver, all delays in the transmission of aiding signals to the RM/IPM must be minimized and accounted for in the aiding estimation algorithms. Errors introduced into the tracking loop by sources such as the IMU-data extrapolation algorithm or frequency-reference acceleration-sensitive drift, limit the extent to which tracking-loop noise bandwidth can be reduced.

ADDENDUM

In recent studies where IMU aiding was used in the carrier tracking loop, it was found that a 4-ms lag in the transmission of IMU data to the RM/IPM has created problems (Refs. 13 and 14). A new algorithm has been developed which accounts for the presence of this transport lag. Simulation results are presented to show the maximum carrier-loop tracking errors as a function of tracking-loop noise bandwidth. Also included are time histories of the carrier-loop tracking errors. No input noise or frequency-reference errors are included in any of the test runs, and a linear error detector is assumed.

The main point of interest is that with the transport lag accounted for in the extrapolation algorithm, a significant reduction in carrier tracking error (with respect to the data of Refs. 13 and 14) is obtained at the 100-Hz data-rate case. Under these conditions a significant reduction in peak tracking error is obtained by increasing the IMU data rate, as indicated in Figure 1.

143

REFERENCES FOR APPENDIX A

1. "System Specification for the NAVSTAR Global Position System Phase 1", SS-GPS-101B, SAMSO/YE.

2. Stonestreet, W.M., "A Functional Description of the NAVSTAR GPS Receiver Model X", CSDL Report R-981, Rev. 1, February 1977.

3. Hildebrand, F.B., Introduction to Numerical Analysis, McGraw-Hill 1956.

4. Kriegsman, B.A., Stonestreet, W.M., and Cox, D.B., Jr., "IMU Aiding for GPS X-Set Receiver", CSDL Report for SAMSO Constract F04701-75-C-0212, currently in preparation.

5. Taylor, R.E., "Satellite Tracking Simultaneous-Lobing Mono-pulse Receiving System with Polarization Diversity Capability", IEEE Transactions Aerospace and Electronics Systems, Vol. 3, No. 4, July 1967.

6. Filippi, E., "CO2 Laser Ranging Systems Study", Old Dominion Systems, Inc., May 1975, N75-29410.

7. Jaffe, R., and Rechtin, R., "Design and Performance of Phase-Lock Circuits Capable of Near-Optimum Performance over a Wide Range on Input Signal and Noise Levels", IRE Transaction on Information Theory, Vol. IT-1, March 1955.

8. Lewis, P.W., and Weingarten, W., "A Comparison of Second, Third, and Fourth Order Phase-Locked Loops", IEEE Transactions on Aerospace and Electronics Systems, Vol. AES-3, No. 4, July 1967.

9. "Time and Frequency" Theory and Fundamentals", NBS Monograph 140, May 1974.

10. Hellwig, H., "A Review of Precision Oscillators", NBS Technical Note 662, February 1975.

11. Harton, P.L., "Frequency-Standard Stability for Doppler Measurements On-Board the Shuttle", Lockheed Electronics Co., Inc., Report LEC-3964.

REFERENCES (cont'd) FOR APPENDIX A

12. Przyjemski, J., and Konop, P., "Limitations on GPS Receiver
     Performance Imposed on Crystal Oscillator G-Sensitivity",
     CSDL Report P-432, March 1977.

13. Kriegsman, B.A., "Transport Lags on IMU-Aiding Data," Draper
     Laboratory Memo BAK-GPS-8, May 25, 1977.

14. Kriegsman, B.A., Cox, D.B., Jr., Stonestreet, W.M., "IMU-Aided
     GPS Receiver," Draper Laboratory Report P-490, June 1977.
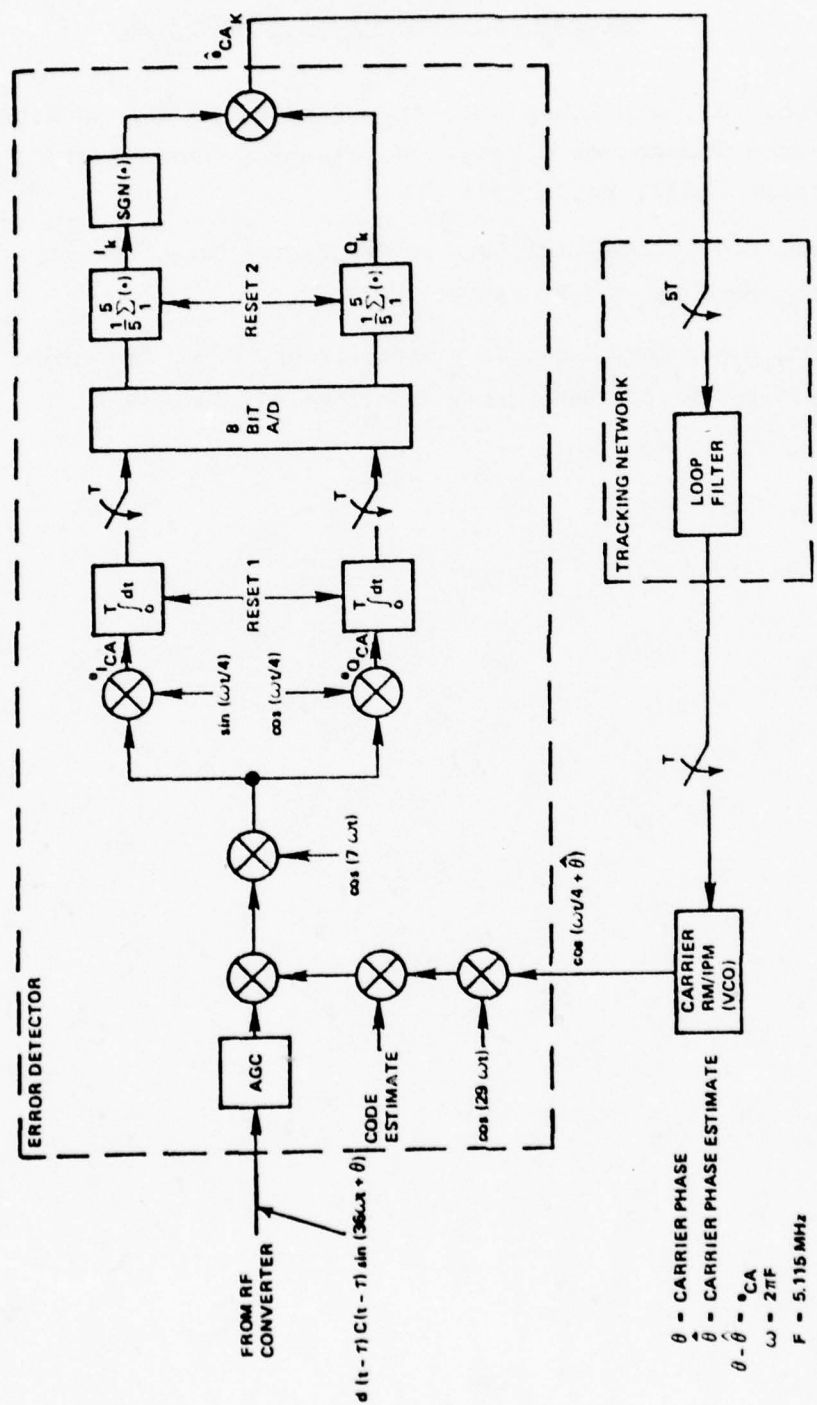
Figure A-1. X-Set Costas Loop Implementation.

146

Figure A-2 X-Set Code Loop Implementation.

147

7706A2522

Figure A-3 Linear Carrier Tracking Errors for High-Jerk Trajectory.

148
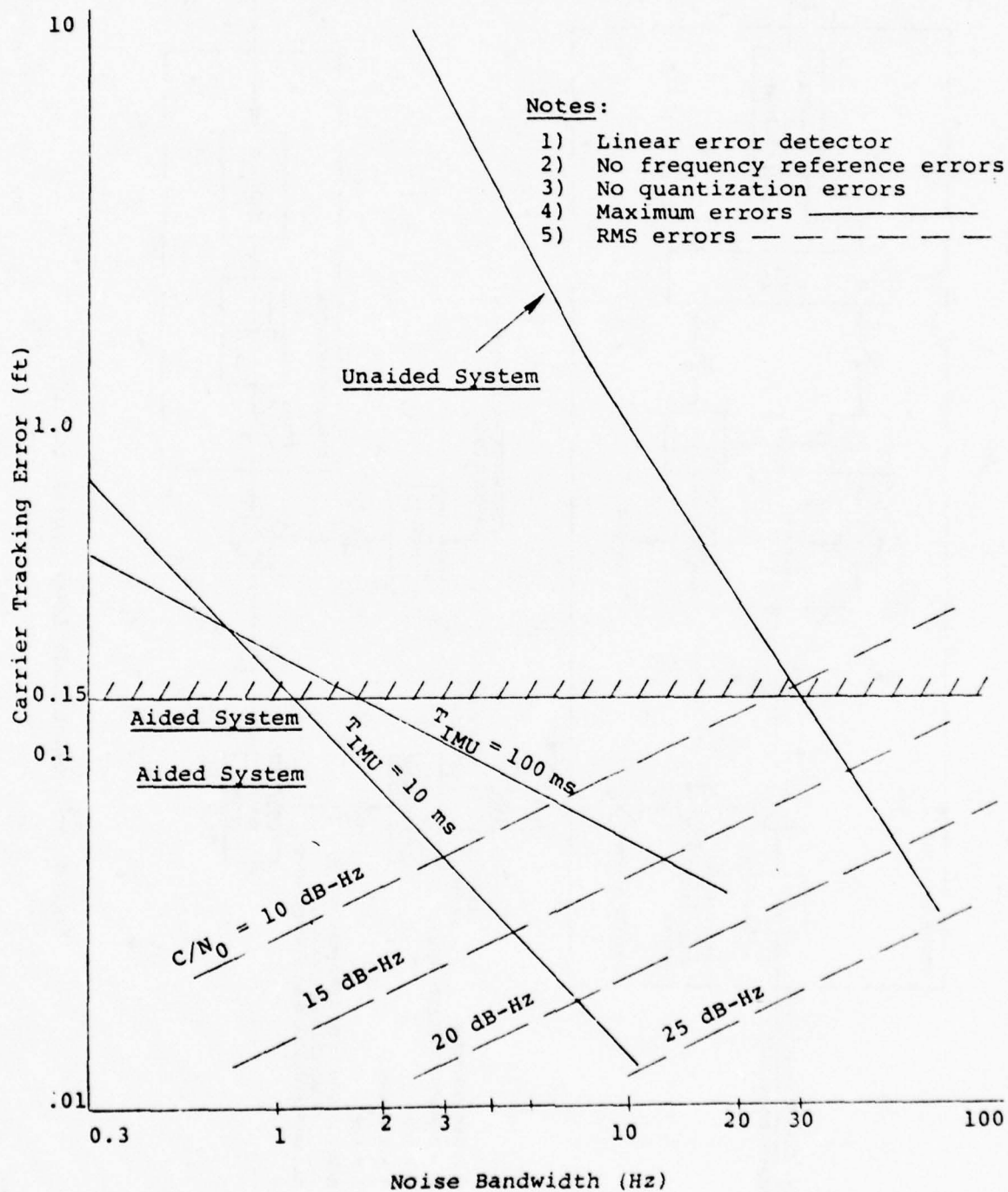
Figure A-4. Carrier-Loop Errors for Phase-Step and High-Jerk Inputs

Mallinckrodt design with B_n = 32 Hz.

Notes:
1) Linear error detector
2) No input noise
3) No frequency-reference errors

High-Jerk Input

Phase-Step Input (0.1 ft)

149
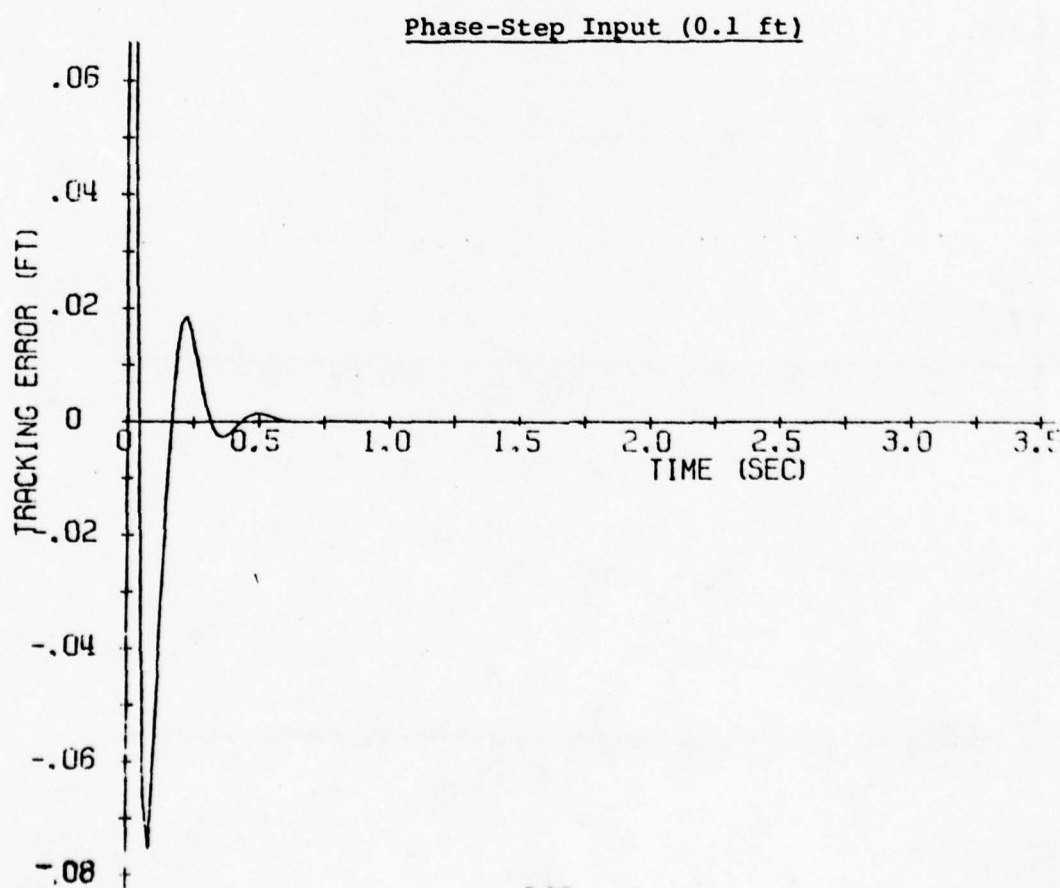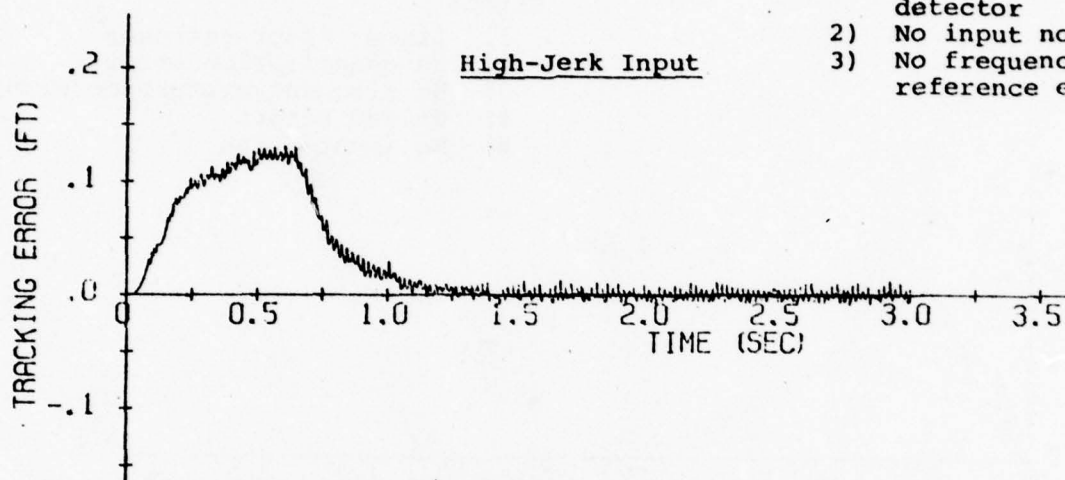
Figure A-5. <u>IMU-Aiding (T = 100 ms) for High-Jerk Trajectory</u>.

Carrier Tracking Errors

<u>Notes:</u>
1) Linear error detector
2) No quantization errors
3) No frequency-reference errors
4) No IMU errors
5) No input noise
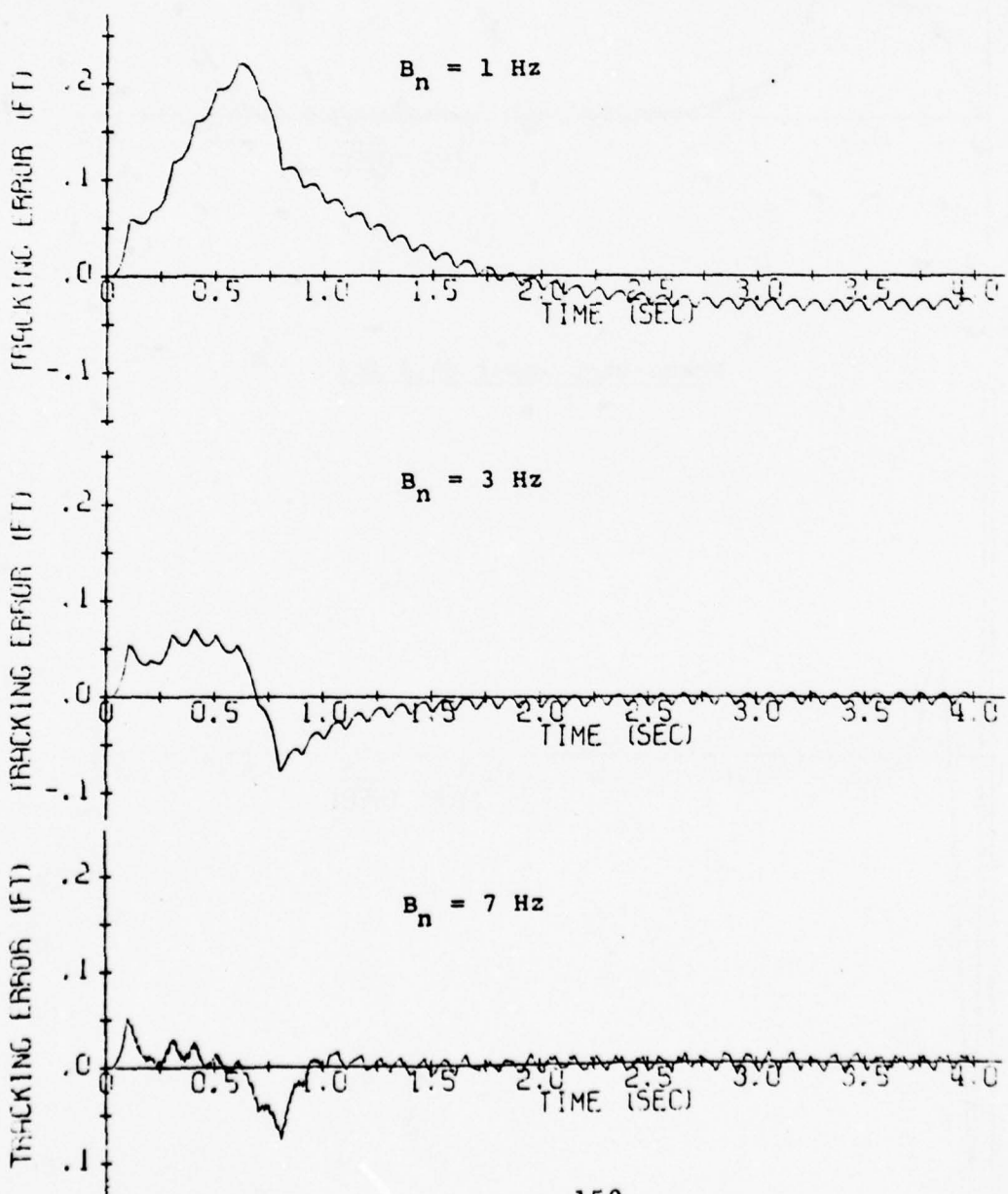
Figure A-6. <u>IMU-Aiding (T = 10 ms) for High-Jerk Trajectory.</u>

Carrier Tracking Errors

Notes:
1) Linear error detector
2) No quantization errors
3) No frequency-reference errors
4) No IMU errors
5) No input noise

$B_n = 1$ Hz

$B_n = 3$ Hz

$B_n = 7$ Hz

151
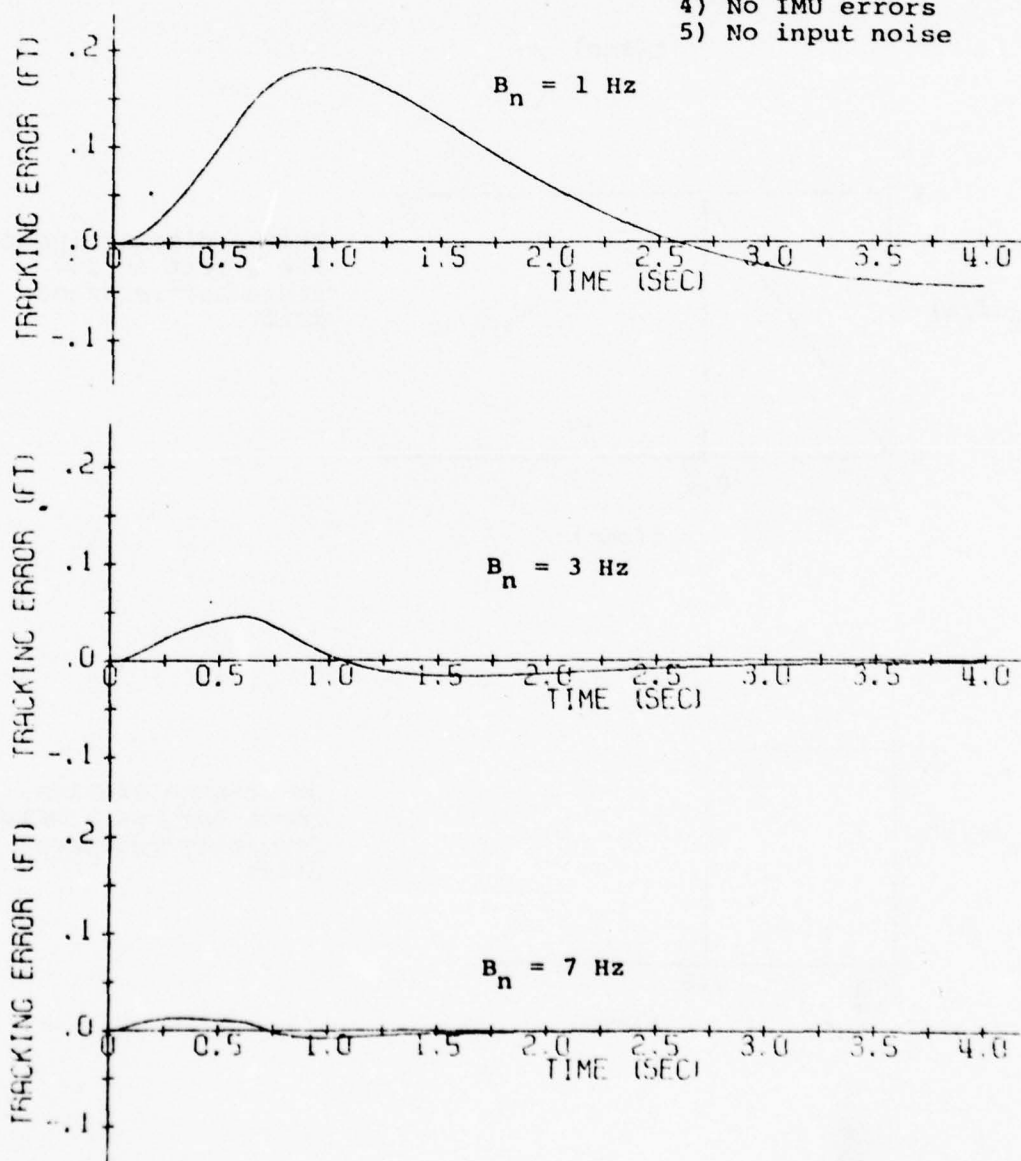
Figure A-7. <u>Acceleration-Sensitive Frequency-Reference Drift During High-Jerk Trajectory.</u>
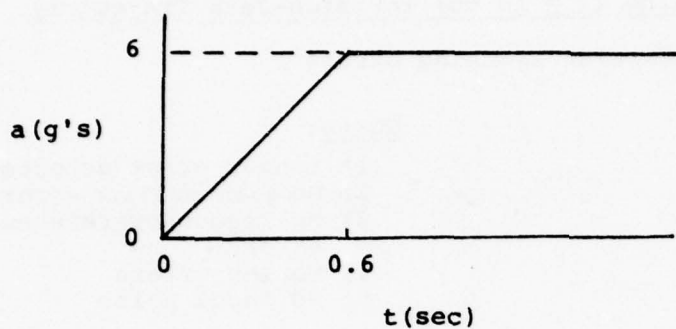
High-jerk input
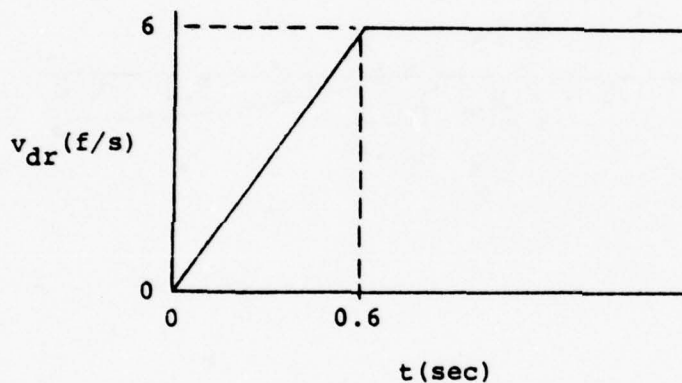
Drift-velocity input for 1 part in 10^9 frequency-reference drift
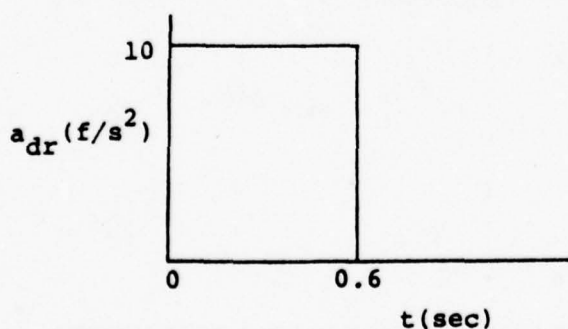
Drift-acceleration input for 1 part in 10^9 frequency-reference drift

152

Figure A-8. **Frequency-Reference Induced Errors on High-Jerk Trajectory.**

153
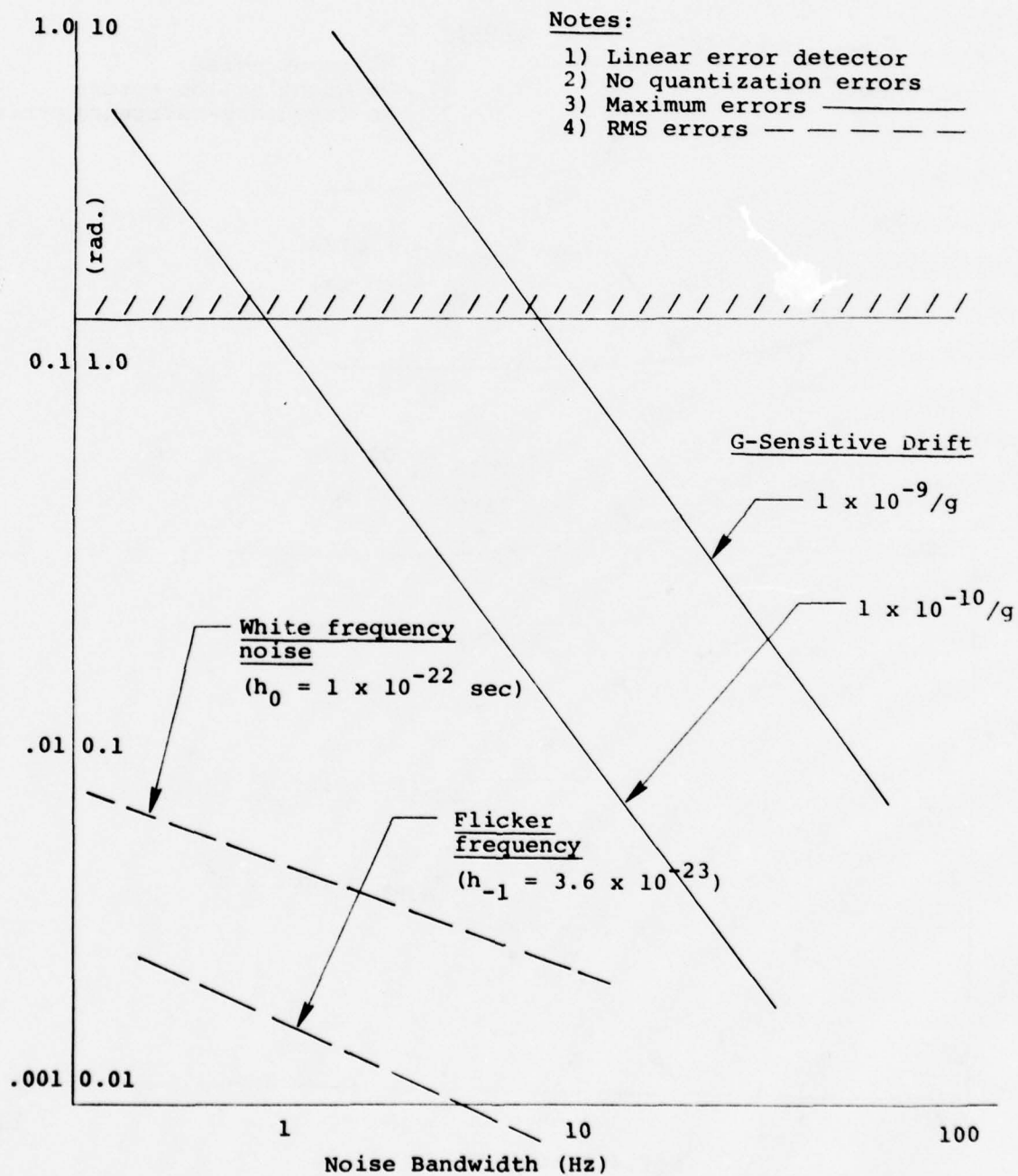
Figure A-9. IMU Measurement Errors for High-Jerk Trajectory.

Maximum Carrier Tracking Errors

154
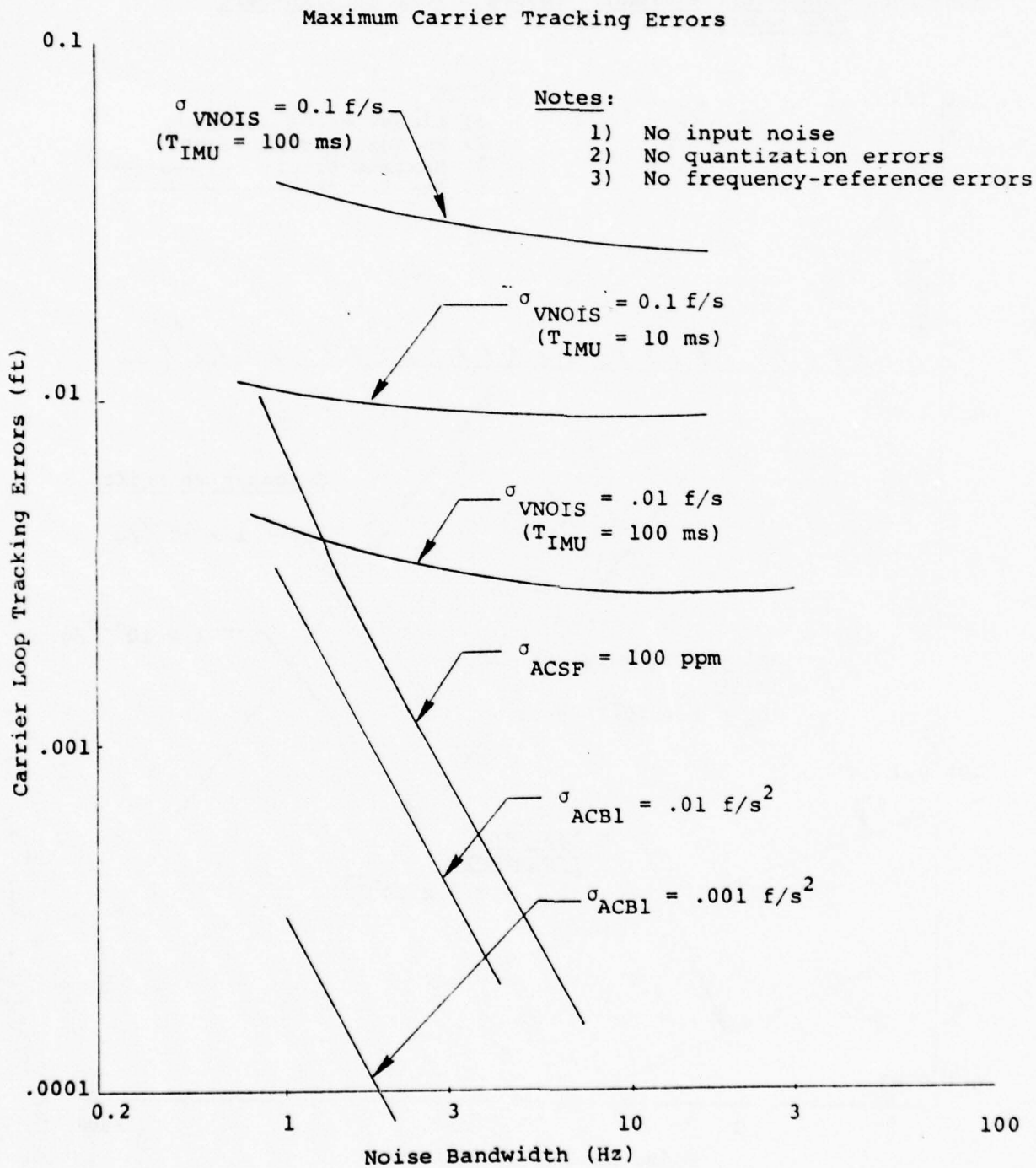
Figure A-10.   Carrier Tracking Errors for Rotational Inputs.

AIDED SYSTEM

155
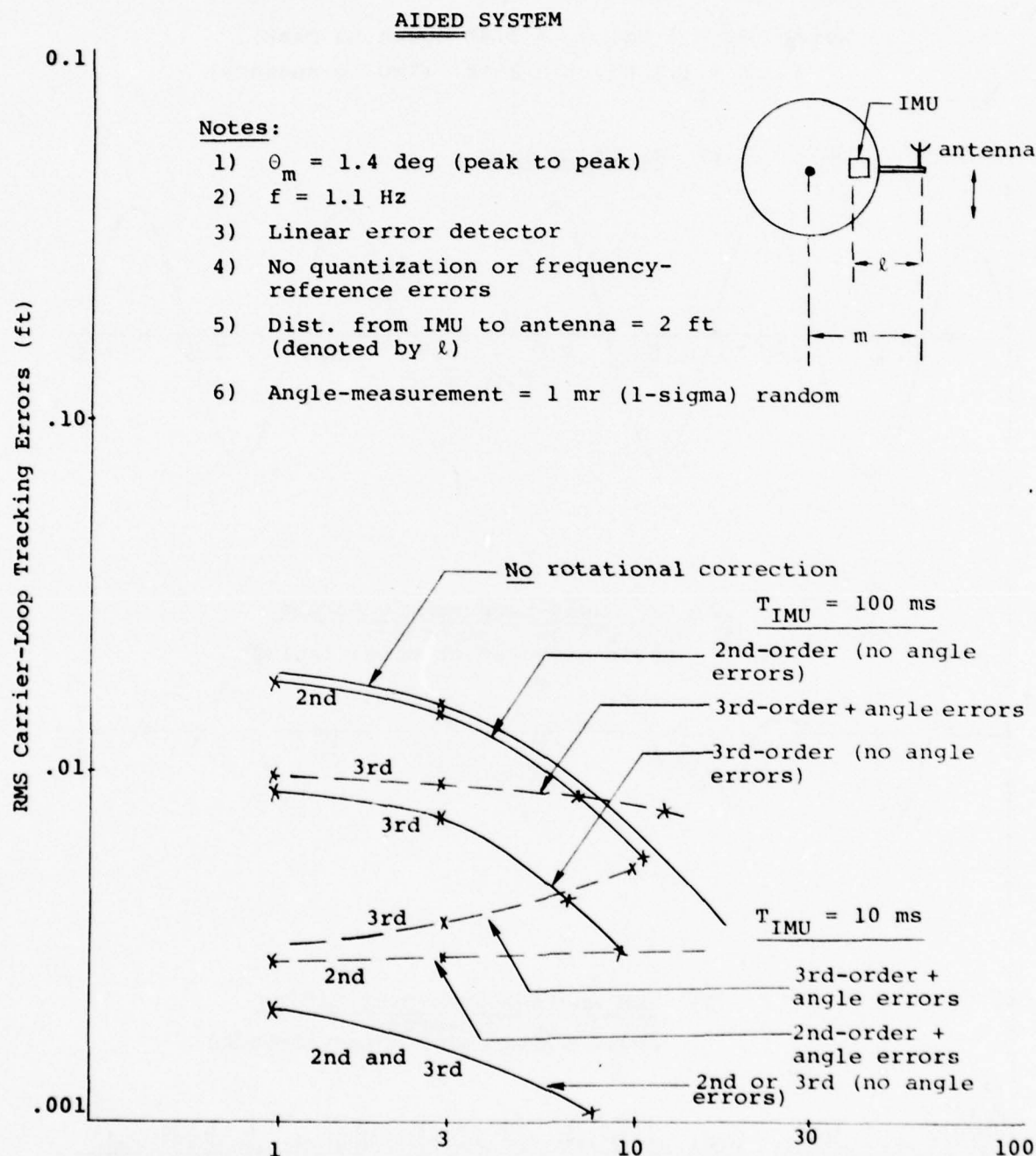
Figure A-11. Carrier Tracking Errors with Rotational Inputs.

Note: B_n = 1 Hz, Θ_m = 1.4° (peak to peak),
f = 1.1 Hz, m = 2 ft. (IMU to antenna)

1) No IMU Aiding

2) IMU Angle-Measurement Aiding
    T = 100 ms, 3rd-order,
    angle-measurement noise included

3) IMU Angle-Measurement Aiding
    T = 10 ms, 3rd-order,
    angle-measurement noise included

156
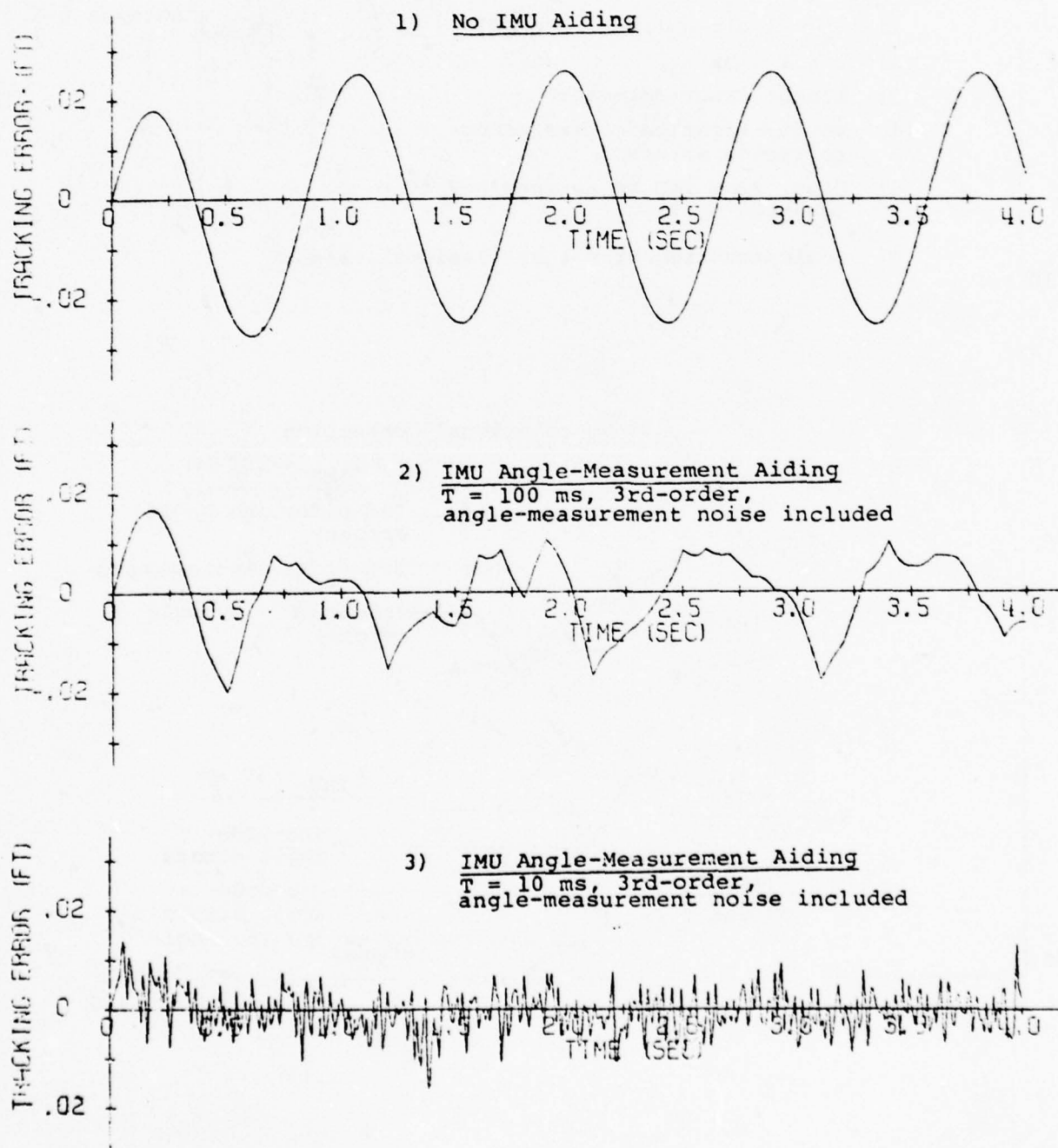
Figure A-12.   Unaided Receiver with High-Jerk Trajectory.

Notes: 1) Typical Monte-Carlo run near threshold
2) C/N_0 = 28 dB-Hz
3) Frequency-reference drift = 1×10^{-9}/g
4) $B_n \approx 60$ Hz, T_{CODE} = 2 sec

CARRIER LOOP TRACKING ERROR

CODE LOOP TRACKING ERROR

157
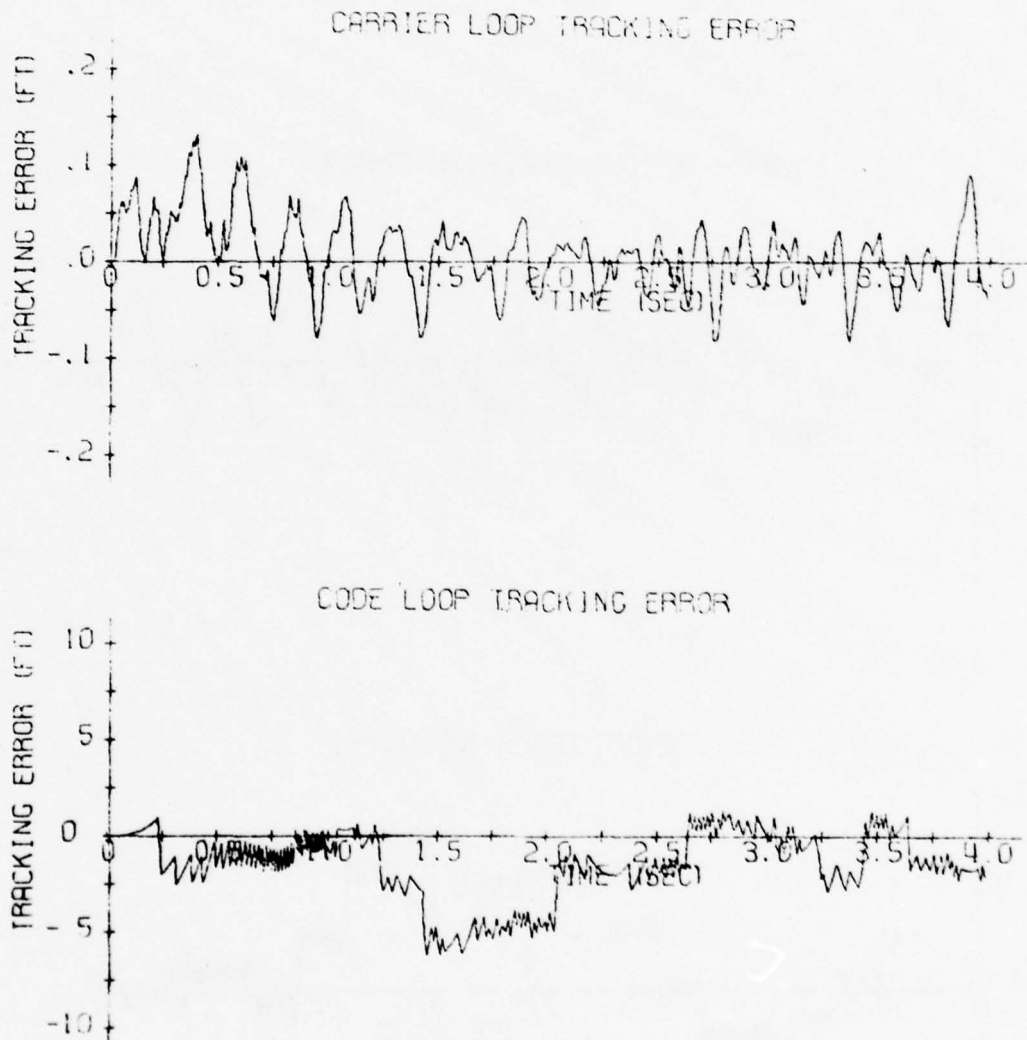
Figure A-13. IMU-Aided (T = 100 ms) Receiver with High-Jerk Trajectory.

Notes: 1) Typical Monte-Carlo run near threshold
        2) C/N_0 = 20 dB-Hz
        3) Frequency-reference drift = $1 \times 10^{-10}/g$
        4) B_n = 11 Hz

CARRIER LOOP TRACKING ERROR

CODE LOOP TRACKING ERROR
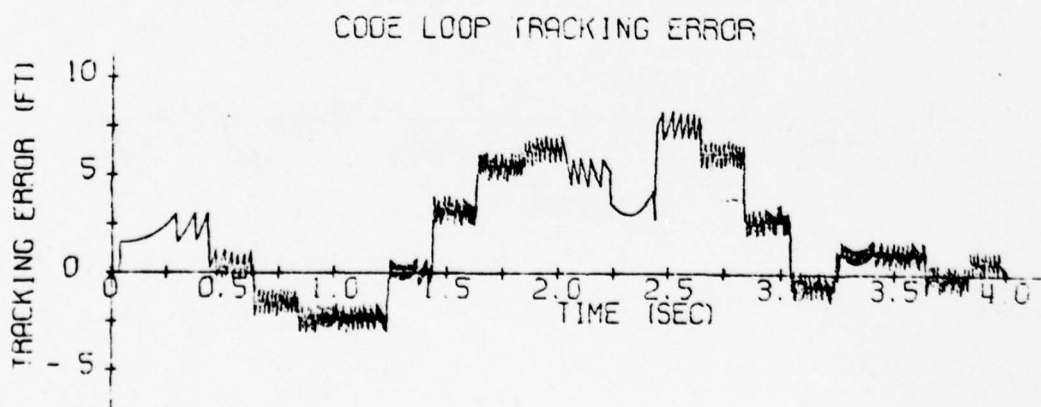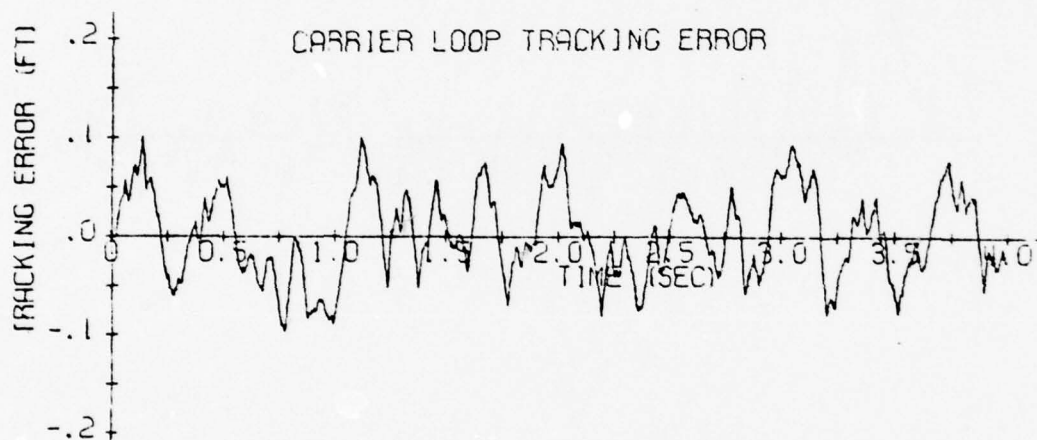
Figure A-14.   IMU-Aided (T = 10 ms) Receiver with High-Jerk Trajectory.

    Notes: 1) Typical Monte-Carlo run near threshold
            2) C/N_0 = 18 dB-Hz
            3) Frequency-reference drift = 1×10^{-10}/g
            4) B_n = 4.5 Hz

CARRIER LOOP TRACKING ERROR

CODE LOOP TRACKING ERROR

159
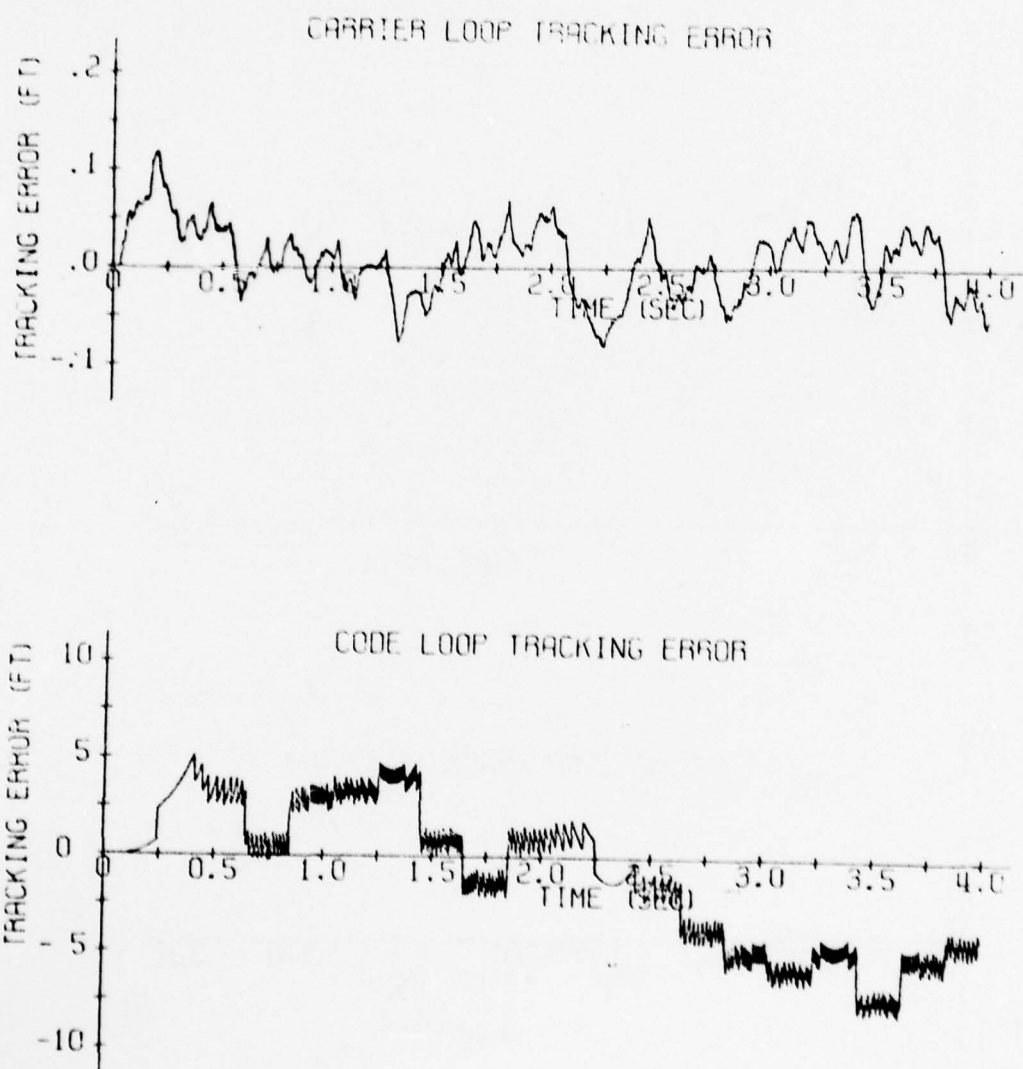
Figure A-15.   IMU-Aided Receiver - Carrier Cycle Slipping.

Notes:
1) High-jerk input trajectory
2) C/N_0 = 18 dB-Hz
3) T_{IMU} = 100 ms
4) Frequency-reference drift $\simeq$ 1 x 10^{-10}/g
5) $B_n \approx$ 1 Hz

CARRIER LOOP TRACKING ERROR

CODE LOOP TRACKING ERROR

160
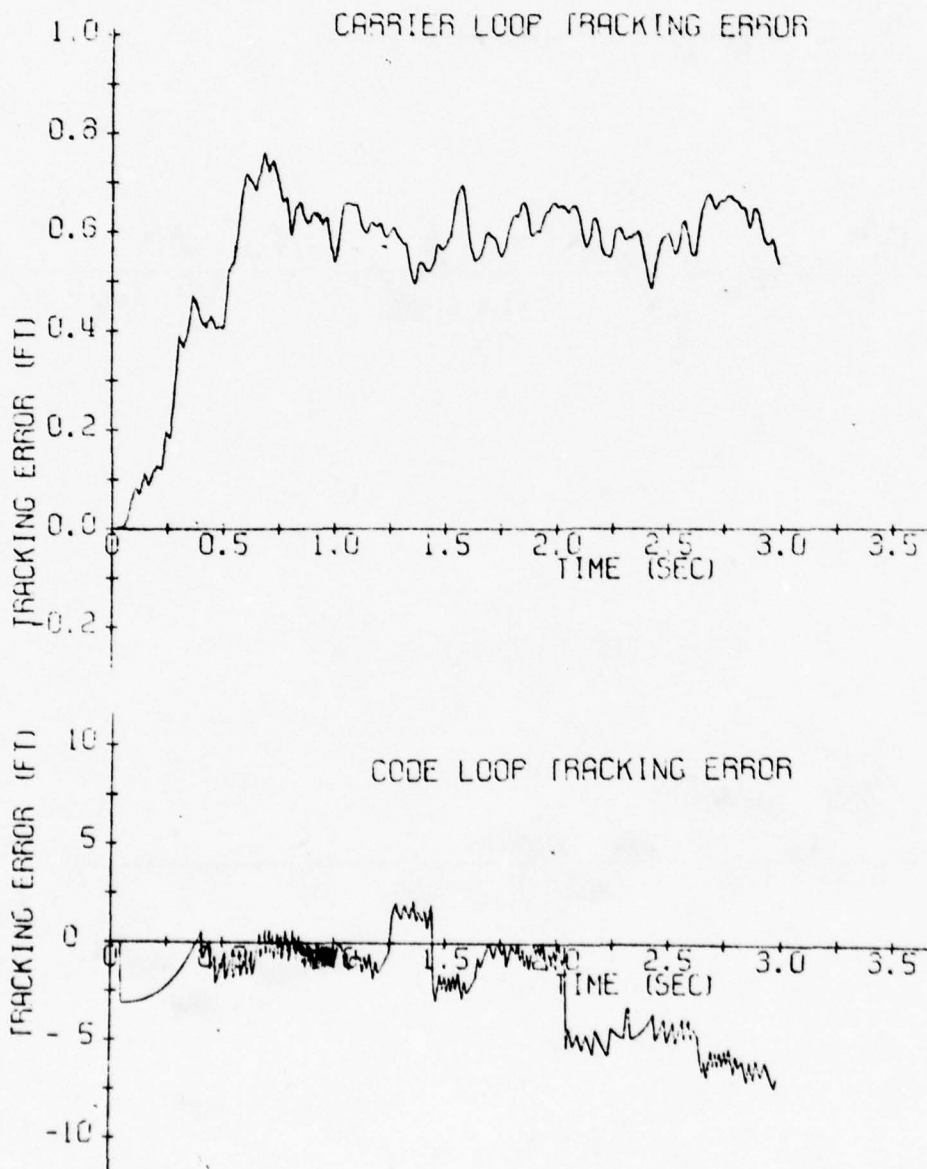
Figure A-16. <u>IMU-Aided Receiver – Carrier Lost Lock</u>

<u>Notes:</u>

1) Carrier loop not tracking
2) IMU aiding code loop and frequency reference
3) T_{IMU} = 10 ms
4) C/N_0 = 12 dB-Hz
5) T_{CODE} ≈ 2 sec
6) Frequency-reference drift = $1 \times 10^{-10}/g$

CARRIER LOOP TRACKING ERROR

CODE LOOP TRACKING ERROR

161
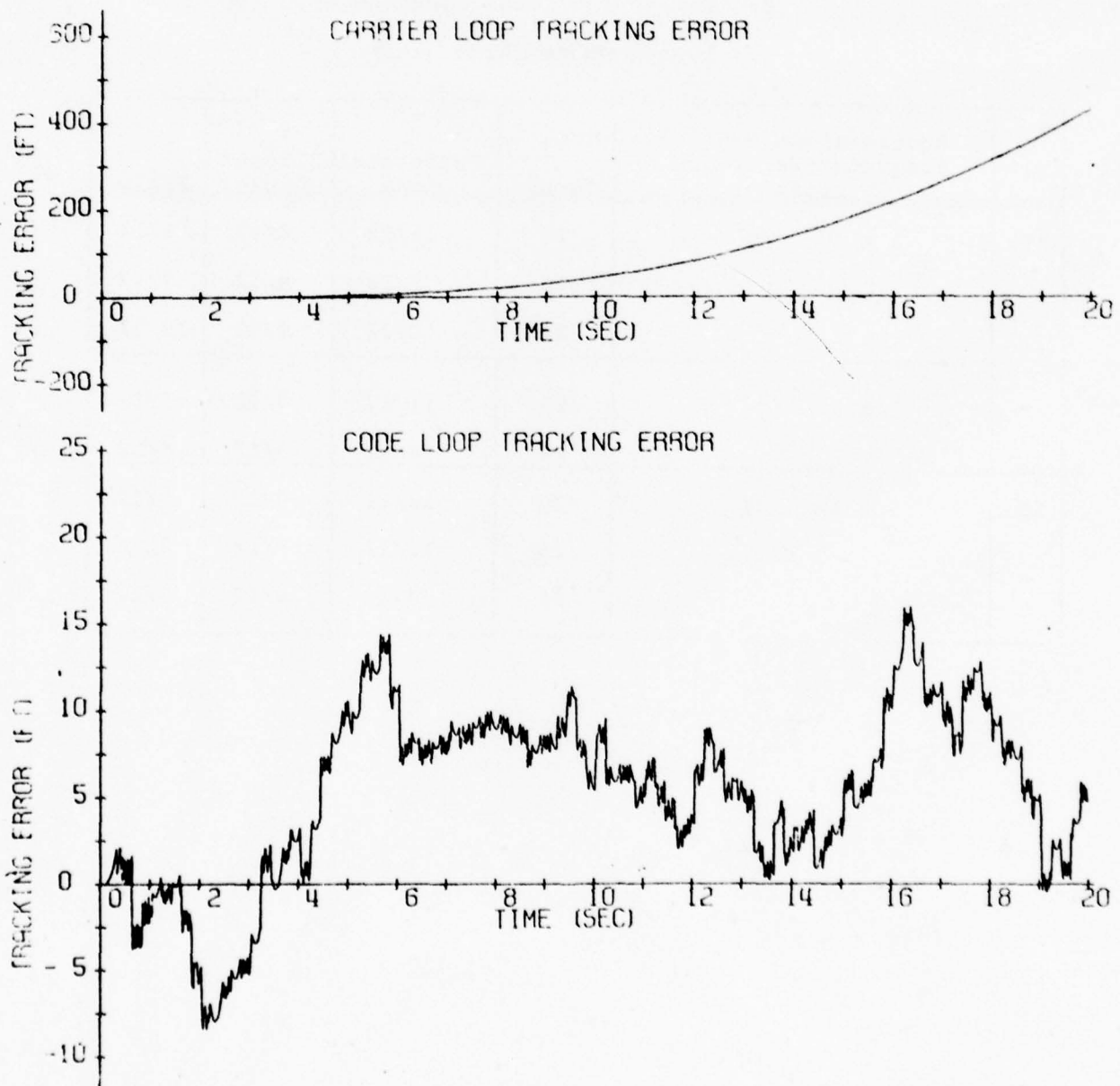
Table 1.   Monte-Carlo Runs - Unaided Receiver.

Notes:
1) High-jerk trajectory input
2) Successful run - maintains lock or temporarily slips cycles
3) Failed run loses lock and does not recover
4) 10-run Monte-Carlo sets

B_n (Hz)	Acceleration Sensitive Frequency Reference Drift	C/N_0 (dB-Hz)	Successful Runs	Slipped Cycles	Failed
60	$1 \times 10^{-10}/g$	28	11/12	0/12	1/12
		26	5/12	0/12	7/12
		24	0/12	0/12	12/12
	$1 \times 10^{-9}/g$	28	11/12	0/12	1/12
		26	4/12	3/12	8/12
50	$1 \times 10^{-10}/g$	30	12/12	0/12	0/12
		28	12/12	0/12	0/12
		26	3/12	0/12	9/12

162

Table 2.   Monte-Carlo-Runs - IMU-Aided Receiver.

Notes:

1) High-jerk trajectory input
2) $T_{IMU} = \underline{100 \text{ ms}}$

B_n (Hz)	Acceleration-Sensitive Frequency-Reference Drift	C/N_0 (dB-Hz)	Successful Tracking	Slipped Cycles	Failed
22	$1 \times 10^{-9}/g$	24	10/10	1/10	--
		22	9/10	2/10	1/10
11	$1 \times 10^{-9}/g$	28	10/10	--	--
		24	7/10	3/10	3/10
		20	4/10	2/10	6/1
	$1 \times 10^{-10}/g$	24	10/10	--	--
		20	10/10	--	--
		18	4/10	3/10	6/10
5	$1 \times 10^{-10}/g$	20	9/10	5/10	1/10

9	$1 \times 10^{-9}/g$	∞	yes
7		∞	no
3	$1 \times 10^{-10}/g$	∞	yes
2		∞	no

163

Table 3. Monte-Carlo-Runs - IMU-Aided Receiver.

<u>Note</u>: 1) High-jerk trajectory input
2) T_{IMU} = <u>10 ms</u>

B_n (Hz)	Acceleration-Sensitive Frequency-Reference Drift	C/N_0 (dB-Hz)	Successful Tracking	Slipped Cycles	Failed
11	1×10^{-9}/g	28	10/10	--	--
		24	9/10	--	1/10
		20	0/10	0/10	10/10
	1×10^{-10}/g	18	7/10	3/10	3/10
		16	0/10	0/10	10/10
5	1×10^{-10}/g	24	10/10	--	--
		20	10/10	1/10	--
		18	9/10	7/10	1/10
		16	6/10	4/10	4/10

9	1×10^{-9}/g	∞	yes
7		∞	no
3	1×10^{-10}/g	∞	yes
2		∞	no
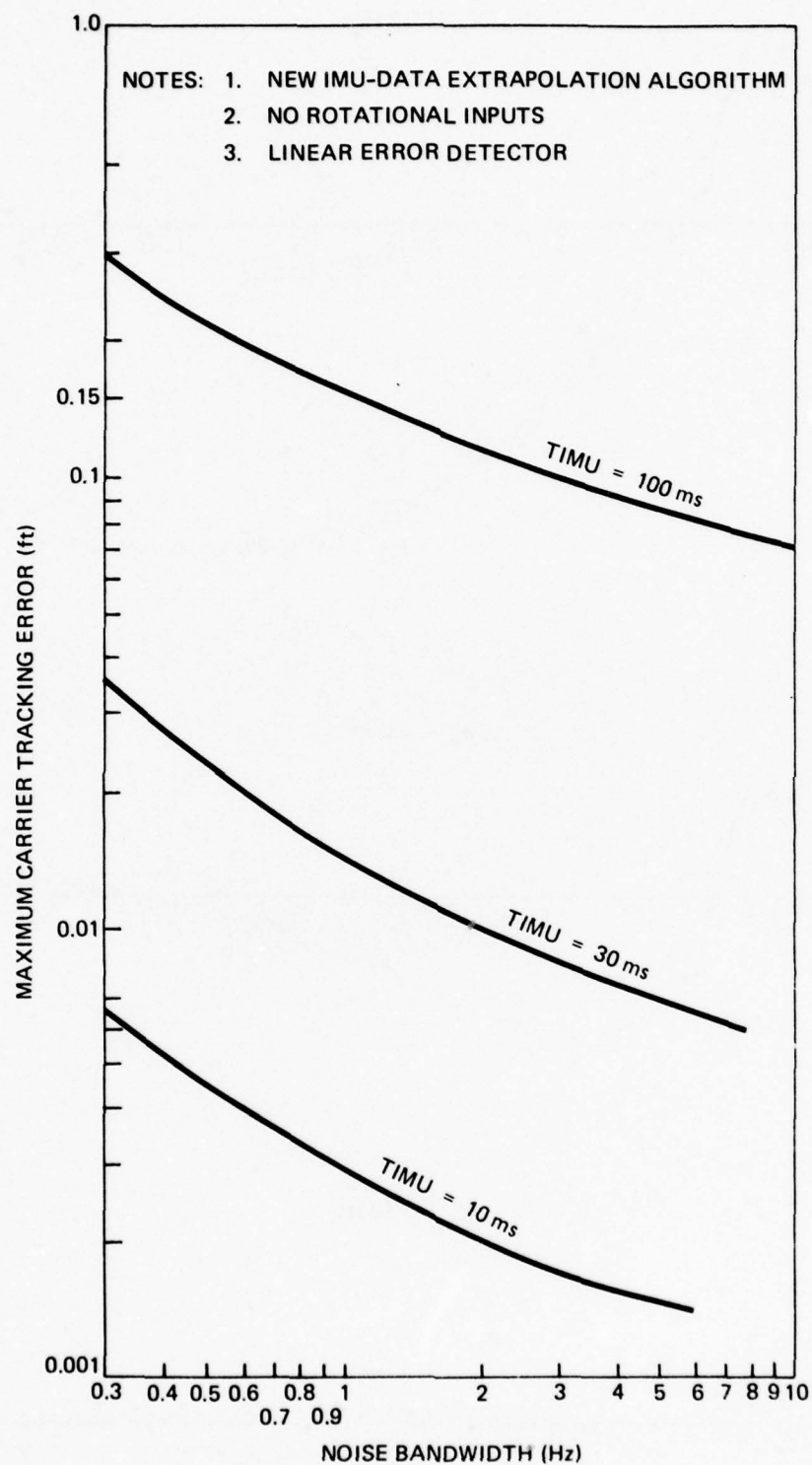
Figure A-17.   Carrier Tracking Errors for High-Jerk Trajectory.

165

Figure A-18. Carrier Tracking Errors — T_{IMU} = 100ms

166
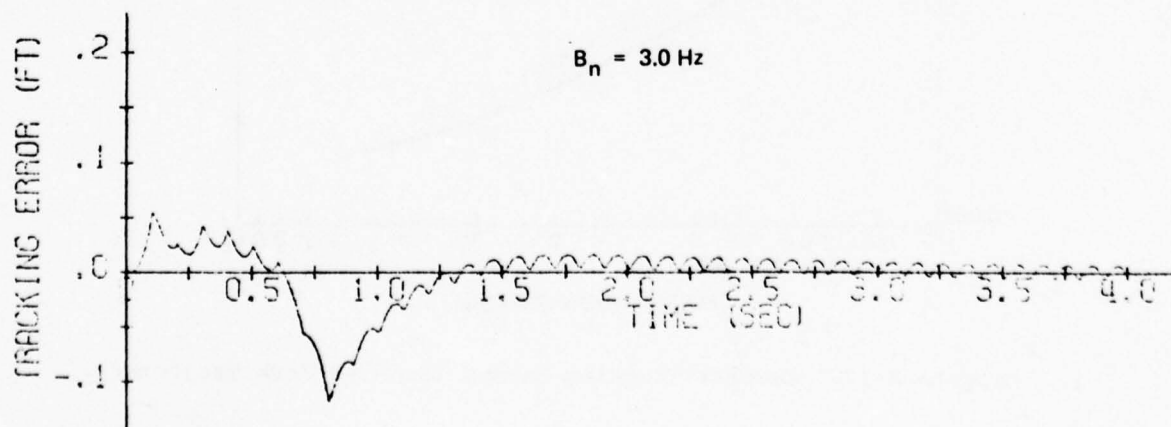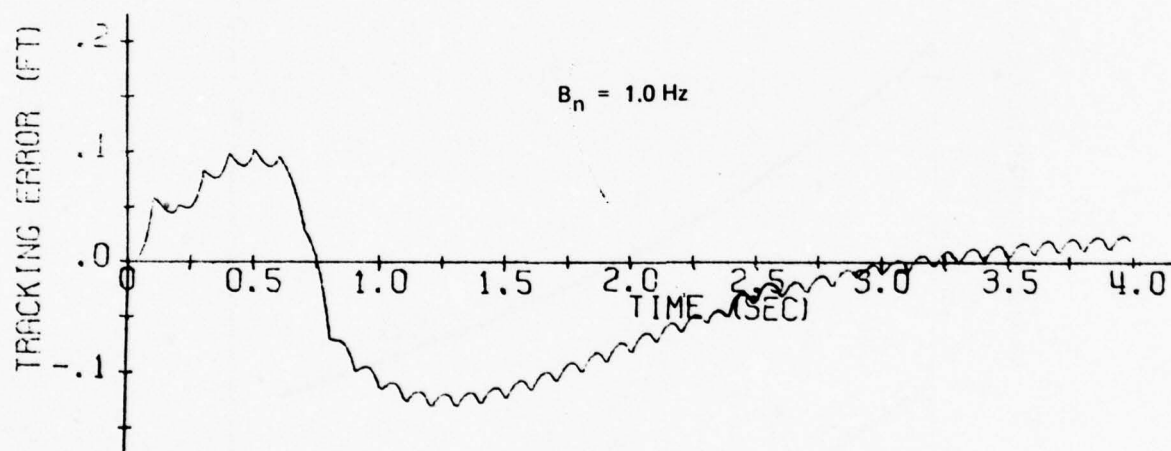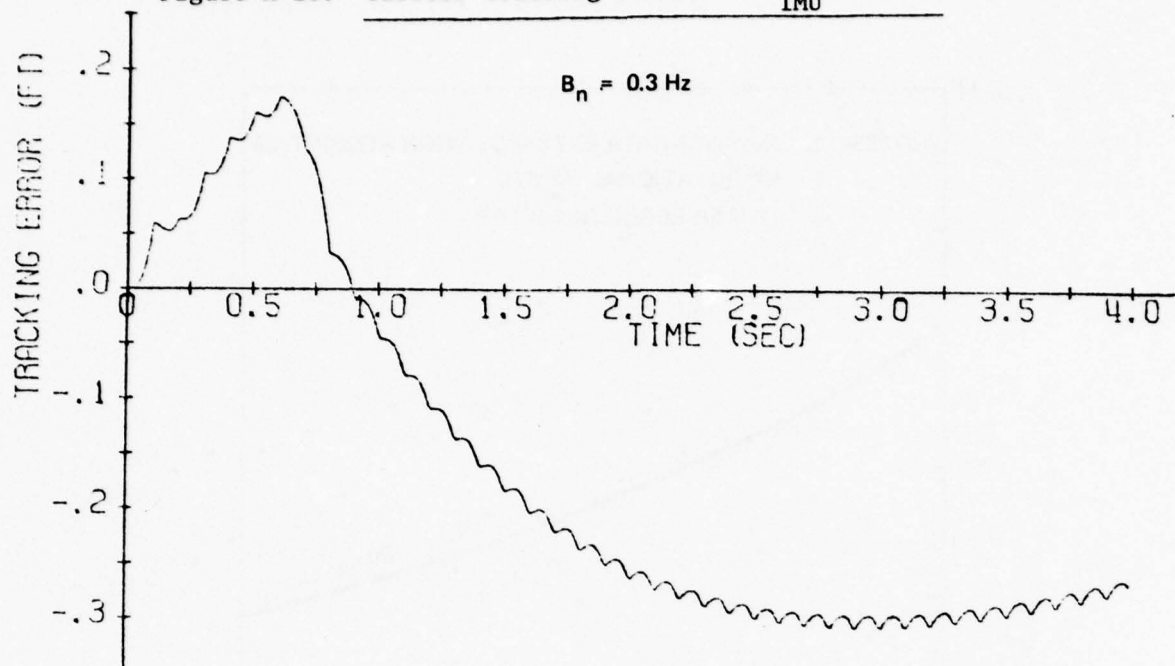
Figure A-19.   Carrier Tracking Errors — T_{IMU} = 30ms

167
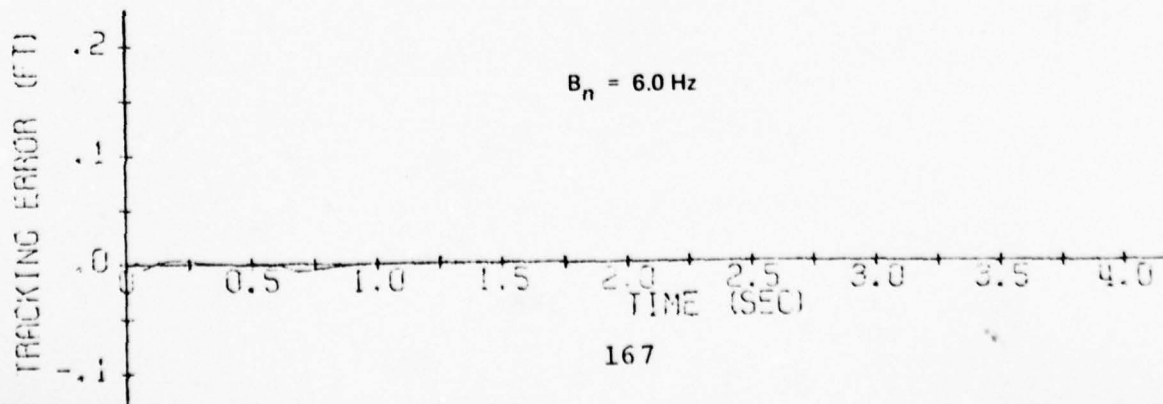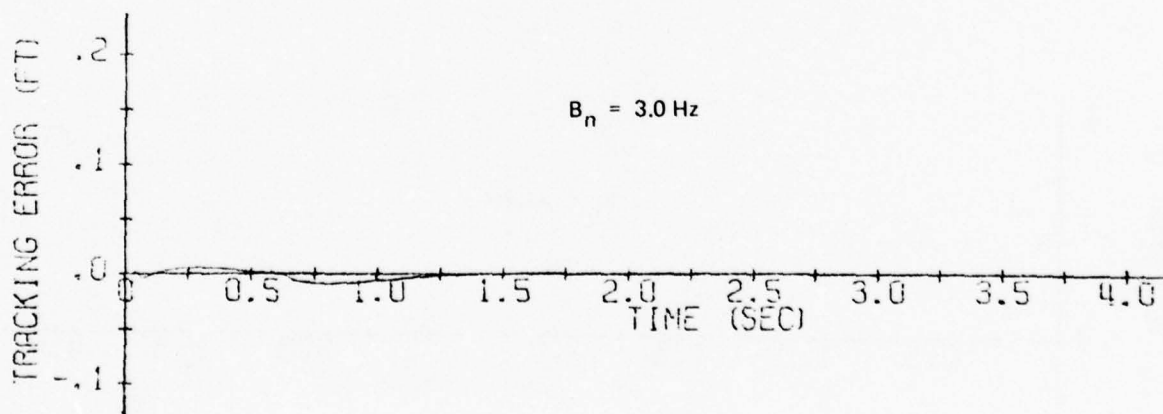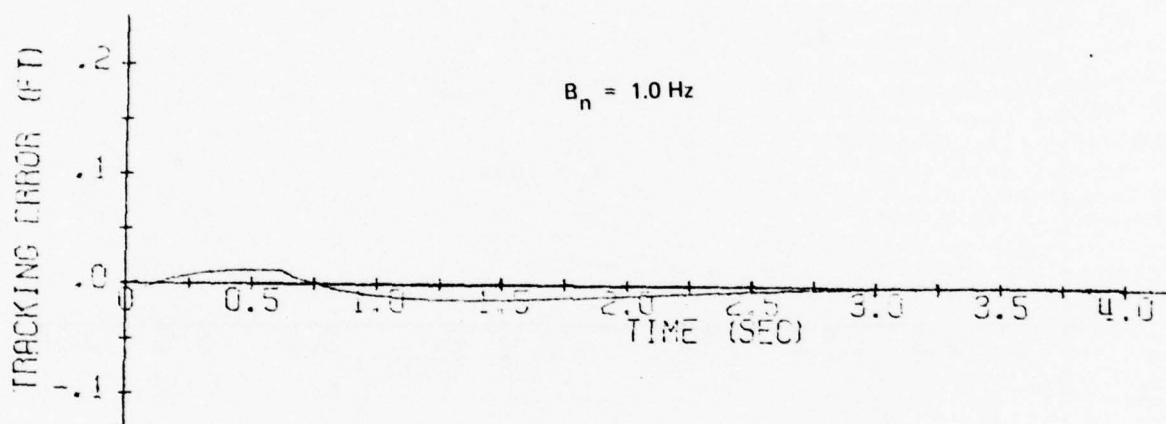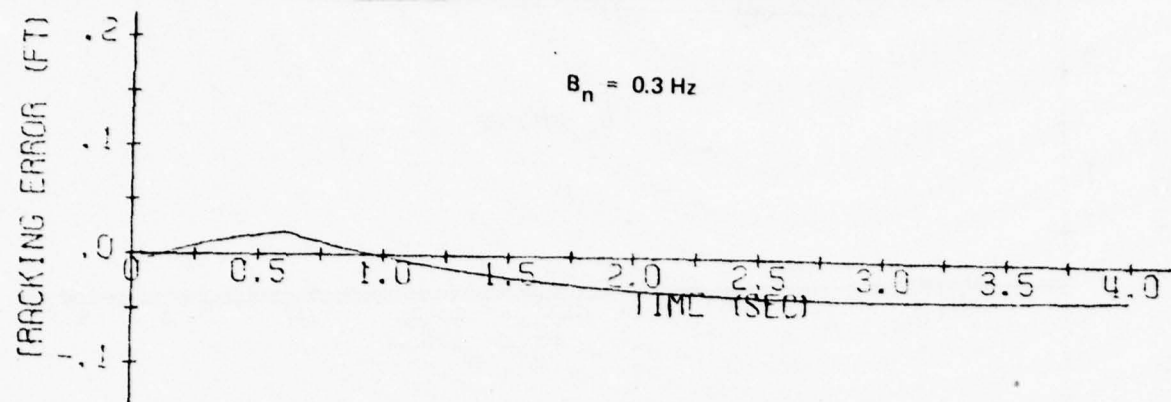
Figure A-20. Carrier Tracking Errors — $T_{IMU} = 10ms$

$B_n = 0.3\text{ Hz}$

$B_n = 1.0\text{ Hz}$

$B_n = 3.0\text{ Hz}$
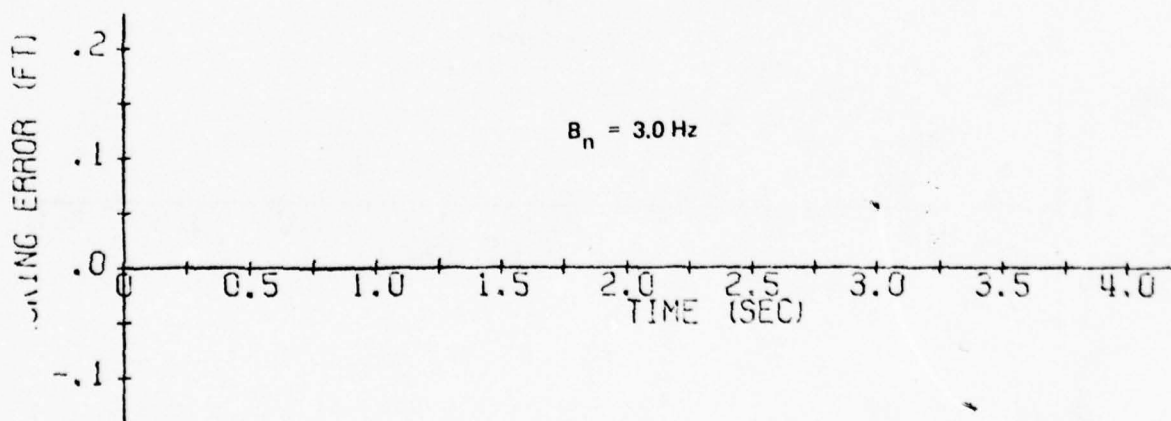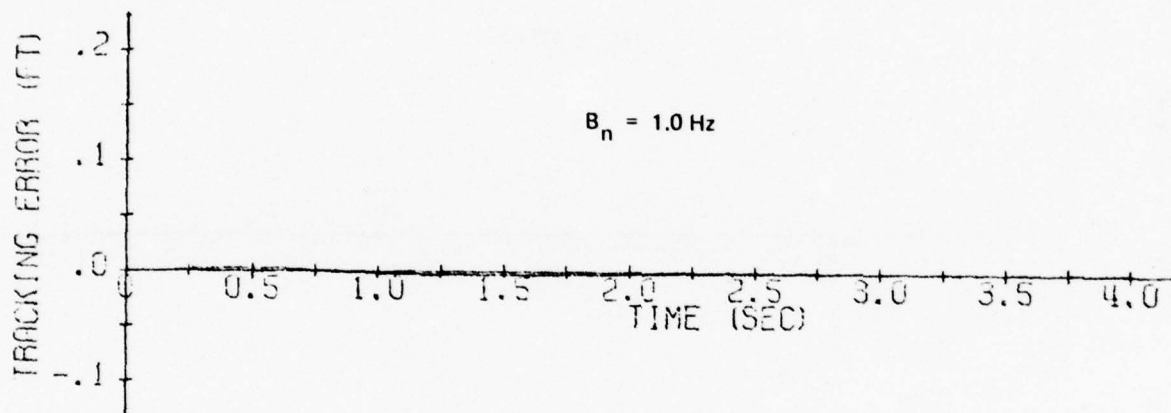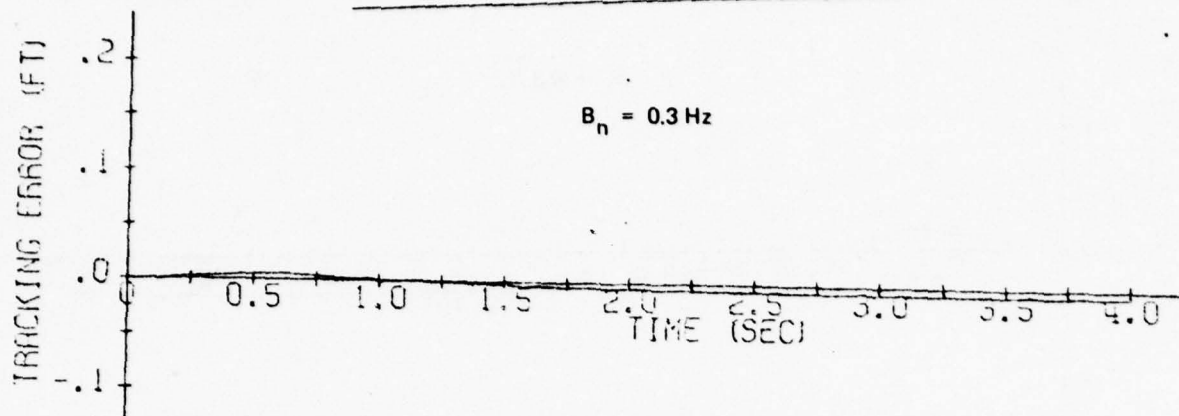
APPENDIX B

CODE DETECTOR NOISE CHARACTERISTICS

The intent is to study the effects of noise on a code detector described by the following equation:

$$\frac{\hat{e}_{CO}}{\Delta} = \frac{|P_E| - |P_L|}{|P_E| + |P_L|} \tag{B1}$$

where

Δ = amount of advance and delay of early and late codes = 0.5 chip.

$\hat{e}_{CO}/\Delta$ = detector output.

P_E = early signal, i.e., the signal contained in the result of correlating the received code with the generated code, but advanced by one half chip.

P_L = late signal, same as early, but delayed by one half chip.

Now,

$$P_E = |I_E| + |Q_E| \tag{B2}$$

where, I_E and Q_E are the in-phase and quadrature components of P_E, respectively. If we assume no phase error in the carrier loop then

$$I_E = -.5 - \varepsilon \text{ chips} \tag{B3}$$

169

and

$$Q_E = 0 \tag{B4}$$

likewise,

$$P_L = |I_L| + |Q_L| \tag{B5}$$

where

$$I_L = 0.5 + \varepsilon; \; Q_L = 0 \tag{B6}$$

Adding noise to I and Q results in

$$P_E = 0.5 - + n_{IE} + n_{QE} \tag{B7}$$

and

$$P_L = 0.5 + + n_{IL} + n_{QL} \tag{B8}$$

Finally, substitution of (B7) and (B8) in (B1) gives

$$\frac{\hat{e}_{CO}}{\Delta} = \frac{[|0.5-\varepsilon + n_{IE}| + |n_{QE}|] - [|0.5+\varepsilon + n_{IL}| + |n_{QL}|]}{|0.5-\varepsilon + n_{IE}| + |n_{QE}| + |0.5+\varepsilon + n_{IL}| + |n_{QL}|} \tag{B9}$$

Equation (B9) without the noise will vary linearly with ε and is equal to 1 at $\varepsilon = -0.5$ and -1 at $\varepsilon = 0.5$. Adding noise will result in a gain reduction.

A series of Monte Carlo computer calculations of $\hat{e}_{CO}/\Delta$ are presented here for various (S/N) ratios and for -0.5 chip $\leq \varepsilon \leq 0.5$ chip.

170

The (S/N) ratio is related to the RMS value σ_N of the independent noises (n_{IE}, n_{QE}, n_{IL}, n_{QL}) as follows

$$\sigma_n = \sqrt{\frac{1}{2\left(\frac{S}{N}\right)T}} \qquad\qquad (B10)$$

where, T is the integrate-and-dump time, which determines the pre-detection bandwidth. In all cases treated here, T is 4 ms.

Figures B1 through B18 are the plotted results of the Monte Carlo runs for values of (S/N) from 51 dB-Hz to 0 dB-Hz, where

and
$$\mu = \text{Ensemble average of } \hat{e}_{CO}/\Delta$$
$$\sigma = \text{RMS error on } \mu$$

Each point represents the mean and rms of 256 Monte Carlo calculations.

From Figures B1-B18 the effective gains $\partial(\overline{e_{CO}/\Delta})/\partial\epsilon$ are estimated for each value of σ_n. These gains are plotted versus $(1/\sigma_n^2)$ in Figure B19. The effective gain is thought to be directly porportional to $(1/\sigma_n^2)$ at low values of $(1/\sigma_n^2)$.
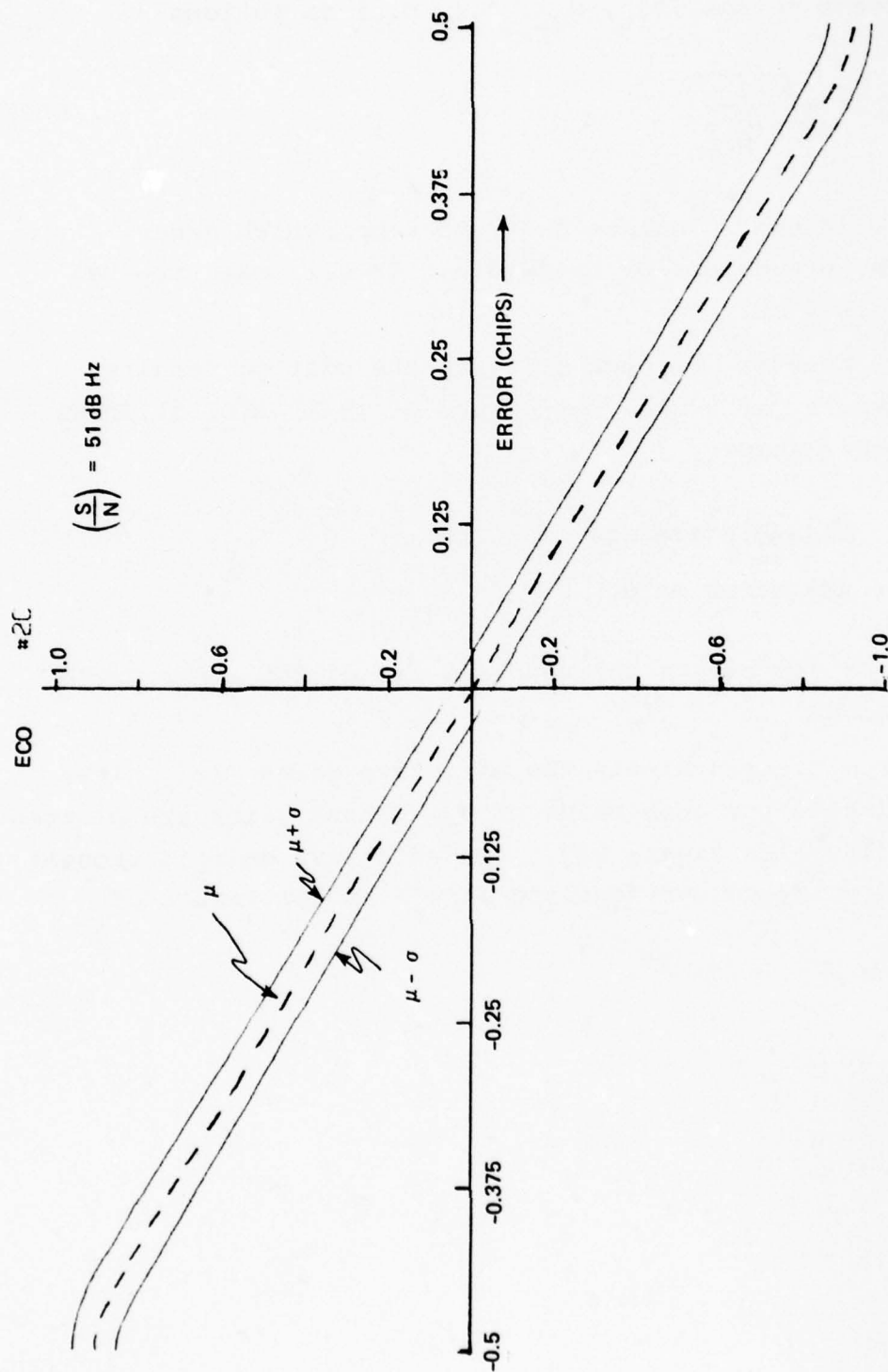
Figure B1.   Average detector output versus tracking error with
S/N = 51 dB-Hz, T = 0.004 sec.
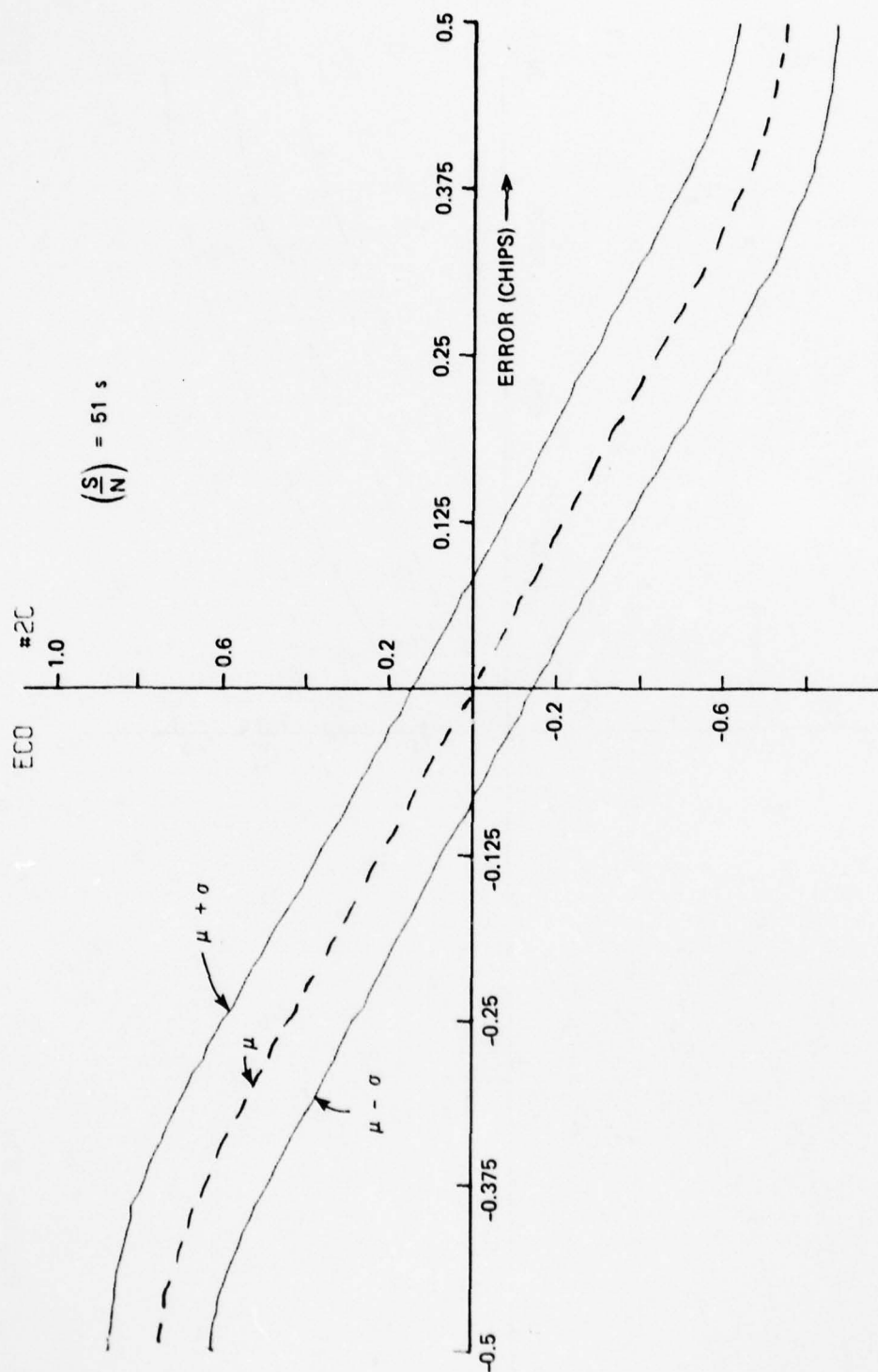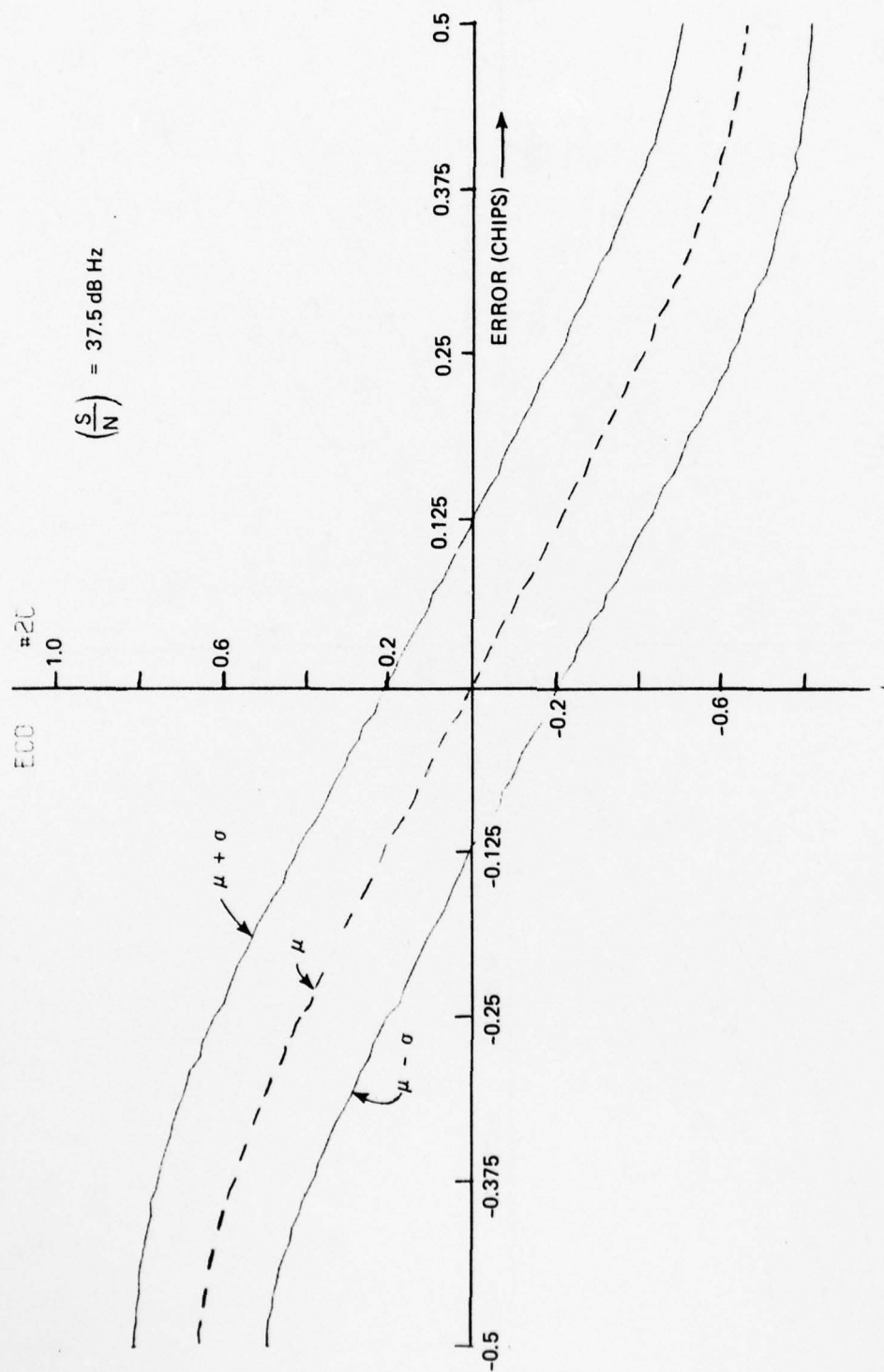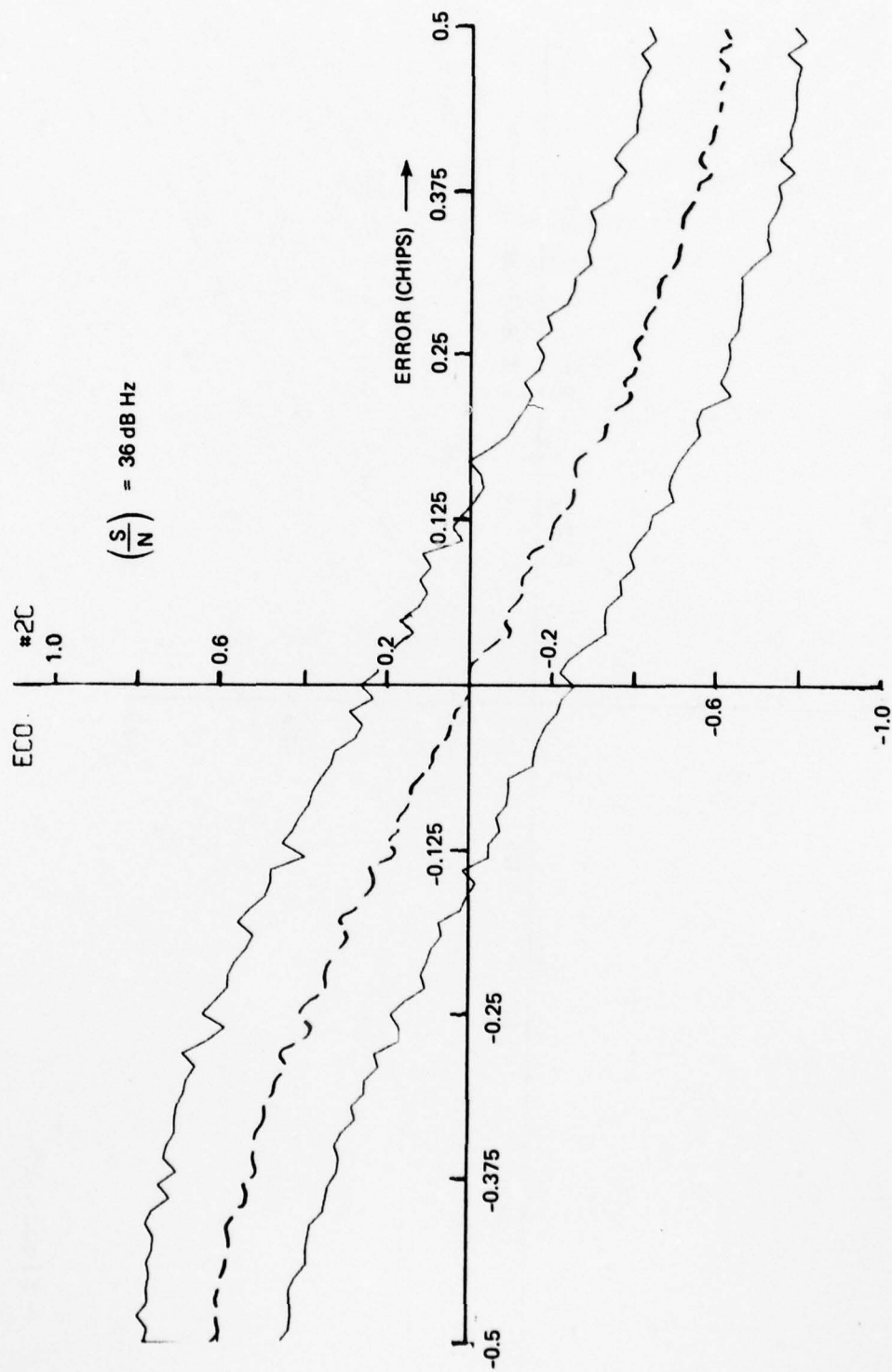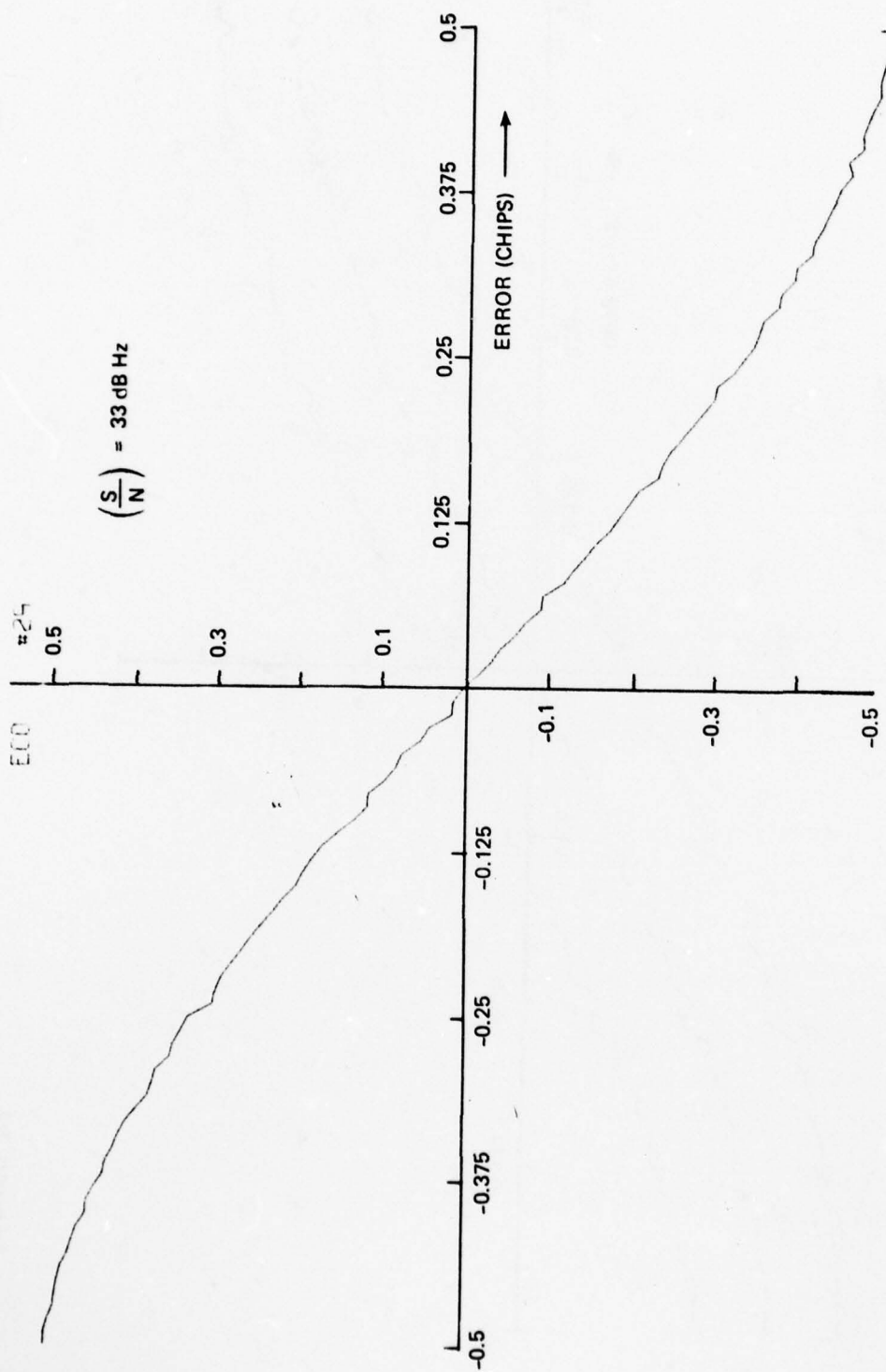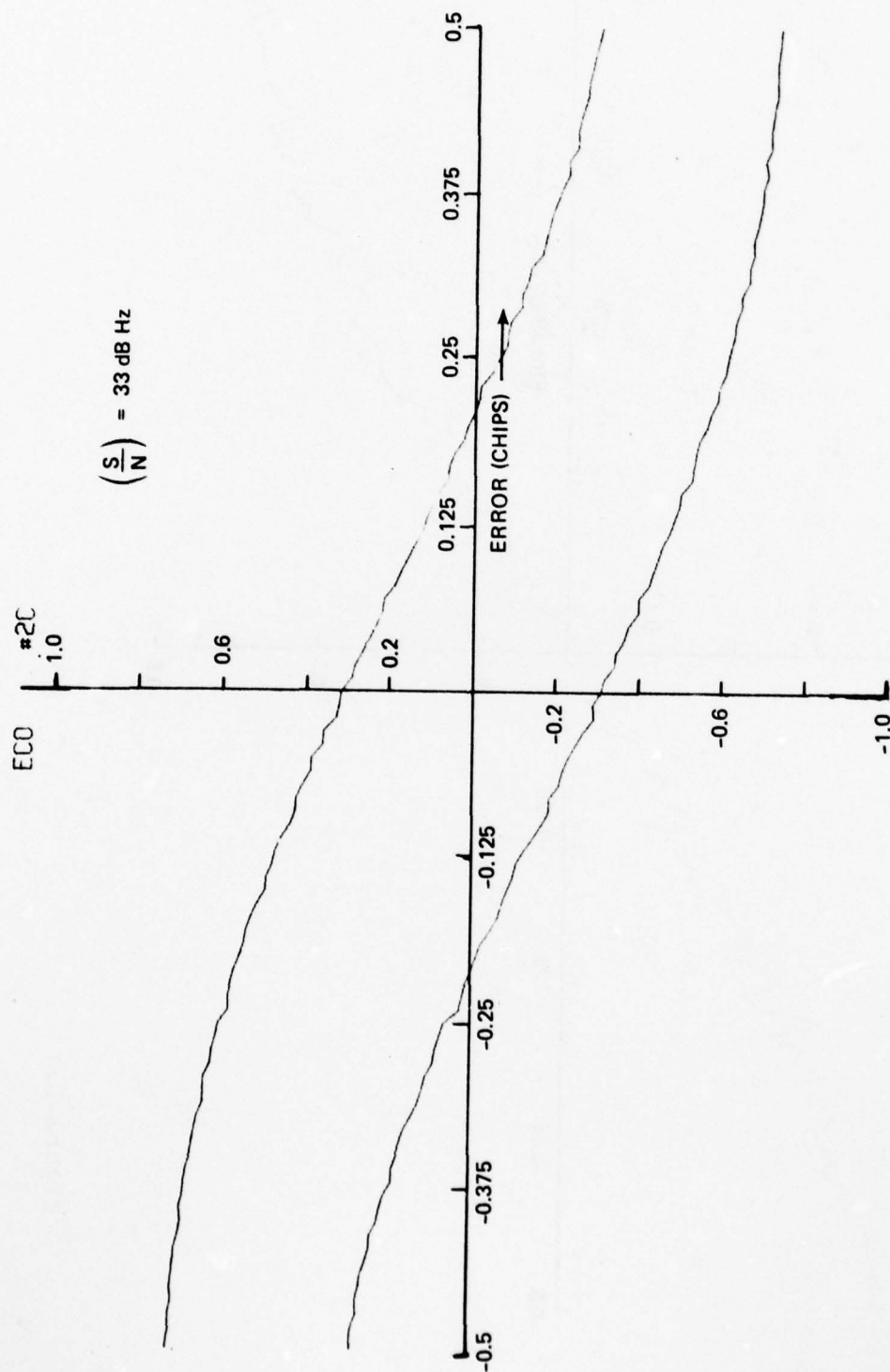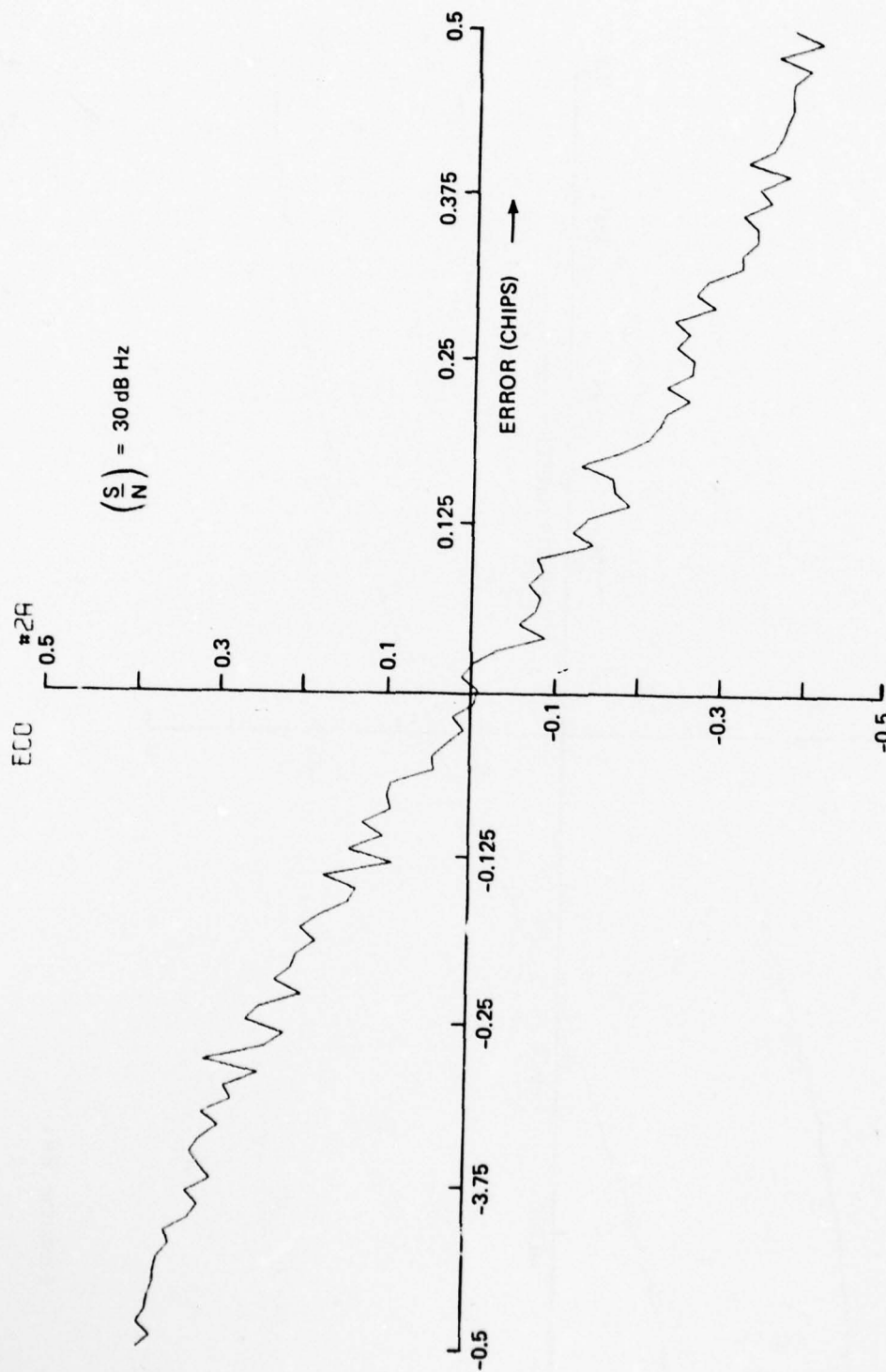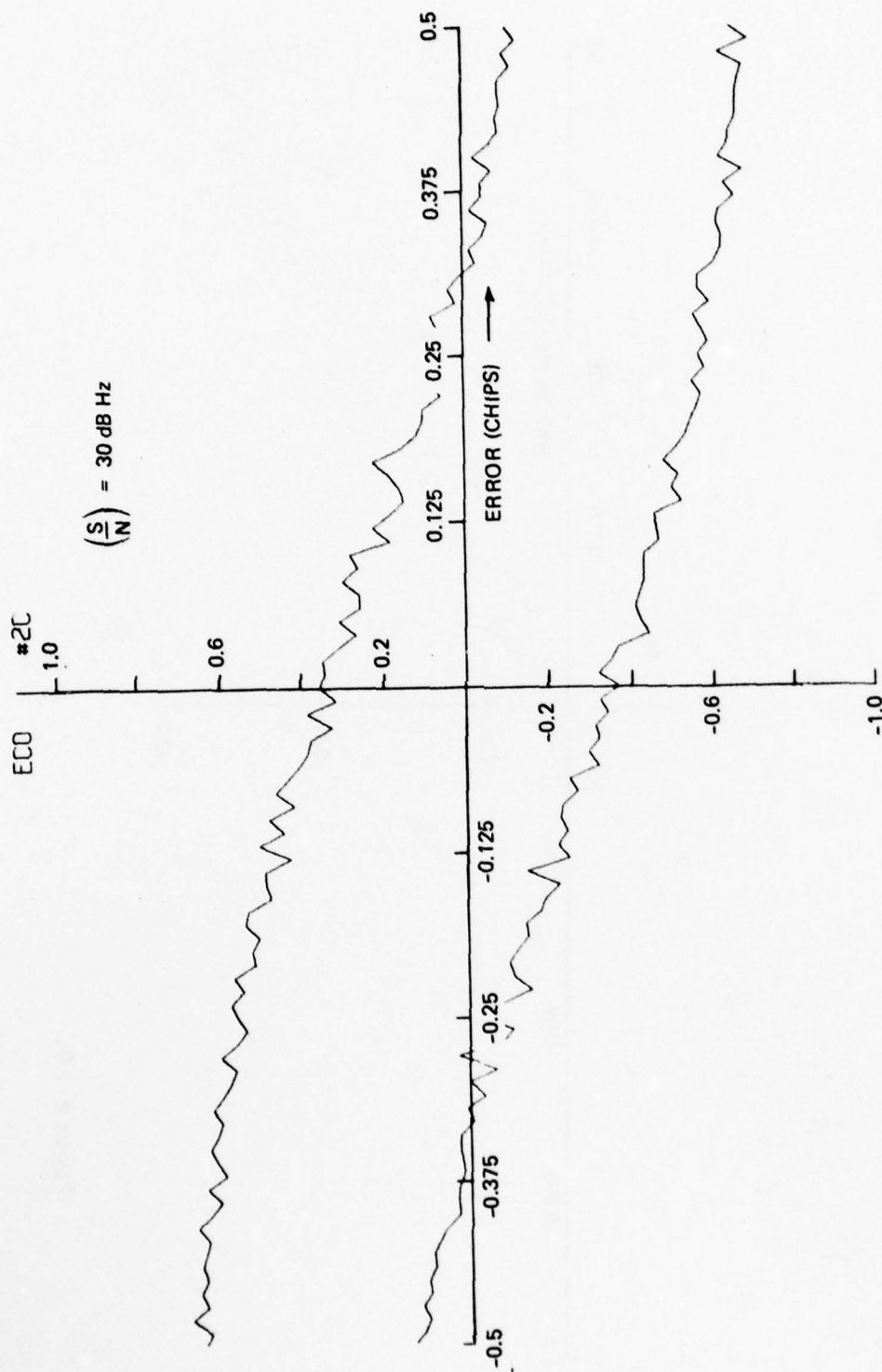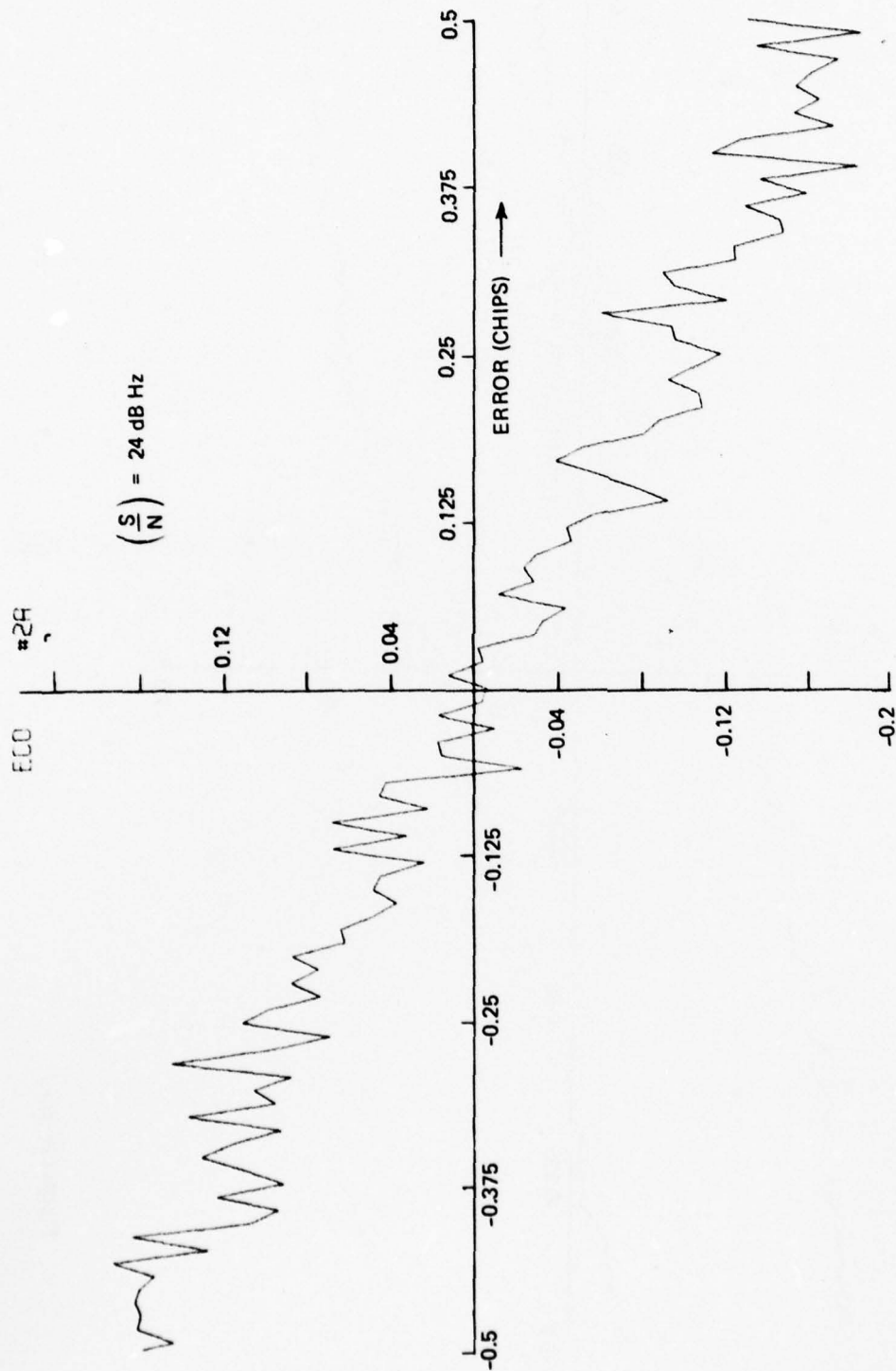
172

Figure B2.

173

Figure B3.

174

Figure B4.

175

ECO   #24

$\left(\dfrac{S}{N}\right)$ = 33 dB Hz

ERROR (CHIPS) →

Figure B5.

176

Figure B6.

177

Figure B7.

178

Figure B8.

179

Figure B9.

180

Figure B10.

181

Figure B11.

182

Figure B12.

183

Figure B13.

Figure B14.

185

Figure B15.

186

MICROCOPY RESOLUTION TEST CHART
NATIONAL BUREAU OF STANDARDS 1963 A
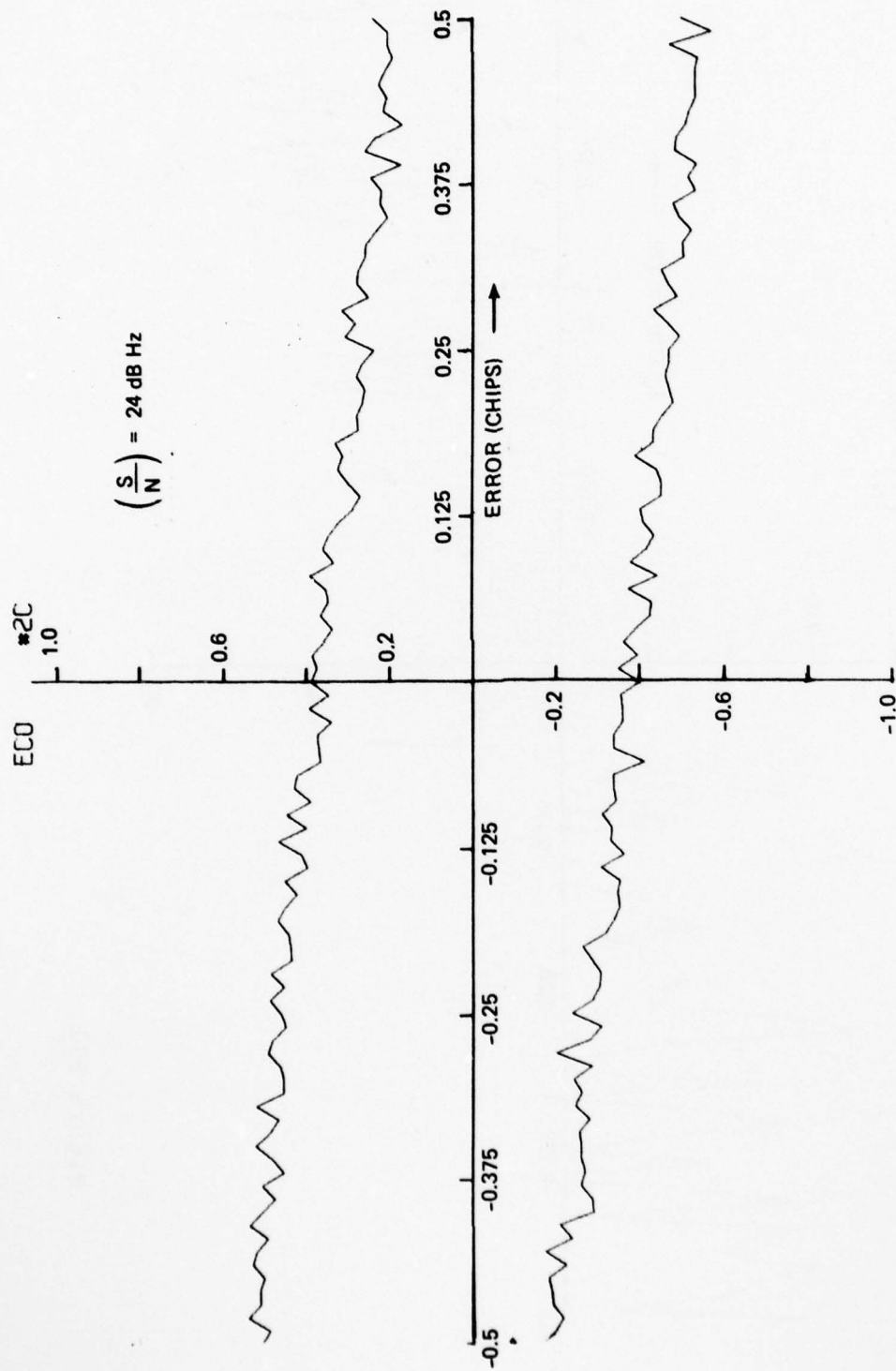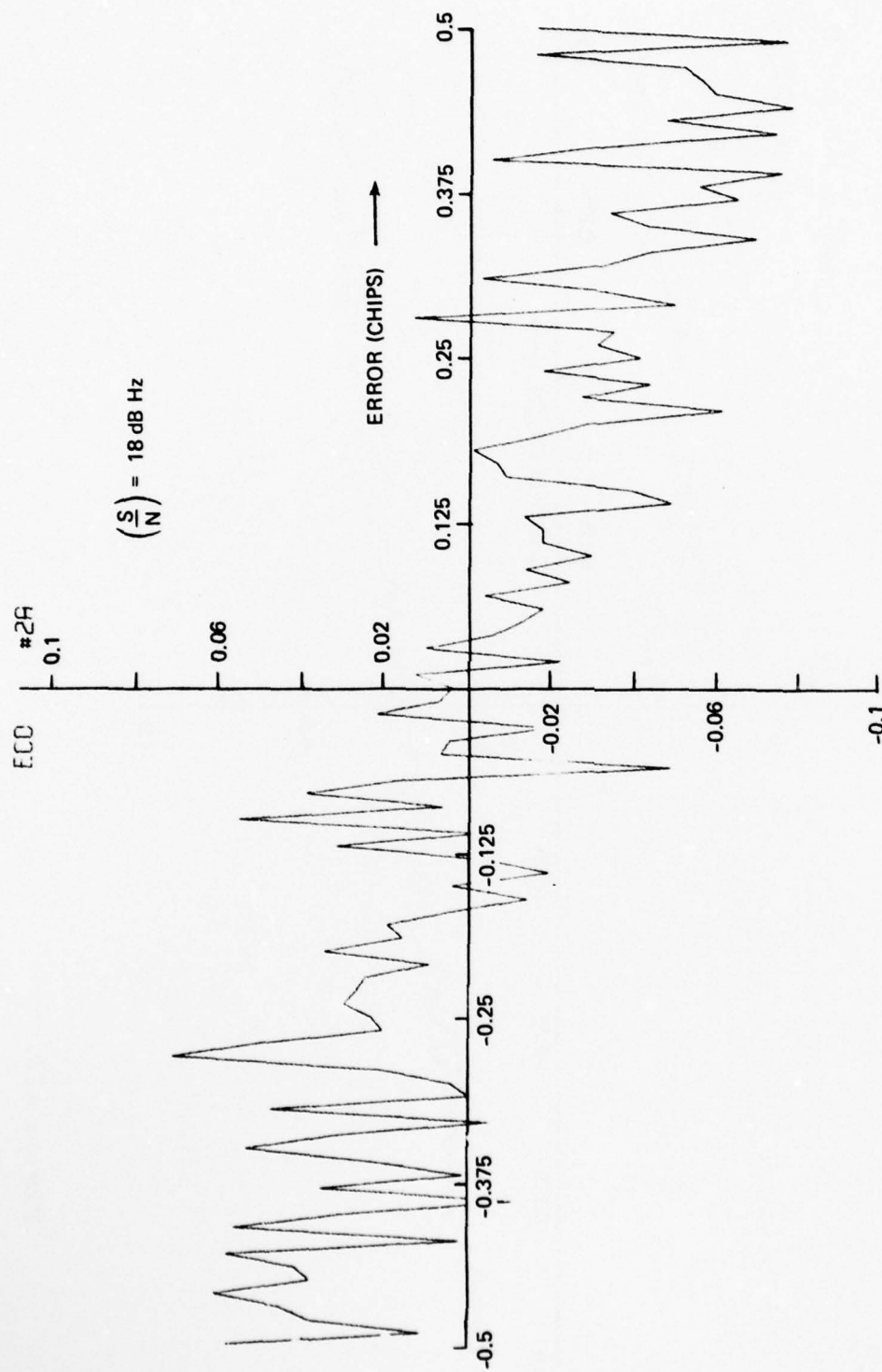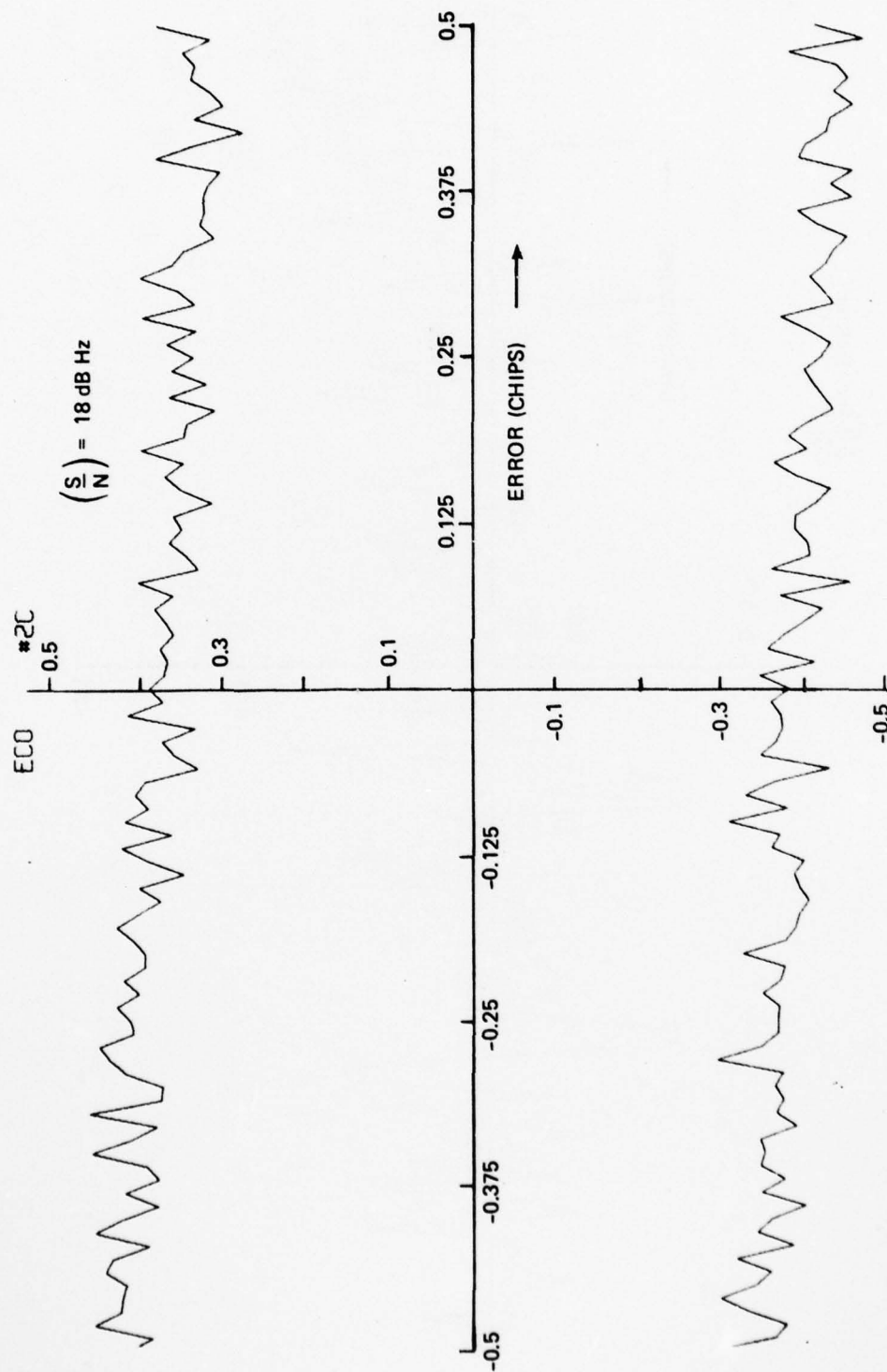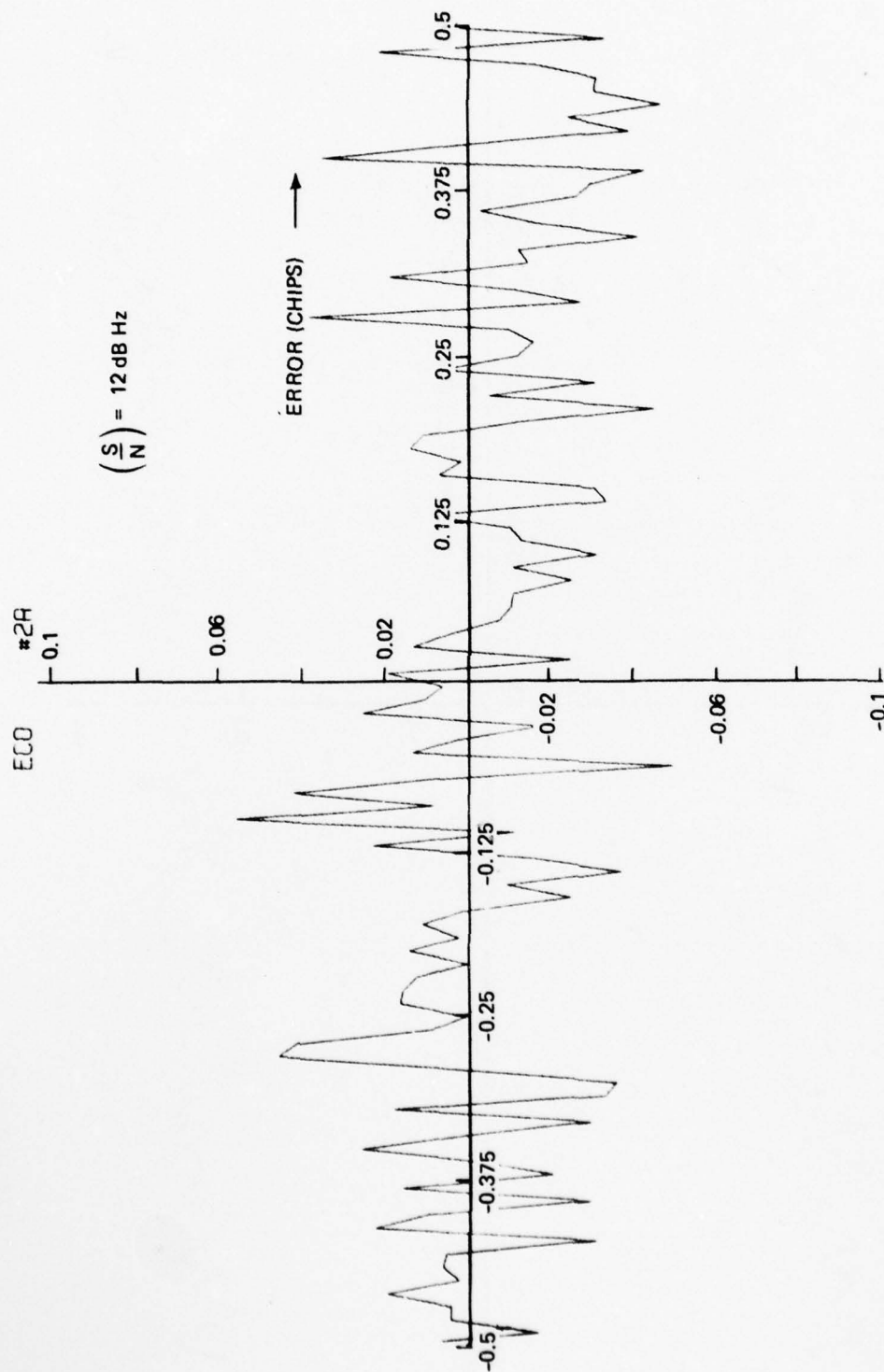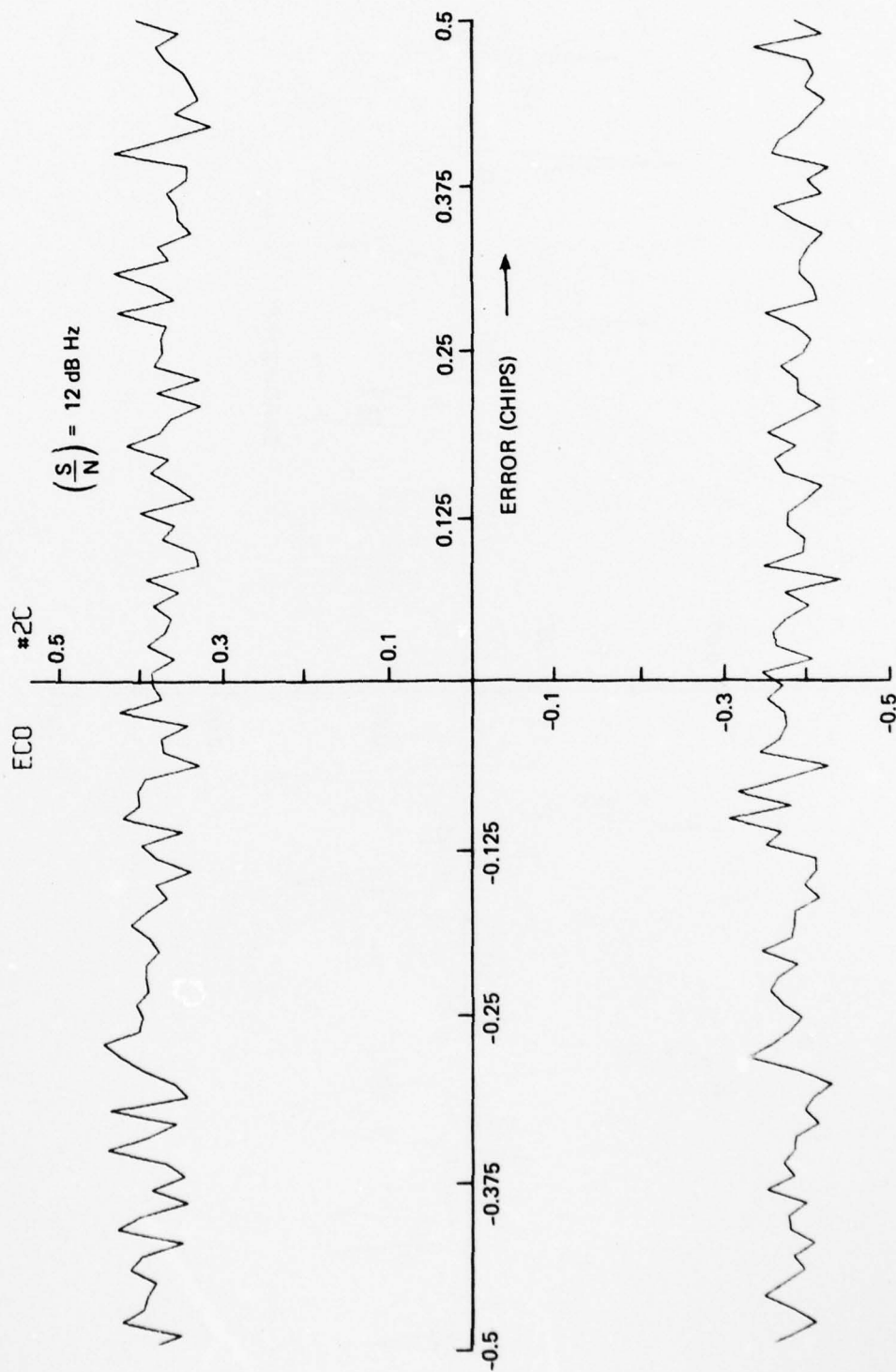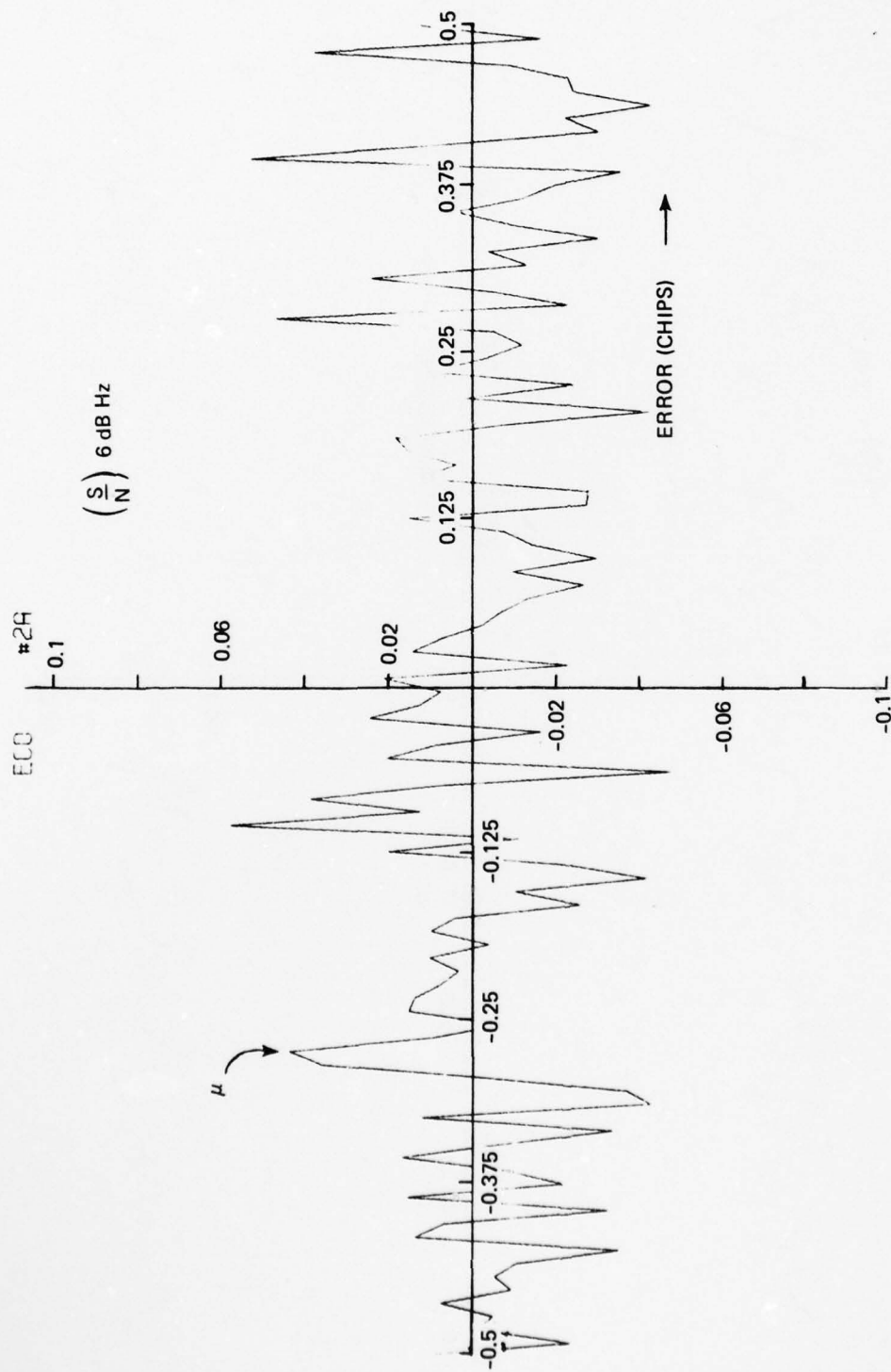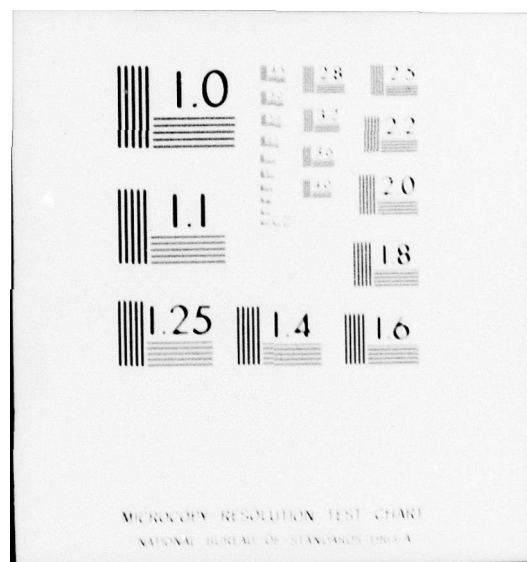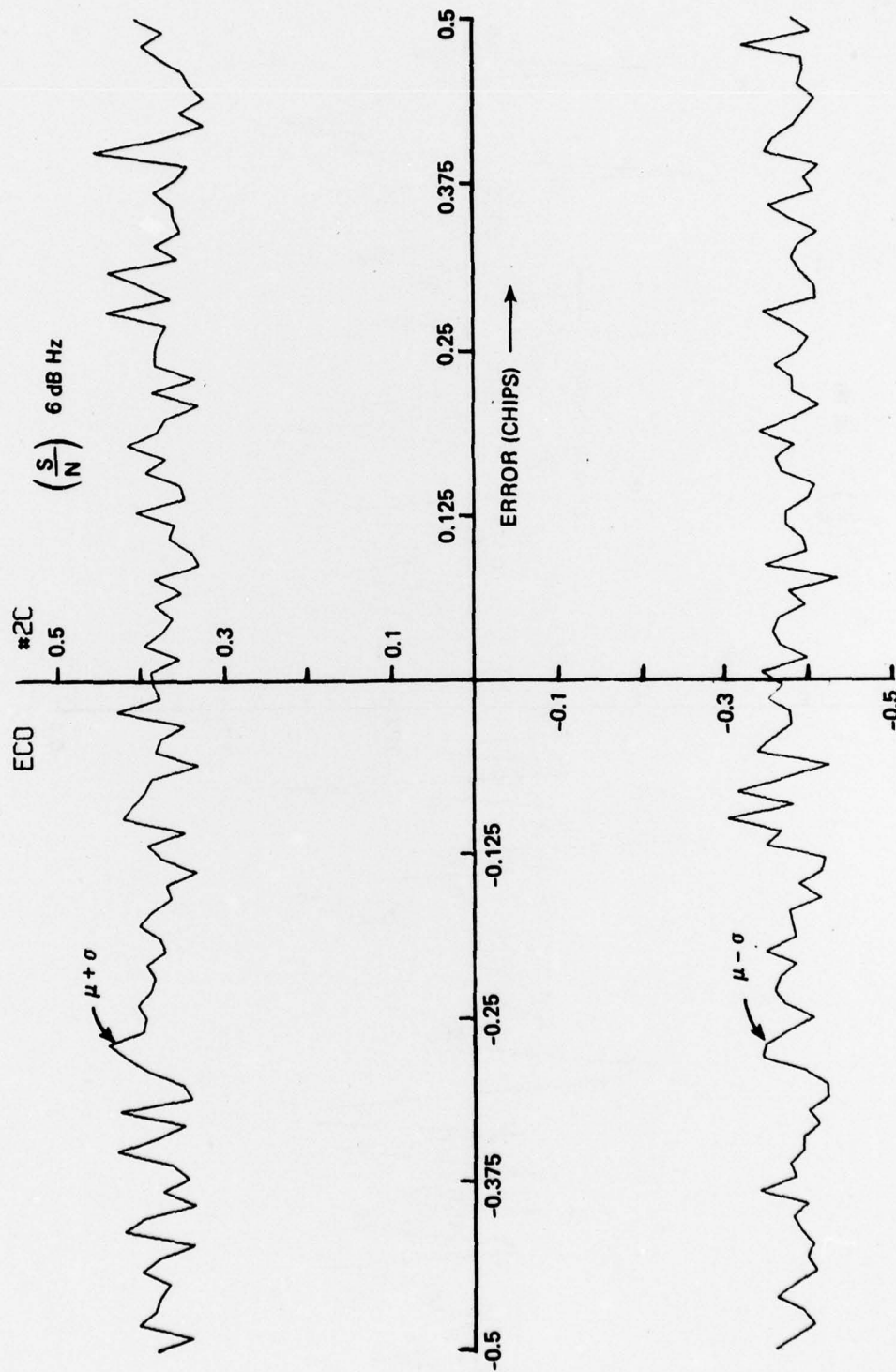
Figure B16.

Figure B17.

Figure B18.

189

LOG $\left(\frac{\partial \tilde{e}/\Delta}{\partial \epsilon}\right)$
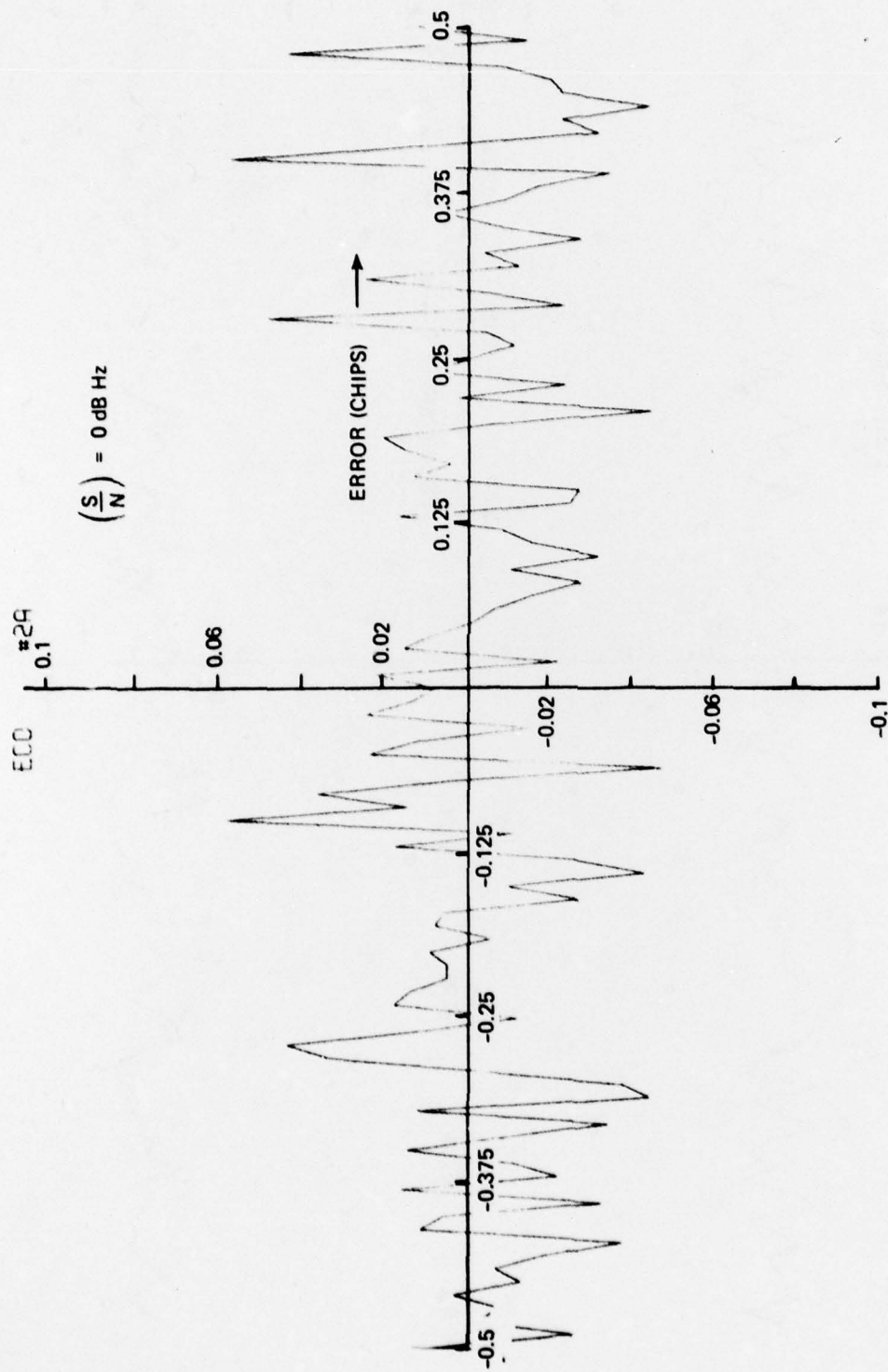
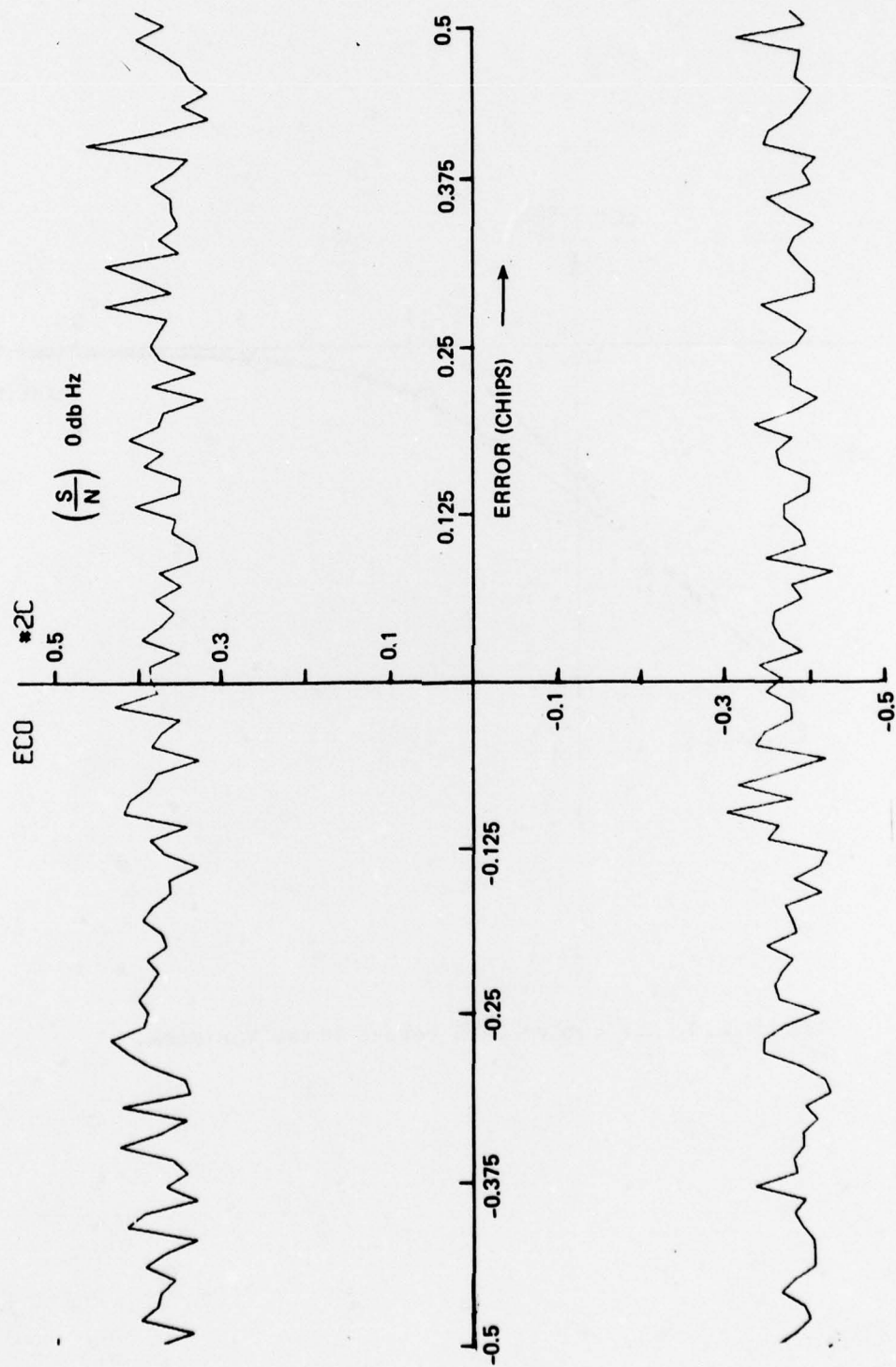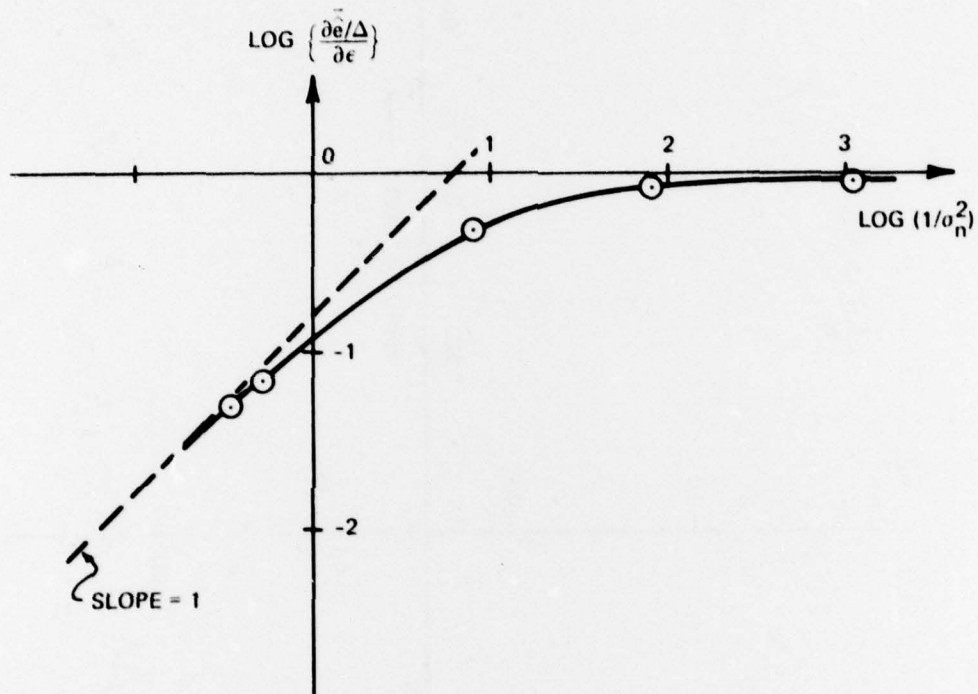LOG $(1/\sigma_n^2)$

0

1

2

3

−1

−2

SLOPE = 1

Figure B19. Effective Gain Versus Noise Variance.

APPENDIX C

DERIVATION OF EFFECTIVE GAIN
AS A FUNCTION OF NOISE POWER

From Equation (8.10)

$$\hat{e}_{CO} = \frac{1}{2} \left[-|(\Delta-\varepsilon) + n_{IE}| - |n_{QE}| + |(\Delta+\varepsilon)| + n_{IL}| + |n_{QL}| \right] \qquad (C1)$$

The effective gain G is

$$G = \frac{\partial \hat{e}_{CO}}{\partial \varepsilon} = \frac{1}{2} \left. \frac{\partial}{\partial \varepsilon} \right|_{\varepsilon=0} \left\{ -\overline{|(\Delta-\varepsilon) + n_{IE}|} + \overline{|(\Delta+\varepsilon) + n_{IL}|} \right\} \qquad (C2)$$

From symmetry

$$G = \left. \frac{\partial}{\partial \varepsilon} \right|_{\varepsilon=0} \overline{|(\Delta+\varepsilon) + n_{IL}|} \qquad (C3)$$

From A. Papoulis, Probability, Random Variables and Stochastic Processes, McGraw Hill Book Co., N.Y., 1965, we find

$$\overline{|X-a|} = \overline{X-m} + 2 \int_a^m (x-a) f(x) dx \qquad (C4)$$

191

where $\overline{}$ denotes expected value, m is the median of X, f(x) is the probability density function of X, and a is an arbitrary constant. So we write Equation (C3) as

$$G = \frac{\partial}{\partial\varepsilon}\Bigg|_{\varepsilon=0}\overline{|n_{IL} - (-\Delta - \varepsilon)|} = \frac{\partial}{\partial\varepsilon}\Bigg|_{\varepsilon=0}\Bigg\{\overline{n_{IL} - o} + 2\int_{-\Delta-\varepsilon}^{o}(n_{IL} + \Delta + \varepsilon)$$

$$f(n_{IL})\ d\ (n_{IL})\Bigg\} \tag{C5}$$

Then

$$G = o + 2\frac{\partial}{\partial\varepsilon}\int_{-\Delta-\varepsilon}^{o} n\ f(n)\,dn + 2\Delta\frac{\partial}{\partial\varepsilon}\int_{-\Delta-\varepsilon}^{o}f(n)\,dn$$

$$+ 2\frac{\partial}{\partial\varepsilon}\ \varepsilon\int_{-\Delta-\varepsilon}^{o}f(n)\,dn \tag{C6}$$

Carrying out the differentiation yields

$$G = (2)(-\Delta)f(-\Delta) + (2\Delta)f(-\Delta) + 2\int_{-\Delta}^{o}f(n)\,dn$$

$$= 2\int_{-\Delta}^{o}f(n)\,dn \tag{C7}$$

where

$$f(n) = \frac{1}{\sigma\sqrt{2\pi}}\ e^{\frac{-n^2}{2\sigma^2}} \tag{C8}$$

so the gain is

$$\boxed{G = \text{erf}\left(\frac{\Delta}{\sqrt{2}\sigma}\right)} \tag{C9}$$

For small $\Delta/\sqrt{2}\sigma$ the gain becomes

$$\boxed{G = \frac{2}{\sqrt{\pi}}\left(\frac{\Delta}{\sqrt{2}\sigma}\right) = 0.798\ \frac{\Delta}{\sigma}} \tag{C10}$$

192